Assessing visual function following the transplantation of mouse ESC-derived rod precursors

Debbie Goh

A thesis submitted to University College London
for the degree of Doctor of Philosophy (PhD)

2016

Institute of Ophthalmology

University College London

Declaration

I, Debbie Goh, confirm that the work presented in this thesis is my own. Where information has been derived from other sources, I confirm that this has been indicated in the thesis.

Debbie Goh, B.Sc.

Abstract

Photoreceptor replacement therapy is a promising strategy for treating retinal degenerative diseases leading to blindness. Previous work by our lab has demonstrated proof-of-concept that mouse embryonic stem cells (ESCs) can be differentiated, in a 3D culture system, into post-mitotic rod photoreceptor precursors for transplantation. However, rescue of visual function following transplantation of ESC-derived rod precursors has yet to be demonstrated. This project therefore sought to optimise the transplantation of mouse ESC-derived rod photoreceptor precursors into mouse models of retinal disease, define the optimal developmental stage for transplantation in an endogenous photoreceptor reporter ESC line, and thereafter, assess the extent to which visual function is restored in recipient animals post-transplantation. We assessed different aspects of optimising the transplantation protocol, such as dissociation method, AAV2 virus pseudotype used for labelling photoreceptors, and host immune suppression, and also characterised photoreceptor differentiation in a *Crx.GFP* ESC line. Additionally, we developed a multi-electrode array (MEA) set up and stimulus protocol that allowed us to detect visual responses from retinal explants. These studies demonstrated the generation of large numbers of healthy, developmentally-homogenous mouse ESC-derived rod photoreceptors for transplantation, and resulted in a significantly increased number of donor-reporter labelled cells observed in the host outer nuclear layer (ONL) following transplantation. Most importantly, using the MEA, we were able to demonstrate for the first time that mouse ESC-derived photoreceptor precursors were capable of transmitting light-evoked responses following transplantation into a mouse model of severe retinal degeneration. Taken together, these are encouraging first steps towards the use of stem cells for photoreceptor replacement therapy in retinal degenerative diseases.

(259 words)

Acknowledgments

This thesis and the findings within would not be possible without the help and support of many people. It will be difficult to fully express my thanks to everyone here, but I will try anyway.

I would first like to thank my primary supervisor Professor Robin Ali, for giving me the opportunity 3 years ago to join the Gene and Stem Cell Therapy group – I have learnt an incredible amount just by being part of such a diverse group. Thank you for your endless support throughout these years, and for pushing me to be a better scientist. To my secondary supervisor Professor Rachael Pearson, thank you for being so approachable and for teaching by example how good science is done. I am deeply grateful to both of you for believing in me, and for your contributions of time, ideas, and funding, which have made my PhD experience thoroughly productive and stimulating.

To the Stem Cell Facility, thank you for being my second family, and for teaching me the tricks of the trade. In particular, I would like to thank Anai, for your contagious enthusiasm that kept me going in the tough times, for providing direction when the way forward seemed unclear, and most of all, for your friendship. To Emma, for helping me find my feet in the early days of my PhD. To my desk buddies, Arifa and Magda, for your immense practical support and for making 'grape Fridays' an occasion to look forward to at the end of each long week. To my fellow PhDs, Kamil and Manjit, for keeping the mundanity of bench work at bay with your banter and ingenious ideas.

I am deeply appreciative of many others in the group too. A special thanks to Sander, for reading through this thesis, and for your astute input over the years. To Yanai, for your help with the animal work, and especially for your beautiful subretinal injections. To Rob, for tirelessly sorting my GFP-labelled cells (sorry I couldn't offer anything more exciting, and I hope someone soon replaces me on your wall of shame for clogging the Fortessa one time too many). To Tassos, for introducing this complete novice to the world of genome editing. To Pete, for generously sharing your expertise on all things immunology-related. To Martha, Paul, Kate and Matteo, for supporting my foray into the intimidating world of neuroscience with such patience, and for your

constructive criticism. To Heather, for tirelessly working behind the scenes to keep everything running so smoothly.

To the Agency of Science, Technology and Research (A*STAR), thank you for your generous funding and for supporting my pursuits in both Medicine and Science. Not to forget Waitrose, for your free coffees that kept me going through the late nights without breaking my bank.

Heartfelt thanks also go to my amazing friends outside of the lab – in particular, Mark & Mel, Murph & Ames, Grace, Ginni, Cher, Anja and Jas – for praying for me, offering practical help, and organising fun things to do to motivate me to work hard. An extra special mention must also be made to those supporting me from miles away in Singapore – Becca, for always being there to listen and pray with, and Chong Yong, for providing me with excellent music to write to and cheering me on when my spirits flagged.

Finally, I would like to dedicate this thesis to my parents, for freeing me to pursue my studies abroad for the past 6 years and for another 3 more. The separation has not been easy, but I thank you for sharing every step of this journey with me even from afar, and for being my pillars of support throughout these years. I could not have made it this far without your love and dedication.

Table of Contents

List of Figures

Chapter 1 : Introduction

1.1 The retina

1.2 Development of the mammalian eye

1.3 Development of the neural retina

1.5 Photoreceptor replacement therapy

Chapter 2 : Methods

Chapter 3 : Optimisation of transplantation protocol

3.2.1 Assessing photoreceptor viability in vitro

5.2.3 Investigating light stimulus-driven RGC responses in the Gnat1$^{-/-}$ retina

5.2.4 Investigating light stimulus-driven RGC responses in the Opn4$^{-/-}$ Gnat1$^{-/-}$ Cnga3$^{-/-}$ retina

5.2.5 Investigating light stimulus-driven RGC responses in the Aipl1$^{-/-}$ retina

List of Tables

Chapter 2 : Methods

Chapter 4 : Development of a photoreceptor reporter knock-in line

List of Abbreviations

3D	Three-Dimensional
ACAID	Anterior Chamber-Associated Immune Deviation
AIPL1	Aryl-hydrocarbon Interacting Protein-Like 1
AMD	Age-related Macular Degeneration
BMP	Bone Morphogenetic Protein
BSA	Bovine Serum Albumin
Cas	CRISPR-associated
cGMP	Cytoplasmic Cyclic Guanosine Monophosphate
CMV	Cytomegalovirus
CRISPR	Clustered Regularly Interspaced Short Palindromic Repeat
CRX	Cone-Rod Homeobox
CUSUM	Cumulative Sum
CyA	Cyclosporine A
DLP	Digital Light Processing
DSB	Double Stranded Break
EB	Embryoid Body
EFTF	Eye Field Transcription Factor
EGF	Epithelial Growth Factor
ERG	Electroretinogram
ESC	Embryonic Stem Cell
FACS	Fluorescence Activated Cell Sorting
FBS	Fetal Bovine Serum
FGF	Fibroblast Growth Factor
FMO	Fluorescence Minus One
FP	Fluorescent Protein
FSC	Forward Scatter
GAP	GTPase-activating Protein
GC	Guanylate Cyclase
GCAP	Guanylate Cyclase-Activating Proteins
GCL	Ganglion Cell Layer
GFP	Green Fluorescent Protein
GFP^+	GFP-positive
Gnat1	Rod α-transducin
G_t	Transducin G-protein

HDR	Homology-directed Repair
ILM	Inner Limiting Membrane
INL	Inner Nuclear Layer
IPL	Inner Plexiform Layer
IPM	Inter Photoreceptor Matrix
iPSC	Induced Pluripotent Stem Cell
IPTG	Isopropyl β-D-1-thiogalactopyranoside
IRES	Internal Ribosome Entry Site
IS	Inner Segment
KSR	Knock-out Serum Replacement
LB	Luria-Bertani / Lysogeny Broth
LCA	Leber Congenital Amaurosis
LD	Live/Dead
LGN	Lateral Geniculate Nucleus
LIF	Leukaemia Inhibitory Factor
MACS	Magnetic Activated Cell Sorting
MEA	Multi-electrode Array
MEK	Mitogen-activated protein kinase kinase
MFI	Median Fluorescence Intensity
MHC	Major Histocompatibility Complex
ND	Neutral Density
NEAA	Non-Essential Amino Acids
NHEJ	Non-Homologous End Joining
NK	Natural Killer
NRL	Neural Retina Leucine zipper protein
OFF-GC	OFF-Ganglion Cells
OGC	$Opn4^{-/-}$ $Gnat1^{-/-}$ $Cnga3^{-/-}$ mouse model
OLM	Outer Limiting Membrane
ON-GC	ON-Ganglion Cells
ONL	Outer Nuclear Layer
OPL	Outer Plexiform Layer
OS	Outer Segment
PCR	Polymerase Chain Reaction
PDE	Phosphodiesterase
PFA	Paraformaldehyde
PKCa	Protein Kinase C alpha subunit

R*	Activated Rhodopsin
RGC	Retinal Ganglion Cell
RK	Rhodopsin Kinase
RMM	Retinal Maturation Media
RP	Retinitis Pigmentosa
RPC	Retinal Progenitor Cell
RPE	Retinal Pigment Epithelium
SDM	Site-Directed Mutagenesis
sFEB	Serum-free Floating culture of Embryoid Body aggregates
SOC	Super Optimal broth with Catabolite repression
SSC	Side Scatter
SSEA-1	Stage-Specific Embryonic Antigen-1 (or CD15)
TGF-β	Transforming Growth Factor-beta
UTR	Untranslated Terminal Region
V1	Primary Visual Cortex
WT	Wild-Type
ZO-1	Zona Occludins-1

Chapter 1 : Introduction

1.1 The retina

1.1.1 Cell types in the retina

The vertebrate retina is a thin sheet of neural tissue at the back of the eye that converts light to an electrical signal. There are six major neuronal classes in the vertebrate retina – rod and cone photoreceptors, bipolar, horizontal, amacrine, and ganglion cells – which are organized in a laminar arrangement and form numerous circuits for the processing of visual information (Figure 1.1).

Broadly, the process of vision is initiated in photoreceptors, which are sensory neurons specialized to capture light quanta and convert them into electrical signals. These signals are integrated and processed by the interneurons – the bipolar, horizontal, and amacrine cells – and subsequently transmitted to ganglion cells, which are the projection neurons of the retina. The axons of ganglion cells converge to form the optic nerve, which relays visual output from the retina to the lateral geniculate nucleus (LGN). This visual information is preserved and retinotopically mapped on to area V1 of the primary visual cortex in the occipital lobe, and from there on, to higher visual processing areas that extract relevant information to construct a coherent perceptual experience (Lamb et al., 2007; Masland, 2001).

Figure 1.1: Anatomy of the mammalian retina, as shown by a representative H&E cross section of an adult mouse retina (left) and by schematics (centre and right). In the retina, the six main neuronal classes are organized into three nuclear layers [outer nuclear layer (ONL), inner nuclear layer (INL) and ganglion cell layer (GCL)], and form synaptic connections in two plexiform layers [outer plexiform layer (OPL) and inner plexiform layer (IPL)]. Cone and rod photoreceptors comprise the outer retina with their cell bodies situated in ONL and their inner and outer segments (IS and OS) located between ONL and the retinal pigment epithelium (RPE). Photoreceptor axons terminate in the OPL and synapse with horizontal and bipolar cells in the INL, which also contains Müller glial and amacrine cells. Bipolar cells relay signals to amacrine and ganglion cells through synapses in the IPL. Ganglion cell axons project towards the optic nerve head and carry signals to the brain. End-feet of Müller glia form the outer and inner limiting membranes (OLM and ILM). Adapted from (Yang et al., 2015)**.**

1.1.2 Retinal structure and organization

The retina is a layered structure with two synaptic ("plexiform") layers sandwiched by three distinct nuclear layers – the outer nuclear layer (ONL), inner nuclear layer (INL) and ganglion cell layer (GCL). This principal laminar structure is conserved in all vertebrate retinae.

The nuclear layers house the three principal neuronal cells that make up the visual pathway: the photoreceptor, bipolar, and ganglion cells. The ONL contains the cell bodies of both rod and cone photoreceptors. The INL contains the cell bodies of horizontal, bipolar, amacrine and Müller glial cells: bipolar cells propagate signal from photoreceptors to ganglion cells, horizontal and amacrine cells provide lateral modulation, and Müller glia spanning the entire breadth of retina provide both metabolic and structural support. The GCL contains ganglion and displaced amacrine cells. Ganglion cell axons pass within the nerve fibre layer to the optic disk, where they converge to form fibres of the optic nerve.

The plexiform layers contain the dendrites and synapses: the outer plexiform layer (OPL) lies between the ONL and INL, and is where the photoreceptors communicate with horizontal and bipolar cell dendrites; the inner plexiform layer (IPL) separates the INL and GCL, and is where the bipolar cell axons interact with amacrine and ganglion cells.

The outer limiting membrane (OLM) is located at the outer edge of the ONL, between photoreceptor inner segments and the apical end feet of Müller glia. It comprises a network of zonula adherens junctions formed from heterotypic cadherin-catenin transmembrane protein complexes (Figure 1.2b,c) (Tepass, 2002). Apart from providing adhesive contacts between photoreceptors and Müller cells, these junctions are also a source of polarity signals that control morphogenesis and lamination (Popp et al., 2004) and provide a semi-permeable barrier preventing the diffusion of phototransduction cascade molecules. They are linked to the actin cytoskeleton within the cell cytoplasm, via adapter proteins such as ZO-1 and Crb1 (Figure 1.2c) (Alves et al., 2014).

The retinal pigment epithelium (RPE) is a monolayer of pigmented epithelial cells connected by tight junctions, which control intercellular communication and electrical potential differences. The RPE has multiple vital functions, many of which relate to the normal function and survival of photoreceptors; death of either cell type can therefore result in secondary degeneration of the other. RPE cells have a polarised apical-basal orientation: the apical membranes contain microvilli extending into the interphotoreceptor matrix (IPM), which are involved in the renewal of photoreceptor outer segments by phagocytosis, whereas the basolateral aspect contacts Bruch's membrane, which maintains the outer blood-retinal barrier and the immune-privileged status of the retina. In addition, pigmented melanin granules in RPE cells absorb light that is not captured by adjacent photoreceptors, thereby reducing backscatter and improving image resolution. RPE also plays major role in the visual cycle, and is the principle site of 11-*cis*-retinal regeneration.

Figure 1.2: (a) Schematic of a Müller cell (grey) illustrating its location within a representative H&E-stained mouse retina. (b) Confocal image of a retinal section from an Nrl.gfp (green) mouse, stained for zonula occludins-1 (ZO-1; red), a zonula adherens junction protein. Scale bar, 20 mm. (c) Schematic illustrating the zonula adherens junctions (red) that form the OLM, between the cells of the mammalian retina (green photoreceptors; grey Müller cells; blue nuclei). An enlargement of an adherens junction demonstrates the presence of the actin-binding protein ZO-1 at the OLM (insert). Adapted from (West et al., 2008).

1.1.3 Photoreceptors

There are two types of photoreceptors – rods and cones. In both mouse and human retinae, rods account for approximately 97% of retinal photoreceptors, and cones make up the remaining 3%. The combined action of rods and cones allow visual perception over 10 log units of magnitude in light intensity. Rods mediate scotopic vision under conditions of dim illumination, and can respond to single light quanta. Cones are a 100-fold less sensitive than rods, but they are able to provide high-acuity, photopic colour vision in bright daylight conditions with greater temporal resolution than rods.

The mammalian retina only expresses one type of rod visual pigment (rhodopsin, which has a peak spectral sensitivity at ~500 nm). In contrast, cones express a variety of visual pigments, or opsins, whose spectral sensitivity varies based on the cone's subtype. Most mammals have two types of cone opsins that confer dichromatic colour vision: S-opsin (or blue-sensitive opsin), which has peak sensitivity in the short wavelength (430nm) region of the spectrum, and M-opsin (or green-sensitive opsin), which has peak sensitivity in the medium-long wavelength (530nm) region of the spectrum. Human cones can express an additional type of opsin, L-opsin (or red-sensitive opsin), which is sensitive to longer wavelength (561nm) light and, together with S-opsin and M opsin, confers trichromatic colour vision.

Despite being functionally and morphologically distinct from each other, both rod and cone photoreceptors are highly polarised, elongated cells that can be described as having four subcellular compartments: the outer segment (OS), the inner segment (IS), the nucleus, and the synaptic terminal (Figure 1.3a).

Figure 1.3: (a) Diagram of rod and cone morphologies and the varying functions in each subcellular compartment. Adapted from (Swaroop et al., 2010)**. (b) Simplified diagram of rod and cone presynaptic terminals. Rod synaptic terminals ("spherules") possess only a single, large active zone with a single synaptic ribbon whereas cones synaptic terminals ("pedicles") have multiple active zones. Abbreviations: RPE, retinal pigmented epithelium; OS, outer segment; IS, inner segment; Syn, synaptic terminus; CB, cell body; sv, synaptic vesicle; h, horizontal cell postsynaptic dendrite; b, bipolar cell postsynaptic dendrite. Adapted from** (Schmitz et al., 2012)**.**

The OS contains all the components necessary for phototransduction, and the biochemical cascade of phototransduction is restricted to the OS. Stacks of discs derived from invaginations of the photoreceptor plasma membrane are found throughout the length of the OS, and each OS disc incorporates several million opsin molecules. OS disc renewal occurs continually, and entails the shedding of distal discs and phagocytosis by the enveloping apical microvilli of the RPE.

The IS lies immediately proximal to the OS, and contains all the protein synthesis and metabolic machinery required to assemble and transport opsin molecules to the OS discs. Mitochondria also manufacture ATP to power the sodium-potassium pump necessary for stabilising the resting potential.

Cone nuclei are situated at the outer apical edge of the ONL near the OLM, whereas rod nuclei lie basal to cone nuclei in the inner regions of the ONL. Additionally, cone cell nuclei have irregularly-shaped clumps of heterochromatin, whereas rods have a single large central clump instead.

Light-evoked signals are relayed passively down the photoreceptor axon to the synaptic terminals located in the OPL. Rod terminals are generally found at the outer regions of the OPL, and lie basal to cone terminals. The structure of photoreceptor terminals is unique in the nervous system, as they contain a specialised structure called a synaptic ribbon that facilitates the release of the excitatory neurotransmitter glutamate on to second-order retinal neurons. The rod synaptic terminal, called a spherule, appears smaller in size than cone synapse terminals, as it contains a single invagination with a single ribbon synapse. Processes from two horizontal cells and two to five bipolar cells can be found within a rod synaptic cleft. Conversely, the cone synaptic terminal, termed a pedicle, has multiple ribbon synapses and several synaptic cell invaginations, each containing processes from two horizontal cells and multiple bipolar cells (Figure 1.3b).

1.1.4 Phototransduction cascade of rods

Phototransduction is a biochemical cascade that converts a captured photon of light into an electrical signal. Thus far, only rod and cone photoreceptors as well as melanopsin-containing photosensitive retinal ganglion cells (RGCs) have been found to be capable of phototransduction; of these, rod phototransduction is the most well-characterised (Figure 1.4).

In the dark, rods are constitutively depolarized. This depolarization is due to a steady inward electrical 'dark current' caused by Na^+ and Ca^{2+} cations moving into the cell along their concentration gradient, through open cyclic guanyl monophosphate (cGMP)-gated (cG-gated) Na^+/Ca^{2+} ion channels. cG-gated ion channels in the OS plasma membrane remain open due to high cGMP levels within the photoreceptor OS, and the resultant Ca^{2+} influx stimulates the rod photoreceptor to continuously release the neurotransmitter glutamate onto post-synaptic bipolar cells (Yau, 1994).

In darkness, the rod visual pigment, rhodopsin, exists as a dimer comprising the chromophore 11-*cis*-retinal covalently coupled to the opsin protein, which is a transmembrane G-protein-coupled receptor. Photon absorption causes dissociation of rhodopsin into opsin and all-*trans*-retinal, resulting in a conformational change of rhodopsin to its activated state (denoted as R*). In turn, R* activates hundreds of transducin G-protein molecules ($G_{t\,\alpha\beta\gamma}$) by causing GTP to bind to the $G_{t\,\alpha}$ unit of $G_{t\,\alpha\beta\gamma}$. The activated $G_{t\alpha}$-GTP (denoted as G*) then dissociates from $G_{t\,\alpha\beta\gamma}$ and binds to the inhibitory γ-subunits of phosphodiesterase 6 (PDE6), thereby removing the inhibition on the catalytic α- and β-subunits of PDE6. PDE6 is the primary regulator of cytoplasmic cyclic guanosine monophosphate (cGMP) concentration. The activation of PDE6 therefore leads to cGMP hydrolysis and a rapid reduction in cytoplasmic cGMP concentration, causing closure of cG-gated channels. Levels of Na^+ and Ca^{2+} fall, causing hyperpolarisation and thereby decreased glutamate release from the rod spherule.

Figure 1.4: Schematic of the molecular steps in phototransduction, as taking place in the outer membrane of a rod OS disc. Step 1: Incident photon (hv) is absorbed and activates conformational change of rhodopsin (R) to R*. Step 2: R* catalyses transducin (G) activation to G* by the release of bound GDP in exchange for cytoplasmic GTP. The β and γ subunits dissociate. Step 3: G* binds inhibitory γ subunits of phosphodiesterase-6 (PDE), allowing activation of its α and β subunits. Step 4: Activated PDE rapidly breaks down cGMP. Step 5: Reduced levels of cytosolic cGMP cause cGMP (cG)-gated channels to close, preventing further influx of Na^+ and Ca^{2+}. Adapted from (Leskov et al., 2000)**.**

Following light stimulation, the phototransduction cascade has to be terminated in order to restore cGMP levels and allow re-opening of the cG-gated channels. When intracellular Ca^{2+} levels fall following phototransduction, Ca^{2+} is released from recoverin (Rec), a calcium-binding protein that forms a complex with rhodopsin kinase (RK) and inhibits its activity. Ca^{2+} release allows for the dissociation of RK, which inactivates the photoactivated R* to a phosphorylated form (R-P) that binds preferentially to another cytoplasmic protein, arrestin (Arr). This rapidly reduces the amount of R* available for the activation of transducin, and thereby quenches R* activity (Figure 1.5a). Low Ca^{2+} levels also stimulate the release of Ca^{2+} from guanylate cyclase-activating proteins (GCAPs), allowing GCAP to bind to retinal guanylate cyclases (GCs), which are membrane-associated enzymes that catalyse the formation of cGMP from GTP (Figure 1.5b). Apart from increased cGMP synthesis, cGMP hydrolysis by activated PDE is also reduced by GTPase-activating proteins (GAPs) (Figure 1.5c). GAPs bind to activated $G_{t\,\alpha}$-GTP, inducing rapid hydrolysis of the bound GTP and causing G* to break off from PDE. This allows inhibitory action of the β-subunits of PDE once again, halting the hydrolysis of cGMP by PDE (Wert et al., 2014; Pugh and Lamb, 2000). Finally, as light exposure causes the conversion of 11-*cis*-retinal to all-*trans*-retinal, in order to maintain light responses, rods recycle this chromophore through the visual cycle that takes place in the RPE.

Figure 1.5: Schematic of the deactivation of the phototransduction cascade. (a) Inactivation of R* (b) GC activation and cGMP synthesis (c) Inactivation of PDE and reduced cGMP hydrolysis. Adapted from (Pugh and Lamb, 2000)**.**

1.1.5 Retinal circuitry and cortical processing

Having an understanding of retinal circuitry and cortical processing is important if we are to assess the integration of transplanted photoreceptor precursors. In the retina, scotopic and photopic visual signals are propagated along separate neuronal pathways which have various points of convergence. Rods and cones are pre-synaptic to different second-order bipolar cells, which are responsible for transmitting the visual signal received onwards to the inner retina. The dendrites of rod bipolar cells are highly branched, and receive input from as many as 120 rods, conferring high sensitivity but low acuity. In contrast, in animals with foveas, cones are responsible for higher-acuity vision than rods, with bipolar cells that transmit signals from just a few cones and drive ganglion cells with very small receptive fields.

There are three known pathways available for signals from rods to reach retinal ganglion cells. First, in the classical primary rod pathway (Figure 1.6a), rod photoreceptors synapse with ON-bipolar cells, which express the metabotropic glutamate receptor mGluR6. In darkness, constant glutamate binding to mGluR6 inhibits the opening of the non-selective cation channel TRPM1-L, and the reduction of cation influx causes the bipolar cell to hyperpolarize. A light-evoked decrease in glutamate release opens these channels, causing a depolarising 'ON' response of the ON-bipolar cell (Nawy and Jahr, 1991). A majority of rod ON-bipolar cells project onto AII amacrine cells instead of ganglion cells. These AII amacrine cells facilitate the piggybacking of rod signals on to the cone pathway, either via inhibitory glycinergic synapses with OFF-cone bipolar cells, or by providing electrical input into ON-cone bipolar cells via gap junctions. This dual convergence with the cone visual pathway allow both ON and OFF signals to be generated in scotopic conditions.

There is a secondary rod pathway (Figure 1.6b), where rod-cone gap junction coupling at the level of the photoreceptor enables rods to signal via cone pathways (Asteriti et al., 2014; Tsukamoto et al., 2001). Unlike rods, which only synapse with the rod ON-bipolar cell, cones synapse on to both ON and OFF bipolar cells, of which there are 13 different recorded types. An increase in glutamate release at the cone bipolar-ganglion cell synapse can therefore signal either the presence of light (via ON bipolar cells) or its absence (via OFF bipolar cells) (Kolb et al., 1995; Nelson and Kolb, 1983). The difference in response between ON and OFF bipolar cells is governed by expression of different post-synaptic glutamate receptors (Masland, 2001).Unlike ON

bipolar cells, which express mGluR6, OFF bipolar cell express either kainate or AMPA ionotropic receptors (Yang et al., 2003), which have different kinetics – AMPA receptors resensitize to glutamate much faster than kainate receptors, and are more selective for transient signal components, rather than sustained characteristics (DeVries, 2000). Glutamate release in darkness causes both AMPA and kainite glutamate receptors to open, allowing calcium influx, which depolarizes the OFF bipolar cell. When glutamate release from cones falls upon light detection, the calcium channels close and the OFF bipolar cell hyperpolarizes.

Figure 1.6: Schematic of rod and cone visual pathways in the retina. (a) In the classical primary rod pathway, rod signals are transmitted via the ON-rod bipolar cell (ON-RBP) then onto the AII amacrine cell. The AII then inputs either into ON-cone bipolar cell via gap junctions in connexion 36 (Cx 36) and then ON-ganglion cells (ON-GC), or into OFF-cone bipolar cell and then OFF-ganglion cells (OFF-GC). (b) In the secondary rod pathway, rods convey visual signal directly to cones via gap junctions in Cx36. Adapted from (Seeliger et al., 2011)

Finally, there is a third pathway for rod signals through a mixed rod-cone OFF bipolar cell. Unlike the metabotropic mGluR6 receptors used by the rod ON-bipolar, glutamate released from rods at these synapses is detected by ionotropic AMPA receptors. These light-hyperpolarizing cells have been demonstrated in rodents (Hack et al., 1999; Pang et al., 2012; Soucy et al., 1998; Tsukamoto et al., 2001; Tsukamoto and Omi, 2013).

In addition to synapsing with bipolar cells, photoreceptors also synapse with horizontal cells. Horizontal cells provide negative feedback to photoreceptors via lateral inhibition, thereby modulating multiple photoreceptor input to bipolar cells and controlling the resulting magnitude of bipolar activation. They are thus crucial for background subtraction, making it possible to focus on low-contrast details in a visual scene. Similarly, bipolar cell input to ganglion cells is modulated by amacrine cells, which are a diverse group of mostly inhibitory interneurons that use a variety of neurotransmitters for signalling, of which the most commonly used are GABA and glycine. One major role of amacrine cells is thus to provide a level of negative feedback to bipolar cells; however they also serve many other functions, such as feature extraction and lateral inhibition.

Ganglion cells are the output neurons of the retina, encoding visual information in the rate of action potential generation, which is modulated by bipolar and amacrine cells as described above. Action potentials are transmitted along the axons of ganglion cells over long distances to the higher visual centres in the brain. Ganglion cells are physiologically and morphologically diverse, with at least 15–20 different types, each of which is thought to transmit independent, parallel channels of visual information that serve specific functions. Vast majority of ganglion cells axons terminate in the lateral geniculate nucleus (LGN) of the thalamus, which in turn relays information mostly to the primary visual cortex (V1) in the occipital lobe of both hemispheres of the brain for visual processing (Figure 1.7a). The visual cortex in each hemisphere receives input from the ipsilateral half of the visual field, and different areas of the visual cortex process various aspects of visual information, such as form, colour or movement (Figure 1.7b).

Figure 1.7: (a) Visual pathway from the retina to the brain. Ganglion cells from the retina project to the lateral geniculate nucleus (LGN) via the optic nerve, and from here, signals are relayed to the visual cortex. Adapted from https://sites.google.com/site/physiologysite/the-visual-pathway-from-eye-to-primary-visual-cortex (b) Areas of the visual cortex. The visual cortex is divided into five main areas – V1 to V5. Area V1, which is known as the striate cortex or the primary visual cortex, receives most of the visual input before relaying it to the appropriate area of the extrastriatal cortex for complex visual processing. Adapted from http://mikeclaffey.com/psyc170/notes/images/vision-v-areas.jpg.

1.2 Development of the mammalian eye

The eye originates from the neuroepithelium of the ventral forebrain, which develops into distinct ocular tissues through an extremely complicated process involving derivatives from mesoderm, neural crest and ectoderm. Critical steps during eye development include the formation of the eye field, specification of the neural retina and RPE, and retinogenesis. Any disruption of these steps in development can result in severe eye defects. As such, the development of ocular tissues must be precisely coordinated, and this is achieved through extrinsic signalling molecules acting closely in concert with intrinsic cell determinants to control development.

1.2.1 Formation of the eye field

Although the first morphological evidence of eye formation in vertebrates is the bilateral evagination of neuroepithelium within the anterior neural plate to form the optic vesicles, modern molecular evidence shows that the eye primordium is specified at an earlier stage.

During late gastrulation, a process known as neural induction drives ectodermal cells in the dorsal ectoderm to adopt a neural fate at the expense of epidermal differentiation. This region of neuroectoderm is called the neural plate; the anterior region of which is specified to give rise to the retina, and is therefore referred to as the eye field (Figure 1.9a). A group of transcription factors – the eye field transcription factors (EFTFs), namely *ET*, *Rx1*, *Pax6*, *Six3*, *Lhx2*, *tll* and *Optx2/Six6* – are expressed in overlapping temporal and spatial patterns during eye field formation to selectively activate genes important for eye development (Figure 1.8)(Zuber et al., 2003; Andreazzoli, 2009).

Figure 1.8: Summary of different stages in eye field specification in the anterior neural plate in *Xenopus*. Top panel: Light blue indicates the neural plate, blue shows the area of *Otx2* expression, and dark blue represents the eye field. Middle panel: Complex genetic regulatory network activated at the corresponding stages. *ET* at the front induces *Rx1*, which activates a cross-regulatory network, including *Pax6*, *Six3*, *Lhx2* and *tll*, followed by *Optx2* induced by *Pax6*. Bottom panel: Representative *in situ* hybridization for several of the EFTFs at the same stage as drawn above to show localization in *Xenopus* embryos. From left to right – *Otx2*, stage 12; *Otx2*, stage 13; *Otx2* (purple) and *Rx1* (red), stage 13; *Rx1* alone, stage 13. Adapted from (Zuber et al., 2003; Reh, 2013).

While the expression of EFTFs in the eye field establishes a genetic network to control eye field specification, concomitant inhibition of two branches of the TGFβ signalling pathway, namely Activin/Nodal and bone morphogenetic protein (BMP) signalling, is also required. Both signalling pathways strongly inhibit neural development; as such, their activity in the ectoderm needs to be repressed for the induction and maintenance of neural fate (Wong et al., 2015). Expression of Wnt/β-catenin signalling in an increasing anterior to posterior gradient along the brain (i.e. low Wnt in anterior) is also crucial for the maintenance of anterior neural tissue. To this end, the expression of secreted antagonists (e.g. Dickkopf-1/Dkk-1), SFRP1, and Tlc) or intracellular inhibitors (e.g. ICAT, TCF-3/*headless*, Axin1/*masterblind*, Shisa) of the Wnt/β-catenin pathway is required in the anterior neural plate. Loss of function

in these inhibitors or ectopic activation of the Wnt/β-catenin pathway usually results in posteriorisation and often truncation of forebrain, and consequently, decreased or ablated expression of eye-specific genes (Fuhrmann, 2008).

1.2.2 Establishment of retinal identity

The eye field is initially centrally-positioned and continuous across the anterior neural plate. However, following neurulation, this single eye field undergoes lateral division and evagination to form two symmetric bilateral optic vesicles (Figure 1.9B). This occurs in response to secreted factors, namely sonic hedgehog (Shh) and FGF.

Figure 1.9: Schematic of vertebrate eye development. A. Specification of the eye field within the anterior neural plate. B. Formation of the optic vesicle. C. Specification of the RPE, neural retina and optic stalk domains within the optic vesicle and formation of the lens placode from the surface ectoderm. D. Formation of the optic cup and the lens vesicle. E. Mature optic cup and lens. Abbreviations: C: Cornea; ef: eye field; L: lens; LP: lens placode; LV: lens vesicle; MS: mesenchyme; NR: neural retina; ON: optic nerve; OS: optic stalk; OV: optic vesicle; RPE: retinal pigment epithelium; S: sclera; SE: surface ectoderm. Adapted from (Vergara and Canto-Soler, 2012).

Extension of the distal portion of the optic vesicles allows for contact with the overlying surface ectoderm (lens ectoderm) (Figure 1.9B). This area of contact develops into the lens placode, as well as the primordia of other anterior structures such as the cornea and conjunctival epithelium. Moreover, the interaction triggers the simultaneous invagination of the overlying lens placode and optic vesicles, resulting in the formation of a pair of bilayered optic cups and lens vesicle (Figure 1.9C). The inner layer of the optic cup develops into the presumptive neural retina, whereas the outer layer acquires pigmentation and develops into the non-neural retinal pigment epithelium (RPE).

Although both are derived from the optic vesicle, these two tissues are quite distinct: the neural retina is a multi-layered structure containing millions of neurons and photoreceptors, whereas the pigment epithelium is a single layer of non-neural, pigmented, cuboidal cells. This distinction is a result of their expression of different domain-specific genes, the earliest being the homeobox gene Vsx2 (formerly Chx10) and the basic helix–loop–helix (bHLH) transcription factor Mitf for the neural retina and RPE respectively.

Figure 1.10: Specification of RPE and retina in the optic vesicle. A. RPE specification (early optic vesicle stage): the extraocular mesenchyme induces Mitf expression throughout the optic vesicle, possibly by activin-like signalling. B. Retina specification (late optic vesicle stage): Activation of ERK by FGF secreted from the lens ectoderm induces Vsx2 and Sox2 expression in the distal optic vesicle, which requires Vsx2-mediated repression of Mitf. Adapted from (Jayakody et al., 2015).

Two key transcription factors, Otx2 and Mitf, are required for the acquisition and preservation of RPE fate (Nguyen and Arnheiter, 2000) (Figure 1.10A). Otx2 is one of the EFTFs, and persists till the late optic vesicle stage to prime the optic vesicle to respond to inducing signals. In the early optic vesicle stage, activin-like signalling from the extraocular mesenchyme induces Mitf expression throughout the optic vesicle. Both Otx2 and Mitf are subsequently downregulated in the presumptive neural retina domain when Vsx2 expression is initiated (Nguyen and Arnheiter,

2000). Otx2 and Mitf work in cooperation to transactivate the expression of crucial genes for terminal pigment differentiation (Martinez-Morales et al., 2001, 2003). Otx2 is required for Mitf expression, and the expression of Otx2 along with Wnt can in fact convert neural retina to RPE (Westenskow et al., 2009). For further reviews, readers are directed to (Fuhrmann, 2010; Martínez-Morales et al., 2004; Bharti et al., 2006).

Additionally, several other upstream regulators – intrinsic and extrinsic – ensure that Mitf is sufficiently expressed to promote RPE cell fate. Extracellular signalling by S*hh,* Wnt, and BMP is known to regulate early aspects of RPE induction and development (Fuhrmann et al., 2000). Other intrinsic signals such as the EFTFs Rx3 (Rojas-Muñoz et al., 2005) or Pax6 (Bäumer et al., 2003) have also been proposed to be involved in RPE specification.

The paired-like homeodomain transcription factor *Vsx2* (formerly *Chx10*) specifies the neural retinal domain of the optic cup. Loss of function mutations in *Vsx2* leads to a conversion of the neural retina into RPE (Rowan et al., 2004). Vsx2 is one of the earliest markers in the presumptive neural retina; it is initially expressed within all retinal progenitor cells (RPCs), but is later restricted to post-mitotic bipolar and a subpopulation of Müller glial cells in the postnatal retina. Vsx2 is important for RPC proliferation, and also activates the transcription factor Crx, which in turn activates downstream transcription factors known to be involved in photoreceptor generation, such as NeuroD and neural retina leucine zipper (Nrl) (Burmeister et al., 1996; Green et al., 2003).

Extrinsic signaling factors are also important in the specification of the neural retinal domain. High MAPK FGF signalling from the overlying lens ectoderm is required – first, to induce neural retinal specification in the distal optic vesicle by promoting *Vsx2* expression; second, for the driving of retinal differentiation (Cai et al., 2010). *Vsx2* mediates the effect of FGF potentially by directly repressing the expression or activity of Mitf, allowing the distal optic vesicle to develop into retina (Horsford et al., 2005; Bharti et al., 2008)(Figure 1.10B). Additionally, BMP signalling has been proposed to be involved in neural retina specification or maintenance of the neural retina domain in the optic vesicle (Murali et al., 2005; Morcillo et al., 2006).

1.3 Development of the neural retina

1.3.1 Histogenesis of retinal cell types

All cell types of the neural retina are derived from a population of retinal progenitor cells (RPCs) in the developing optic cup. RPCs have been shown to be inherently multipotent and competent to give rise to any class of retinal cell type (Turner et al., 1990; Holt et al., 1988; Turner and Cepko, 1987). Gradual changes in intrinsic and extrinsic determinants increasingly restrict lineage choices and shift the competence of RPCs to generate the different retina cell types (Swaroop et al., 2010).

During retinal development, RPCs proliferate extensively to generate a robust pool of multipotent progenitors for later differentiation. Several extrinsic factors previously involved in the earlier stages of eye development, including Notch, Shh, FGFs and epithelial growth factor (EGF), have been shown to participate in the maintenance of the RPC progenitor pool (Chen et al., 2012; Anchan et al., 1991; Jensen and Wallace, 1997; Levine et al., 1997; Lillien and Cepko, 1992; Lillien, 1995). Notably, high concentrations of Notch allow for the maintenance of cycling RPCs by regulating the expression of multiple intrinsic bHLH transcription factor genes – bHLH repressors such as *Hes1* and *Hes5* are upregulated, which act to repress proneural bHLH activators such as NeuroD1 and Mash1, thereby promoting proliferation and inhibiting neural differentiation (Hatakeyama and Kageyama, 2004; Le et al., 2006).

As development progresses, some RPCs exit the cell cycle and differentiate into different post-mitotic retinal cell subtypes. The different retinal subtypes are 'born' in a distinctive order that has been highly conserved across vertebrates: retinal ganglion cells, horizontal cells, cone photoreceptors, and amacrine cells of at least one class are born first; rod photoreceptors and the remaining amacrine cells are next to be born, followed by bipolar cells and finally Müller glial cells (Marquardt and Gruss, 2002; Marquardt, 2003)(Figure 1.11A). In the mouse, cone genesis begins as early as embryonic day (E) 12 and is complete by birth, whereas rod genesis begins at E14 and continues until P10, peaking at birth (Morrow et al., 1998; Young, 1985; Carter-Dawson and LaVail, 1979; Rapaport et al., 2004)(Figure 1.11B).

After exiting the cell cycle, these photoreceptor precursors can take up to two weeks after birth to mature, the process of which involves a substantial increase in opsin expression levels, extension of outer segments towards the RPE, and formation of synapses with horizontal and bipolar interneurons. S-opsin is first expressed in cones at E18 whereas M-opsin is expressed later in development at P6, while rhodopsin starts to be expressed in rods after birth at P2 (Swaroop et al., 2010).

Figure 1.11: A. The sequential birth of cell classes in the vertebrate retina. B. Photoreceptor genesis and maturation in mice. The relative numbers of cone and rod precursor cells that are born over time are shown. In mice, cones are generated prenatally as early as embryonic day (E) 12. Rods, which vastly outnumber cones, are generated both before and after birth, from around E14 to postnatal day (P) 10. Expression of S opsin begins at ~E18, that of M opsin at ~P6 and that of rhodopsin at ~P2. Opsin levels increase substantially until after weaning in mice. As photoreceptors mature, outer segments (OS) and synapses form. A. Adapted from (Cepko, 2014)**. B. Adapted from** (Swaroop et al., 2010)**.**

1.3.2 Photoreceptor development

It is well-established that following cell cycle exit, bHLH and homeobox-type transcription factors cooperate to specify the various neuronal cell types – homeodomain genes appear to determine layer specificity whereas bHLH activators determine neuronal fate within the specified layers (Cepko, 1999; Hatakeyama and Kageyama, 2004). In particular, early post-mitotic photoreceptor precursors co-express the homeobox genes cone-rod homeobox (Crx) and orthodenticle homeobox 2 (Otx2), along with the bHLH genes NeuroD and Mash1 (Hatakeyama and Kageyama, 2004) (Figure 1.12).

Otx2 plays an instructive role in specifying photoreceptor lineage by directly regulating the expression of the key transcription factor Crx and its target genes. Crx acts downstream of Otx2; it transactivates many photoreceptor-specific genes and is necessary for the terminal differentiation, maturation and maintenance of rods and cones (Furukawa et al., 1999; Nishida et al., 2003; Hennig et al., 2008).

Following commitment to a photoreceptor cell fate, additional transcription factors come into play to promote the generation of either rod or cone photoreceptors. Of key importance in specification of the rod fate is the transcription factor, neural retina leucine zipper (Nrl). Nrl is a basic motif-leucine zipper transcription factor of the Maf subfamily that is preferentially expressed in rod photoreceptor precursor cells shortly after terminal mitosis, and as such, it is regarded as one of the earliest rod-specific photoreceptor markers (Akimoto et al., 2006). Nrl interacts with multiple transcription factors in order to promote a rod lineage – for example, it acts synergistically with Crx to activate the Rhodopsin promoter. Nrl also directly activates the orphan nuclear receptor Nr2e3, which co-activates rod genes with Nrl and Crx, and concomitantly suppresses the expression of cone-specific genes, thereby irreversibly committing Nrl-expressing precursors to a rod fate (Oh et al., 2008). Other factors involved in rod development include neurogenic differentiation factor 1 (NeuroD1) and achaete-scute homologue 1 (Ascl1, or Mash1).

Figure 1.12: Cooperation of bHLH and homeodomain genes for retinal subtype specification. *Hes1* (together with *Hes5*) acts as an effector of Notch signalling to maintain RPC proliferation and inhibit neuronal differentiation. Differentiating neurons lose *Hes1* expression. It is likely that homeodomain factors regulate layer specificity while bHLH activators determine neuronal fate within the layers. Cells that retain *Hes1/Hes5* expression during neurogenesis adopt the final available cell fate, Müller glial cells. Of particular interest is the photoreceptor developmental pathway, demarcated in the black box. Adapted from (Hatakeyama and Kageyama, 2004).

While the specification of a cone lineage is less well-understood than that of a rod, several genes have been implicated in this process. The retinoid-related orphan receptor RORβ is a dual regulator in both rod and cone differentiation that appears to lie upstream of Nrl in the photoreceptor differentiation pathway. Like Crx, RORβ is essential for the formation of photoreceptor outer segments and synapses (Jia et al., 2009), and has been shown to act synergistically with Crx to initiate S-opsin transcription in cones (Srinivas et al., 2006). Separately, the nuclear thyroid hormone receptor β2 (Trβ2) responds to increasing levels of circulating thyroid hormone during development to direct the differentiation of M-opsin-expressing cone photoreceptors (Ng et al., 2001; Roberts et al., 2006; Ng et al., 2009). Other factors involved in M-opsin and S-opsin patterning include retinoid X receptor-γ (RXRγ)(Roberts et al., 2005).

Current molecular evidence pertaining to the abovementioned transcription factors appears to support a "transcriptional dominance" model of photoreceptor cell fate determination as proposed by Swaroop et al. (2010) (Figure 1.13). In this model, Otx2 biases a RPC to a photoreceptor precursor fate, which will then go on to differentiate into an S-cone by default, unless diverted otherwise to a rod or M-cone differentiation programme by intervening signals. Action by Nrl and its downstream target Nr2e3 will induce a rod state and suppress S-opsin and other cone genes, whereas in the absence of Nrl and Nr2e3 action, Trβ2 can induce M-opsin and suppress S-opsin expression.

Figure 1.13: "Transcription dominance" model of photoreceptor cell fate determination, as proposed by Swaroop et al. (2010). The model suggests that the S-cone pathway (red) is the default pathway, and that intervening action of other transcription factors, such as Nrl and Nr2e3 (green) or Trβ2 (blue), is necessary to drive the differentiation programme towards that of a rod or L/M-cone respectively. Adapted from (Swaroop et al., 2010)**.**

1.4 Retinal degeneration

Retinal degeneration is the leading cause of blindness in the developed world (Bunce et al., 2010). Causes of degeneration may be age-related, hereditary, and/or environmental. Hereditary conditions include retinitis pigmentosa (RP), Leber Congenital Amaurosis (LCA), Stargardt disease and Ushers disease, and these arise from mutations in over 200 different genes. As such, onset and rate of progression is highly variable across the different conditions. On the other hand, age-related macular degeneration (AMD) occurs predominantly in the elderly.

RP is probably the best characterised out of the retinal degenerative conditions, and is also the most common form of inherited retinal degeneration, with an incidence of 1 in 3000 worldwide (Shintani et al., 2009). RP encompasses a genetically and phenotypically heterogeneous group of conditions, with a wide range of causes that manifest in highly variable clinical presentations and progressions. To date, over 240 gene mutations have been associated with RP (Retinal Information Network), causing defects in a variety of cellular components involved in rod structure and function, in particular those involved in the biosynthesis and folding of rhodopsin, as well as failure of the underlying RPE. Most patients initially present with night blindness and loss of peripheral vision due to damage of rod photoreceptors. As the disease progresses, secondary cone death occurs, which results in deterioration of central vision, visual acuity, and colour vision (Hartong et al., 2006). Currently, there are no routinely available treatment options; management of the disease, for example with vitamin A supplementation, can at best slow down the disease progression (Berson, 2007). Clinical trials are currently under way to test the use of gene therapy to correct underlying genetic abnormalities and halt degeneration at early disease stages. Notably, recently published results of a Phase II clinical trial using rAAV2/2-mediated *RPE65* gene supplementation for the treatment of LCA demonstrated improved retinal sensitivity, albeit modestly and temporarily (Bainbridge et al., 2015).

AMD affects 10% of people over the age of 60 – a figure set to rise with population aging (Minassian et al., 2011; Owen et al., 2012). The pathogenesis of AMD has yet to be delineated; however, four key risk factors have been identified – age, genetics, high body mass index, and smoking (Evans, 2001). In particular, single nucleotide polymorphisms in genes encoding proteins of the innate immune system, such as complement factor H, B or C3, have been strongly linked with AMD

development (Haines et al., 2005; Klein et al., 2005). AMD is thought to be a result of chronic, low-grade inflammation in the macular region, which leads to degeneration of RPE and Bruch's membrane (Jager et al., 2008). There are two forms of AMD – 'dry' non-exudative AMD, which affects 90% of AMD patients (Curcio et al., 1996), and 'wet' exudative AMD, which is more severe but also treatable. In the dry form, gradual accumulation of extracellular deposits (drusen) between the RPE and Bruch's membrane leads to geographic atropy of the RPE, photoreceptors, and underlying choriocapillaris (Anderson et al., 2002; Tezel et al., 2004; Donoso et al., 2006; Shen et al., 2007). In the wet form, rapid and destructive choroidal neovascularisation breaks through Bruch's membrane and the RPE into the subretinal space, and occasionally, the retina. These vessels are often leaky, leading to the accumulation of blood below the macular, causing secondary photoreceptor damage especially in the cone-rich macular region and thereby a loss of central vision. Recent years have seen major advances in the treatment of wet AMD with anti-vascular epithelial growth factor (VEGF) agents such as ranibizumba (Lucentis) and bevacizumba (Avastin). However, there is a scarcity of treatment options for the more common dry AMD.

Despite the diverse aetiologies and phenotypic heterogeneity of retinal degenerative disorders like AMD and RP, these disorders culminate in a common final pathway – the loss of photoreceptors. As such, photoreceptor replacement by transplantation of new photoreceptors holds much potential as a broad treatment strategy for retinal degenerative disorders. Furthermore, despite degeneration of the overlying photoreceptor layer, much of the inner retina and visual circuits remain intact (Santos et al., 1997; Damiani et al., 2012; Mazzoni et al., 2008). This presents a window of opportunity for photoreceptor replacement therapy, in the expectation that transplanted photoreceptors, which are afferent neurons, need only to make short, single synaptic connections in order to reconstitute the existing retinal circuits, contribute to the retinotopic map, and restore visual function (MacLaren et al., 2006).

1.5 Photoreceptor replacement therapy

Efforts in photoreceptor replacement therapy have largely taken on one of two transplantation strategies: whole retinal sheet transplantation, or transplantation of dissociated cell suspensions. The former strategy would be particularly relevant in severe retinal degeneration where the endogenous photoreceptor layer may be largely absent; however, results to date show only limited connectivity between grafted sheets and the recipient visual circuitry (Seiler et al., 2008; Humayun et al., 2000; Radtke et al., 1999). A comprehensive discussion of retinal sheet transplantation can be found in reviews by Seiler and Aramant (2012) and Ghosh and Ehinger (2000).

Greater success has been achieved with the transplantation of dissociated cell suspensions. Effective photoreceptor replacement by this strategy requires the identification of an appropriate donor cell that has the ability to migrate from the site of transplantation, correctly integrate within the recipient retina with high efficiency, differentiate into mature photoreceptors, and ultimately form synapses with inner retinal neurons in order to restore visual function.

1.5.1 Defining the donor cell

Given that progenitor cells and immature neurons demonstrate an intrinsic ability to migrate and differentiate during development, several early studies examined the potential of brain- and retina-derived neural stem/progenitor cells as donor cells for transplantation (Sakaguchi et al., 2004; Young et al., 2000; Chacko et al., 2000; Van Hoffelen et al., 2003; Klassen et al., 2007; Mellough et al., 2007; Yang et al., 2002). However, these appear to lack the ability to migrate and integrate correctly within the adult host retina (Young et al., 2000; Sakaguchi et al., 2005). Moreover, they neither differentiate into mature photoreceptors, nor form functional synapses with recipient inner retinal neurons (Young et al., 2000; Sam et al., 2006). It was suggested that this was because the non-neurogenic, adult recipient retina is unable to provide the developmental cues required for a stem/progenitor cell to differentiate into a mature photoreceptor.

Later studies, however, provided strong evidence to show that transplantation success depends more on the developmental stage of the donor cell, than on that of the recipient. A key proof-of-concept study by MacLaren and Pearson et al. using a transgenic mouse model, in which GFP reporter expression is driven by the Nrl promoter (Akimoto et al., 2006), demonstrated that the transplantation of post-mitotic Nrl-expressing donor-derived rod precursors leads to significantly higher numbers of GFP^+ cells present in the ONL of the recipient retinas (MacLaren et al., 2006). These findings define the optimal developmental stage of donor cells for successful rod photoreceptor transplantation. To date, studies by other groups have similarly shown that successful transplantation can indeed be achieved using immature post-mitotic rod precursor cells, but not progenitor cells or photoreceptors at later stages of development (MacLaren et al., 2006; Pearson et al., 2012; Lakowski et al., 2010, 2011; Bartsch et al., 2008; Eberle et al., 2011; Gonzalez-Cordero et al., 2013; Decembrini et al., 2014; Gust and Reh, 2011). Moreover, the reporter-labelled donor cells in the host ONL exhibit specialised morphological features of mature rod photoreceptors, such as synapses with inner retinal neurons and outer segments (Pearson et al., 2012; Barber et al., 2013; Eberle et al., 2012; Singh et al., 2013).

1.5.2 Immunological response to transplanted cells

In addition to the transplanted donor cells being intrinsically at the optimal developmental stage, their interactions with the recipient retinal microenvironment are likely to be another crucial aspect in influencing their successful migration and integration. In particular, immune rejection of transplanted allogeneic tissue grafts is often a major complication in transplantation. However, the eye is often described as enjoying a unique immune privilege, particularly in the anterior chamber, corneal stroma, vitreous cavity, and subretinal space. Of particular relevance to photoreceptor precursor transplantation is the extent to which the subretinal space is an immune-privileged site, since immune privilege is likely to aid transplantation outcome by inhibiting immune rejection. In the healthy retina, the RPE and retina microvasculature act as an outer and inner blood-retina barrier respectively, physically preventing the systemic immune system from interacting with the subretinal space (Kaestel et al., 2005; Zamiri et al., 2005). Moreover, a number of studies have observed an anterior chamber-associated immune deviation (ACAID)-like induction of immune tolerance to alloantigens introduced in the subretinal space,

albeit to a lesser extent (Wenkel and Streilein, 1998; Jiang et al., 1993; Wenkel et al., 1999). There, alloantigens captured by antigen-presenting cells (APCs) induce the generation of antigen-specific regulatory T cells in the spleen, resulting in an active downregulation of conventional systemic cell-mediated immune responses (Medawar, 1948; Niederkorn, Streilein, et al., 1981; Niederkorn, Shadduck, et al., 1981; Streilein et al., 1980; Stein-Streilein and Streilein, 2002; Wilbanks and Streilein, 1990; Streilein and Niederkorn, 1985). Furthermore, under normal physiological conditions, the subretinal space possesses an immunosuppressive microenvironment, in which antigen-driven T cell activation is actively suppressed by means such as the constitutive secretion of cytokines (e.g. TGF-β) from RPE cells and direct contact inhibition from Muller glia (Jiang et al., 1993; Katamay and Nussenblatt, 2013).

Nevertheless, there are several lines of evidence indicating that this immune privilege is neither extended uniformly to all antigens, nor necessarily permanent. Allogeneic retinal allografts placed in different immune-privileged sites in the eye were observed to deteriorate more rapidly compared to syngeneic counterparts, whereas in mice lacking an immune system, retinal allografts survived for a duration that was comparable to their syngeneic counterparts (Streilein, 1999; 1999; Jiang et al., 1995). Moreover, it is reasonable to speculate that immune privilege can be abolished by pathological processes in which RPE cell viability is compromised or resident retinal macrophages are activated by photoreceptor death (for example, in AMD), or by mechanical trauma during the surgical procedures itself (Wenkel and Streilein, 1998). Indeed, in a proportion of transplants, our group has observed increased macrophage recruitment to the site of transplantation as well as autofluorescent cell debris within the subretinal space, suggesting an acute innate inflammatory response against transplanted cells by 1 month post-transplantation. This is always associated with significantly fewer integrated photoreceptors (West et al., 2010; Goh, unpublished observations).

Apart from an innate immune response against transplanted allogeneic retinal tissue, work by our group and others have shown evidence of donor-specific delayed hypersensitivity, as early as 5 weeks and as late as 4 months post-transplantation (Jiang et al., 1993; Streilein et al., 2002; Jiang et al., 1995; West et al., 2010). West et al. (2010) observed that $CD4^+$ and $CD8a^+$ T cells were not only present in the neural retina and subretinal space near surviving transplanted photoreceptors, but also,

more extensively, in the choroid around the transplantation site, indicating specific alloantigen-induced T-cell recruitment to the site of transplantation. Transplanted cells were also rejected more rapidly in recipients which had been "primed" by an initial transplantation, suggesting that the immune response was antigen-specific.

Taken together, the reported immune responses mounted against transplanted donor cells are a concern for the efficiency and durability of stem cell transplantation strategies, and is therefore an area that warrants further investigation.

1.5.3 Restoration of visual function

Earlier work indicates that the likelihood of a positive functional response to visual stimulation is positively correlated to the number of reporter-labelled donor cells present in the host ONL following transplantation (Pearson et al., 2012; Barber et al., 2013; MacLaren et al., 2006; Lamba et al., 2009), whereas the presence of a large mass of donor cells in the subretinal space is detrimental (West et al., 2010). A major challenge for the cell suspension approach to photoreceptor replacement is therefore to generate sufficient numbers of optimally-staged donor cells and to achieve a large number of reporter-labelled donor cells present in the host ONL post-transplantation.

In 2012, Pearson et al. provided the first definitive proof of functional rescue following the transplantation of Nrl.GFP donor-derived rod precursor transplantation in a mouse model of congenital stationary night blindness, the *Gnat1*$^{-/-}$ mouse at 3 weeks post-transplantation. Immunohistochemically, these GFP-labelled cells in the host ONL displayed evidence of forming classic triad synapses with second-order bipolar and horizontal cells in the recipient retina. Suction electrode recordings revealed that the GFP-labelled cells present in the host ONL were light sensitive, and displayed dim-flash kinetics similar to that of wild type rods. Moreover, *Gnat1*$^{-/-}$ animals receiving Nrl.GFP^{+} rod precursor transplants demonstrated robust responses to scotopic stimuli in the visual cortex, optokinetic head-tracking abilities, as well as improved visually-guided task-solving behaviour in response to scotopic stimuli (Pearson et al., 2012), These responses and behaviours were absent in uninjected and sham-injected animals. However, the numbers of reporter-labelled cells present in the host ONL achieved in the study were insufficient to drive a robust electroretinogram (ERG) response in the recipient retinae. By using gene replacement

in the same *Gnat1*$^{-/-}$ model, Pearson et al. demonstrated that approximately 150,000 reporter-labelled cells present in the host ONL are required to generate a reproducible scotopic ERG response (Pearson et al., 2012).

Nonetheless, while the numbers of reporter-labelled cells present in the ONL following transplantation may be too few to mediate a sufficiently large response for ERG detection, studies have demonstrated restoration of other aspects of visual function, even in models of end-stage retinal degeneration. Notably, Singh et al. (2013) investigated the transplantation of Nrl.GFP donor-derived rod precursors into an *rd1* mouse model of severe human retinitis pigmentosa, which, in contrast to the *Gnat1*$^{-/-}$ model, undergoes complete rod degeneration and significant ONL loss by 3 weeks of age. At 2 weeks post-transplantation, the transplanted cells appeared to mediate functional improvements in pupillary light responses and light avoidance behaviour, as well as changes in cerebral visual cortical blood flow in animals with no previous baseline rod function (Singh et al., 2013).

Moreover, in parallel to ongoing work on rod precursor transplantation, the transplantation of cone-like photoreceptor precursors has also seen promising results with regards to the restoration of visual function. Santos-Ferreira et al. (2014) showed the detection of responses to photopic stimuli in cone-depleted retinas of cone photoreceptor function loss 1 (Cpfl1) mice by multi-electrode array recordings, although these could not be detected by ERG (Santos-Ferreira et al., 2014).

Taken together, there is an increasing body of evidence demonstrating the potential for restoration of visual function in the diseased retina following the transplantation of immature photoreceptor precursors. Both adult and degenerate retinal environments appear capable of incorporating and maintaining these transplanted rod precursors, albeit to varying extents depending on disease phenotype (West et al., 2010; MacLaren et al., 2006; Barber et al., 2013; Pearson et al., 2010). It is of particular clinical interest to investigate the extent to which transplanted immature photoreceptor precursors can restore visual function in advanced retinal degenerative disease phenotypes, a good example of which is the *Aipl1*$^{-/-}$ mouse model (see Section 5.1). The lack of production of the photoreceptor-specific aryl hydrocarbon receptor-interacting protein-like 1 (Aipl1) protein leads to rapid death of both rod and cone photoreceptors by 4 weeks of age (Ramamurthy et

al., 2004; Dyer et al., 2004), which is likely to reflect the clinical picture in patients with end-stage retinal degeneration.

1.6 Directed differentiation of pluripotent stem cells to generate transplantation-competent donor cells

The findings discussed above provide strong support for photoreceptor replacement therapy as a feasible strategy, provided the donor cell is at the optimal developmental stage at the time of transplantation – specifically, a post-mitotic photoreceptor precursor cell. However, the equivalent stage of development in humans occurs early in the second trimester. This presents not only an obvious ethical but also a practical problem, as donor cell material from developing embryos will be in very limited supply and of variable quality.

An expandable, renewable source of cells that could be cultured *in vitro* to the correct developmental stage for transplantation may, therefore, represent a more appropriate and reproducible source of photoreceptor precursor cells. To this end, pluripotent embryonic stem cells (ESCs), which have the potential to be differentiated into nearly all cell types, represent a potential alternative cell source. Given the wealth of knowledge to date regarding the intrinsic and extrinsic mechanisms driving retinal development, much progress has been made in the last decade in the *in vitro* differentiation of ESCs towards photoreceptor lineages (Figure 1.14).

Figure 1.14: A. Summary of the main signalling factors required for normal eye development, from neural progenitors to retinal progenitors and finally photoreceptor precursors. B. Representation of the signalling factors used in some of the key ESC/iPSC differentiation protocols published to date. Adapted from (Jayakody et al., 2015).

ESCs are derived from the inner cell mass of the pre-implantation blastocyst, and can either be maintained in an undifferentiated state, or directed to differentiate toward various lineages deriving from all 3 germ layers. Several studies have reported successful generation of photoreceptors *in vitro* from mouse, monkey and human ESCs, using a variety of sequential differentiation protocols mimicking stepwise eye development *in vivo* (Lamba et al., 2009; Osakada et al., 2009).

Building on the ground-breaking work by Watanabe et al. demonstrating telencephalic differentiation from mouse ESCs (Watanabe et al., 2005), Ikeda et al. used antagonists of the nodal (LeftyA) and Wnt/β-catenin (Dkk-1) pathways in a serum-free floating culture of EB aggregates (SFEB) system, with later addition of activin-A and 5% serum, to derive $Rx^+/Pax6^+$ neural retinal progenitor cells (Ikeda et al., 2005). Inhibition of Notch signalling by addition of the γ-secretase inhibitor, DAPT, at the early RPC stage was able to steer mitotic RPCs to differentiate into post-mitotic $rhodopsin^+/recoverin^+$ photoreceptor precursors. The efficiency of photoreceptor differentiation was further improved with the addition of a combination of factors known to be involved in rod genesis, namely acidic FGF, basic FGF, taurine, Shh and retinoic acid (RA) (Osakada et al., 2008).

In a similar study using human ES cells, Lamba et al. used an antagonist of BMP signalling (Noggin) – the other branch of the TGFβ signalling pathway known to inhibit neural development besides Nodal – in combination with Dkk-1 and IGF-1, another known neural induction factor. Under these conditions, ~80% of the hESCs differentiated into $Pax6^+/Chx10^+$ retinal progenitors, and ~12% of which developed into Crx^+ photoreceptor precursors (Lamba et al., 2006). Meyer et al. was also able to demonstrate the efficient generation of Rx^+ neural rosettes that gave rise to neurospheres highly enriched for $Chx10^+$ retinal progenitors, using a culture system that relied on endogenous secretion of Dkk-1 and Noggin by ESCs instead of introducing exogenous inductive agents. By day 80 of culture, approximately 15% of all neurospheres contained Crx^+ photoreceptor precursors, of which almost 53% of these expressed Recoverin (Meyer et al., 2009).

Together, these studies demonstrated the possibility of directing ESCs to differentiate towards a retinal fate.

Encouragingly, a landmark study by Gonzalez-Cordero et al. was able to demonstrate that stage-specific reporter-labelled photoreceptor precursor cells derived from mouse ESCs cultured in a 3D system may be transplanted into both wild type and degenerating retinas, leading to the presence of reporter-labelled cells in the host ONL, which exhibit characteristics of mature photoreceptors (Gonzalez-Cordero et al., 2013). The authors adapted a novel 3D culture system first established by Eiraku et al. to scale up the production of photoreceptors. Unlike many of the 2D methods described above, this 3D system enables the spontaneous formation of optic cup-like structures from ES cells in a manner closely mimicking morphological retinal development *in vivo*, in the absence of any neighbouring tissues such as surface ectoderm or lens. These optic cup-like structures also contained all major retinal cell types, which were spatially arranged in the correct apical-basal order, closely resembling that of the early neonatal eye (Eiraku et al., 2011).

In close agreement with Gonzalez-Cordero et al., two other groups have recently reported successful transplantation of developmental stage-specific photoreceptor precursors using the 3D culture system, and observed similar numbers of reporter labelled-cells in the host ONL post-transplantation (Decembrini et al., 2014; Lakowski et al., 2015). Decembrini et al. utilised a mouse ES cell line obtained from a Crx.GFP mouse to generate Crx.GFP-positive photoreceptor precursor cells; whereas Lakowski et al. isolated an enriched population of mouse ES cell-derived post-mitotic rod precursors using a cell surface biomarker panel of 5 markers (CD73, CD133, CD24, CD47, and CD15). However, the number of reporter-labelled donor cells in the host ONL post-transplantation in these three studies still significantly fall short of that achieved with the donor-derived photoreceptor precursors, with a range of averages from 276 to 799 reporter-labelled donor cells per retina in eyes injected with mESC-derived photoreceptor precursors (Gonzalez-Cordero et al., 2013; Decembrini et al., 2014; Lakowski et al., 2015), compared to an average of 18,300 reporter-labelled donor cells per retina in eyes injected with donor-derived photoreceptor precursors. Further optimisation is therefore required to increase the number of reporter labelled-cells in the host ONL post-transplantation, in order to assess whether ESC-derived photoreceptor precursor cells are capable of restoring visual function following transplantation to the degenerate retina.

Research Aims and Objectives

Our group and others have shown that subretinal transplantation of optimally-staged post-mitotic photoreceptor precursors labelled with a GFP reporter into various murine models of retinal degeneration results in the presence of GFP-positive (GFP^+) cells with rod-like morphology within the outer nuclear layer (ONL) of the host retina. These GFP^+ cells not only demonstrate robust expression of photoreceptor proteins that are genetically absent in the host photoreceptors, but also display other morphological characteristics of mature photoreceptors (Pearson et al., 2012; Barber et al., 2013; Eberle et al., 2012; Singh et al., 2013). Importantly, these GFP^+ cells respond to light stimuli in a manner similar to wild-type rods, as seen from single cell (Pearson et al., 2012) and whole retinal recordings (MacLaren et al., 2006; Santos-Ferreira et al., 2014; Lamba et al., 2009); and an increased number of GFP^+ cells present in the host ONL following transplantation is positively correlated to a greater extent of functional vision restoration (Pearson et al., 2012; Barber et al., 2013).

In 2013, Gonzalez-Cordero et al. demonstrated for the first time proof of concept that rod photoreceptor precursor cells can be reproducibly differentiated from mouse embryonic stem cells (mESCs) in a modified three-dimensional (3D) culture system (Eiraku et al., 2011), and subsequently isolated for transplantation via GFP expression driven by the rod-specific Rhodopsin gene promoter (Gonzalez-Cordero et al., 2013). GFP^+ cells were similarly present in the host ONL following transplantation, and showed robust expression of both proteins absent from host photoreceptors as well as other markers characteristic of mature rod photoreceptors. However, the observed number of GFP^+ cells present in the host ONL following transplantation of mouse ESC-derived photoreceptor precursors was consistently lower than that seen with transplanted postnatal retina donor-derived photoreceptor precursors.

The aims of this project are, therefore, (1) to optimise the transplantation of mouse ESC-derived rod photoreceptor precursors, in order to increase the number of reporter-labelled donor cells present in the host ONL post-transplantation, (2) to develop an endogenous photoreceptor reporter ESC line in order to define the optimal developmental window for transplantation, and thereafter, (3) to assess the extent to which visual function is restored in various mouse models of retinal disease following the transplantation of reporter-labelled mouse ESC-derived photoreceptor precursors.

Chapter 2 : Methods

2.1 Mouse ESC retinal differentiation culture

A mouse EK.CCE ESC line (129/SvEv; a kind gift of Prof. E. Robertson) as well as a mouse Crx.GFP ESC line (a kind gift of Prof. Y. Arsenijevic, (Decembrini et al., 2014)) were maintained as previously described in GMEM containing 10% Knockout Serum Replacement (KSR), 1% Fetal Bovine Serum (FBS), 0.1mM NEAA, 1mM pyruvate, 0.1mM 2-mercaptoethanol with 2000U/ml LIF, 0.5μM MEK inhibitor (PD0325901) and 1.5μM GSK3 inhibitor (CHR99021) (Gonzalez-Cordero et al., 2013).

For 3D embryoid body (EB) retinal differentiation, on day 0 of culture, ESCs were resuspended in differentiation medium (GMEM containing 1.5% KSR, 0.1mM NEAA, 1mM pyruvate, 0.1mM 2-mercaptoethanol) at $3x10^4$ cells/mL, plated into low-binding 96-well (Nuclon Sphera) plates at a density of $3x10^3$ cells/well, and incubated at 37°C with 5% CO_2. Growth factor-reduced Matrigel (BD Biosciences) was added to cell aggregates on day 1 of culture to a final concentration of 2% (v/v). On day 9 of culture, whole EBs were transferred to low-binding 24-well plates at a density of 6 EBs/cm^2, and cultured in retinal maturation medium (RMM; DMEM/F12 Glutamax containing N2 supplement and Pen/Strep) at 37°C, 5% CO_2. The media was changed every 2–3 days, with the addition of 1mM taurine (Sigma) and 500nM retinoic acid (Sigma) from day 14 of culture onward.

Figure 2.1: Schematic showing early and late mouse ESC retinal differentiation in 3D culture, followed by viral-labelling of rod photoreceptor precursors, and then the transplantation of rod precursors. Adapted from (Gonzalez-Cordero et al., 2013).

2.2 Production of recombinant AAV2/9 and shH10 Rhop.GFP viruses

A pD10/Rhodopsin promoter-GFP construct was used to generate AAV2/9 and ShH10 Rhop.GFP viruses. Recombinant AAV2/2 serotype particles were produced through a previously described tripartite transfection method (Gao et al., 2002) into HEK293T cells, followed by purification using ion exchange chromatography (Davidoff et al., 2004). Viral genome titres were determined by quantitative real-time PCR using a probe-based assay binding the SV40 poly-adenylation signal. Amplicon-based standard series of known amounts were used for sample interpolation. Final titres were expressed as vg/mL.

SV40 Forward primer: 5'-Agcaatagcatcacaaatttcacaa-3'.
SV40 Reverse primer: 5'-AGATACATTGATGAGTTTGGACAAAC-3'.
SV40 Probe: FAM-5'-AGCATTTTTTTCACTGCATTCTAGTTGTGGTTTGTC-3'-TAMRA.

EBs were infected at day 22 of culture with $1.2x10^{11}$ viral particles per EB in 250uL of RMM/well. Each well contained 12 whole EBs, which is approximately $1.5x\ 10^{6}$ cells. Media was topped up after overnight incubation at $37^{o}C$.

2.3 Preparation of mESC-derived embryoid bodies for cell sorting

EBs were dissociated using a papain-based Neurosphere Dissociation Kit (Miltenyi Biotec, 130-095-943). Reagents were made up according to manufacturer's instructions. Briefly, EBs were dissociated by gentle trituration in a papain-based enzyme mix at 37°C for 15 min, and then centrifuged at 900rpm for 7min. Cell pellets were resuspended at 2-3 x 10^7 cells/mL in FACS buffer (66% MEM-E HEPES, 33% HBSS ($+Mg^{2+}$, $-Ca^{2+}$), 1% FBS, Dnase I (10 µL/mL)) and passed through a 35-µm mesh cell strainer (BD Falcon, UK; cat no 352235) before undergoing cell sorting. Fluorescence activated cell sorting (FACS) was performed on a BD Influx Cell Sorter fitted with a 200mW 488nm blue laser to excite GFP, and sorted with a 70 micron nozzle at 50 psi. GFP was collected using the 488-530/40nm detector. FAC-sorted mESC-derived GFP^+ cells were on average >95% pure GFP-positive, and >80% viable. These were collected in 20% FBS in RMM, then subsequently centrifuged and resuspended at a final concentration of 200,000 cells/µL in sterile HBSS ($+Ca^{2+}$, $+Mg^{2+}$) and Dnase I (0.05%) before injection.

For magnetic activated cell sorting (MACS), EBs derived from a transgenic mESC line (CBA.YFP R1/E ESC, ATCC-R) with a YFP reporter cassette driven by the ubiquitously active β-actin promoter were dissociated as above, and then centrifuged at 900rpm for 7min. Cell pellets were resuspended at 2-3 x 10^7 cells/mL in 100µL of MACS buffer (PBS [without Mg and Ca, pH 7.2], 0.5% BSA, 2 mM EDTA). A conjugated antibody against mouse CD73 (APC-conjugated rat IgG1, clone TY/11.8, Miltenyi Biotec, 130-102-586) was added to samples at a 1:50 dilution and incubated for 30 minutes at 4°C in the dark. Cells were then washed with MACS buffer, and centrifuged at 900rpm for 7min. The cell pellet was resuspended in 100µL of anti-APC magnetic beads (80µL MACS buffer and 20µL MicroBeads; Miltenyi Biotec, 130-090-855), and incubated for 20 minutes at 4°C in the dark, followed by washing with MACS buffer and centrifugation. Cell pellets were resuspended in 500µL of MACS buffer prior to magnetic separation. MACS was performed on an AutoMACS Pro Separator (Miltenyi Biotec), and sorted using a positive-selection, double-column program in sensitive mode (denoted as 'Posselds' on the AutoMACS). The eluted MAC-sorted mESC-derived $CD73^+$ cells were subsequently centrifuged and resuspended at a final concentration of 200,000 cells/µL in sterile HBSS (+Ca, +Mg) and Dnase I (3%) before injection.

2.4 Animals

Gnat1$^{-/-}$ (kind gift of J. Lem, Tufts University School of Medicine), triple-knockout *Opn4*$^{-/-}$*Gnat1*$^{-/-}$*Cnga3*−/− (OGC) (kind gift of A. Vugler, University College London), *Aipl1*$^{-/-}$ and C57b6 mice were maintained in the University College London animal facilities on a standard 12h light-dark cycle. Mice received food and water ad lib and were provided with fresh bedding and nesting daily. All recipient animals received transplanted cells at 8–12 weeks of age, keeping with the optimal recipient age as determined by donor-derived precursor cell transplantation (Barber et al., 2013), unless otherwise stated. Experiments were conducted in accordance with the Policies on the Use of Animals and Humans in Neuroscience Research, revised and approved by the ARVO statement for the Use of Animals in Ophthalmic and Vision Research.

2.5 Transplantation of donor cells

Recipient mice were anesthetized with an intraperitoneal injection of 0.2mL of a mixture of Dormitor (1 mg/mL medetomidine hydrochloride; Pfizer Pharmaceuticals), ketamine (100 mg/mL; Fort Dodge Animal Health), and sterile water in the ratio 5:3:42. Recipient eyes were dilated using 1% tropicamide (Bausch & Lomb) and kept moist with Viscotears (Novartis Pharmaceuticals UK Ltd). A glass coverslip placed over the eye and surgery was performed under direct visual control using an operating microscope (Carl Zeiss) as described previously (Pearson et al., 2012). A trans-sclera needle stick puncture was performed prior to subretinal injection at the level of the anterior chamber, using a sterile 8mm 34-gauge hypodermic needle (Hamilton), to relieve pressure in the orbit. 1µl of cell suspension was delivered, using the same needle, as a single injection into the subretinal space in the superior ocular quadrant, unless otherwise stated. The needle was left in place for approximately 20s to allow for re-equilibration of intraocular pressure before slowly withdrawing, leading to self-sealing of the wound tunnel. Careful surgical notes were taken for later reference. Procedured mice were reversed using Antisedan (atipamezole hydrochloride 0.10 mg/ml, Pfizer Pharmaceuticals, Kent UK), and the eyes protected with Viscotears. Mice were placed on heat mats and received softened food until fully recovered.

2.6 Histology and immunohistochemistry

Mice were sacrificed by cervical dislocation 3 weeks after transplantation, unless otherwise stated. Eyes were dissected to remove the cornea, iris, and lens. All samples (EBs and dissected eye cups) were fixed for 1h in 4% paraformaldehyde (PFA), followed by cryoprotection in 20% sucrose (1h at room temperature or overnight at 4^{o}C) and embedding in OCT (TissueTek). Embedded samples were frozen in isopentane pre-cooled in liquid nitrogen. Frozen samples were cryosectioned at 18μm thickness, and all sections were collected for analysis.

For immunohistochemistry, sections were blocked for 2h at room temperature with 5% goat serum and 1% bovine serum albumin (BSA) in PBS with 1% Triton X-100, followed by incubation with primary antibody (Table 2.1) at 4 °C overnight. Subsequently, sections were washed 3 times with PBS for (5 min per wash), incubated with secondary antibody for 2h at room temperature, washed another 3 times with PBS (5 min per wash), then counterstained with DAPI (1:1000, Sigma-Aldrich). The appropriate Alexa-Fluor 488 and 546 secondary antibodies (Invitrogen-Molecular Probes) were used at a 1:500 dilution. For eyes transplanted with Crx.GFP^{+} cells, an Alexa-Fluor 488 anti-GFP rabbit antibody was used at a 1:500 dilution during secondary antibody staining.

Antigen	Host species	Dilution	Supplier
Caspase 3	rabbit	1 in 20	Abcam (Ab2302)
Cone arrestin	rabbit	1 in 250	Millipore (AB15282)
GFP	rabbit	1 in 300	Life Technologies (A-21311)
GFP	goat	1 in 300	(FITC-conjugate) Abcam (ab6662)
Ki67	rabbit	1 in 100	Abcam (Ab15580)
Lamin B	mouse	1 in 200	Abcam (Ab8980)
PKCα	rabbit	1 in 25	Santa cruz (sc10800)
Recoverin	rabbit	1 in 500	Chemicon (AB5585)
Rhodopsin	mouse	1 in 2000	Sigma (O4886)
Ribeye (CtBP2)	mouse	1 in 100	BD Biosciences (612044)
Rod α-transducin (Gnat1)	rabbit	1 in 1000	Santa Cruz (sc389)
S-opsin	rabbit	1 in 300	Millipore (AB5407)
Synaptophysin	mouse	1 in 1000	Sigma-Aldrich (S5768)

Table 2.1: Primary antibodies for immunohistochemical staining

2.7 Cell counts and exclusion criteria

Blinded counts of GFP^+ cells present in the host ONL were taken using a fluorescence microscope (ObserverZ.1, Zeiss). The average number of GFP+ cells per eye was determined by counting all GFP+ cells in alternate serial sections through each eye and doubling the count. GFP+ cells were only counted if the whole cell body was correctly located within the outer nuclear layer, and at least one of the following was visible: spherule synapse, inner/outer processes, or inner/outer segments.

Eyes were omitted from further quantitative analysis if (1) there was clear evidence of an injection having been administered intravitreally, (2) if there was evident reflux of the cell suspension at the time of injection, or (3) if eyes demonstrated evidence of macrophage infiltration, which can be identified under light microscopy as large, autofluorescent cells, accompanied by autofluorescent cell debris.

2.8 Image acquisition

Images were taken on a Leica DM5500Q confocal microscope. Unless otherwise stated, images show merged maximum projection images of an xyz stack through 18-µm thick xy sections. Individual xy images were acquired using a frame average of 2, at 1024 x 1024 resolution, and at 1.6-1.8µm intervals throughout the depth of the stack. The same laser intensity, gain and offset settings were kept constant between samples within the same experiment. LAS AF image software was used for image processing.

2.9 Assessment of cell viability of mouse ESC-derived photoreceptor precursors

2.9.1 Staining of cell suspension for flow cytometry

For flow cytometric analysis, EBs were dissociated using the papain-based Neurosphere Dissociation Kit (Miltenyi Biotec) as detailed above (see Section 2.3). Cells were counted and resuspended in 1% Bovine Serum Albumin (in PBS) to a concentration of $1x10^6$ cells/mL, and staining was performed on 100µL aliquots.

For surface marker analysis, CD73 clone TY/11.8 APC (30 µg/mL; Miltenyi Biotec., UK; 130-102-586) was added at a 1:75 dilution and incubated for 30 minutes at 4°C in the dark. Cells were washed once in 1X Binding Buffer (10X stock diluted in distilled water, eBioscience Ltd., UK; 00-0055). For subsequent viability analysis, Annexin V-eFluor 450 (eBioscience, 88-8006) was added to samples at a 1:20 dilution (in 1X Binding Buffer) and incubated for 15 minutes at room temperature. Cells were washed once in 1X Binding Buffer and resuspended in PBS. DRAQ7 (Biostatus, DR71000) dead cell stain was then added to the samples at a final concentration of 0.3µM for 5 minutes at room temperature before sample acquisition.

2.9.2 Flow cytometric data acquisition and analysis

Compensation was performed using single colour controls prepared from OneComp eBeads (eBioscience Ltd., UK; 01-1111) for cell surface staining. All of the samples were acquired using a BD Fortessa X-20 flow cytometer (BD Biosciences, Oxford, UK), equipped with 355nm, 405nm, 488nnm, 561nm and 640nm excitation lasers. All acquired flow cytometric data was analysed using FlowJo software (10.0.7; FlowJo LLC; USA. Background fluorescence was measured using unstained cells; single-stained and fluorescence minus one controls were used to set gating parameters to distinguish between positive- and negative-staining populations.

2.10 Assessment of recipient immune response to mouse ESC-derived photoreceptors

2.10.1 Preparation of cell suspension

Eyes were dissected individually in 50μL of ice-cold PBS on a Petri dish. Surrounding extraocular tissue was trimmed away, a puncture was made with a 30G needle at the corneal limbus, and curved Vanna scissors were used to extend the incision around the circumference of the limbus. The cornea and iris were removed with forceps, following which, the iris was disposed of and the cornea was inverted to wash out contents of the anterior chamber into the PBS. The lens and lens capsule were extracted anteriorly, and discarded along with the cornea. The vitreous and retina were gently eased from the residual sclera-RPE-choroid complex, and washed in the 50μL of PBS containing the aqueous humour, while the sclera-RPE-choroid complex was tapped sharply on the dish to release any cells before being discarded. The dish was washed with a further 50μL of ice-cold PBS, and the pooled volume of PBS, along with the retina, was transferred to a 1.5 mL Eppendorf tube.

The contents of each tube underwent papain-based enzymatic digestion with the Neurosphere Dissociation Kit (Miltenyi Biotec, 130-095-943), as described in Section 3. The digested material was homogenised by gentle trituration with a pipette, before being filtered through a 70-μm cell strainer and washed with PBS. This was centrifuged at 300g for 5 min, the supernatant discarded, and the remaining cell pellet resuspended in 150μL of PBS for staining.

Splenic tissue samples were prepared by homogenising each spleen with the back of a syringe plunger against a 70-μm cell strainer over a 50 mL Falcon tube containing 5 mL of ice-cold PBS, and washing the filter with another 45 mL of ice-cold PBS. Samples were centrifuged (300 g for 5 min) and cell pellets underwent red blood cell lysis by the addition of 1mL of ACK lysing buffer (Invitrogen; ThermoFisher Scientific, UK, A1049201) for 30s. The lysis reaction was terminated by adding 50 mL of PBS to the sample, following which the sample was filtered with a 70-μm cell strainer and centrifuged (300 g for 5 min). The resultant cell pellet was resuspended in 5 mL of ice-cold PBS and kept at 4^{o}C.

2.10.2 Surface marker staining for flow cytometry

Cell suspensions were blocked with rat anti-mouse CD16/32 clone 93 Fc block (0.5mg/mL; eBioscience Ltd., UK, 14-0161) for 10 min at 4^{o}C. Surface marker staining was performed in the dark for 30 min at 4^{o}C in PBS, using the following antibodies against cell surface proteins: CD4 clone GK1.5 PE (2 ng/uL; BioLegend Ltd., UK; 1000407); CD8a 53-6.7 BV650 (0.2 mg/uL; BioLegend Ltd., UK); CD11b clone M1/70 BV711 (0.5 mg/ml; Biolegend Ltd., UK; 101242); CD45 clone 30-F11 BUV395 (0.2 mg/mL; BD Biosciences, UK; 564279). All antibodies were used at a 1:100 dilution. SYTOX Blue (2.5 mM/mL; Life Technologies; ThermoFisher Scientific, UK; S11348) was used for live-dead discrimination after surface staining. Data acquisition was performed as described in Section 2.9.2.

2.11 Immune suppression

In some experiments, recipient animals were immune-suppressed with cyclosporine A (CyA; Rigcharm Pharmacy, UK). The dosing regimen used was in accordance to that recommended by Jensen et. al. (2012) for human ES cell-derived neural progenitor transplantation into rats; briefly, mice were given subcutaneous injections of 10 mg/kg/day CyA for 10 days, starting 2 days prior to subretinal transplantations, followed by 50mg/kg/day in the drinking water until culling (B. Jensen, 2012).

2.12 Cell cycle analysis

5-ethynyl-2'-deoxyuridine (EdU, from Click-iT EdU Alexa Fluor 594 Imaging Kit, Invitrogen, C10339) was dissolved in DMSO to give a 10mM stock solution, according to manufacturer's instructions. For birthdating analysis, EBs were incubated on different days in culture with 0.5μM EdU for 8h and collected on day 26. For the proliferation assay, EBs were pulsed with EdU as for birthdating analysis, but collected immediately after the pulse.

For immunohistochemistry, EBs were collected and fixed in 4% PFA prior to embedding, freezing, and cryosectioning as described earlier. Slides were prepared as above (see section 2.6), and an Alexa-Fluor 488 anti-GFP secondary antibody was used prior to the Click-it EdU detection reaction to retain GFP signal. For the Click-iT reaction, slides were incubated with 200μL of Click-iT reaction cocktail per slide (86μL of 1x Click-iT® reaction buffer, 4μL of $CuSO_4$, 0.25μL of Alexa Fluor-594 picolyl azide, and 10μL 1x reaction buffer additive) for 30 mins at room temperature in the dark, before proceeding with PBS washes and DAPI staining.

For flow cytometric analysis, EBs were dissociated as described above (see Section 2.3), washed with PBS, and resuspended in 100μL per sample of Zombie Violet Fixable Viability dye (BioLegend, 423113) at 1:500 dilution, for 30 minutes at 4°C in the dark. Samples were then washed with PBS, pelleted, and fixed in 100μL per sample of fixative (4% PFA), for 15 minutes at room temperature in the dark. Following fixation, samples were washed with 1% BSA in PBS, pelleted and re-suspended in 100μL per sample of 1x Click-iT saponin-based permeabilisation/wash buffer (in 1% BSA). After 15min of incubation at room temperature, 500μL per sample of a 1x Click-iT reaction cocktail (438μl PBS, 10μl $CuSO_4$, 2μl Picolyl azide-AF647, 50μl of 1x Reaction buffer additive in diH2O) was added to the sample and incubated for 30 minutes at room temperature in the dark. Following incubation, samples were washed with the permeabilisation/wash buffer, and resuspended in PBS for sample acquisition on the BD LSRFortessa X-20 flow cytometer. Background fluorescence was measured using unstained cells; single-stained and fluorescence minus one controls were used to set gating parameters between positive and negative populations. The controls for each time point were collected on corresponding days in culture for accurate gating.

2.13 Generation of endogenous triple reporter mouse ESC line using CRISPR-Cas9

2.13.1 Amplification of rod gene promoters

Regions of the 3'UTR of rod-specific genes, rhodopsin and α-transducin (Gnat1), were selected for amplification, in order to drive reporter expression through endogenous promoters without disrupting normal transcription. Primers were designed for the selected 3'UTR regions using NCBI Primer Blast software. The selected 3'UTR regions were amplified from mouse ESC genomic DNA by PCR, using the GoTaq Green Master Mix. Gradient PCR was used to determine the optimal annealing temperature for each primer set; full PCR cycle conditions can be found in Table 2.2. PCR reactions were analysed by gel electrophoresis. Samples were loaded with 6X loading dye (Promega) and run with a 1kb DNA ladder (Promega) at 180V for 50 minutes in a 1% agarose gel. Desired bands were cut out from the agarose gel and DNA was extracted using the Qiagen Gel Extraction Kit, following manufacturer's instructions.

Primer set	**Product size**	**PCR cycle conditions**
mRhoF AAGGGCATCCATCCACCAAG **mRhoR** CTAGCCAGCC TGAAGTGGAG	1925bp	95°C for 30s 35 cycles of: 95 °C for 15s 61 °C for 15s 68 °C for 120s 68°C for 5min
mGnat1F 5' CCAGACTTTCCGCCATCCTT 3' **mGnat1R** 5' GGAGAGGTTGTGCCCTAGTC 3'	1444bp	95°C for 30s 40 cycles of: 95 °C for 15s 58 °C for 15s 68 °C for 100s 68°C for 5min

Table 2.2: Primer sets, product sizes, and PCR cycle conditions for amplification of rod 3' UTR regions.

2.13.2 Vector construction for repair template

The reporter gene vectors Rho.mCherry and Gnat1.Katushka were constructed using the pGEM-T Easy vector backbone (Promega). Amplified 3'UTR regions were cloned into pGEM-T Easy Vector plasmid (Promega), following manufacturer's instructions. A 1:1 insert:vector ratio was used for both rhodopsin and Gnat1 PGEM-T Easy cloning.

The amplified rhodopsin 3'UTR contains SapI and BamHI restriction sites, which are required for later insertion of the fluorescent protein (FP); likewise, the α-transducin 3'UTR contains BciVI and NdeI restriction sites required for FP ligation. Site-directed mutagenesis was performed using the QuikChange Lightning Site-Directed Mutagenesis Kit (Agilent Technologies), according to manufacturer's instructions, to remove additional SapI or BciVI and NdeI sites that were present on the original pGEM-T Easy backbone.

The FP insert was designed and synthetized to contain the appropriate restriction sites at either end (SapI and BamHI for rhodopsin; BciVI and NdeI for Gnat1) as well as an internal ribosome entry site (IRES) preceding the 5'-CCACC-3' Kozak sequence and FP sequence.

Final mutagenized rhodopsin-/Gnat1-PGEM vectors and synthetized FP inserts were digested with the appropriate enzymes, and separated by gel electrophoresis as above. DNA was extracted from excised gel bands as above, and the concentrations were determined using a Nanodrop Spectrometer. FP inserts were ligated to their respective vectors in a 2:1 insert:vector ratio for Rho.mCherry and a 1:1 ratio for Gnat1.Katushka. T4 ligase and 10X ligation buffer were added to the reaction mixture and incubated at 4^{o}C overnight.

2.13.3 Vector construction for CRISPR Guides

A pUC backbone vector was opened by BbsI digestion. U6 promoter guides (1 µg/µL) were annealed by heating equal amounts of forward and reverse primers at 95°C for 3 min. 40ng of the BbsI-digested backbone was ligated to 1µg of the annealed U6 guides using T4 ligase and 2X rapid ligation buffer, with 1h incubation at room temperature. Site-directed mutagenesis was then performed using the QuikChange Lightning Site-Directed Mutagenesis Kit (Agilent Technologies) to insert the H1 promoter guides into the U6 guide-containing pUC backbone (see Table 2.3). SDM primers contained the 20 base pair-long H1 guide sequence, flanked by 30 base pair-long unmodified sequences upstream (H1 promoter) and downstream (tracRNA).

Primer set	**PCR cycle conditions**
mRho H1 guides F 5'TCTTATAAGTTCTGTATGAGACCACAGATC **TGCCAATATGCCCACCTTCA** GTTTTAGAGCTAGAAATAGCAAGTTAAAAT 3' **mRho H1 guides R** 5'ATTTTAACTTGCTATTTCTAGCTCTAAAAC **TGAAGGTGGGCATATTGGCA** GATCTGTGGTCTCATACAGAACTTATAAGA 3'	95°C for 120s 18 cycles of: 95 °C for 20s 60 °C for 10s 68 °C for 105s 68°C for 5min
mGnat1 H1 guides F 5'TCTTATAAGTTCTGTATGAGACCACAGATC **TCCAACACGTGTCCACCCAG** GTTTTAGAGCTAGAAATAGCAAGTTAAAAT 3' **mGnat1 H1 guides R** 5'ATTTTAACTTGCTATTTCTAGCTCTAAAAC **CTGGGTGGACACGTGTTGGA** GATCTGTGGTCTCATACAGAACTTATAAGA 3'	As above

Table 2.3: Primer sets and PCR cycle conditions for introduction of H1 guides via site-directed mutagenesis.

2.13.4 Transformation into competent cells

Samples were transformed into α-Select Gold Competent Cells (Bioline) according to manufacturer's recommendations. Briefly, 20µL of reaction was added per 25µL of thawed cells and mixed gently. Following 30min of incubation on ice, the cells were heat-shocked for 45s at 42°C and recovered on ice for 2min. 100µL of Super Optimal broth with Catabolite repression (SOC) Medium was then added to the transformation reaction, which was subsequently incubated for 60min at 37°C with 200rpm shaking. Each transformation reaction was then spread onto LB agar plates containing 100µg/mL of Ampicillin, and incubated overnight at 37°C. For PGEM-T Easy vector cloning, prior to plating the transformation reaction, 40µL of 20mg/mL X-gal and 4µL of 200mg/mL IPTG was spread onto the agar plates for blue/white screening of bacterial colonies. The following day, colonies were picked and cultured overnight at 37°C in 5mL of LB broth inoculated with 100µg/mL of Ampicillin.

2.13.5 Miniprep of samples

Minipreps were carried out on bacterial cultures of picked colonies using a GenElute Plasmid Miniprep Kit (Sigma), according to manufacturer's instructions. Samples were eluted in a final volume of 40µL ddH_2O.

Diagnostic digests were carried out at each stage where possible in order to decide which clones to send for final validation by Sanger sequencing. Digestions were performed at 37°C for 2h before analysis by gel electrophoresis on a 1% gel, unless otherwise required. Glycerol stocks of the correct clones were made and stored at -80°C.

2.13.6 Megaprep of samples

Megapreps were generated from glycerol stocks of the correct clones. For this, 500mL of LB broth with 100µg/mL of Ampicillin was inoculated with bacterial stock and incubated at 37°C overnight. The Plasmid Mega Kit (Qiagen) was used according to manufacturer's instructions, and samples were eluted in 1mL of ddH_2O. Megapreps were Sanger sequenced to validate successful and correctly-oriented insertion of reporter fluorescent protein into vector backbone (see Table 2.4).

Sequencing primers	**Sequence (5' to 3')**
Rho 3'UTR	AAAGCATCGAGACCAGGGG
Gnat1 3'UTR	ACTCAGCAGTGCCCTAGTGAC
U6 forward	CCCATGATTCCTTCATATTTG
H1 forward	AATTCGAACGCTGACGTC

Table 2.4: Sequencing primers

2.14 *In vitro* Multi-Electrode Array recordings

Mice were kept on a standard 12h light-dark cycle and dark-adapted overnight (>16 h) before the experiment to ensure maximal photoreceptor sensitivity. Mice were sacrificed under dim red light by cervical dislocation, following which each eye was enucleated and kept in bicarbonate-buffered Ames media (Sigma-Aldrich, A1420) bubbled with carbogen (5% CO_2/95% O_2) up to the point of dissection. All procedures carried out prior to and during recording were performed under dim red light (λ_{MAX} = 650nm), which is reported to be below the spectral sensitivity of murine detection and has minimal impact on rod photopigment activation.

Prior to MEA recordings, each eye was dissected to remove the cornea, iris, and lens, in order to access the retina. Care was taken to remove as much vitreous from the retinal surface as possible, in order to get good electrode contact. Retinal slices from eyes receiving transplanted cells were examined for GFP fluorescence in order to isolate and excise the region with the GFP^+ cell mass. The excised piece of retina was then mounted ganglion-side down in the recording chamber of a 60-channel MEA having 30µm-diameter electrodes spaced 100µm apart (60-channel pMEA 100/30iR-Ti, Multi Channel Systems, Reutlingen, Germany). Negative pressure was applied to the underside of the retina explant through the perforated MEA, in order to achieve good electrode contact and to keep the explant in position. As GFP^+ rods would have been photobleached by the GFP-excitation light (approx. 10min exposure), the mounted retina was perfused with 100 µM 9-*cis*-retinal (analog of 11-*cis*-retinal; Sigma-Aldrich, R5754) in carbogen-saturated, bicarbonate-buffered Ames solution containing 0.2% BSA for 30 minutes in the dark at 37°C before light stimulation began. This incubation period was also to allow the retina to equilibrate before recording.

During recording, the mounted retina was constantly perfused with carbogen-saturated Ames medium containing 9-*cis*-retinal (as above) maintained at 37°C (temperature was monitored by a thermistor in the perfusion circuit). Care was taken to ensure that 9-*cis*-retinal was not exposed to light at any point in the experiment, as it is light-sensitive. Control eyes were subject to the same light exposure and rhodopsin regeneration procedure prior to recording. Recordings from each retinal slice typically lasted for 3 hours.

2.15 Design and delivery of *in vitro* light stimuli

2.15.1 Light path

Light stimulation was delivered to the retina patch using the output of a digital light processing (DLP) projector (Texas Instruments) focused through a 10X objective (Nikon). Position of the DLP microcontrolled mirrors that form image pixels were driven by HDMI output produced by custom software written in MATLAB using PsychToolbox. Each image pixel, once magnified, covered an area of approximately $55um^2$ on the retina patch.

The light path contained two filter wheels with a set of neutral density (ND) filters (Thorlabs), having optical densities from 1 ('ND1') to 4 ('ND4'). To achieve light attenuation stronger than 4 log units, I serially combined an ND4 filter in one filter wheel with another ND1 filter in the second filter wheel. The filter settings will hereafter be referred to as ND0 (brightest setting used, no ND filter and hence no light attenuation) to ND5 (darkest setting used, 10^5-fold light attenuation). Recordings were taken across 5 log units of light intensity, in discrete 1 log unit increments, from the lowest light intensity (ND5) to the highest (ND0), in order to avoid bleaching by the stimulus. There was a 10min adaptation period following each neutral density filter change, to allow for the retina to adapt to the new ambient light level before recording.

2.15.2 Visual stimuli

The DLP projector was used to deliver a square pulse of white light stimulus to the mounted retina patch, followed by a defined recovery period before the next sweep. This was done for 20 sweeps continuously per stimulus light level.

2.15.3 Data acquisition

Extracellular voltage traces were recorded from 60 electrode channels at an amplified gain of 1200 and data sampling rate of 32 kHz/channel, with a bandpass filter of 10-3000Hz, by an MC_Card system using MC_Rack software (Multi Channel Systems).

2.16 Statistical analysis

All means are presented ± standard error of mean (s.e.m.), unless otherwise stated; N, number of animals or independent experiments performed; n, number of eyes, EBs, retinal explants, or differentiation cultures, where appropriate. For cell counts in recipient eyes, statistical analysis is based on at least three independent transplantation sessions (cell preparation, FACS and transplantation). Statistical significance was assessed using GraphPad Prism 5 (Graphpad software Inc., USA) to conduct appropriate statistical tests, including unpaired student t-test or Mann-Whitney U test for comparisons between two groups, and ANOVA with Tukey's test or Kruskal-Wallis with Dunn's test for multiple comparisons. In figures, *P< 0.05, **P< 0.01, and ***P< 0.001.

Chapter 3 : Optimisation of transplantation protocol

3.1 Introduction

Early studies by our group have demonstrated that the subretinal transplantation of GFP reporter-labelled, post-mitotic donor-derived Nrl.GFP-positive photoreceptor precursors into the *Gnat1*$^{-/-}$ mouse model of retinal degeneration results in the presence of rod-like, GFP-positive (GFP^{+}) cells within the recipient outer nuclear layer (ONL). Notably, an increased number of GFP^{+} cells present in the host ONL following transplantation was found to be positively correlated to the extent of functional vision restored (Pearson et al., 2012; Barber et al., 2013), suggesting that these GFP^{+} cells were able to relay photoresponses down visual pathways. While a reliable electroretinogram (ERG) response could be only achieved with an estimated minimum of 150,000 GFP^{+} cells, the presence of an average of 25,000 GFP^{+} cells in the host ONL was sufficient to generate primary visual cortical activity in response to visual stimuli, and also restore visually-guided behaviour such as optokinetic head-tracking and solving a water-maze task (Pearson et al., 2012).

More recent work in our lab on transplanting optimally-staged mouse ESC-derived Rhodopsin.GFP-positive rod precursors into *Gnat1*$^{-/-}$ recipient mice demonstrated that an average of 276 GFP^{+} cells were present in the host ONL following transplantation (Gonzalez-Cordero et al., 2013), which was significantly lower than what was achieved with the transplantation of donor-derived rod precursors (Figure 3.1). The assessment of visual function in animals transplanted with reporter-labelled mouse ESC-derived photoreceptor precursors therefore required further optimisation of the transplantation protocol in order to increase the number of reporter-labelled donor cells present in the host ONL following transplantation.

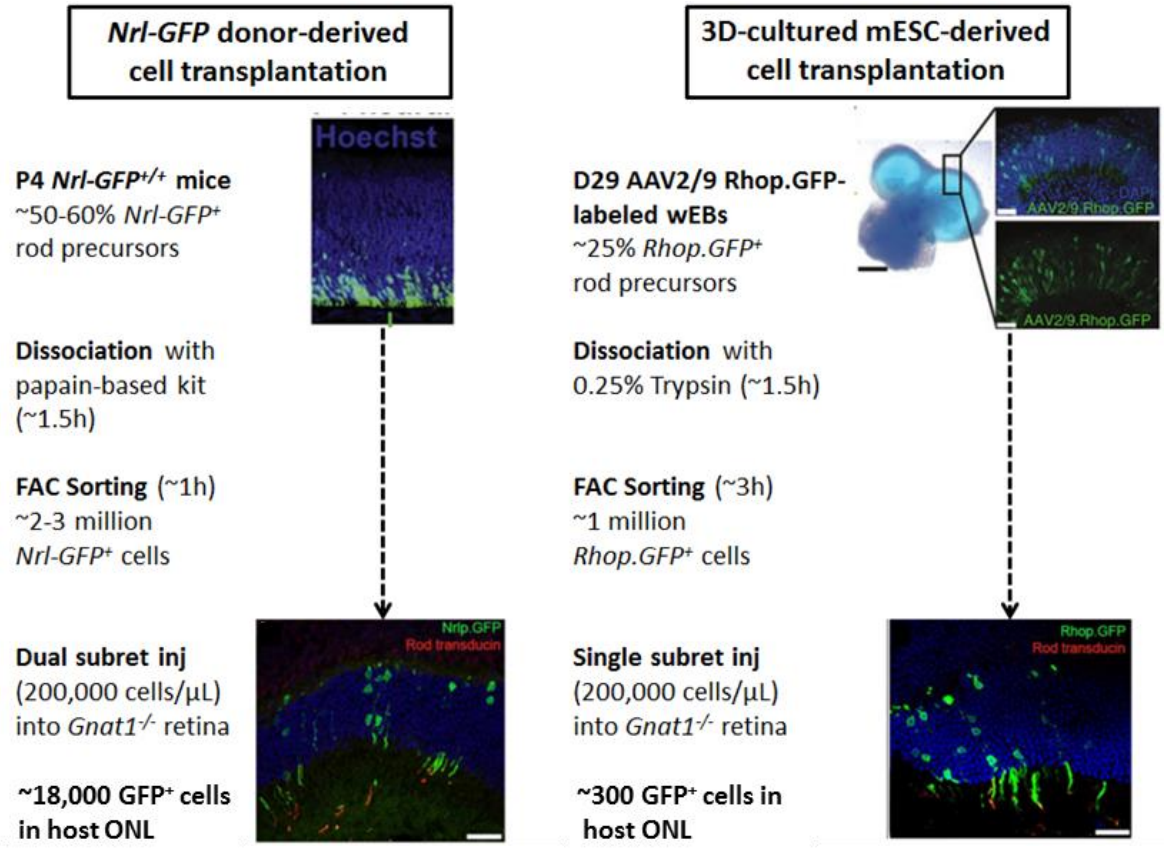

Figure 3.1: Schematic comparing *Nrl.GFP* donor-derived cell transplantation with 3D-cultured mouse ESC-derived cell transplantation. wEBs: whole embryoid bodies.

We hypothesised that poor viability of photoreceptor precursor cells may compromise their ability to survive and develop into mature photoreceptors *in vivo* following transplantation. Although dead, GFP-negative cells are excluded from the transplanted population during the process of cell sorting, cells that are beginning apoptosis may still contain GFP and be included in the injected donor cell population. Apoptotic cells can compromise the survival, differentiation, and migration of viable neighbouring cells in the microenvironment through contact or production of soluble factors such as TGF-β and cytochrome c (Gregory and Pound, 2010, 2011; Fan and Bergmann, 2008). As such, the presence of early apoptotic photoreceptor precursors in the *in vitro* 3D culture and in the transplanted cell population may contribute to poor survival and development post-transplantation. We therefore began by assessing the levels of early apoptosis in our 3D *in vitro* cultures, and we investigated the effect of excluding apoptotic cells from the GFP-labelled mESC-derived photoreceptor precursor population during fluorescent activated cell sorting (FACS) prior to transplantation, on the number of GFP$^+$ cells present in the host ONL following transplantation.

Next, I compared different methods of embryoid body (EB) dissociation and single cell sorting to improve cell yield and viability prior to transplantation. Purification of donor cell population by cell sorting to isolate only photoreceptor precursors for transplantation has been shown to have the greatest impact on the numbers of reporter-labelled donor cells present in the host ONL, compared with other procedural manipulations (Pearson et al., 2012; West et al., 2012). A critical step in cell sorting is the dissociation of tissue into a single cell suspension, and the dissociation protocol employed should enable a maximum yield of functionally viable single cells and retention of important cell surface antigens. I focused on the retention of CD73, which is a glycosylphosphatidylinositol-anchored ecto-5'-nucleotidase expressed in both photoreceptor precursors and mature photoreceptors, and its usefulness as a cell surface marker to enrich for post-mitotic rod precursors for transplantation has recently been demonstrated by Lakowski et al. (2015). As an additional readout, I investigated the effect of different dissociation protocols on the numbers of reporter-labelled donor cells present in the host ONL following transplantation into *Gnat1*$^{-/-}$ mice. The *Gnat1*$^{-/-}$ mouse lacks rod α-transducin (Gnat1), a protein essential for rod phototransduction; as such, it has no rod function or behavioural responses to scotopic visual stimuli. It has been shown to undergo progressive loss of rods (~10% loss) over a period of 12 months, and is a model of stationary night-blindness as the retina remains anatomically stable (Calvert et al., 2000).

Additionally, in our previous studies, mouse ESC-derived rods were labelled for transplantation using an AAV2/9 Rhodopsin.GFP virus. Increased transduction efficiency can allow additional scaling up of the yield of Rhop.GFP^{+} cells from *in vitro* cultures for transplantation. As such, I added different viral vector capsids to differentiating EBs to compare the various AAV2 pseudotypes based on their efficiency and specificity in photoreceptor transduction *in vitro*, as well as their effect on cell viability.

Finally, the potential host immune rejection of allogeneic retinal cell grafts presents a major challenge that remains to be fully addressed before photoreceptor precursor transplantation can be applied to the clinic. Our chosen site of donor cell transplantation – the subretinal space – is often described as an immune-privileged site, in which the systemic immune response to alloantigens is actively modulated in

a manner that limits conventional immunogenic inflammation. However, this fragile state of immune privilege can be compromised by the transplantation procedure itself, which may inadvertently introduce mechanical trauma to the outer blood-retinal barrier. Indeed, previous work in our lab using allogeneic neonatal donor-derived Nrl.GFP^{+} photoreceptor precursors transplanted into recipient mice with partially mismatched H2 haplotypes, found that majority of transplanted eyes showed evidence of an adaptive T cell-mediated immune response initiated against donor cells by 3-4 weeks post-transplantation, resulting in evident cell loss by 2-4 months (West et al., 2010). This response could be modulated through the use of cyclosporine A (CyA). CyA is a widely-used immunosuppressant that reduces the activation and proliferation of antigen-reactive T cells by inhibiting the early Ca^{2+}-dependent steps of the T cell response. This prevents the synthesis and secretion of IL-2 from MHC II-restricted CD4^{+} T cells, as well as IFN-γ from MHC I-restricted cytotoxic CD8^{+} T cells, both of which are key players in late acute and chronic graft rejection in the eye (Snyder, Sabatini, et al., 1998; Boisgérault et al., 2001). The host adaptive immune response to ESC-derived photoreceptor precursor cells has yet to be investigated. Given that these cells are likewise being transplanted into recipient mice with partially mismatched H2 haplotypes, and are potentially more immunogenic than donor-derived cells due to prolonged *in vitro* culture with animal-derived components (Tang et al., 2013), I therefore aimed to investigate whether ESC-derived photoreceptor precursor cells would induce a host adaptive immune response post-transplantation, and if suppression of this immune response would increase the number of reporter-labelled donor cells in the host ONL following transplantation.

3.2 Results

3.2.1 Assessing photoreceptor viability in vitro

We first assessed the viability of photoreceptors in our *in vitro* culture conditions by quantifying the proportion of early apoptotic cells within the neuroepithelia region of EBs grown to later time points in culture. Early apoptotic cells were identified based on active Caspase-3 and Lamin B immunohistochemistry as well as condensation of nuclear chromatin (Figure 3.2A). Active Caspase-3 is an effector caspase associated with initiation of the apoptotic signalling pathway (Nicholson et al., 1995), whereas degradation of the nuclear envelope marker Lamin B is caspase-dependent and a feature of apoptosis (Burke, 2001).

Neuroepithelial regions were examined at 3 late timepoints in differentiation – day 29, 34, and 36 – which approximately correspond to postnatal day 8, 12, and 16 respectively in normal retinal development *in vivo* (Gonzalez-Cordero et al., 2013). The proportion of apoptotic cells was significantly higher in day 36 differentiation cultures compared with day 29 cultures (Figure 3.2B; 16.0 ± 2.4% vs. 7.7 ± 1.1%, $p < 0.01$, Mann-Whitney, $n \geq 11$ EBs per group). Furthermore, while clear neuroepithelial morphology was maintained till day 29, by day 34 there were signs of rosette formation and increased neuroepithelial disorganization. By day 36, the majority of the EBs did not have clear neuroepithelial regions, and there was a greater prevalence of small neural rosettes (Figure 3.2C, day 36, arrow heads).

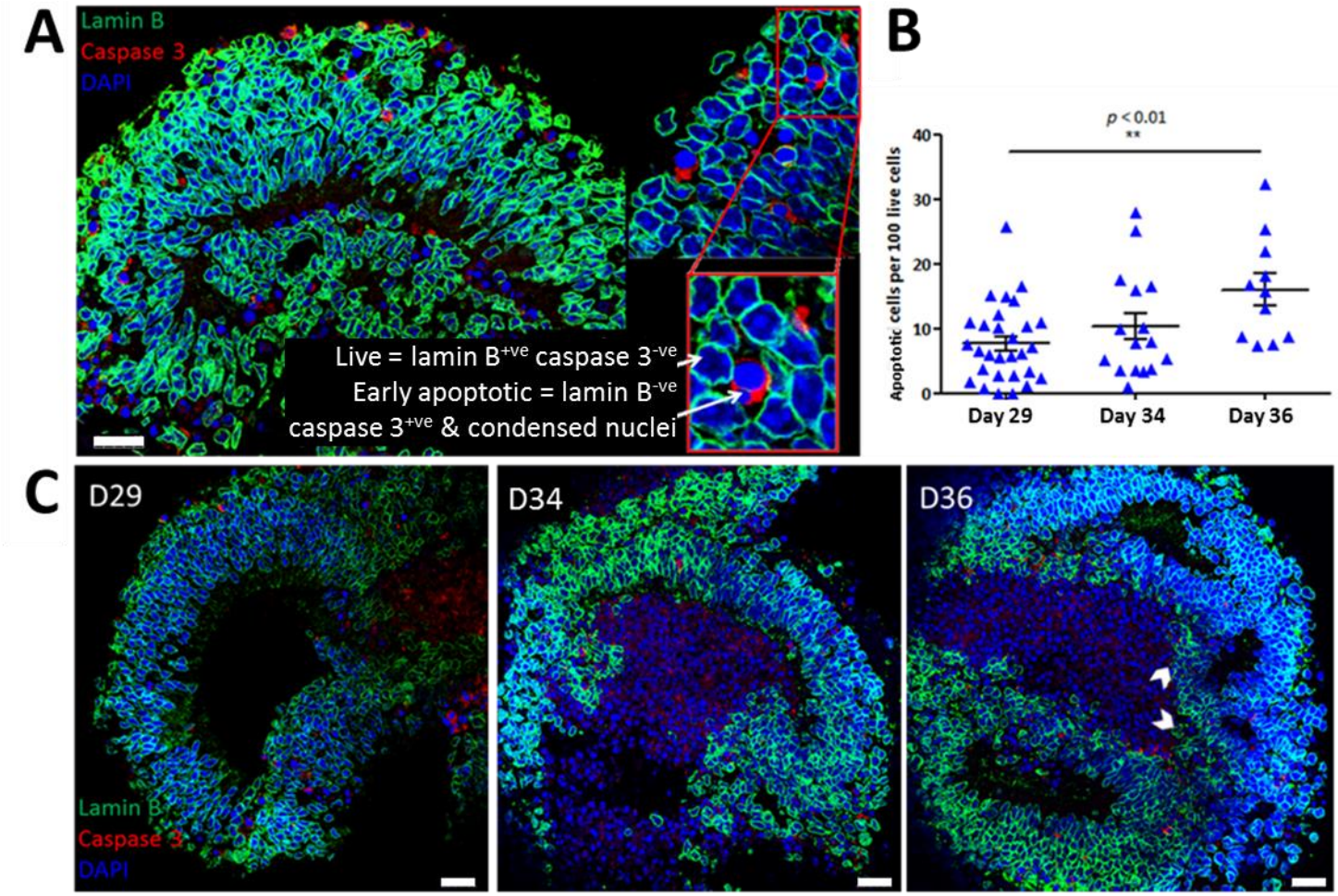

Figure 3.2: Levels of early apoptosis in neuroepithelia region of EBs grown at day 29, 34, and 36. A. Regions of neuroepithelia were examined for presence of early apoptotic cells. Live cells were defined as Caspase-3$^-$ and Lamin B$^+$ with an intact nuclear envelope, whereas early apoptotic cells were Caspase-3$^+$ and Lamin B$^-$, with an absent nuclear envelope and condensed nuclei. B. Proportion of early apoptotic cells out of live cells in regions of neuroepithelia in EBs at different days in culture was quantified. C. Representative images of neuroepithelia morphology in EBs at different days in culture. Rosette formation was observed later in culture at day 36 (arrow heads). Scale bar: 25µm.

We next investigated the hypothesis that poor viability of the photoreceptor precursor cells prior to transplantation may compromise their ability to survive and mature *in vivo*, resulting in low numbers of reporter-labelled donor cells observed in the host ONL following transplantation. To do this, an AAV2/9.Rhodopsin.GFP (Rhop.GFP) virus was added to the differentiation culture on day 22. On day 29 in culture, EBs were then dissociated with 0.25% Trypsin and stained with Annexin V, which like Caspase-3, is an early marker of apoptosis. This was followed by staining the cell suspension with a Live-Dead dye, DRAQ7, prior to fluorescence activated cell sorting (FACS). For FACS, a sequential gating strategy was first applied to exclude debris, cell aggregates, and dead cells; following which, the selected single live cell population was either sorted on the basis of GFP expression alone, or on the expression of GFP as well as the absence of Annexin V staining (Figure 3.3). The control population of cells sorted on GFP alone would therefore be likely to comprise a proportion of Annexin V-positive, early apoptotic cells; whereas the population of GFP^+/Annexin V^- cells would comprise only live cells, having excluded Annexin V-positive, early apoptotic cells.

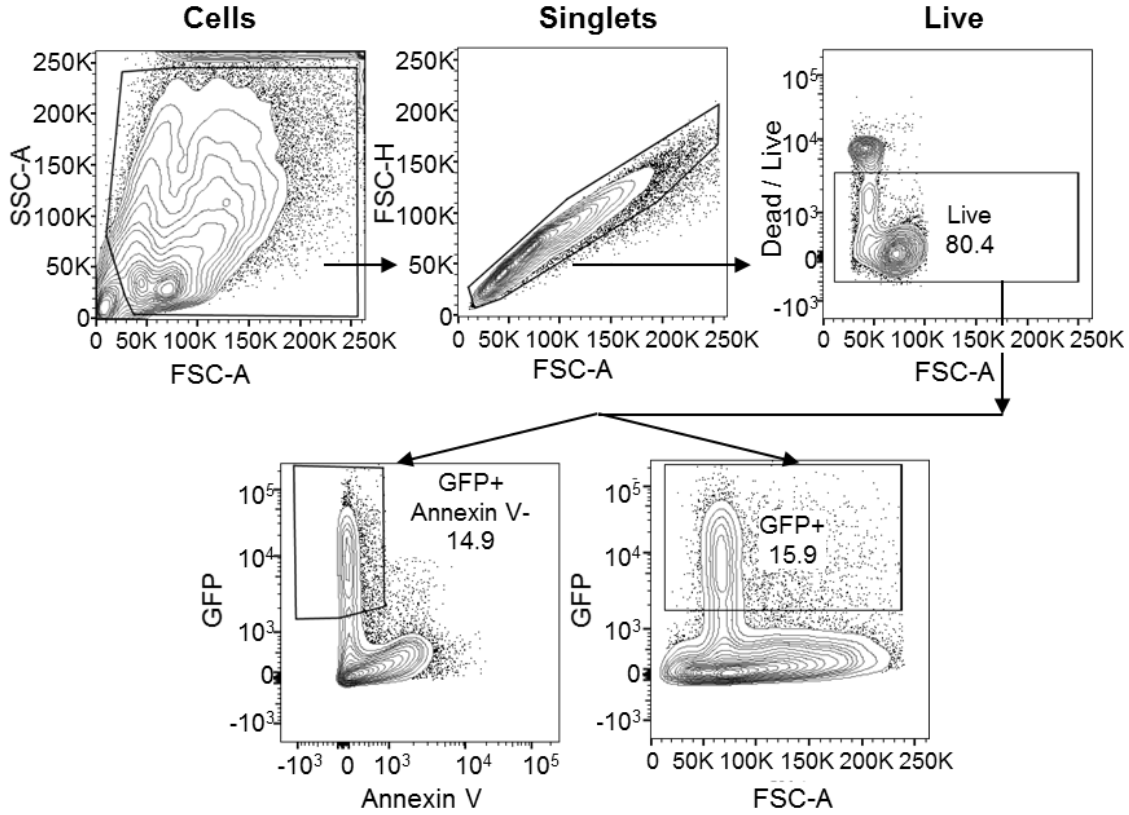

Figure 3.3: Flow cytometry gating showing sequential exclusion of debris, cellular aggregates, and dead cells in the cell suspension derived from dissociated day 29 Rhop.GFP-labelled EBs. The single live population was then either sorted on the basis of GFP expression and absence of Annexin V expression, or on GFP expression alone, prior to transplantation. Numbers in plots indicate percentage of parent population.

At 3 weeks post-transplantation, GFP$^+$ cells could be observed appropriately located and orientated in the host ONL in both groups of transplants (Figure 3.4A). These cells were morphologically very similar to wild-type rods and correctly expressed the mature outer segment protein Gnat1, rod α-transducin, which is absent in endogenous *Gnat1*$^{-/-}$ rods. While one of the eyes treated with GFP$^+$/Annexin V$^-$ cells had a markedly high number of GFP$^+$ cells present in the host ONL, overall, there was no statistically significant increase in the number of GFP$^+$ cells present in the host ONL following the transplantation of GFP$^+$/Annexin V$^-$ cells as compared with GFP$^+$ cells (Figure 3.4B; 359.3 ± 256.1% vs. 298.5 ± 68.35%; $p > 0.05$, Mann-Whitney, $n \geq 4$ eyes).

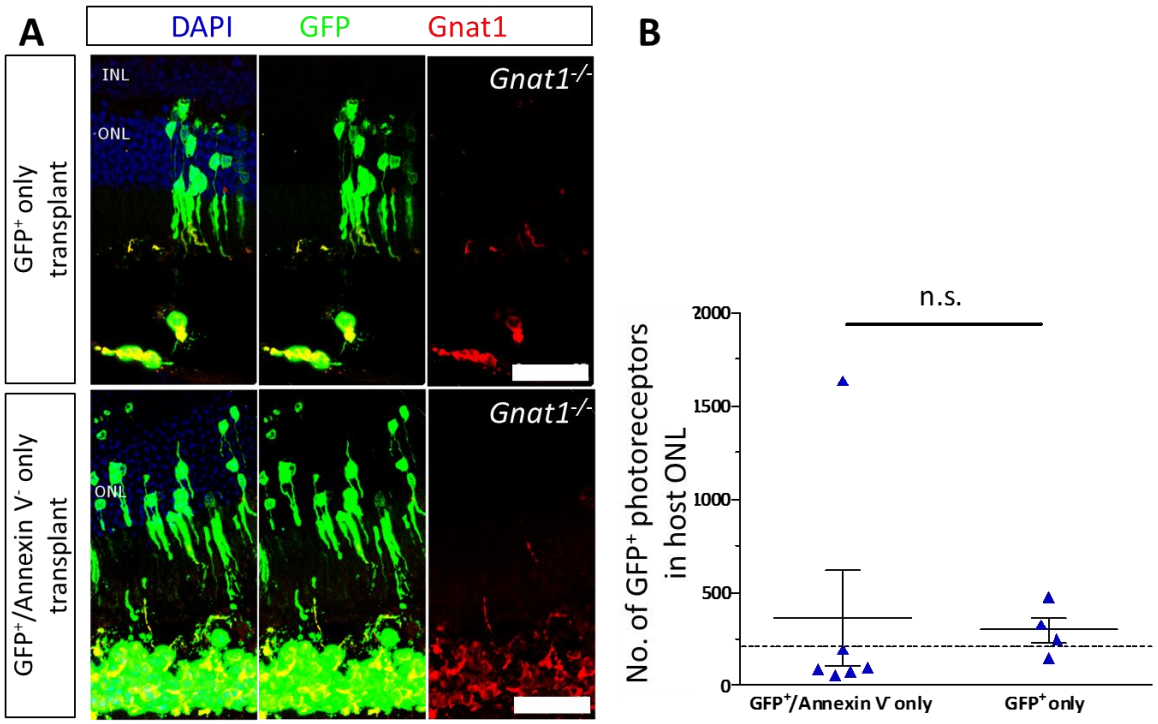

Figure 3.4: Assessing the effect of excluding early apoptotic cells on the number of GFP$^+$ cells in the *Gnat1*$^{-/-}$ host ONL at 3 weeks following transplantation. A. In both groups of transplants, GFP$^+$ cells were observed in the host ONL, a proportion of which also expressed Gnat1. Scale bar: 25µm. B. Exclusion of Annexin V-positive early apoptotic cells did not significantly increase the number of GFP$^+$ cells present in the host ONL following transplantation. The dotted line indicates the previously reported average number of GFP$^+$ cells present in the host ONL at 3 weeks post-transplantation (Gonzalez-Cordero et al., 2013).

Our assessment of photoreceptor viability *in vitro* indicated that our current 3D culture conditions are unable to fully support EB differentiation and photoreceptor survival in the long term. However, the proportion of early apoptotic cells at day 29 of culture was small, and the exclusion of early apoptotic cells from the GFP-labelled population prior to transplantation did not appear to increase the number of GFP-labelled cells present in the host ONL at 3 weeks following transplantation, indicating that the viability of transplanted cells may not be the primary cause for the observed low numbers of GFP-labelled cells present in the host ONL following transplantation.

3.2.2 Testing different dissociation methods of EBs for transplantation

We previously used a specialised papain-based kit (Worthington Papain Dissociation System) to prepare donor-derived cells for transplantation, whereas mouse ESC-derived 3D EBs were dissociated using 0.25% Trypsin, mainly due to a quicker incubation period (8 minutes as opposed to 45 minutes with the Worthington Papain kit). A number of dissociation kits are available and these claim to enable efficient and reproducible yields of single, viable cells with preserved membrane and epitope integrity. Here, I compared five of these methods for EB dissociation prior to FACS on the basis of dissociation efficiency, cell viability, retention of CD73 antigenicity, and most importantly, the number of GFP^+ cells in the host ONL post-transplantation. The 0.25% trypsin-based dissociation method employed in the original mESC-derived photoreceptors transplantation protocol, was compared with the Worthington Papain Dissociation System used for the donor-derived photoreceptor transplantation protocol (hereinafter referred to as 'Papain'), along with three other papain-based Miltenyi Biotec Dissociation Kits for Neural Tissue, Neurosphere, and Embryoid Body.

As before, an AAV2/9.Rhop.GFP virus was added to EBs at day 22 in culture, and EBs were then dissociated on day 29 and stained for Annexin V and DRAQ7 for flow cytometric analysis (Figure 3.5A). Here, the Live/Dead DRAQ7 stain was first plotted against Annexin V, and the double-negative population was selected; within this double-negative population, another gate was then drawn around debris, which could be identified on the basis of its low forward- and side-scatter profile (denoted as FSC-A and SSC-A respectively). The same gating was subsequently applied back to the entire cell population to distinguish between debris and 'not debris', so as to exclude small debris and cell fragments from downstream analysis. Cellular aggregates were also excluded from the 'not debris' population, allowing for the quantification of the total yield of single intact cells (Figure 3.5A, blue box), as well as live Rhop.GFP^+ photoreceptor cells (Figure 3.5B, blue box). The viability of dissociated cells was also assessed by plotting Annexin V against the Live/Dead stain, which allowed us to identify early apoptotic (Annexin V^+/LD^-), late apoptotic (Annexin V^+/LD^+), necrotic (Annexin V^-/LD^+), and live populations (Annexin V^-/LD^-) (Figure 3.5C, blue box). Fluorescence minus one controls, in which each control is stained with

all fluorochromes except one, were used to set gating parameters to distinguish between positive- and negative-staining populations.

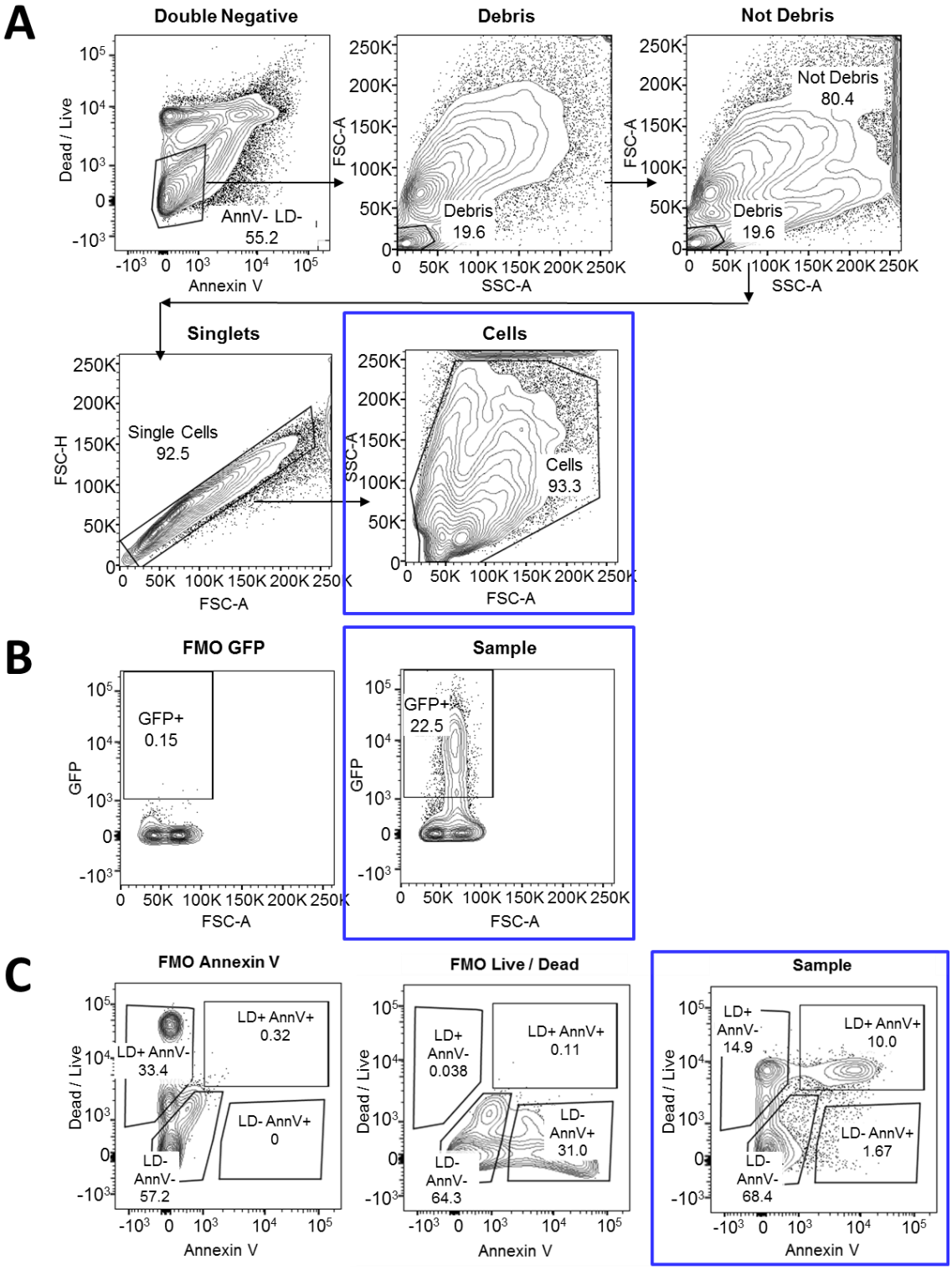

Figure 3.5: A. Flow cytometry gating showing sequential exclusion of debris and cellular aggregates in the cell suspension derived from dissociated day 29 Rhop.GFP-labelled EBs. B. The percentage of live GFP-labelled cells in each sample was determined, using the FMO GFP control to distinguish between positive- and negative-staining populations. C. Annexin V was plotted against the Live/Dead stain in order to determine the relative proportions of early and late apoptotic, live, and necrotic populations. FMO Annexin V and FMO Live/Dead controls were used to distinguish between positive- and negative-staining populations. Numbers in plots indicate percentage of parent population.

There was no significant difference in total yield of intact cells and Rhop.GFP$^+$ yield between the methods tested (Figure 3.6A). However, the period of time required to generate the desired single cell suspension for transplantation varied between the methods (Figure 3B). While 0.25% trypsin was the quickest method (8 minutes), the viability of the cells isolated with trypsin was the poorest (Figure 3.6C). The proportion of early apoptotic cells was significantly higher in trypsin-dissociated cell suspensions compared with the other papain-dissociated suspensions within the total population (Figure 3.6C; 15.2 ± 2.3% vs. <6.5% respectively; $p<0.05$, Kruskal-Wallis, n=3) as well as in the Rhop.GFP$^+$ population (19.3± 3.1% vs. <3% respectively; Figure 3.6D; $p<0.05$, Kruskal-Wallis, n=3). The proportion of live cells was correspondingly significantly lower in trypsin-dissociated cell preparations compared with the other papain-dissociated methods within the total population (62.4 ± 6.6% vs. >78.5% respectively; Figure 3.6C; $p<0.05$, Kruskal-Wallis, n=3 differentiation cultures) and Rhop.GFP$^+$ population (74.0 ± 2.1% vs. >91.5% respectively; Figure 3.6D; $p<0.05$, Kruskal-Wallis, n=3 differentiation cultures). The comparison of the 5 different dissociation methods showed that the papain-based Neurosphere Dissociation Kit provided the best balance of dissociation efficiency, cell viability, and a short protocol length of only 15 minutes.

We also assessed the retention of CD73 antigenicity following dissociation (Figure 3.6E). Flow analysis for CD73 following dissociation demonstrated that 0.25% trypsin treatment cleaves CD73, with only 11% of the cells expressing this marker, whereas the papain-based dissociation methods were able to preserve CD73 antigenicity (~45-60% CD73$^+$ cells).

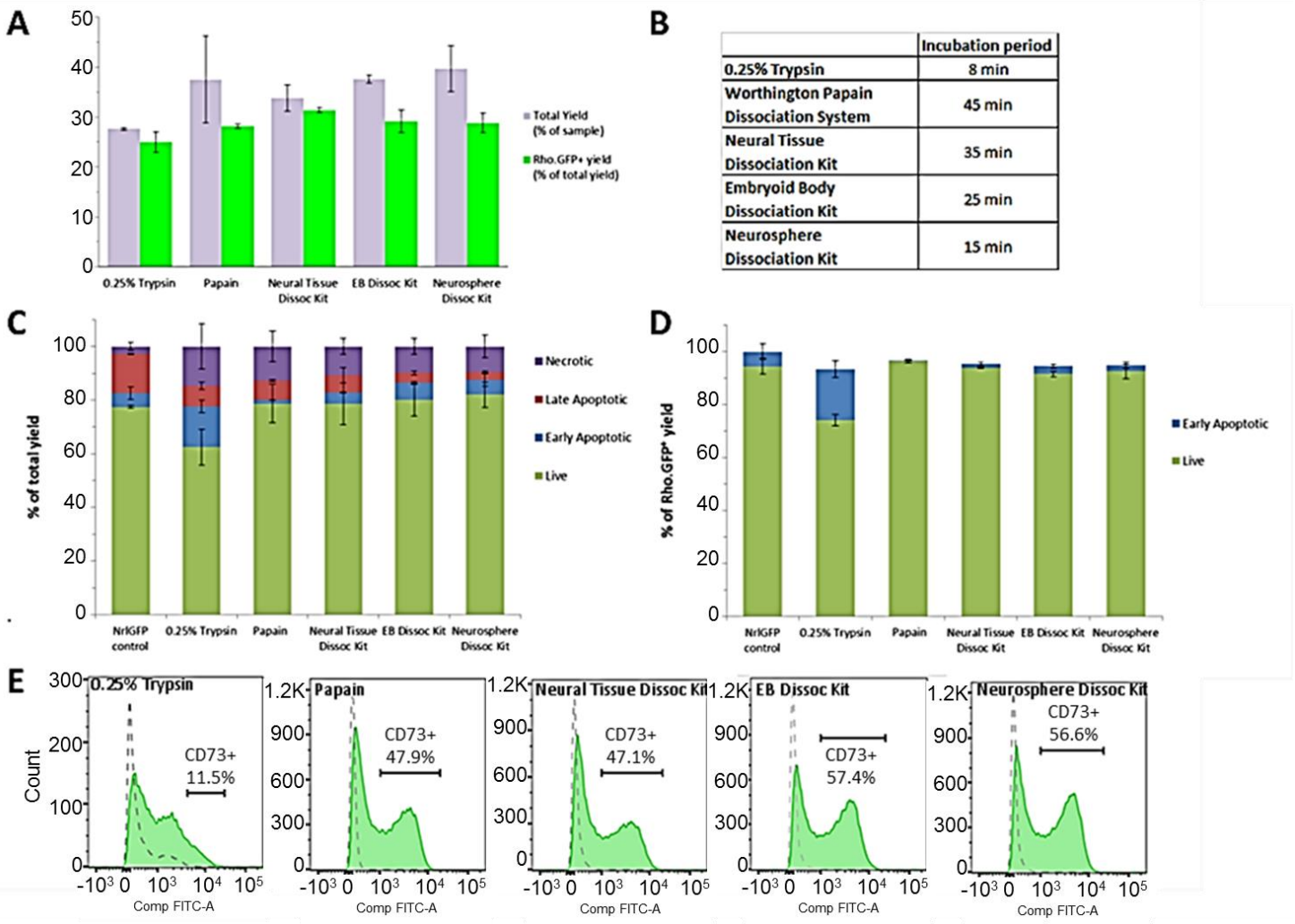

Figure 3.6: Effect of dissociation method on: A. dissociation efficiency; B. length of protocol, C. and D. viability; and E. retention of CD73 antigenicity. Papain-dissociated NrlGFP donor-derived cells (prior to sorting) were included as a control.

Finally, to establish if the different methods of dissociation had an impact on the number of GFP$^+$ cells in the host ONL following the transplantation of mouse ESC-derived rod photoreceptors, we transplanted Rhop.GFP$^+$ cells dissociated either by the original 0.25% trypsin protocol or by the papain-based Neurosphere Dissociation kit into the *Gnat1*$^{-/-}$ mouse model. Notably, use of the papain-based Neurosphere Dissociation kit instead of trypsin to dissociate mESC-derived EBs saw a significant three-fold increase in the number of GFP$^+$ cells in the host ONL following transplantation (1712.4 ± 534.4 photoreceptors vs. 511.5 ± 129.0 photoreceptors; $p < 0.05$, Mann-Whitney, n= 5 and 4 eyes respectively), with a maximum of 3606 GFP$^+$ cells in the host ONL in the papain-based Neurosphere Dissociation kit group (Figure 3.7A). There was a slightly greater proportion of eyes rejected from downstream quantitative analysis due to macrophage infiltration in the 0.25% Trypsin group, as compared with the Neurosphere Dissociation Kit group (Figure 3.7B). Furthermore, the GFP$^+$ cells present in the host ONL following the transplantation of Rhop.GFP$^+$ cells dissociated with the Neurosphere Dissociation kit were appropriately orientated within the host ONL and morphologically similar to wild-type rods (Figure 3.7C). In addition, they correctly expressed Gnat1, which is absent in endogenous *Gnat1*$^{-/-}$ rods (Figure 3.7D).

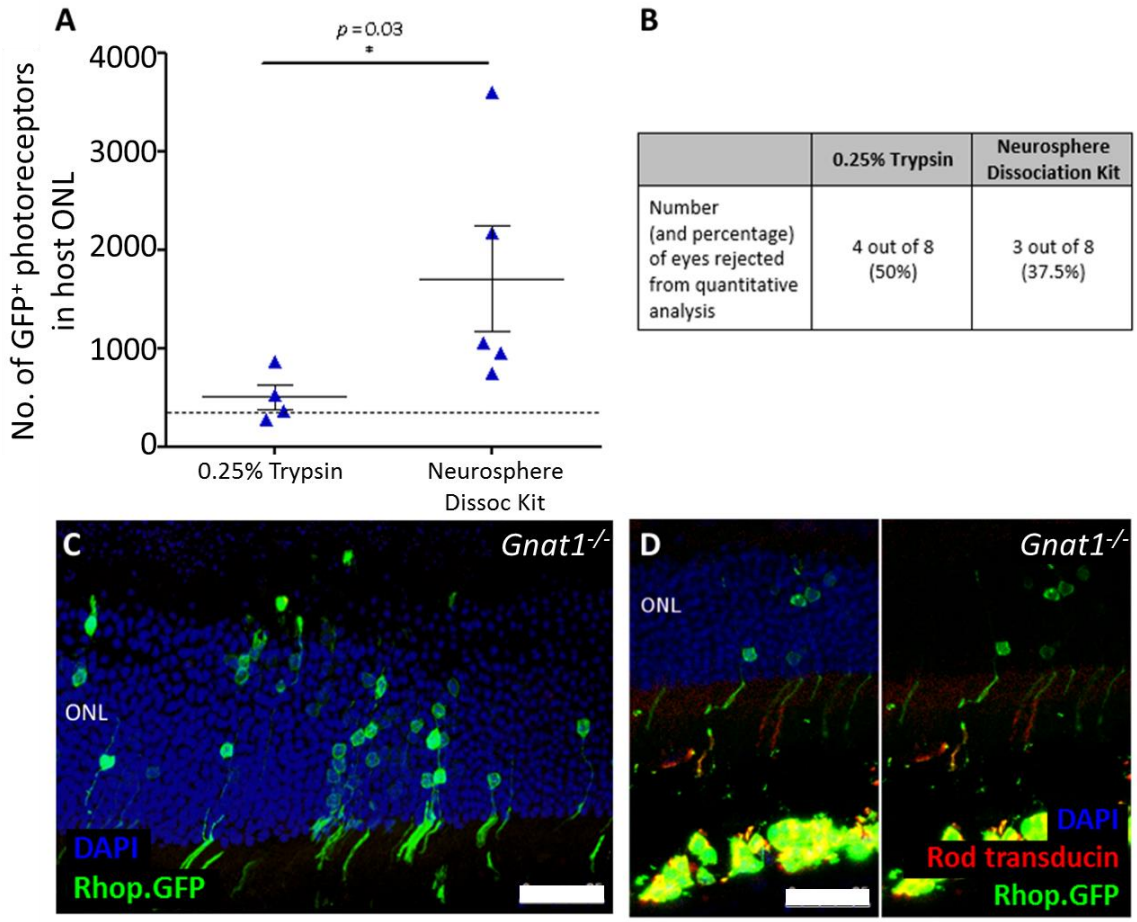

Figure 3.7: Comparison of 0.25% Trypsin and the papain-based Neurosphere Dissociation Kit. A. Use of the Neurosphere Dissociation Kit significantly increases the number of GFP⁺ cells present in the host ONL at 3 weeks post-transplantation. The dotted line indicates the previously reported average number of GFP⁺ cells present in the host ONL at 3 weeks post-transplantation (Gonzalez-Cordero et al., 2013). B. Number of eyes rejected from further quantitative analysis in each group. C. Transplanted Rhop.GFP⁺ rod precursors dissociated with the Neurosphere Dissociation Kit are correctly localised and orientated in the recipient *Gnat1*$^{-/-}$ ONL, and also D. express Gnat1 in their outer segments. Scale bar: 25µm.

3.2.3 Testing different cell sorting methods for transplantation

Using the papain-based Neurosphere Dissociation Kit, which ensured preservation of the CD73 surface antigen, I was able to compare Magnetic Associated Cell Sorting (MACS) and FACS as methods to isolate rod precursors for transplantation. Day 29 EBs derived from a transgenic mESC line (CBA.YFP R1/E ESC; ATCC-R) with a YFP reporter cassette driven by the ubiquitously active β-actin promoter were first dissociated and labelled with CD73-APC, followed by secondary labelling with anti-APC microbeads. The ATCC mESC line follows the same time course of development in our *in vitro* 3D differentiation cultures as the E16 line, and the pattern of CD73 expression is similar to that of Rhodopsin in E16 differentiation cultures (Gonzalez-Cordero et al., 2013; Lakowski et al., 2015). CD73 labelling of day 29 ATCC EBs was therefore chosen as a developmentally-equivalent substitute for Rhop.GFP-labelled day 29 E16 EBs for MACS. This substitution was necessary as MACS is not dependent on GFP reporter expression, as described below, but it was still important to be able visualise the transplanted cells in the host ONL.

Anti-CD73-APC microbead-labelled ATCC photoreceptor cells were subsequently isolated using the AutoMACS machine and transplanted into the subretinal space of *Gnat1*$^{-/-}$ recipient mice. In agreement with findings by Marius Ader's and Jane Sowden's groups, GFP^{+} cells were observed in the ONL of recipient *Gnat1*$^{-/-}$ retinas (Postel et al., 2013; Eberle et al., 2012, 2011, Lakowski et al., 2011, 2015). The number of GFP^{+} cells present in the host ONL appeared to be slightly lower for MAC-sorted cells (725.0 ± 262.6, n=4 eyes) compared with FAC-sorted cells (1750 ± 285.1, n=10 eyes), although this difference was not significant (Figure 3.8A; $p>0.05$; Mann-Whitney) (Figure 3.8A). MAC-sorted cells were observed to be correctly orientated within the host ONL (Figure 3.8B) and contained Gnat1 (Figure 3.8C). Presence of the biodegradable microbeads attached to the labelled cells did not appear to have any apparent detrimental effect on transplanted cell survival at 3 weeks post-transplantation. In addition, the yield of CD73^{+} cells post-MACS (35-40%) was comparable to that of Rhop.GFP^{+} cells post-FACS (25-30%).

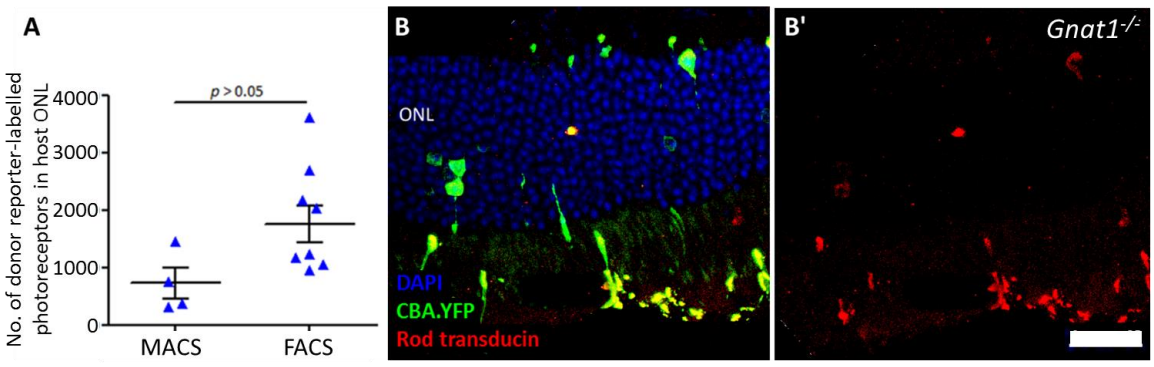

Figure 3.8: Comparison of different cell sorting methods. A. The number of reporter-labelled donor photoreceptors present in the host ONL following transplantation of CD73⁺ cells isolated by MACS vs. Rhop.GFP⁺ cells isolated by FACS are not statistically significant. B. Reporter-labelled donor cells are present in the recipient *Gnat1*$^{-/-}$ mouse retina following transplantation, and B'. express Gnat1.

Therefore, given that both the length of the sort for MACS and FACS (approximately 30-45min), as well as the viability of sorted cells post-sort (>90% viable) are comparable, I decided to choose FACS over MACS as a method for cell sorting due to the increased incubation time involved in the two-step indirect magnetic labelling of dissociated cells for MACS. Furthermore, sorting for multiple surface markers as in Lakowski et al. (2015) will prove costly as microbeads have to be purchased for individual markers. Importantly, the possibility of isolating ESC-derived rod photoreceptor precursors with the surface marker CD73 by MACS emphasises the importance of preserving cell surface antigens when choosing a method of dissociation.

As such, all subsequent experiments necessitating the dissociation of 3D mESC-derived EBs into a single cell suspension for flow cytometry were carried out using the Neurosphere Dissociation Kit for dissociation instead 0.25% Trypsin.

3.2.4 Improving AAV transduction efficiency of mouse ESC-derived rod photoreceptors

The previously established transplantation protocol for mESC-derived rod precursors employed an AAV2/9 Rhop.GFP virus to infect mESC-derived EBs, in order to enable isolation of rod precursors by GFP expression, which is driven by the Rhodopsin promoter. Increased transduction efficiency can allow additional scaling up of the yield of Rhop.GFP$^+$ cells from *in vitro* cultures for transplantation. To this end, I sought to assess different AAV2 pseudotypes for their efficiency and specificity in photoreceptor transduction, as well as their effect on cell viability.

3.2.4.1 Establishing AAV2 tropism in mouse ESC-derived EBs

To investigate AAV tropism in mouse ESC-derived EBs, I tested 6 different AAV2 psuedotypes driving GFP expression under the control of the ubiquitous cytomegalovirus (CMV) promoter. A schematic of the 3D differentiation and virus infection protocol is shown in Figure 3.9A. Titre-matched viruses were added to EBs at day 22 in culture, following which EBs were collected for cryopreservation and flow cytometric analysis 7 days later.

The AAV2 pseudotypes exhibited different tropisms efficiency *in vitro* (Figure 3.9B-G). Low magnification images of virus-transduced EBs at day 29 in culture showed GFP$^+$ cells in regions of neuroepithelia across all tested pseudotypes (Figure 3.9 B-G, arrow heads). In particular, ShH10 appeared to strongly transduce cells only in the neuroepithelial regions, whereas some pseudotypes appeared to transduce other non-neuroepithelial regions of EBs (Figure 3.9H, asterisk). Flow cytometric quantification of GFP expression indicated that the percentage of cells transduced by ShH10 was significantly greater (53.0 ± 8.7%) than all the other pseudotypes tested (Figure 3.9H). AAV2/9 (16.4 ± 7.5%), AAV2/8 (20.0 ± 4%), AAV2/8T (15.7 ± 1.3%) and AAV2/5 (12.0 ± 5.3%) pseudotypes had similar transduction efficiencies, whereas AAV2/2 only transduced 6.0 ± 2.6% of the total number of cells (Figure 3.9H**;** $p<0.001$, ANOVA, n=3 differentiation cultures).

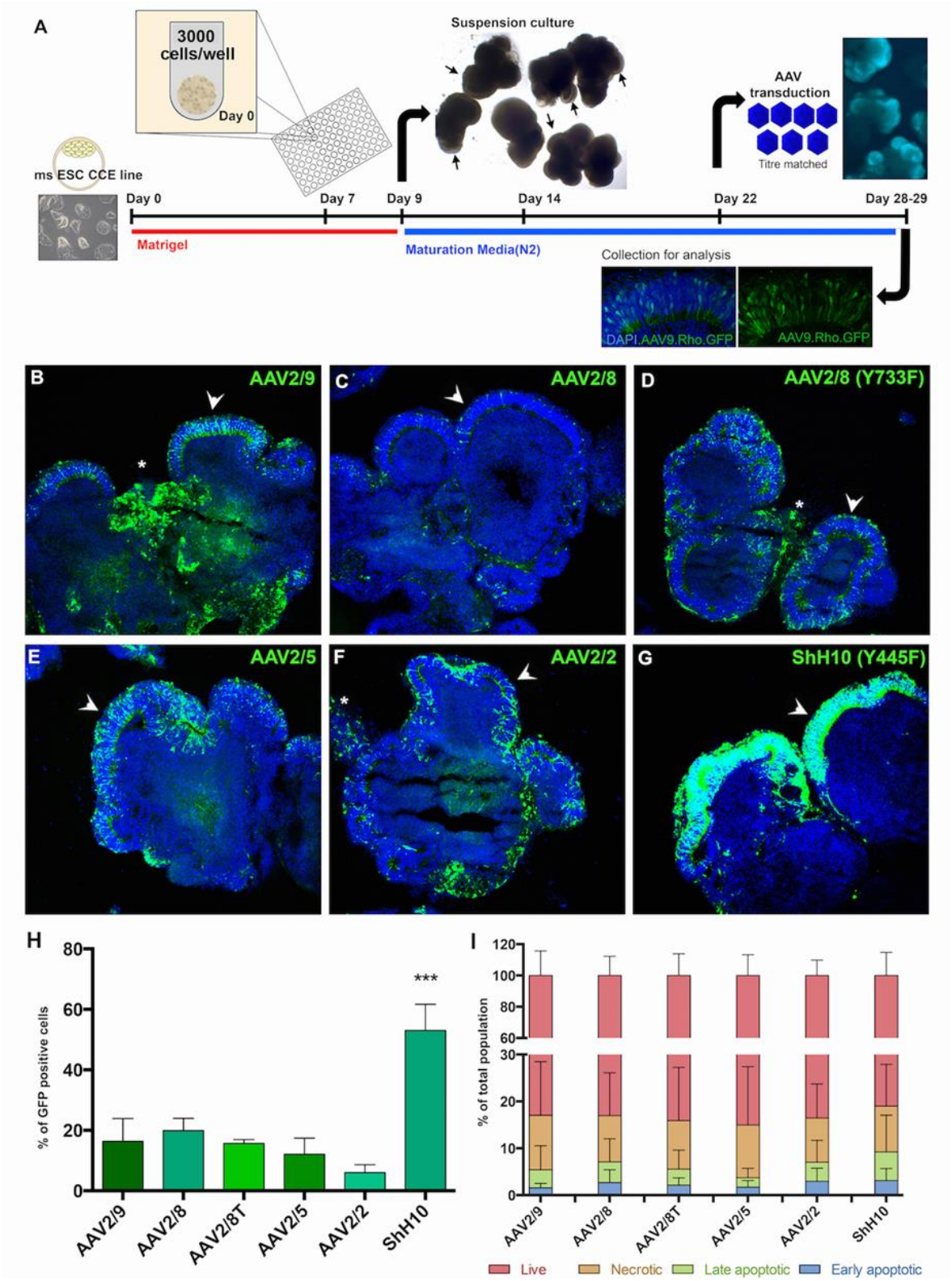

Figure 3.9: Establishing AAV2 tropism in mouse ESC-derived EBs. A. Schematic of 3D differentiation and virus infection protocol. B-G. All tested pseudotypes can transduce neuroepithelial regions (arrow heads), although some also label non-neuroepithelial cell types (asterisk). H. ShH10 demonstrates a significantly higher transduction efficiency in EBs (n = 3; $p < 0.001$), I. without any detrimental effect on cell viability.

Furthermore, inspection of the EBs under light microscopy demonstrated that ShH10.CMV.GFP^{+} labeled cells were not only more numerous but also had a stronger and brighter GFP expression. This was confirmed by flow cytometric measurements of the Median Fluorescent Intensity (MFI), which was normalised to the MFI of a non-virus-tranduced control (Figure 3.10). Such strong expression of GFP in ShH10.CMV.GFP-transduced cells led us to question if there was any detrimental effect on the overall viability of ShH10.CMV.GFP-transduced cultures compared with cultures transduced with the other pseudotypes. This was assessed by staining for Annexin V and DRAQ7, as was done in Section 2.9.1, which allowed us to identify early apoptotic (Annexin V^{+}/DRAQ7^{-}), late apoptotic (Annexin V^{+}/DRAQ7^{+}), necrotic (Annexin V^{-}/DRAQ7^{+}), and live populations (Annexin V^{-}/DRAQ7^{-}). Based on flow cytometric quantification of the percentages of early and late apoptotic, necrotic, and live cells, there appeared to be no significant difference in cell viability following viral transduction between all pseudotypes (Figure 3.9I).

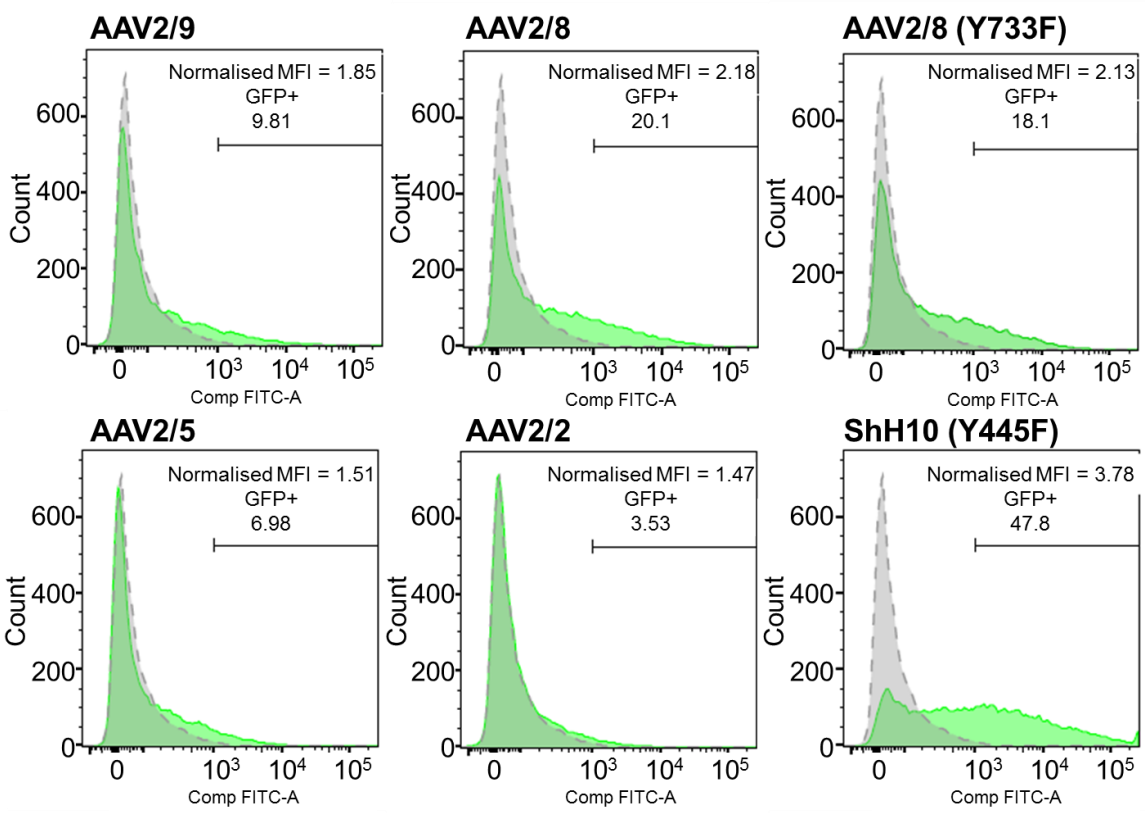

Figure 3.10: Median Fluorescence Intensity measurements of different virus-transduced EBs (normalised to a non-virus-transduced sample).

3.2.4.2 Establishing AAV2 tropism in mouse ESC-derived photoreceptors

Having established the ability of all tested pseudotypes to transduce neuroepithelial regions in EBs, I next sought to compare their efficiency and specificity in the transduction of mouse ESC-derived photoreceptors, which we identified using CD73 as a photoreceptor-specific cell surface marker. The percentage of CD73$^+$ photoreceptor cells at day 29 in culture was consistently around 30-40%, irrespective of differentiation batch or the virus pseudotype used for transduction (Figure 3.11A). The percentage of CD73$^+$ photoreceptors that was labelled with CMV.GFP was significantly greater when cells were transduced with the ShH10 pseudotype (24.7 ± 10.5%) than with the other pseudotypes (Figure 3.11A; $p < 0.001$, ANOVA; n=3 differentiation cultures). As before, flow cytometric analysis of the viability of virus-transduced CD73$^+$/GFP$^+$ double-positive photoreceptors demonstrated that viral transduction by either pseudotype did not cause any detrimental effect on the viability of CD73$^+$ photoreceptors (Figure 3.11B).

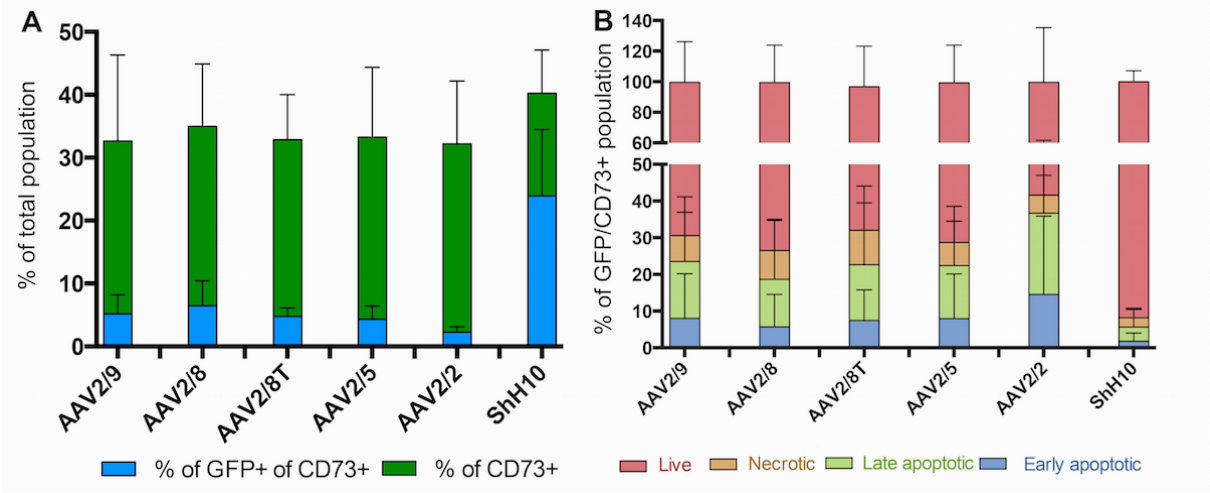

Figure 3.11: Establishing AAV2 tropism in mouse ESC-derived photoreceptors. A. ShH10 demonstrates a significantly higher transduction of CD73$^+$ photoreceptors (n = 3; p = 0.01), B. without any detrimental effect on cell viability.

3.2.4.3 Testing rod promoter specificity in mESC-derived photoreceptors

Having established different pseudotypes' tropism in mouse ESC-derived EBs and photoreceptors, I then sought to assess rod photoreceptor transduction efficiency following infection with the previously-used AAV2/9 capsid and ShH10, the most efficient virus under CMV control as determined previously. To do this, we produced AAV2/9 and ShH10 vectors that each contained the rod-specific bovine Rhodopsin (Rhop.GFP) promoter. At 7 days post-virus transduction, EBs were collected for immunohistochemical staining as well as flow cytometric analysis. Immunohistochemical staining for murine rhodopsin showed that both AAV2/9 and ShH10 Rhop.GFP viruses were selectively expressed in rods, as seen from the co-expression of GFP with rhodopsin in cells within neuroepithelia (Figure 3.12A). Flow cytometric analysis revealed that the percentage of Rhop.GFP$^+$ rods was significantly higher in ShH10.Rhop.GFP-transduced EBs than in AAV2/9.Rhop.GFP-transduced EBs (Figure 3.12B; 23.58 ± 2.3% vs. 16.50 ± 1.6%; $p < 0.05$, unpaired t-test; n=9). Furthermore, the majority (~80%) of the Rhop.GFP$^+$ rod photoreceptors were viable following virus transduction, and no significant difference in viability was observed between AAV2/9.Rhop.GFP and ShH10.Rhop.GFP (Figure 3.12C).

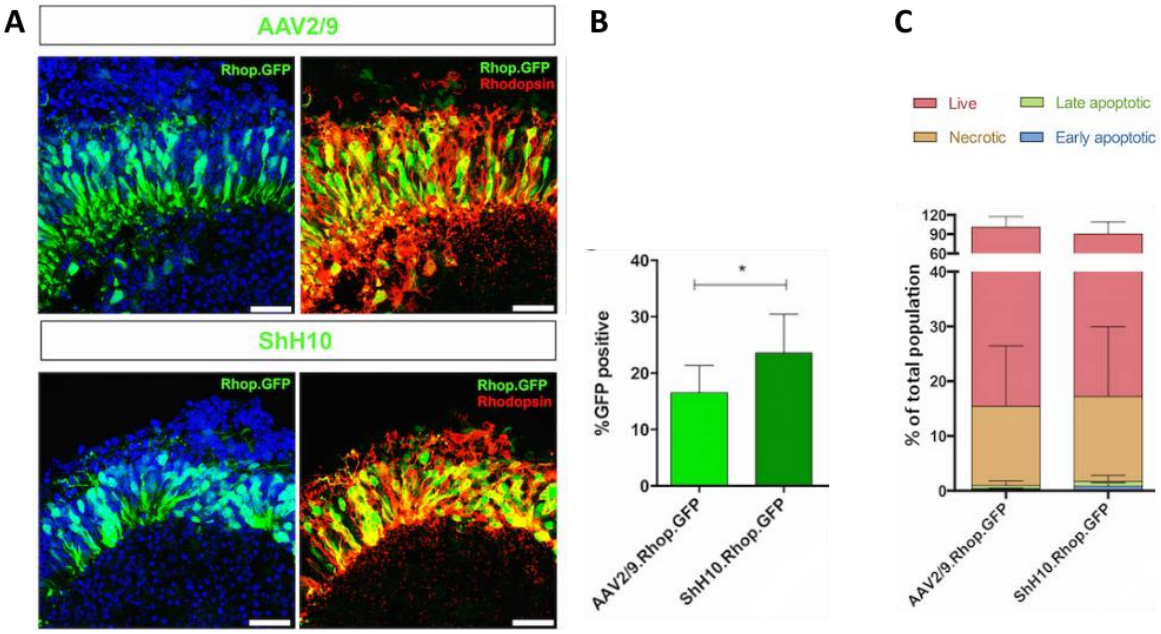

Figure 3.12: Assessing rod promoter specificity in mouse ESC-derived photoreceptors. A. Both AAV2/9 and ShH10 Rhop.GFP effectively label Rhodopsin$^+$ rod photoreceptor precursors in the neuroepithelial layer of EBs. B. ShH10.Rhop.GFP labels a significantly higher proportion of rod precursors compared to AAV2/9 Rhop.GFP (n=3; $p < 0.05$), C. without any detrimental effect on cell viability.

Finally, we compared the number of GFP$^+$ cells in recipient *Gnat1*$^{-/-}$ ONLs following the transplantation of mouse ESC-derived rod photoreceptors labelled with either ShH10.Rhop.GFP or AAV2/9.Rhop.GFP. As done in previous transplantation experiments, 200,000 GFP$^+$ cells/µL was injected in the superior subretinal space of each eye. There was no statistically significant difference between number of GFP$^+$ cells in the host ONL observed between eyes transplanted with ShH10.Rhop.GFP$^+$ cells (1,789.2± 281.8 photoreceptors, n=5 eyes) and those transplanted with AAV2/9.Rhop.GFP$^+$ cells (1,712.4 ± 534.4 photoreceptors, n=5 eyes; $p > 0.05$, Mann-Whitney; Figure 3.13). In addition, there was no difference in the number of eyes rejected from downstream quantification due to macrophage infiltration between both groups (3 out of 8 eyes were rejected from each group). Most importantly, GFP$^+$ cells in the host ONL of eyes transplanted with ShH10.Rhop.GFP$^+$ cells were morphologically similar to wild-type rods (Figure 3.13B), and correctly expressed Gnat1 (Figure 3.13C).

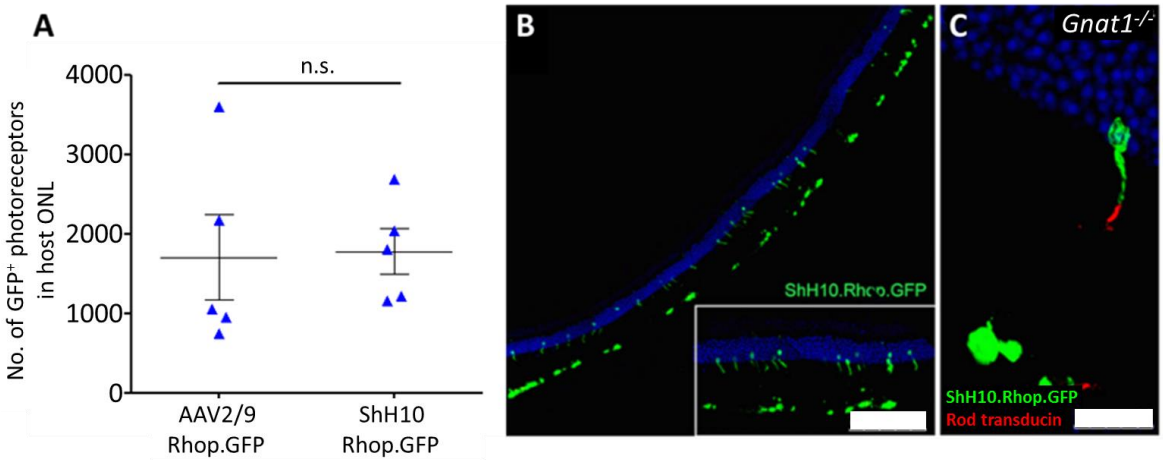

Figure 3.13: Comparing the transplantation of AAV2/9 Rhop.GFP$^+$ and ShH10 Rhop.GFP$^+$ cells. A. The numbers of GFP-labelled photoreceptors present in the host ONL following transplantation of AAV2/9 Rhop.GFP$^+$ versus ShH10 Rhop.GFP$^+$ cells are not statistically significant. B. GFP-labelled cells are present in the recipient *Gnat1*$^{-/-}$ mouse retina following transplantation of ShH10 Rhop.GFP$^+$ cells, and C. correctly express Gnat1. Scale bars: B – 75µm; C – 25µm.

In summary, in light of the above findings, subsequent transplantations of mESC-derived rod photoreceptors were carried out using a ShH10.Rhop.GFP virus to label the EBs *in vitro*, and the Neurosphere Dissociation kit was used for the dissociation of EBs into a single cell suspension for FACS. We have demonstrated that these two changes to the original transplantation protocol were able to increase the proportion of rod photoreceptor precursors labelled *in vitro*, improve the viability of dissociated cells, preserve CD73 antigenicity, and increase the number of GFP^+ cells present in the host ONL following transplantation. With this optimised protocol, an average of 59.4 ± 14.4% (n=5 eyes) of the GFP^+ cells present in the host ONL following transplantation were also $Gnat1^+$, which is comparable to the ~80% of $Gnat1^+$/$Rhop.GFP^+$ cells reported in Gonzalez-Cordero et al. (2013). Most importantly, the average number of GFP^+ cells present in the host ONL following transplantation was increased to an average of 1789.2 ± 281.8 photoreceptors, compared with the initial average of 236 ± 44 photoreceptors (Gonzalez-Cordero et al., 2013).

3.2.5 Understanding and suppressing the recipient immune response to mouse ESC-derived photoreceptors

Allogeneic neonatal donor-derived NrlGFP^{+} photoreceptor precursors were previously shown to induce both an acute innate inflammatory responses as well as an adaptive T cell-mediated immune response following transplantation into recipient mice with partially mismatched H2 haplotypes (West et al., 2010). Similarly, in approximately 30% of eyes transplanted with mESC-derived photoreceptor precursors, we observed macrophage infiltration into the recipient eye by 3 weeks post-transplantation, suggesting an innate inflammatory response. Macrophages appear as distinct large, autofluorescent cells under the light microscope. Macrophage infiltration is always associated with the presence of autofluorescent cell debris within the subretinal space as well as a significant decrease in donor-labelled photoreceptors within the host ONL, and is therefore one of the criteria for exclusion of eyes from further quantitative analysis (see Section 2.7 for details). However, the adaptive immune response to mESC-derived photoreceptor precursor cells has yet to be investigated. As such, I sought to investigate whether mESC-derived photoreceptor precursor cells would elicit an adaptive immune response from the recipient mouse following transplantation, and if suppression of this host immune response would increase the number of reporter-labelled donor cells present in the host ONL post-transplantation.

3.2.5.1 Understanding the adaptive immune response to mESC-derived photoreceptors

A flow cytometric gating strategy was designed to analyse the T cell population in the *Gnat1*$^{-/-}$ eye at 3 weeks after the transplantation of shH10 Rho.GFP-positive cells, using antibodies specific to the cell surface proteins CD45, CD11b, CD4, and CD8a, in combination with a live/dead discrimination dye and the FSC and SSC parameters (Figure 3.14). CD45 was chosen for the panel in order to select for CD45-positive leukocytes, whereas CD11b, a pan-myeloid marker (for macrophages and monocytes, neutrophils, etc.) that also labels non-myeloid natural killer cells, was chosen to identify CD11b-negative lymphocytic T and B cells. Each eye was prepared in a uniform manner, allowing cells in the aqueous humour and vitreous to be analysed together with the retina. Splenic tissue was used for positive controls, whereas uninjected *Gnat1*$^{-/-}$ eyes were used for negative controls.

Debris and cellular aggregates were first excluded, following which, live-dead discrimination was performed to exclusively analyse single live cells. Plotting CD11b against CD45 allowed for isolation of a population of T and B lymphocytes ($CD45^+CD11b^-$), from which CD4-positive and CD8a-positive T cells could be identified. This gating strategy was first validated in splenocytes, before it was applied to cell suspensions prepared from mESC-derived $Rho.GFP^+$ photoreceptor precursor-treated and untreated control eyes.

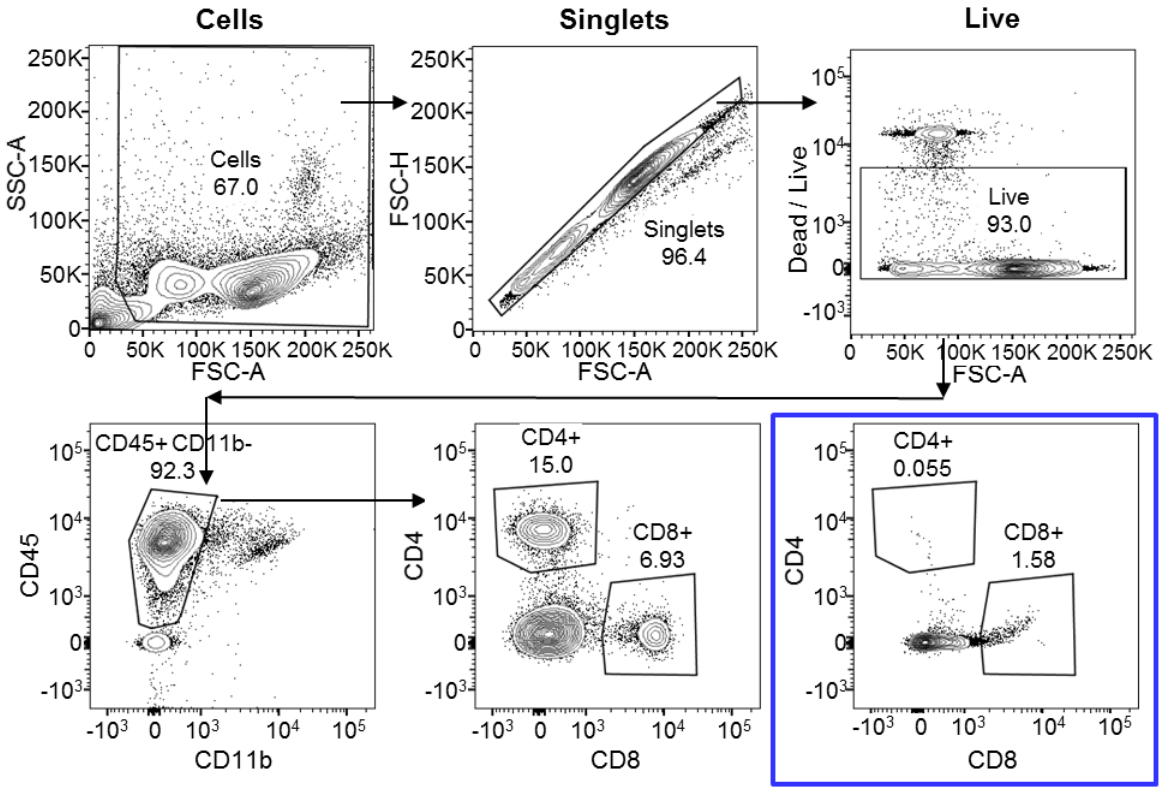

Figure 3.14: Flow cytometry gating showing sequential exclusion of debris, cellular aggregates, and dead cells from $Gnat1^{-/-}$ splenocytes. Lymphocytes were isolated by gating on the $CD45^+CD11b^-$ population, to exclude non-leukocytic ($CD45^-$) as well as myeloid and NK cells ($CD45^+CD11b^+$). The same gating was then applied to treated $Gnat1^{-/-}$ eyes (representative FACS plot in blue box) and negative control untreated $Gnat1^{-/-}$eyes. Numbers in plots indicate percentage of parent population.

The numbers of $CD45^+CD11b^-$ lymphocytes were significantly higher in mESC-derived $Rho.GFP^+$ photoreceptor precursor-treated eyes than in untreated control eyes at 3 weeks post-transplantation (Figure 3.15A; 11,859 ± 6537 vs. 493.7 ± 152.8; $p<0.02$, Mann-Whitney; $n \geq 3$ eyes). Within this lymphocytic population, the majority of cells stained negative for CD4 and CD8; nonetheless, the number of $CD8a^+$ cells was significantly higher in the treated eyes than in the control eyes (Figure 3.15B;137.0±38.4 vs. 34.7±3.5; $p<0.05$, Mann-Whitney; $n \geq 3$ eyes), whereas there was no statistically significant difference between the number of $CD4^+$ cells in the treated eyes and in the control eyes (Figure 3.15B; 4.6 ± 2.9 vs. 0.0 ± 0.0; $p>0.05$, Mann-Whitney; $n \geq 3$ eyes). The total number of T cells present in the treated eyes was significantly greater in treated eyes than in control eyes (Figure 3.15B; 141.6 ± 39.6 vs. 34.7 ± 3.5; $p<0.05$, Mann-Whitney; $n \geq 3$ eyes), which is certainly a result of the increased presence of $CD8^+$ cells in the retina following the transplantation of mESC-derived $Rho.GFP^+$ photoreceptor precursors.

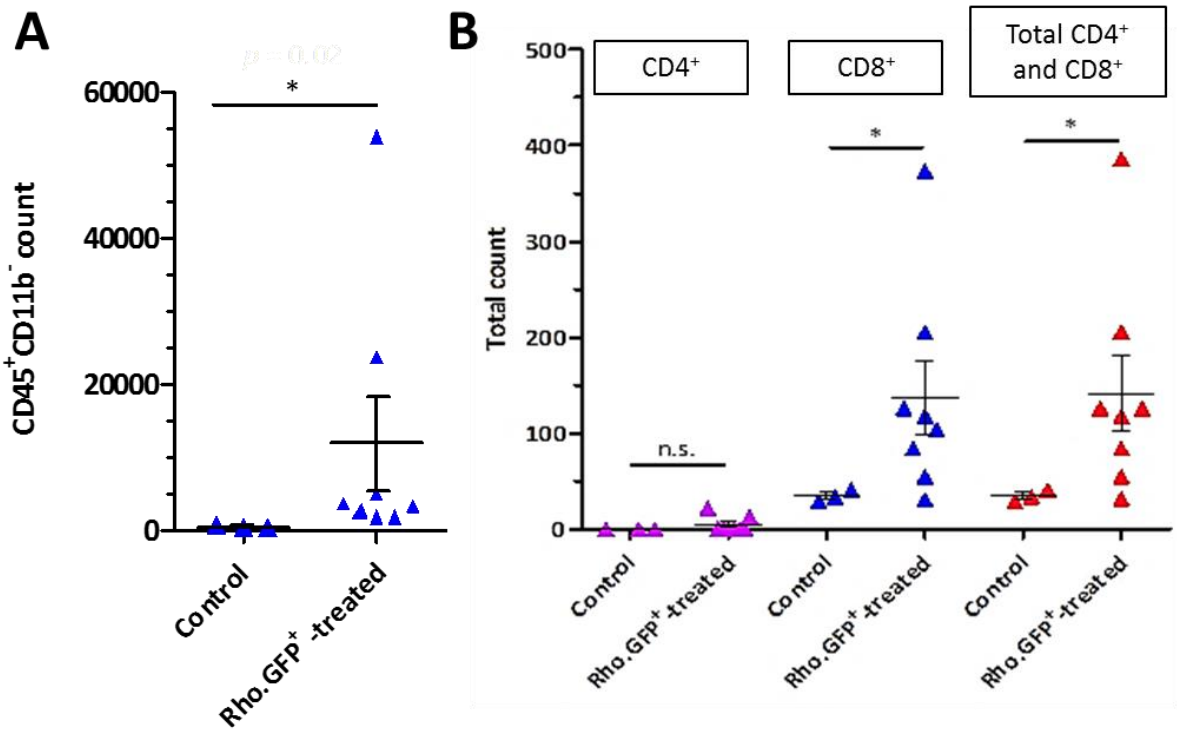

Figure 3.15: Analysis of cell suspensions derived from $Rho.GFP^+$- treated and untreated eyes, using the gating strategy. A. Compared with untreated eyes, a statistically significant increase in the number of $CD45^+CD11b^-$ lymphocytes can be seen in treated eyes. Mann-Whitney, n≥3. B. Compared with untreated eyes, a statistically significant increase in the number of $CD8a^+$ T cells can be seen in treated eyes, whereas the number of $CD4^+$ T cells is similar between treated and untreated eyes. Each point represents one eye, with data pooled from two independent experiments. Mann-Whitney, n≥3. Mean ± SEM is shown in graphs.

In addition, we were able to use flow cytometry to estimate the number of surviving GFP⁺ cells present in each retinal suspension (Figure 3.16A). We excluded the possibility that GFP+ cells included resident or infiltration macrophages that had phagocytosed GFP, by plotting GFP against CD45 (Figure 3.16B). Less than 1.03% of GFP+ cells co-stained with CD45 in any of the 8 retinae, confirming that they were not macrophages or of any leukocytic lineage. Of the 8 treated retinae examined, the average number of GFP⁺ cells present was 2255±1153; however, this was not significantly higher than that present in untreated control retinae (56.0±12.4; Figure 3.16C; $p>0.05$, Mann-Whitney; $n \geq 3$ eyes). The presence of GFP-positive events in the untreated control samples are likely to be due to autofluorescent artefacts which may not have been adequately excluded by the gating strategy (see Figure 3.14); nonetheless, these numbers are small relative to the number of GFP-positive events detected in treated eyes. In addition, the number of CD4⁺ and CD8⁺ T cells did not appear to be proportional to the number of ESC-derived donor GFP⁺ cells present in the eye (Figure 3.16D; $r_s=0.036$, $p>0.05$, Spearman correlation; n = 8 eyes).

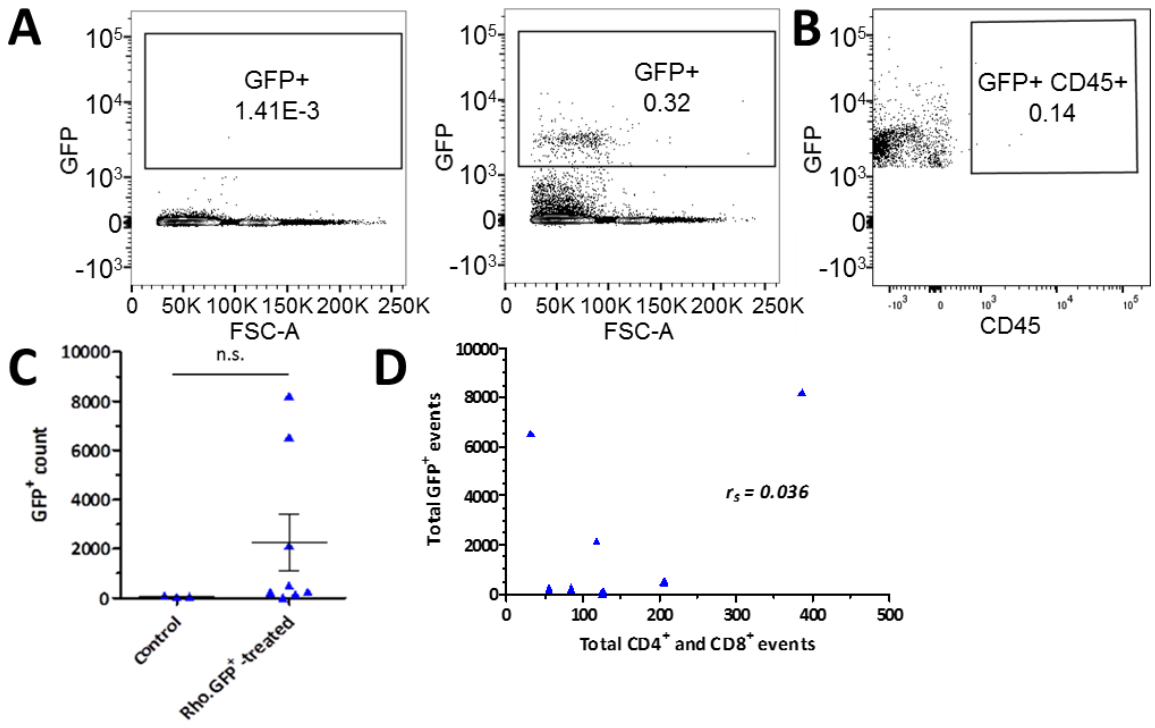

Figure 3.16: A. Flow cytometry gating showing the selection of GFP⁺ events for quantification. B. GFP⁺ populations were assessed for co-staining with CD45, in order to ensure that autofluorescent macrophages were not included in downstream assessment. C. The difference in the mean number of GFP⁺ cells present in treated eyes was not statistically significant, and D. There was no correlation between the number of GFP⁺ cells present in treated eyes and the number of infiltrating CD4⁺ and CD8⁺ cells (Spearman correlation, n=8). Mean ± SEM is shown in graphs.

3.2.5.2 Suppression of adaptive immune responses to mESC-derived photoreceptors with Cyclosporine A (CyA)

To assess the impact of suppressing T cell-mediated immunogenic events following transplantation of mESC-derived photoreceptor precursor cells, I evaluated the use of the T cell-targeting immunosuppressant cyclosporine A (CyA). Here, I hypothesised that if a CD8+ T cell-mediated immune response was a cause of the low numbers of reporter-labelled donor cells present in the host ONL following the transplantation of mouse ESC-derived rods, treatment of the recipient mouse with CyA should increase the number of reporter-labelled donor cells present in the host ONL post-transplantation.

We observed significantly increased numbers of GFP-labelled cells in the recipient ONL of eyes from *Gnat1*$^{-/-}$ mice that had been immune-suppressed with CyA, compared to those from mice that had not received CyA (Figure 3.17A; 3162 ± 501.6 vs. 1750 ± 285.1; p=0.013, Mann-Whitney; n ≥ 9 eyes) across 4 different cohorts of transplantations. Further, CyA administration appeared to have had no adverse effects on the numbers of GFP-labelled cells present in the host ONL following transplantation. Notably, in one of the immune-suppressed *Gnat1*$^{-/-}$ recipients, there was a significantly higher number of GFP-labelled cells in the ONL of one eye, approximately double that of the maximum number seen in the non-immune suppressed recipients (6688 vs. 3606). In both eyes of this particular *Gnat1*$^{-/-}$ recipient, the majority of the GFP-labelled cells in the host ONL expressed Gnat1 (Figure 3.17B(i)'). In addition, in both eyes, transplanted GFP-labelled cells appeared to have migrated away from the site of injection, and were present across the rest of the host ONL in a widespread manner (Figure 3.17B(i)'' and B(ii)). This was not often the case with the majority of our transplants; GFP-labelled cells would typically be observed in close proximity to the transplanted cell mass in the subretinal space. However, an improvement to this degree was not observed in all immune-suppressed mice receiving mESC-derived rod precursor transplants.

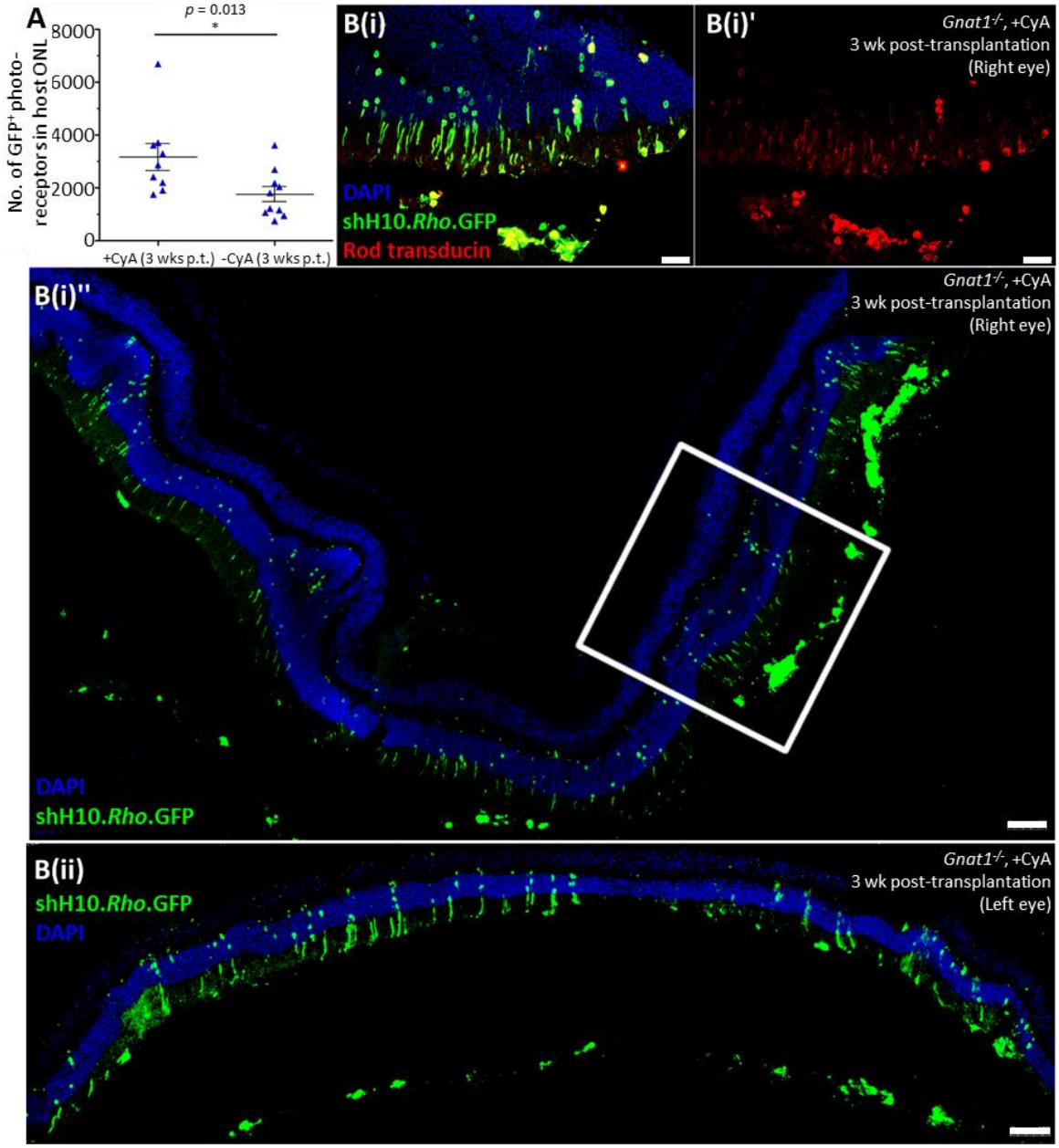

Figure 3.17. Effect of immune suppression with CyA on photoreceptor integration and survival. A. Number of GFP-labelled cells present in host ONL in immune-suppressed vs. untreated recipients, at 3 weeks post-transplantation (mean ± SEM). B(i) and (i)'. Projection confocal images (40X) of GFP-labelled photoreceptors expressing Gnat1, in an immune-suppressed *Gnat1*$^{-/-}$ recipient at 3 weeks post-transplantation. B(i)'' and B(ii). Tile-scan confocal images (10X) of GFP-labelled photoreceptors in the host ONL of either eye of an immune-suppressed *Gnat1*$^{-/-}$ recipient. The region of interest indicated by the white square in B(i)'' is the approximate region where B(i) and (i)' were imaged, using a different slide taken from the same eye. Scale bars: B(i) and B(i)' – 25µm; B(i)'' and B(ii) – 100µm.

In addition, masked assessments were made for evidence of macrophage recruitment in immune-suppressed and untreated control mice. Under light microscopy, macrophages were autofluorescent and had markedly larger nuclei than retinal cells. 5 out of 14 eyes (35.7%) from immune-suppressed recipient mice, compared with 8 out of 18 eyes (44.4%) from untreated control mice, were excluded from further quantitative analysis because of the presence of macrophages in the subretinal space. In keeping with our earlier observations, in eyes showing evidence of macrophage recruitment, there was either a low number or complete absence of GFP-labelled cells in the recipient ONL. As such, compared with non-immune suppressed recipients, a similar proportion of transplants into CyA-treated recipients were subject to an acute inflammatory response, which is expected from using a T cell-targeting immunosuppressant such as CyA.

As a pilot assessment of the long-term survival of GFP-labelled photoreceptors in the host ONL in immune-suppressed recipients, a couple of immune-suppressed *Gnat1*$^{-/-}$ recipients of mESC-derived rod precursors were culled at 6 weeks post-transplantation for quantitative analysis of the transplanted eyes, as previous groups have observed donor-specific delayed hypersensitivity as early as 5 weeks post-transplantation (Jiang et al., 1993; Streilein et al., 2002; Jiang et al., 1995). In the first immune-suppressed recipient, macrophage infiltration had occurred in one eye, whereas there were 2708 GFP-labelled photoreceptors in the ONL of the other eye. In the second immune-suppressed recipient, no cell mass nor evidence of macrophage infiltration was seen in one eye, whereas there were 1120 GFP-labelled cells present in the ONL of the other eye. The GFP-labelled cells present in the host ONL of both eyes displayed normal mature rod morphology with inner and outer segments.

Taken together, these results suggest that both innate and adaptive immune responses mounted by the recipient may collectively compromise the survival of allogeneic mESC-derived rod precursors following transplantation. Suppression of the adaptive T cell response by the use of CyA may have the potential to increase the number of GFP-labelled cells present in the host ONL at the 3-week time point following transplantation; however, this remains to be verified in the long term. Given the wide variation between injections, greater n numbers will be necessary to allow conclusions to be drawn.

3.2.6 Dual subretinal injections

Previous work in our lab has shown that dual subretinal injections of 200,000 donor-derived Nrl.GFP$^+$ cells/1uL injection volume can significantly increase the number and spread of GFP-labelled cells in the host ONL following transplantation (Pearson et al., 2012), although dual injections were also subject to a higher failure rate (R. Pearson, 2016, pers. comm.). Nonetheless, given the improvements seen thus far with the optimised transplantation protocol for mESC-derived photoreceptor precursors, I investigated whether doubling the density of mESC-derived photoreceptor precursors transplanted by giving recipient mice dual injections would further increase the number of reporter-labelled donor cells present in the host ONL following transplantation.

For this set of experiments, the donor photoreceptor precursors were derived from a transgenic mESC line in which GFP expression is driven by the endogenous Crx promoter (Decembrini et al., 2014). This Crx.GFP mESC line is characterised in greater detail in Chapter 4, where Crx.GFP$^+$ cells isolated at day 26 in culture were shown to be developmentally equivalent to P7-8 Nrl.GFP$^+$ photoreceptors. The Crx.GFP line was therefore chosen over the previously-used E16 line, in order to ensure that there would be a sufficient number of GFP-expressing photoreceptor precursors available for dual injections into each eye, without having to produce large amounts of ShH10.Rhop.GFP virus to label the E16 line.

Unfortunately, 6 out of 6 eyes (100%) that were given dual injections of day 26 Crx.GFP$^+$ photoreceptor precursors either showed evidence of macrophage infiltration, or had no cell mass present when assessed at 3 weeks post-transplantation. In comparison, 6 out of 20 (30%) eyes that received a single injection of day 26 Crx.GFP$^+$ photoreceptor precursors showed evidence of macrophage infiltration.

This result may be indicative of the greater immunogenicity of mESC-derived photoreceptor precursors compared to donor-derived photoreceptor precursors, which would account for the higher frequency of innate macrophage-mediated responses mounted in recipient animals treated with dual injections of mESC-derived photoreceptor precursors.

3.3 Discussion

3.3.1 Assessing photoreceptor viability in vitro

Previous work in our lab on transplanting mouse ESC-derived Rhodopsin.GFP-positive rod precursors into *Gnat1*$^{-/-}$ recipient mice observed a consistently lower number of GFP^{+} cells present in the host ONL following transplantation (Gonzalez-Cordero et al., 2013), compared with that achieved with the transplantation of donor-derived rod precursors. We hypothesized that the presence of early apoptotic photoreceptor precursors in the *in vitro* 3D culture at late time points, and subsequently in the donor cell population, may contribute to poor survival and development post-transplantation, resulting in low numbers of reporter-labelled donor cells observed in the host ONL following transplantation of Rhop.GFP^{+} cells at later days in culture.

As such, we first assessed the viability of cells in the neuroepithelial layer of EBs on days 29, 34, and 36 of culture, which correspond to P4-6, P8, and P12 wild-type retinas respectively in terms of developmental stage. Our assessment of photoreceptor viability *in vitro* indicated that our current 3D culture conditions are unable to fully support EB differentiation in the long term, as seen from the increased neuroepithelial disorganisation after day 29 in culture. Although there was a trend towards an increase in the proportion of early apoptotic cells present in the neuroepithelial at later time points in culture, the proportion of early apoptotic cells was relatively low even at the later time points (~8-16%). However, while long term support of retinal differentiation *in vitro* may indeed be beneficial for other purposes such as disease modelling, for the purpose of transplantation, the low proportion of early apoptotic cells as well as the preservation of neuroepithelial morphology at day 29 indicates that the viability of the *in vitro* culture prior to transplantation is unlikely to be the primary cause for the observed low numbers of GFP-labelled cells present in the host ONL following transplantation.

Furthermore, the exclusion of early apoptotic cells from the transplanted mESC-derived Rhop.GFP^{+} donor population did not significantly increase the number of GFP^{+} cells observed in the host ONL following transplantation. Taken together, the presence of early apoptotic cells in *in vitro* cultures and in the transplanted donor

population did not appear to account for the low numbers of GFP$^+$ cells observed in the host ONL following transplantation of mESC-derived Rhop.GFP$^+$ rod precursors.

3.3.2 Optimisation of dissociation method

Methods of tissue dissociation vary widely in dissociation efficiency, viability, and antigen retention. These effects are dependent on numerous parameters, including tissue type, dissociation media, type and concentration of enzymes used, incubation times and temperature. It is therefore crucial to choose a dissociation protocol that will enable us to obtain a maximum yield of functionally viable, single cells. Papain has been widely used for isolating high yields of viable, morphologically intact neuronal cell types from the cortex and retina (Huettner and Baughman, 1986; Hilgenberg and Smith, 2007; Tabata et al., 2000); however, the incubation time required tends to be significantly longer as papain is more gentle compared with other proteases. In addition, EBs are aggregates grown in suspension culture, which are particularly difficult to dissociate into single-cell suspensions without killing a substantial proportion of cells. In the original mESC-derived photoreceptor transplantation protocol, 0.25% trypsin was chosen over the Worthington Papain Dissociation System used for the donor-derived photoreceptor transplantation protocol, because trypsin is a stronger protease than papain and also required a significantly shorter incubation time. Earlier work by colleagues had found that 0.25% trypsin was the minimum concentration required for efficient dissociation of EBs (A. Gonzalez-Cordero, pers. comm.), whereas collagenase was not effective for deriving a single cell suspension from neonatal retinal tissue (R. Pearson, pers. comm.). As such, here I compared three specialised papain-based kits for Neural Tissue, Neurosphere, and Embryoid Body dissociation (Miltenyi Biotec, UK) with the previously-used 0.25% Trypsin and the Worthington Papain Dissociation System, on the basis of dissociation efficiency, cell viability, retention of CD73 antigenicity, and most importantly, the number of reporter-labelled donor cells in the host ONL post-transplantation.

Notably, across the different dissociation protocols assessed, all the papain-based protocols consistently yielded efficient dissociation of mouse ESC-derived EBs into single viable cells, with significantly lower levels of early and late apoptosis compared with the 0.25% trypsin protocol. This confirms findings from other groups, who have shown that trypsin is more toxic to neuronal cell types compared with

papain (Kaiser et al., 2013; Fitzgerald et al., 1992). The papain-based Neurosphere Dissociation Kit, which has the shortest incubation time, appeared to offer the best balance of a short incubation time without compromising on dissociation efficiency and cell viability, which were at levels comparable to that of Nrl.GFP donor-derived rod photoreceptor precursors dissociated with the Worthington Papain Dissociation Kit. Furthermore, there was a slight trend towards a greater proportion of transplanted eyes being rejected from downstream quantitative analysis due to macrophage infiltration in the 0.25% Trypsin group, as compared with the Neurosphere Dissociation Kit group. This may indicate that a higher proportion of apoptotic cells within the transplanted donor cell population could lead to the invasion of macrophages and increased frequency of macrophage-mediated graft rejection.

The choice of enzyme for tissue dissociation is also known to affect antigen retention. Distinct antigen epitopes have been shown to exhibit characteristic sensitivities to either trypsin or papain, or both (Panchision et al., 2007; Pennartz et al., 2009). Here, I focused on the retention of CD73, an established cell surface marker of post-mitotic photoreceptor precursor cells and mature photoreceptors that has been shown to be important for the isolation of transplantation-competent cells (Koso et al., 2009; Eberle et al., 2011; Lakowski et al., 2011; Eberle et al., 2012, 2014; Lakowski et al., 2015). Flow cytometric analysis showed that trypsin degraded CD73, whereas all the papain-based protocols preserved CD73 antigenicity. This lends further support to the use of papain instead of trypsin for dissociating EBs prior to cell sorting. Although our lab has focused our efforts thus far on isolating transplantation-competent ESC-derived donor cells via photoreceptor-specific transgene expression, the preservation of cell surface biomarkers enabling the isolation of similarly-staged transplantation-competent donor cells is nonetheless pertinent for clinical application, as established by Lakowski *et al.* (2015). This recent study demonstrated for the first time the possibility of using a cell surface biomarker panel to effectively enrich 3D retinal differentiation mESC cultures for rod precursors at a developmental stage equivalent to the postnatal time window of transplantation competence (P4–P8) for donor cells isolated from the developing retina. In this study, CD73 and CD133 were used to delineate developing rods, CD24 and CD47 were used as markers of immature postnatal retinal cells, and the retinal progenitor marker CD15 (SSEA-1) was utilised for negative selection to remove mitotically active

progenitor cells. Interestingly, while Panchision et al. (2007) showed preservation of CD133 and CD15 but not CD24 antigenicity after papain dissociation of mouse fetal cortex tissue (12 units/mL papain, 30min) (Panchision et al., 2007), Lakowski et al. (2015) showed retention of all three markers following papain dissociation (20 units/mL papain, 30-40min) of mouse ESC-derived EBs. This difference may have been due to variation in enzyme composition, lot-to-lot variability, tissue handling or tissue type; regardless, it demonstrates the necessity of verifying that the dissociation method chosen is compatible with target antigens.

Finally, we demonstrated that the use of the papain-based Neurosphere Dissociation Kit instead of 0.25% Trypsin to dissociate mouse ESC-derived EBs for FACS and transplantation, significantly increased the number of reporter-labelled donor cells present in the host ONL post-transplantation. While this could be due in part to the higher viability of papain-dissociated cells, papain digestion may have allowed for the retention of particular cell surface proteins essential for cell survival, migration or maturation, which were previously lost after trypsin digestion. Others in the lab have observed significantly increased numbers of reporter-labelled donor cells present in the host ONL post-transplantation with the use of collagenase over the Worthington Papain Dissociation Kit for the dissociation of Nrl.GFP retinas, despite poorer single cell isolation with the collagenase (R. Pearson, pers. Comm.). These observed differences in transplantation outcome between the dissociation enzymes may reflect differing effects of the dissociation enzyme used on the retention of cell surface proteins. Future work could therefore investigate the differences in cell surface marker retention between different dissociation enzymes, which may have an impact on the number of donor-reporter labelled cells present in the host ONL following transplantation.

Given that the papain-based Neurosphere Dissociation Kit was able to give us high yields of viable photoreceptor precursor cells within a short incubation time, and resulted in significantly higher numbers of reporter-labelled donor cells present in the host ONL post-transplantation, this dissociation protocol was used for all subsequent experiments requiring the dissociation of EBs into single cell suspensions.

3.3.3 Optimisation of viral pseudotype for labelling of rod precursors

To increase the yield of rod photoreceptor precursors that could be obtained from *in vitro* cultures for transplantation, I compared the transduction efficiency of six AAV2 pseudotypes (AAV2/9, AAV2/8, AAV2/8T(Y733F), AAV2/5, AAV2/2 and ShH10(Y445F)) driving eGFP expression on mouse ESC-derived photoreceptors. A wide range in transduction efficiencies was observed across the different pseudotypes. Notably, the ShH10 pseudotype, a AAV6 variant generated through directed evolution, demonstrated the most robust transduction of mouse ESC-derived rod photoreceptor precursors, on the basis of significantly improved efficiency in the labelling of rod precursors.

In addition, photoreceptors are very metabolically active, and may therefore be sensitive to changes in gene expression levels. The ideal viral pseudotype for our purposes should demonstrate specific tropism for photoreceptor cells in order to achieve sufficient levels of transgene expression without causing photoreceptor toxicity. We established that even the high level of GFP expression achieved by ShH10 transduction does not have any detrimental effects in terms of cell viability.

Cell replacement therapy requires large numbers of donor cells, and by testing the optimal AAV2 pseudotypes for transduction of photoreceptors, we were able to demonstrate that a greater number of Rhop.GFP$^+$ cells can be obtaining when the ShH10.Rhop.GFP virus is used as opposed to the AAV2/9. Rhop.GFP virus used in our previous studies. Most importantly, GFP-labelled cells are present in the recipient *Gnat1*$^{-/-}$ mouse retina following the transplantation of ShH10 Rhop.GFP$^+$ cells, at levels similar to those in eyes transplanted with AAV9 Rhop.GFP$^+$ cells, and also correctly express Gnat1.

3.3.4 Immune response of recipient mice and immune suppression

Earlier work by our lab demonstrated that the transplantation of allogeneic neonatal donor-derived Nrl.GFP$^+$ rod precursors into the subretinal space of wild-type mice induces both innate and adaptive host immune responses, despite the subretinal space being commonly thought of as an immune-privileged site (West et al., 2010). We have observed a similar macrophage presence in a proportion of injected eyes by 3 weeks post-transplantation, which is suggestive of an innate inflammatory response. In Section 3.2.5.1, we assessed the adaptive immune response directed against allogeneic mESC-derived Rho.GFP$^+$ rod precursors *in vivo* following transplantation, as well as the effect of suppressing this response with CyA on the presence of GFP-labelled cells in the host ONL following transplantation.

Our data suggests that a predominantly CD8$^+$ T cell-mediated immune response is mounted against mESC-derived rod precursor donor cells by 3 weeks following transplantation into the subretinal space of *Gnat1*$^{-/-}$ mice. The induction of an adaptive immune response is unsurprising, given that our mESC-derived Rho.GFP$^+$ cells (E16 line; 129/SvEv; H2^b) are transplanted into *Gnat1*$^{-/-}$ recipients (129S1/Sv x BALB/c; H2$^{b/d}$), constituting a partial mismatch of H2 haplotypes (or, the major histocompatibility class (MHC) molecule profile in mice). This partial mismatch is also present in the transplantation of donor-derived Nrl.GFP precursors (C57BL/6 x SJL/J Nrl.GFP; H2$^{b/s2}$) into C57BL/6 (H2^b) recipients. A difference in the H2 haplotype between donor cells and recipient mice is one of the key players in stimulating alloantigen recognition. Classically, the host T cell immune response is triggered through two possible pathways: in the direct pathway, the recognition of intact allogeneic MHC molecules on donor cells is mediated by donor antigen-presenting cells (APCs) that express co-stimulatory molecules; whereas in the indirect pathway, recognition of processed alloantigens in peptide form, derived from allogeneic MHC molecules or minor histocompatibility (miH) antigens, is mediated by host APCs. In the context of mESC-derived photoreceptor precursor transplantation, it is likely that the indirect pathway is the dominant pathway for the induction of a T cell response, given that ESC-derived tissues are likely to lack donor-derived APC. In contrast, allogeneic neonatal donor-derived tissue grafts are likely to trigger a T cell response via the direct pathway, as they may contain passenger APCs that have the potential to migrate to secondary lymphoid organs and elicit a robust, accelerated adaptive immune response (Wu et al., 2008; Streilein et al., 2002).

We observed a significant increase in T cell presence at 3 weeks post-transplantation; however, we were unable to establish by flow cytometry whether this T cell mediated response was correlated to a decreased number of surviving GFP$^+$ cells. This may be due to the variation between injections, as well as limitations in the method of tissue preparation, in which a proportion of injected GFP$^+$ cells may have adhered to the RPE and been discarded. Immunohistochemical staining may prove to be a more reliable method of assessing the correlation between the T cell response and the number of surviving transplanted GFP$^+$ cells over time. Similar to our observations, West et al. (2010) showed immunohistochemical evidence of a T cell response to transplanted allogeneic Nrl.GFP$^+$ cells at 3-4 weeks, although a corresponding decrease in the number of surviving GFP$^+$ cells was only observed between 2-4 months post-transplantation (West et al., 2010). Initial studies on the transplantation of full thickness neonatal retinal sheet allografts in the subretinal space reported deterioration of the grafts as early as 1 month post-implantation, apparently coinciding with onset of donor-specific delayed hypersensitivity (Jiang et al., 1993; Jiang et al., 1995; Streilein et al., 2002), which was likely to have been triggered via the direct pathway. We hypothesized that the immunogenicity of mESC-derived Rho.GFP$^+$ rod precursors would be less compared with retinal sheet allografts, but more compared with neonatal donor-derived Nrl.GFP$^+$ rod precursors. There is evidence to suggest that prolonged maintenance and differentiation of ESCs *in vitro* may lead to cell surface expression of novel immunogenic molecules, while embryonic antigens may persist even after directed differentiation, both of which represent additional targets of immunological attack on ESC-derived rod precursors (Tang et al., 2013; Nasonkin and Koliatsos, 2006). For these reasons, we expect allogeneic ESC-derived rod precursors to elicit a more robust T cell-mediated rejection response compared with donor-derived Nrl.GFP$^+$ rod precursors. Further work is necessary to investigate the correlation between T cell response and the survival of injected ESC-derived rod precursors at later time points, in order to determine whether the T cell response mounted against ESC-derived rod precursors is sufficient to cause significant cell loss in the long term, and to compare this with donor-derived precursors.

Our flow cytometric data also showed that the majority of the T cells present in the retinal suspensions derived from treated eyes were CD8a-expressing cytotoxic T cells, whereas CD4-expressing helper T cells were not significantly upregulated compared with untreated eyes. There appears to be much controversy in existing literature over the mechanisms and interactions underlying T cell responses, and it is difficult to make comparisons between studies owing to a variety of factors influencing the nature of the response, such as the source of the donor graft, the immune profile of the recipient, as well as the site of transplantation. While some studies argue that $CD4^+$ T cells are necessary and sufficient to cause allogeneic graft deterioration without the need for $CD8^+$ T cells (Anosova et al., 2001; Janssen et al., 2003; Shedlock and Shen, 2003; Johansen et al., 2004), others have conversely demonstrated that $CD8^+$ T cells are able to independently generate both effector and memory T cells, prevent tolerance induction by co-stimulatory molecule blockade, and mount an effective rejection of allogeneic tissue in the complete absence of $CD4^+$ T cells (Jones et al., 2000; Trambley et al., 1999; Jones et al., 2006). In addition, the majority of the $CD45^+CD11b^-$ population present in treated eyes was $CD4^-CD8^-$. In the context of the spleen, these would presumably be B lymphocytes; however, it would be unexpected to see B lymphocytes infiltrating the eye in an adaptive immune response to a transplanted allograft. Including a B-cell specific marker, such as B220, in the FACS panel may be helpful for verifying the identity of this population. Alternatively, immature natural killer cells, which may not have commenced expression of CD11b (Vosshenrich et al., 2005) may constitute a proportion of the $CD45^+CD11b^-$ population.

We hypothesized that ESC-derived photoreceptor precursors are more immunogenic than neonatal donor-derived photoreceptor precursors, and would therefore elicit a more rapid and robust immune response following transplantation in immunocompetent hosts. This may account for the lower number of reporter-labelled donor cells present in the host ONL following transplantation of ESC-derived photoreceptor precursors compared with neonatal donor-derived photoreceptor precursors. As we observed a predominantly $CD8^+$ T cell-mediated response against ESC-derived photoreceptor precursors by 3 weeks post-transplantation, we investigated whether the immunosuppression of recipient *Gnat1*$^{-/-}$ mice with CyA would result in an increased number of GFP^+ cells present in the host ONL at 3 weeks after the transplantation of mESC-derived Rho.GFP^+ rod precursor cells.

At 3 weeks post-transplantation, in immune-suppressed recipient mice that were given subretinal injections of mESC-derived Rho.GFP$^+$ rod precursor cells, there was a statistically significant increase in the mean number of GFP$^+$ cells in the host ONL compared with recipients that were not treated with CyA, and this increase was particularly marked in one of the CyA-treated recipients. However, this degree of improvement was not observed in the other immune-suppressed recipients. This variation in the number of surviving reporter-labelled donor cells present in the host ONL following transplantation is likely to represent not only variation during the transplantation protocol, but also the significant variation in the extent of immune suppression effected on individual recipient animals. Undergoing long-term, regular injections is painful for the animals and may confound any downstream behavioural analysis by inducing behavioural changes, while oral drug delivery does not permit accurate dosing, and our mice were occasionally observed to avoid drinking water containing CyA. An alternative method of administrating CyA, such as incorporating the drug into a standardised volume of sweet jelly that recipient mice are trained to eat (Zhang, 2011), may reduce variation between individuals. A method of CyA administration that allows long term dosing would be advantageous for future studies on the effect of CyA immunosuppression on long term survival of transplanted ESC-derived cells in the recipient. Jensen et al. (2012) demonstrated that the subcutaneous injection of 10mg/kg/day of CyA for 7 days, beginning 2 days prior to grafting, followed by 10 μg/mL in drinking water was sufficient to suppress the recipient rat T cell response against intracerebral human ESC-derived neural progenitor grafts, and had a pro-survival effect at 2 weeks post-transplantation (B. Jensen, 2012). For our purposes, we modified this protocol by increasing the duration of subcutaneous injections from 7 to 10 days, keeping the CyA dosage constant. Nonetheless, to account for the results seen in our CyA-treated recipient mice, it may be beneficial to assess the extent of T cell suppression in each individual. This could be done by examining the cervical lymph nodes following the 10 day CyA injection period, as well as 3 weeks after (corresponding to when recipient mice are usually culled for analysis). FACS analysis of T cell proliferation following T cell receptor stimulation in the draining cervical lymph nodes will reflect the environment local to the subretinal space and enable us to verify immune suppression following the CyA regime.

In 2 out of 4 eyes of CyA-treated recipients examined at 6 weeks post-transplantation, we found the persistence of reporter-labelled donor cells in the host ONL. The number of reporter-labelled donor cells present in these 2 eyes were similar to the average number seen at 3 weeks post-transplantation in an immune-suppressed recipient. Further experiments including non-immune suppressed recipient controls at later time points after transplantation will be necessary to ascertain the effect of CyA immune suppression on the long term survival of ESC-derived donor cells. 6 weeks post-transplantation may be too early to assess any long term effect of CyA; a longer survival period of up to 4 months may prove more revealing (West et al., 2010).

Finally, we have consistently observed evidence of increased macrophage recruitment corresponding to low numbers of reporter-labelled donor cells present in the host ONL following transplantation in approximately 30-45% of our transplants. Our assessment of macrophage recruitment showed that a similar proportion of CyA-treated immune-suppressed and non-immune suppressed recipient mice mounted an innate immune response against transplanted ESC-derived photoreceptor precursors. This is in agreement with previous reports noting that acute innate inflammatory responses are largely unaffected by CyA (Snyder, Lai, et al., 1998; Lu et al., 1996). Additional short-term control of the early inflammatory response against injected cells, such as the use of steroids like dexamethasone, may be beneficial in further limiting graft destruction and leaving sufficient functional cells to exert a therapeutic effect. Suppressing the early innate macrophage-mediated host response against injected ESC-derived photoreceptor precursors may also allow an increased density of ESC-derived photoreceptor precursors to be injected into recipient mice via dual subretinal injections with minimal macrophage recruitment.

The use of transgenic animals lacking specific immune cells may be useful in demonstrating proof of concept of the nature of host immune responses mounted against ESC-derived photoreceptor precursors. In addition, numerous other methods of immune modulation are now available (see review by (Wood et al., 2016)), and the use of these methods to target specific aspects of host immune response to ESC-derived donor cells may greatly aid the translation of stem cell therapy to the clinic.

3.4 Conclusion

In this chapter we investigated various ways of optimising the transplantation of mouse ESC-derived rod photoreceptor precursors in order to increase the number of reporter-labelled donor cells present in the recipient retina post-transplantation.

Notably, the choice of a papain-based dissociation method over the use of trypsin appeared to be a crucial factor for improving the number of donor-reporter labelled cells observed in the host ONL following transplantation, which may be a result of increased cell viability and/or the retention of specific cell surface antigens. This is an important principle to bear in mind when choosing a dissociation protocol for preparing single cell suspensions, as the effect of various dissociation techniques and proteases will differ depending on the nature of the tissue being dissociated, and it is essential to systematically characterise these effects before moving forward. As the papain-based Neurosphere Dissociation Kit provided the best balance of a high dissociation efficiency, improved cell viability, a short protocol length, CD73 retention, and was shown to significantly increase the number of donor-reporter labelled cells observed in the host ONL following transplantation, all future experiments involving the dissociation of mESC-derived EBs into single cell suspensions were performed using the papain-based Neurosphere Dissociation Kit.

Another principle arising from these experiments was the importance of selecting the appropriate AAV pseudotype for transducing specific cell types. We compared the AAV transduction efficiencies of mouse ESC-derived cultures *in vitro*, and found that the ShH10 pseudotype demonstrated superior transduction of mouse ESC-derived rod photoreceptor precursors compared with the other AAV2 pseudotypes tested, without having any detrimental effects on cell viability. The use of the ShH10.Rhop.GFP virus instead of the AAV2/9.Rhop.GFP virus to label mESC-derived rod precursors therefore enabled us to obtain a greater number of rod precursors from *in vitro* cultures for transplantation. We later acquired a Crx.GFP mESC line, in which GFP expression is driven by the endogenous Crx promoter (kind gift of Prof. Y. Arsenijevic, (Decembrini et al., 2014)), thereby negating the need for viral labelling of photoreceptor precursors in subsequent experiments. Nonetheless, these experiments emphasise the benefits of testing promoter specificity and choosing the appropriate AAV pseudotype for efficient transduction of the targeted cell type, in order to achieve sufficient but non-toxic levels of transgene expression.

Similar experiments of this nature will be particularly relevant in establishing the most efficient pseudotypes for transducing different human pluripotent stem cell-derived cell types, which will be a crucial step for gene therapy clinical trials where targeted gene supplementation is crucial (Gonzalez-Cordero et. al., in press).

Finally, we developed a flow cytometric panel and gating strategy to allow quantitative analysis of the T cell response to donor cells transplanted in the subretinal space of recipient mice. We established that an adaptive $CD8^+$ T cell-mediated response was mounted against mESC-derived Rhop.GFP^+ photoreceptor precursors with partially-mismatched H2 haplotypes, and assessed the effect of suppressing this T cell response with CyA on the number of GFP^+ cells present in the host ONL at 3 weeks post-transplantation. Our results suggest that treating recipient mice with CyA may improve this outcome measure, although it will be necessary to develop a long-term dosing method as well as an assessment of the extent of immune suppression by CyA. Nonetheless, these experiments confirmed the presence of a host immune response against transplanted mESC-derived photoreceptor precursor cells, and represent the first steps towards addressing this challenge for the translation of ESC-derived photoreceptor precursor transplantation to the clinic.

Chapter 4 : Development of a photoreceptor reporter knock-in mESC line

4.1 Introduction

In the previous chapter, we optimised the transplantation protocol by using an ShH10.Rhop.GFP virus to label the mESC-derived EBs and dissociating the EBs with the papain-based Neurosphere Dissociation Kit for FACS and transplantation. This increased the number of reporter-labelled donor cells present in the host ONL at 3 week post-transplantation by more than three-fold – at present, the average number of reporter-labelled donor cells observed in the host *Gnat1*$^{-/-}$ ONL following a single subretinal injection of shH10.Rhop.GFP^{+} cells without host immunosuppression is 1,750±285.1, with a maximum of 3,606 GFP^{+} cells. However, this is still significantly lower than the average and maximum numbers observed in recipient *Gnat1*$^{-/-}$ eyes given dual injections of P8 Nrl.GFP^{+} cells (18,300±1474; maximum of 32,015 GFP^{+} cells respectively). Excluding early apoptotic cells from the donor population and suppressing the host T cell response only partially mitigates this problem and a significant proportion of the transplanted mESC-derived rod precursors remains in the cell mass at the site of injection.

While measures such as suppressing the host immune response and administering dual injections do indeed have the potential to increase the number of GFP^{+} cells present in the host ONL and warrant further investigation, as discussed in the previous chapter, they are based on the assumption that that day 29 Rhop.GFP^{+} mESC-derived rod precursors are developmentally equivalent to postnatal day 8 Nrl.GFP^{+} cells. It is, however, possible that due to the heterogeneous nature of the mESC differentiation *in vitro* (Decembrini et al., 2014; Gonzalez-Cordero et al., 2013; Eiraku et al., 2011), the Rhop.GFP^{+} population presently isolated by FACS for transplantation on day 29 in culture is comprised of a mixed population of rod precursors of varying maturity, whose birth times span a wide range of days in culture. Furthermore, *in vivo*, rods are born over a broad developmental window, and, depending on the time of their birth ('early' or 'late'), post-mitotic rod precursors exhibit variable delays before expressing rhodopsin (Akimoto et al., 2006). The capacity to migrate from the injected cell mass and integrate into the host ONL may thus vary widely even within this post-mitotic rod precursor population. Taken together, these points suggest that further specification of the donor cell population may be required.

Therefore, in this chapter, we aimed to investigate whether there is a window of optimal transplantation competence in our mouse ESC-derived rod precursor population, the beginning and end of which could be defined and selected for using temporally-expressed developmental markers. Defining such a window may be necessary for the isolation of a homogeneous population of transplantation-competent donor cells from the otherwise heterogeneous populations that arise from our mESC differentiation protocol, and may contribute towards improving transplantation efficiency.

To this end, we planned to develop a triple transgenic endogenous reporter mESC line (Crx.GFP::Rho.mCherry::Gnat1.Katushka) that will enable us to track the stage of differentiation of *in vitro* cultures and isolate stage-specific, developmentally-homogenous populations, without the need for viral-labelling, which can lead to false-positives, as we have demonstrated previously (West et al., 2012). Crx, Rhodopsin, and Gnat1 were chosen as developmental markers that represent early, mid and late stages of post-mitotic rod photoreceptor maturation. Crx is a transcription factor expressed early on in photoreceptor specification, whereas the rod visual pigment rhodopsin is expressed slightly later on around the onset of segment formation. Gnat1 was chosen as a marker for defining the end of the transplantation-competent window, in view of observations that mESC-derived rod precursors transplanted at day 26–29 of culture were consistently Gnat1-negative and led to higher numbers of GFP^+ cells present in the host ONL, compared with ESC-derived rod precursors transplanted on day 34 of culture, which were predominantly $Gnat1^+$ and had significantly lower numbers of GFP^+ cells present in the host ONL (Gonzalez-Cordero et al., 2013).

Having a reporter gene under the same transcriptional control as the gene of interest itself allows for accurate representation of the gene's activity. As mentioned briefly in Section 3.2.6, we were able to obtain a transgenic mESC line in which GFP expression is driven by the endogenous Crx promoter (kind gift of Prof. Y. Arsenijevic, (Decembrini et al., 2014)). Crx is expressed in the early stages of photoreceptor differentiation, soon after a cell fated to be a photoreceptor cell becomes post-mitotic, and is maintained in mature differentiated photoreceptors (Samson et al., 2009). The Crx.GFP transgenic ESC line therefore labels all post-mitotic developing and mature cone and rod photoreceptors (Decembrini et al., 2014).

I differentiated the Crx.GFP line using the same differentiation protocol that we developed for the E16 CCE line (Gonzalez-Cordero et al., 2013). This is similar to the protocol reported by Decembrini et al. (2014) but key differences in maintenance and differentiation culture conditions are noted below in Table 4.1. Given these differences, the progression of photoreceptor birth and development may differ. As such, I sought to characterise photoreceptor birth and differentiation in this line, with a view to introducing additional retina-specific promoter-driven fluorescent reporters for mid- and late-developmental markers to the line, as mentioned above.

Decembrini et al. (2014)	Gonzalez-Cordero et al. (2013)
No MEK inhibitor or GSK3 inhibitor in maintenance media	Addition of 0.5μM MEK inhibitor and 1.5μM GSK3 inhibitor to maintenance media
Seeding density of 3000-5000 cells per well in a 96 well plate on day 0 of differentiation	Seeding density of 3000 cells per well in a 96 well plate on day 0 of differentiation
1% B27 added to DMEM/F12 with Glutamax + N2 from day 7/9 to day 12 of differentiation	No B27 added to DMEM/F12 with Glutamax + N2 from day 9 of differentiation
1%FCS + 1%N2 + 2% B27 added to DMEM/F12 with Glutamax + N2 media from day 12 of differentiation onwards	1mM taurine and 500nM retinoic acid added to DMEM/F12 with Glutamax + N2 from day 14 of differentiation onwards
Aggregates kept in 40% O_2 from day 12 of differentiation onwards	Aggregates kept in normoxic atmospheric conditions (20% O_2) throughout

Table 4.1: Differences in 3D mESC culture conditions between Decembrini et al. (2014) and Gonzalez-Cordero et al. (2013).

Next, I explored the use of CRISPR (clustered regularly interspaced short palindromic repeat)-Cas (CRISPR-associated) technology to introduce a Rhodopsin.mCherry construct and a Gnat1.Katushka construct into the Crx.GFP line. This would enable us to monitor the progression of photoreceptor differentiation, and facilitate the selection of developmentally homogenous subpopulations of post-mitotic precursors.

The CRISPR-Cas nuclease system is a microbial adaptive immune mechanism that uses RNA-guided nucleases to cleave foreign genetic material. In particular, the Type II CRISPR-Cas9 system can be manipulated to facilitate efficient and precise RNA-guided genome editing in multiple eukaryotic systems (Hsu et al., 2014; Mali et al., 2013; Ran et al., 2013; Sander and Joung, 2014). The Cas9 nuclease is guided to target DNA sequences by small 'guide' RNAs, and thereby generates a double stranded break (DSB) at specific genomic loci. This cleavage leaves the target locus amenable to modification via DNA repair, which typically occurs via either the error-prone non-homologous end joining (NHEJ) or the high-fidelity homology-directed repair (HDR) pathway. Depending on the nature of the target cell, both pathways can potentially be harnessed to achieve different outcomes. Notably, for precise gene editing, HDR can be leveraged to generate site-directed edits at an endogenous target locus in the presence of a donor repair template containing regions of homology to the target locus, such that the exogenous repair sequence is inserted between two homologous 'arms'.

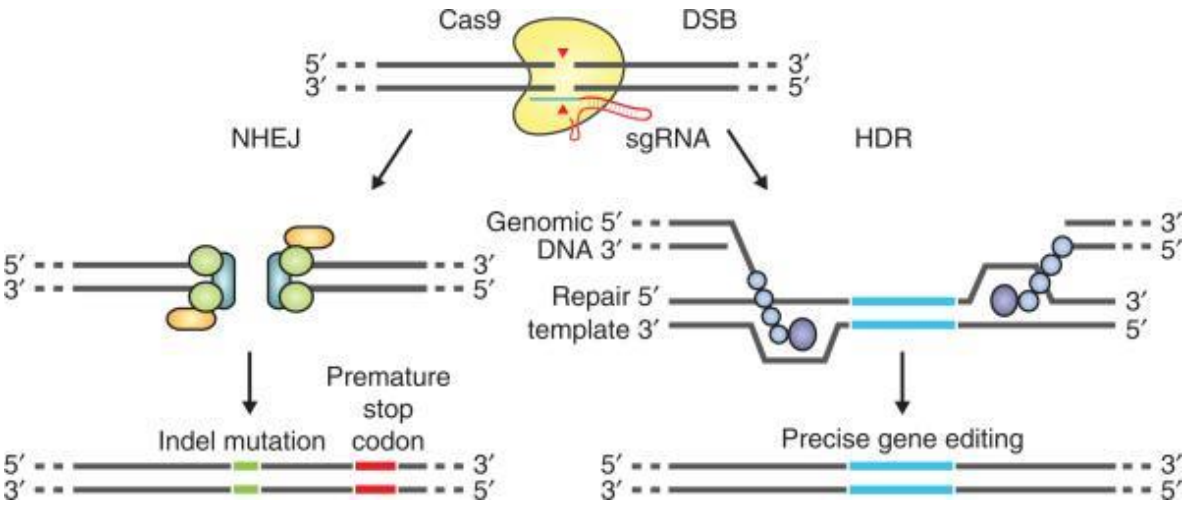

Figure 4.1: Cas9-induced DSBs will typically be repaired by either the NHEJ or the HDR pathway. NHEJ is error-prone, and will likely result in random indel mutations and the creation of a premature stop codon, resulting in gene knockout. Alternatively, HDR can be leveraged with introduction of a repair template to bring about high-fidelity, precise site-directed gene editing. Adapted from (Ran et al., 2013)**.**

The Type II CRISPR-Cas9 system comprises the nuclease Cas9, a CRISPR RNA (crRNA) array that encodes for a guide RNA sequence, and a trans-activating crRNA (tracrRNA) that facilitates processing of crRNA. The guide RNA is 20 nucleotides long and directs Cas9 to a 20-base pair DNA target via Watson-Crick base pairing; additionally, the DNA target must immediately precede a 5'-NGG protospacer adjacent motif (PAM) in order for Cas9 to cleave at the target site. The DSB is made 3-bp upstream of the PAM. Given these requirements, the requisite RNA components – the crRNA and tracrRNA – can be fused together to create a chimeric single-guide RNA (sgRNA), and Cas9 can be easily programmed to cleave any target of interest upstream of a PAM sequence by altering the 20-nt sequence within this sgRNA.

Figure 4.2: Schematic of the Cas9 nuclease. Cas9 can be directed to cleave genomic DNA at a specific target site by a sgRNA comprising a 20 nucleotide guide sequence (in blue) and an invariant scaffold (in red). This guide sequence base pairs with the corresponding 20 base pair DNA target (blue bar), which is immediately upstream of a requisite 5'-NGG PAM (in pink). Cas9 mediates a DSB 3 base pairs upstream of the PAM (red triangles). Adapted from (Ran et al., 2013).

Although the 20-nt guide sequence contributes towards a high degree of cleavage specificity, off-target cleavage can be further minimized through the use of a mutant nickase version of Cas9 (Cas9n) together with a pair of offset sgRNAs complementary to opposite strands of the target site. Simultaneous single-stranded nicks on both strands of the target DNA can introduce a DSB, while significantly reducing off-target nuclease activity, as both sgRNAs will need to recognise the target in order for DSB to occur and single-strand nicks in the genome are preferentially repaired via the high-fidelity HDR pathway. Pairs of sgRNAs were therefore designed for use with the Cas9n protein to introduce Rhodopsin.mCherry and Gnat1.Katushka constructs into the Crx.GFP mESC line.

Figure 4.3: Design of sgRNA pair for double nicking. To facilitate efficient double nicking, the pair of sgRNAs must be designed such that 1) 5' overhangs are generated upon nicking, and 2) the target locus for the sgRNA pair must be offset with an optimal gap of 0-20 base pairs. Adapted from (Ran et al., 2013).

4.2 Results

4.2.1 Assessing proliferation in Crx.GFP embryoid bodies

In order to assess cell proliferation in Crx.GFP differentiation cultures, Crx.GFP EBs were collected on either day 13, 16, 19, 21, or 23 and stained for Ki67, a proliferation marker expressed during interphase (Figure 4.4). Ki67 staining was most prevalent on day 13, and was mostly detected in the neuroepithelial region. As such, it likely corresponds to retinal progenitor cell proliferation. Ki67 expression in neuroepithelial regions was substantial on days 16 and 19, but decreased drastically from day 21 onwards, which is expected as cells exit the cell cycle and commit to a specific cell fate. No co-localisation of Crx.GFP with Ki67 was observed, confirming the expression of Crx in non-proliferative and post-mitotic photoreceptors.

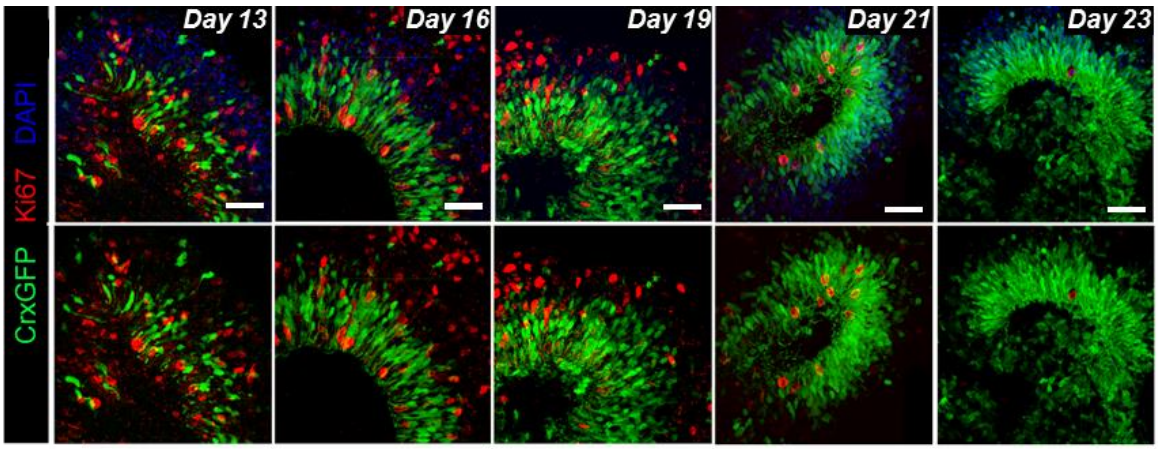

Figure 4.4: Proliferation in Crx.GFP differentiation cultures. Ki67 staining was most prevalent on day 13, and was mainly localised to the neuroepithelial layer. Few Ki67-positive cells were observed from day 21 onwards.

4.2.2 Birthdating of photoreceptors with EdU pulse-labelling

Next, in order to determine the peak of photoreceptor birth *in vitro*, I attempted to pulse-label Crx.GFP 3D differentiation cultures with 5-ethynyl-2'-deoxyuridine (EdU), a nucleoside analogue of thymidine that is taken up during cell division and incorporated into cellular DNA. The EdU label will persist in a cell if the cell exits the cell cycle to mature and differentiate (for example, into a rod); whereas cells that take up EdU but continue dividing are likely to dilute out EdU beyond the limits of detection. When EBs are collected at a later time point in culture (for example, day 26) and stained for EdU, EdU should be strongly detected in CrxGFP$^+$ cells that were undergoing their final mitosis (i.e. onset of differentiation) on the day that EdU was added to the culture media. Cells retaining EdU are therefore likely to have been passing through S phase during or shortly after EdU pulsing, and turned post-mitotic after the following M phase.

The manufacturer's recommended concentration of EdU for *in vitro* experiments is 10μM, and several studies have used this amount in 24-hour labelling protocols (Decembrini et al., 2014; Ning et al., 2013). As the S phase of mitotic progenitors in the postnatal developing mouse retina is roughly 16 hours (Young, 1985), we began by treating day 13 Crx.GFP differentiation cultures with 10 μM EdU for 16 hours. Surprisingly, upon visual inspection, this concentration led to a noticeable loss of EB morphology and high levels of debris in the culture media within 24 hours of EdU addition, suggesting that 10μM EdU may be too toxic for our ESC differentiation cultures.

We titrated the concentration of EdU added, aiming to achieve a balance between preserving cell viability and minimising toxicity whilst ensuring that EdU could be detected by immunohistochemistry and flow cytometry. Day 13 Crx.GFP EBs were first treated with 1μM, 2μM, or 5μM for 16 hours, following which EdU was removed from the media and fresh media was added. Untreated EBs and EBs treated with 10μM EdU were included as positive and negative controls respectively. At 8 hours following the removal of EdU, EBs were dissociated for flow cytometric analysis of viability and EdU expression (Figure 4.5A, n=3 differentiation cultures).

While increasing EdU concentration from 1μM to 5μM did not lead to a relevant difference in the total number of EdU$^+$ cells detected (Figure 4.5B), the resolution of EdU$^+$ and EdU$^-$ populations by flow cytometry was substantially improved with higher EdU concentrations (Figure 4.5B,D). In keeping with our earlier observations, the higher EdU concentrations were more toxic to our ESC differentiation cultures, as seen from the larger percentage of debris present at the higher EdU concentrations (Figure 4.5C) and the fall in the overall proportion of live cells as EdU concentration was increased (Figure 4.5E).

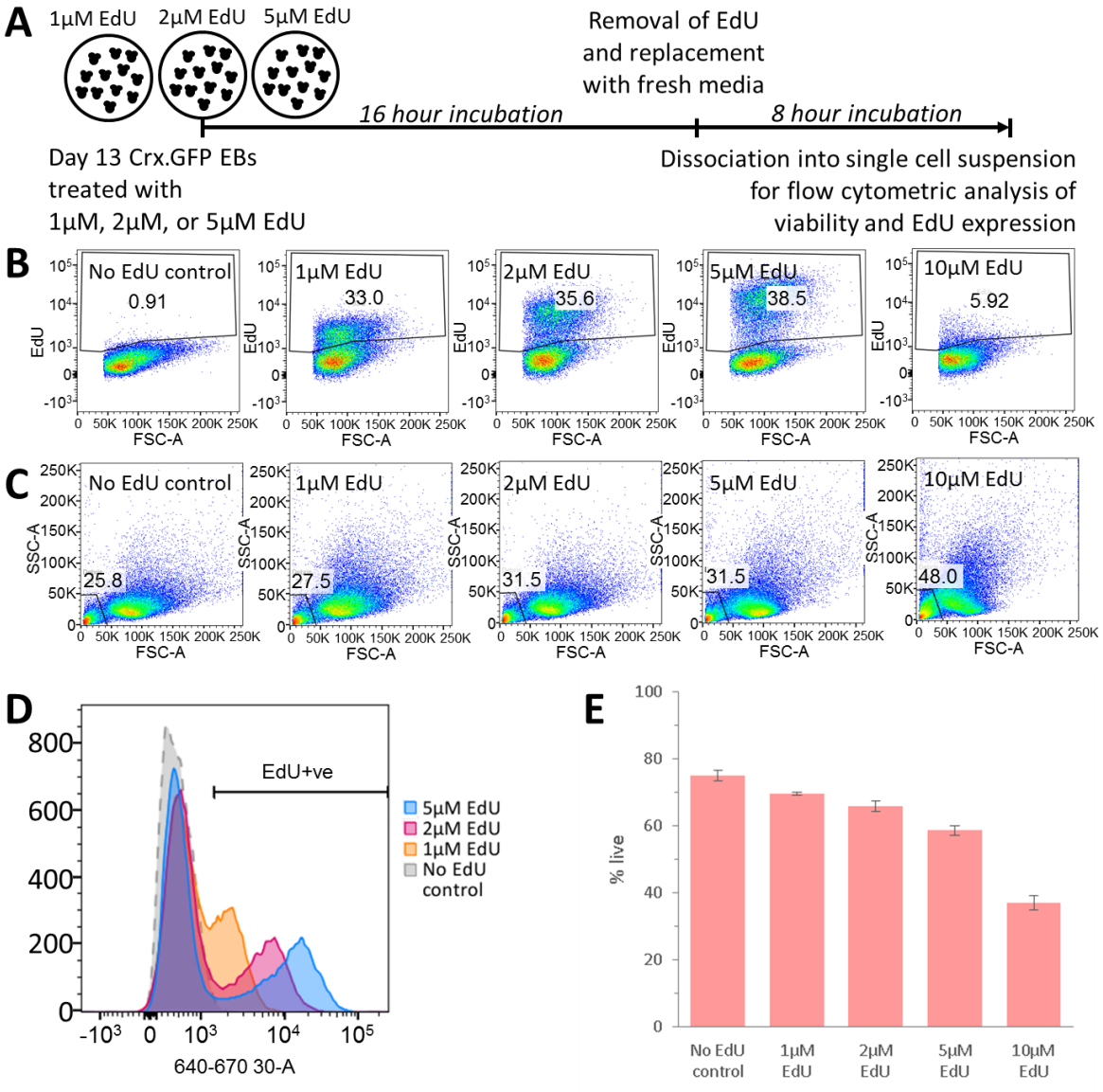

Figure 4.5: A. Schematic showing the titration of EdU concentration for pulse-labelling of Crx.GFP EBs in day 13 *in vitro* cultures. B. Increasing EdU concentration did not lead to a relevant difference in the number of EdU+ cells detected C. A corresponding increase in debris was noted with increased EdU concentrations. D. Higher EdU concentrations allowed for better resolution between EdU$^+$ and EdU$^-$ populations. E. There was a reduction in overall viability as EdU concentration was increased, which was most marked with the use of 10μM EdU.

However, we noticed a marked loss of neuroepithelial morphology in all of the EBs by 48 hours after the start of the 16-hour EdU pulse, even in the EBs pulsed with the lowest concentration of EdU (1μM). By day 26, there was complete disorganisation of neuroepithelial morphology in all of the EBs, and evidence of high levels of debris in the culture media. This was confirmed by dissociating EBs that had been given a 16-hour 1μM EdU pulse and quantifying by flow cytometry the proportion of live cells, which was markedly reduced from 70-80% live in untreated controls, to 15-20% live in EBs pulsed with 1μM EdU.

Therefore, to preserve neuroepithelial morphology in EdU-pulsed EBs till day 26 of culture, we reduced the EdU concentration to 0.5μM and decreased the duration of the EdU pulse to 8 hours. This allowed for preservation of neuroepithelial morphology until day 26 in approximately 30-40% of EBs. EBs were therefore treated with an 8-hour pulse of 0.5μM EdU on either day 13, 16, 19, 21, or 23 in culture, and then collected on day 26 for immunohistochemical staining. Three fields of view over a section of neuroepithelium were imaged for each time point (n=2 differentiation cultures per time point) and blinded counts of the number of EdU^+/$Crx.GFP^+$ cells and $Crx.GFP^+$ cells within each field of view were carried out.

Photoreceptor birth was substantially increased between days 19 and 21 of culture, as seen from the proportion of cells that were $Crx.GFP^+$/EdU^+ double-positive in day 26 EBs given a pulse of EdU on day 19 or day 21. In contrast, the proportion of $Crx.GFP^+$/EdU^+ cells was lower in day 26 EBs that were given a pulse of EdU on day 13, 16, or 23, which suggests that substantially fewer photoreceptors were being born by this time point (Figure 4.6A, B). The majority of EBs that were EdU-pulsed on day 13 or day 16 were observed to have poor neuroepithelial morphology. This may be because younger cells are more susceptible to EdU toxicity, as EdU incorporation is higher and therefore has a proportionally greater toxic effect. Alternatively, this may be due to a greater length of time for the toxic effects of EdU to be manifested in these early-pulsed EBs compared to the late-pulsed EBs.

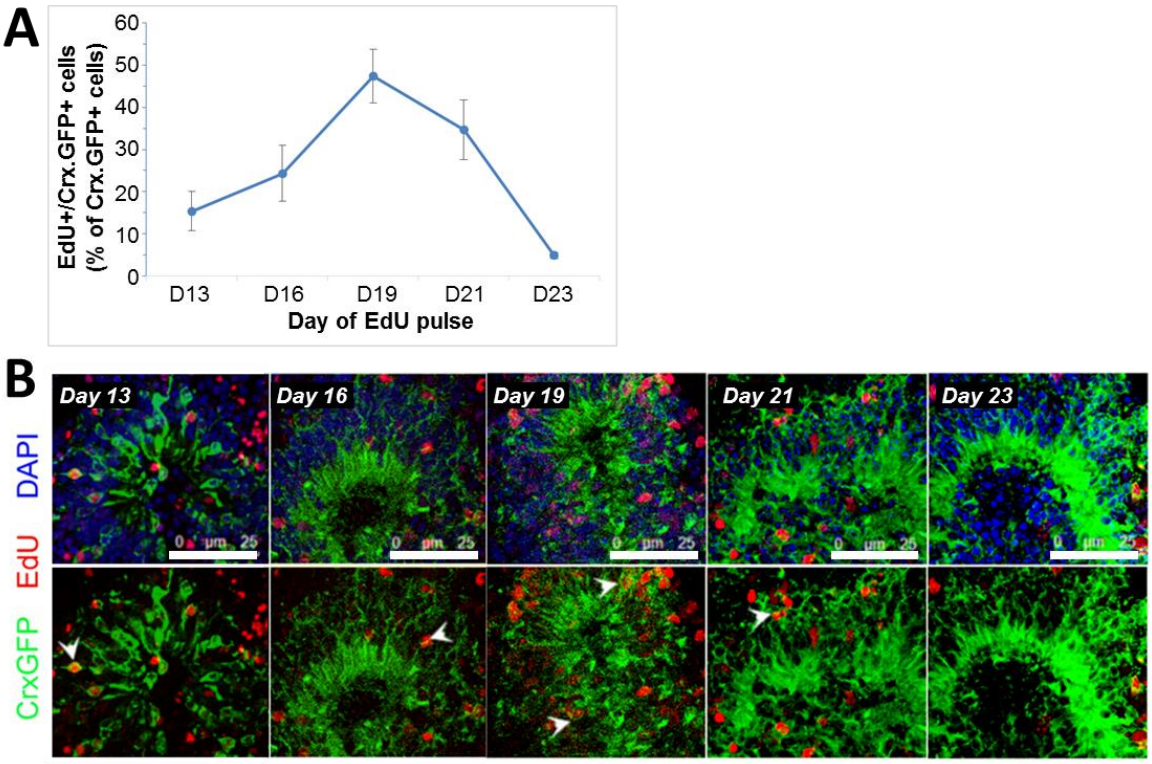

Figure 4.6: Time course of photoreceptor birth. A. The proportion of Crx.GFP⁺ cells that were EdU⁺/GFP⁺ double-positive were substantially increased on day 19 in culture (mean ± SEM). B. Representative images of neuroepithelial regions in day 26 EBs pulsed with 0.5µM EdU for 8 hours on days 13, 16, 19, 21, or 23. White arrows indicate Crx.GFP⁺ /EdU⁺ cells. Scale bar: 25µm.

Unfortunately, I was unable to confirm the immunohistochemical data by flow cytometric analysis as there appeared to be a substantial loss of viability following the dissociation of EdU-pulsed cultures collected at day 26 (overall percentage of live cells was between 30-40% after dissociation), and the percentages of EdU⁺ cells detected were unusually low across all samples. This indicated that the EdU-pulsed EBs were too fragile to undergo dissociation by day 26 of culture.

4.2.3 Time course of photoreceptor development

Next, I sought to characterise photoreceptor development in the Crx.GFP mESC line by examining the expression of photoreceptor-specific proteins over the differentiation culture period, and comparing the profile with a previously-characterised mESC line differentiation (Gonzalez-Cordero et al., 2013), as well as the developing wild-type retina.

In normal mouse development, expression of *Crx* commences at embryonic day (E)10.5-12.5, coinciding with cone birth, and peaks at postnatal day (P)5, which corresponds to the onset of rod maturation (Hennig et al., 2008; Bibb et al., 2001). *Crx* is expressed predominantly in rod and cone photoreceptor precursors, although it is also expressed at relatively low levels in bipolar cells, and its expression is maintained at a lower level in mature adult photoreceptors (Samson et al., 2009). In our cultures, Crx.GFP$^+$ cells were first observed on day 12 of culture in a dispersed fashion throughout the neuroepithelial region, similar to *in vivo* observations of the developing retina at E13. By day 15, the Crx-GFP$^+$ cells were localised to the apical side (the concave inner side of the optic cup), forming a dense, well-aligned layer of photoreceptors resembling the outer nuclear layer, akin to P0 *in vivo* (Figure 4.7A). After day 26 in culture, neuroepithelial layers began to form rosettes and started showing loss of neuroepithelial morphology. These observations were confirmed by flow cytometric analysis, which showed a marked increase in the percentage of Crx.GFP$^+$ cells from 6.6 ± 1.1% on day 13 to 88.1 ± 1.3% on day 28, followed by a decrease in overall GFP expression after day 28 corresponding to the loss of neuroepithelial morphology (Figure 4.7D).

As cones are born before rods *in vivo*, it is likely that the first cells that express Crx are the cone progenitors. Indeed, the short wavelength-responsive cone opsin (S-opsin, or blue opsin) was first detected in a few cells at day 15 in culture, and majority of these were Crx.GFP$^+$/S-opsin$^+$ double-positive (Figure 4.7A). The number of S-opsin expressing cones increased over days in culture, and persisted until day 26, which was the last time point tested. Interestingly, S-opsin was expressed throughout the cell and did not become localised to the outer segment region, indicating that these cells are not fully mature. *In vivo,* the first cones are born at E12.5, although S-opsin is only found in mature cone outer segments and is first detected around E18 (Hennig et al., 2008; Swaroop et al., 2010).

The rod-specific marker Rhodopsin was first detected at day 19 in culture (Figure 4.7B), placing cells at day 19 of culture similar to P2 *in vivo* (Bibb et al., 2001; Swaroop et al., 2010). Like S-opsin, Rhodopsin expression increased over days in culture and persisted till day 30. In vivo, qualitative assessments indicate that protein levels of the late rod marker Gnat1 increases substantially between P8 and P12, coincident with the onset of outer-segment formation. Similarly, at day 28 there were very few Gnat1$^+$ cells *in vitro*, but by day 30, the majority of the cells in the neuroepithelial region were Gnat1$^+$ (Figure 4.7C). As an additional marker of rod development, Crx.GFP EBs were dissociated at similar days in culture and stained for the surface marker CD73 for flow cytometric quantification. The percentage of Crx.GFP$^+$/CD73$^+$ double-positive cells increased substantially between day 21 and 28, peaking at day 28 (Figure 4.7D).

Taken together, these results demonstrate that our Crx.GFP differentiation cultures follow the pattern of photoreceptor development seen *in vivo.* Notably, Crx.GFP photoreceptors obtained from day 26 of culture most closely resemble post-natal day 8 photoreceptors. This is earlier than the previously-described E16 CCE line, in which EBs at day 29 of culture were more comparable to P8 (Gonzalez-Cordero et al., 2013).

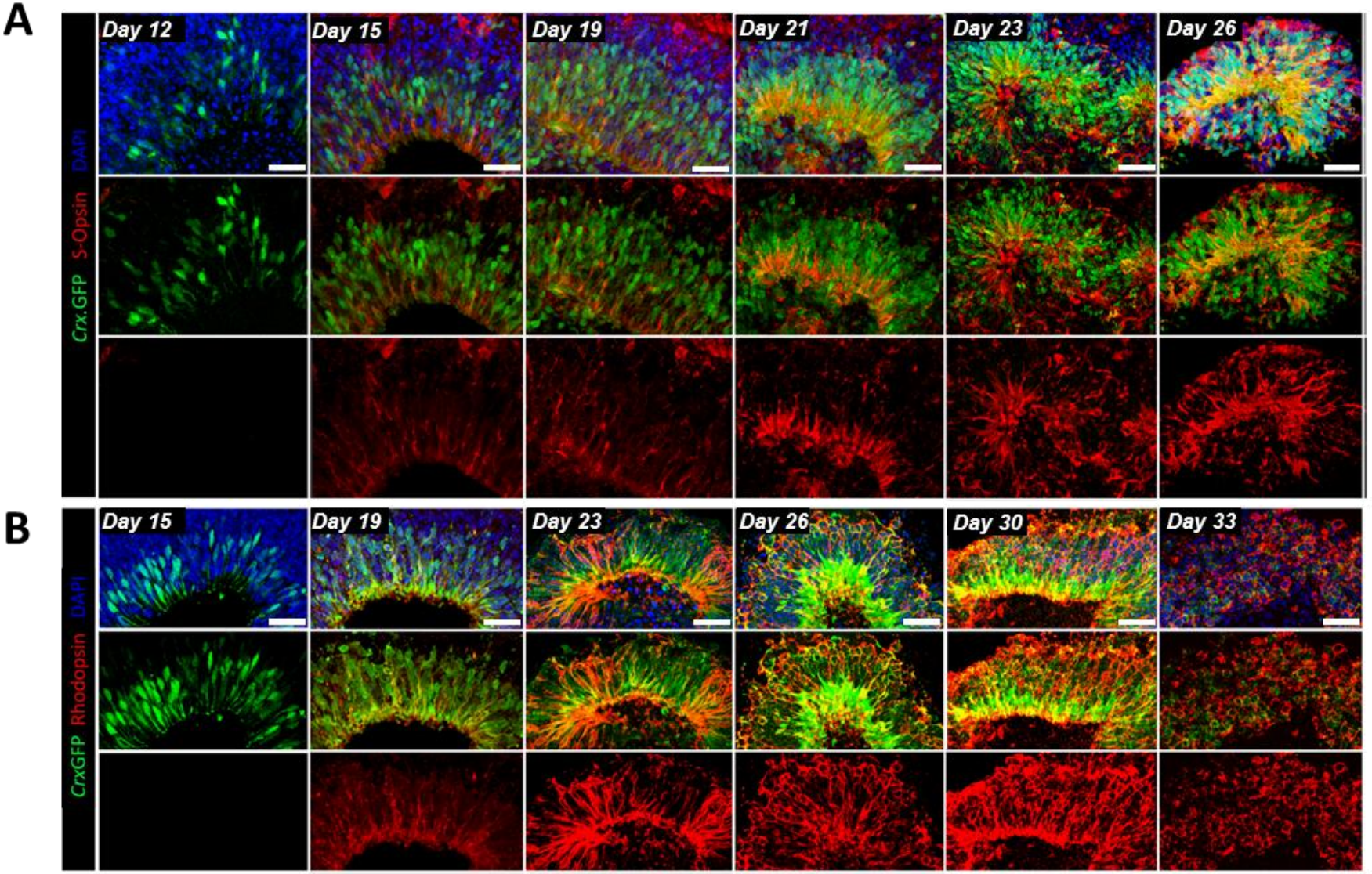
A
Day 12
Day 15
Day 19
Day 21
Day 23
Day 26
DAPI
S-Opsin
Crx.GFP
B
Day 15
Day 19
Day 23
Day 26
Day 30
Day 33
DAPI
Rhodopsin
CrxGFP

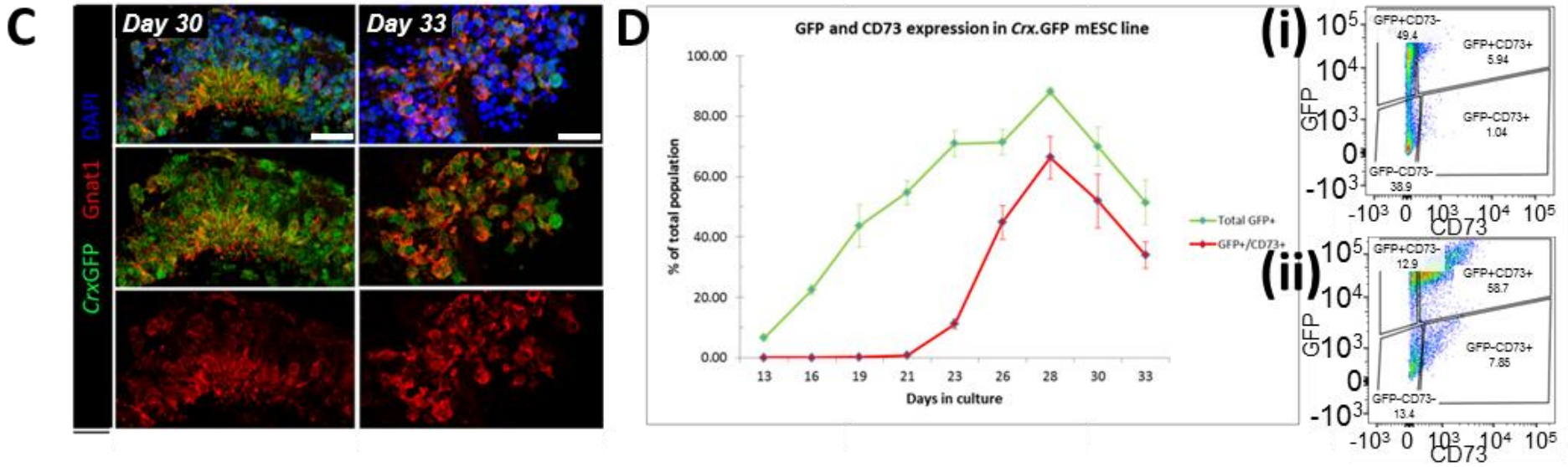

Figure 4.7: Time course of photoreceptor development in Crx.GFP mESC line. Immunohistochemical analysis of temporal expression of A. cone marker S-opsin, B. rod marker rhodopsin, and of C. late rod marker rod α-transducin. D. Crx.GFP and CD73 expression at different days in culture, quantified by FACS analysis (n>3 per time point, mean ± SEM). Representative FACS plots showing Crx.GFP and CD73-APC expression on D(i) Day 21 and D(ii) Day 28. Scale bar: 25µm.

4.2.4 Transplantation of Crx.GFP$^+$ photoreceptor precursors

Given that the peak of photoreceptor birth was around day 19, which is estimated to be equivalent to P0 *in vivo*, I transplanted FAC-sorted Crx.GFP$^+$ cells at different differentiation time points equivalent to early postnatal (days 21 and 26 in culture) and late postnatal (day 29 and 33 in culture) retinal cells, in order to determine whether transplantation outcome, as assessed by the number of GFP$^+$ cells present in the host ONL post-transplantation, is dependent on the developmental stage of the injected Crx.GFP$^+$ photoreceptor precursors.

3 weeks after transplantation, recipient *Gnat1*$^{-/-}$ retinas were harvested and the number of GFP$^+$ cells in the host ONL were quantified. As expected, the average number of GFP$^+$ cells in the host ONL varied in an age-dependent manner, peaking with cells isolated at day 26 of culture (1815 ± 423.3, n=14), which corresponds approximately to P7-8 *in vivo*. This was significantly higher than that achieved with transplants of donor cells isolated at day 21, 29 or 33 of culture (Figure 4.8A, $p<0.005$, Kruskal Wallis; $n>4$). The maximum number of GFP$^+$ cells observed in the host ONL post-transplantation was 5358 with Crx.GFP$^+$ cells transplanted on day 26, compared to 1034 on day 21 and 1833 on day 29. Notably, with transplants of Crx.GFP$^+$ cells isolated on days 21, 29 and 33, there was a higher proportion of cases in which a large subretinal GFP$^+$ cell mass was present with no sign of macrophage infiltration or debris, yet the number of apparently integrated GFP$^+$ cells in the host ONL was very low (<30 cells per eye; Figure 4.8B; 6 out of 7 eyes with D21 transplants, 6 out of 9 eyes with D29 transplants, and 2 out of 4 eyes in D33 transplants, compared to 3 out of 14 eyes in D26 transplants).

The GFP$^+$ photoreceptors observed in the host ONL following the transplantation of Crx.GFP$^+$ cells from different stages of differentiation culture were all observed to be appropriately located within the ONL and morphologically similar to wild-type rods, correctly expressing Gnat1 (Figure 4.8C), which is absent in endogenous *Gnat1*$^{-/-}$ rods. In addition, most of these cell presented with basal processes that terminated as round synaptic bouton-like structures that expressed the rod ribbon synapse marker Ribeye (Figure 4.8D).

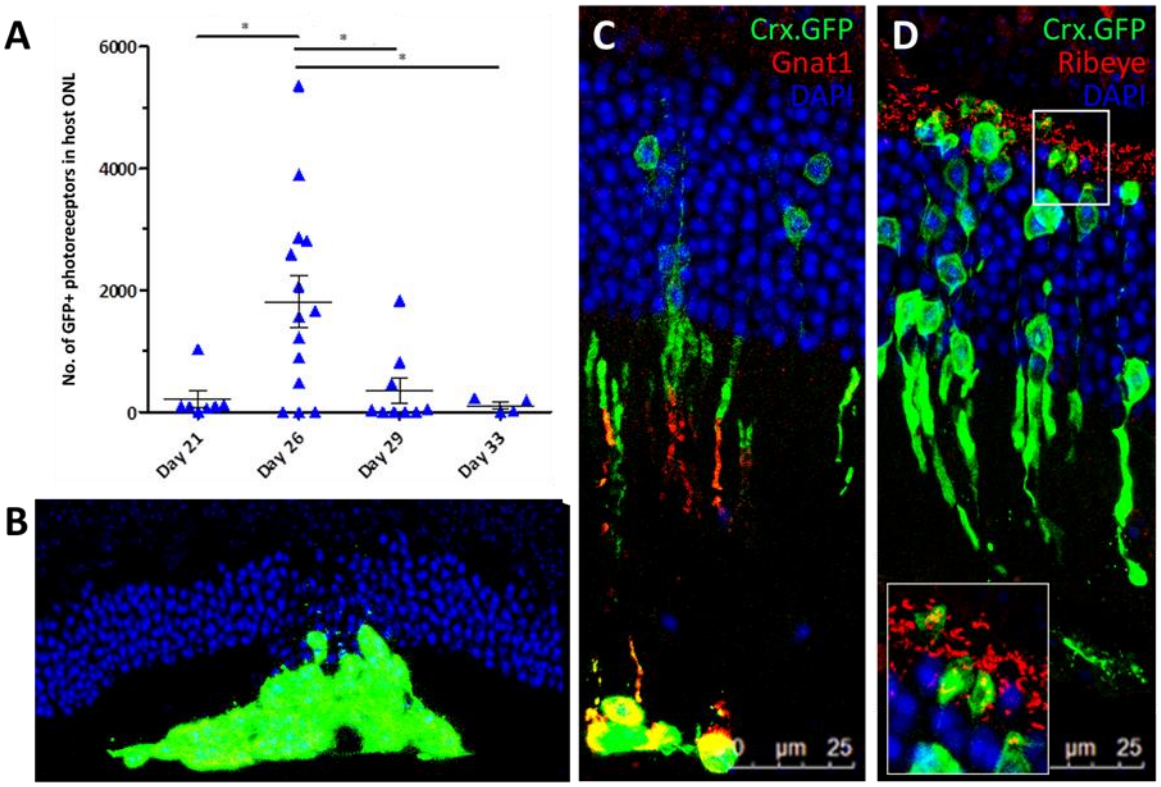

Figure 4.8: Transplantation of Crx.GFP⁺ ESC-derived photoreceptors. A. A significantly higher number of GFP+ cells are seen in the ONL of recipient *Gnat1*$^{-/-}$ mice following the transplantation of Crx.GFP⁺ cells isolated from day 26 of culture, compared to those isolated from day 21, 29, and 33 of culture. B. A large subretinal GFP⁺ cell mass could often be seen with few/no GFP⁺ cells present in the host ONL of eyes injected with Crx.GFP⁺ cells isolated from day 21, 29, and 33 of culture. C. GFP⁺ cells present in the host ONL of eyes injected with Crx.GFP⁺ cells isolated from day 26 of culture correctly express Gnat1, as well as D. the rod ribbon synapse marker Ribeye.

4.2.5 Generation of photoreceptor reporter ESC line with CRISPR-Cas9

Having characterised photoreceptor birth and development in the Crx.GFP mESC line, I next sought to assess the transplantation competence of mESC-derived rod precursors at different developmental stages, by using CRISPR/Cas9 technology to introduce rod-specific reporter gene constructs into the Crx.GFP mESC line in order to create an triple reporter knock-in mESC line (Figure 4.9; Crx.GFP::Rho.mCherry::Gnat1.Katushka). This will potentially allow me to track rod development *in vitro*, and also select for transplantation purposes developmentally-homogenous populations of rod precursors, such as Crx.GFP^{+}Rho.mCherry^{+} Gnat1.Katushka^{-} cells.

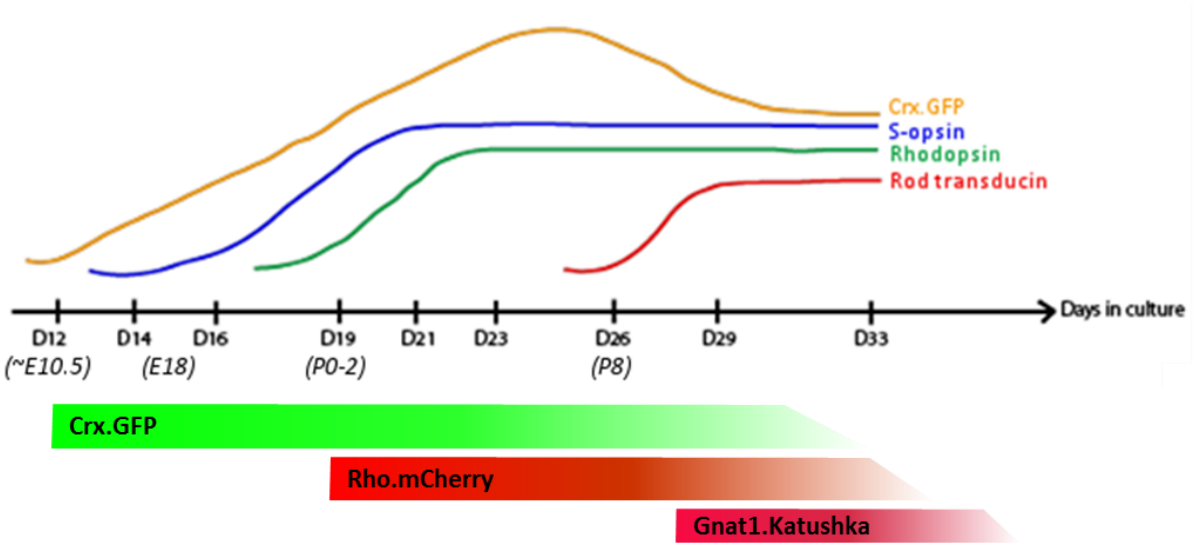

Figure 4.9: Schematic of triple reporter mESC line and corresponding photoreceptor marker expression, as previously characterised.

Given the considerations mentioned in Section 4.1, I decided to employ a dual plasmid strategy in combination with the Cas9n protein to introduce fluorescent protein reporters driven by endogenous rhodopsin and Gnat1 promoters into the Crx.GFP mESC line (Figure 4.10). One plasmid will contain the 'repair template' (fluorescent protein reporter sequence flanked by homology arms targeting the 3' UTR of respective rod gene; Figure 4.10A), whereas the other plasmid will contain a pair of sgRNAs encoding 20-nt guide sequences to direct Cas9n to the site of reporter sequence insertion (Figure 4.10B). Following electroporation of both plasmids with Cas9n protein into Crx.GFP mESCs: cells that successfully take up both plasmids and Cas9n should have fluorescent protein reporter expression driven by the endogenous rod gene promoters (Figure 4.10C). Isolation of clonal Crx.GFP::Rho.mCherry:: Gnat1.Katushka cell lines will then be carried out by single-cell FAC sorting followed by an expansion period till clonal cell lines are confluent enough to be screened by PCR.

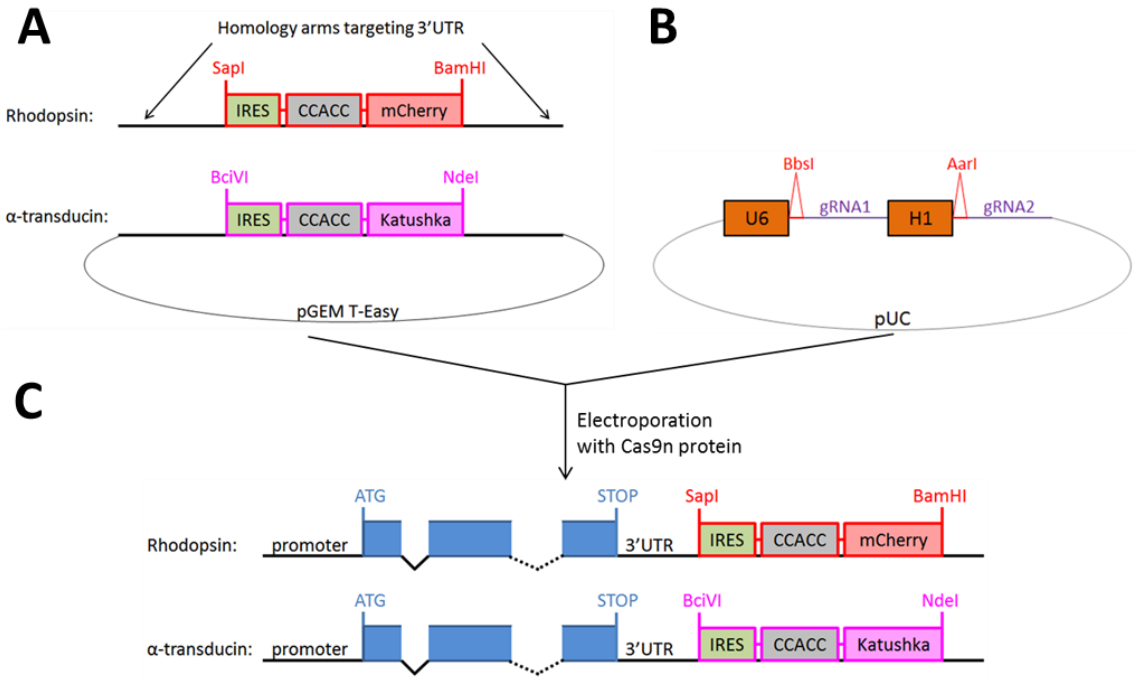

Figure 4.10: Dual plasmid strategy. A. Repair template containing homology arms targeting the 3'UTR of the target gene and the appropriate fluorescent protein reporter insert, on a pGem T-Easy plasmid backbone. B. For each insertion of fluorescent protein reporter, a pUC plasmid was constructed to encode a pair of single guide RNAs encoding target gene-specific 20-nt guide sequences. C. Following electroporation of the plasmids with Cas9n protein into Crx.GFP mouse ES cells, cells which successfully take up both plasmids and the protein should have the fluorescent protein reporter sequences inserted in the 3'UTR of the respective targeted rod genes, where expression will be driven by endogenous promoters. Blue blocks represent exons; black lines represent non-coding sequences.

At the time of writing, both Rho.mCherry and Gnat1.Katushka repair templates have been made successfully (Figure 4.11). Selected 3'UTR regions of the mouse Rhodopsin and Gnat1 genes were PCR amplified from mESC genomic DNA, and cloned into pGEMT-Easy vectors (Figure 4.11A). Site-directed mutagenesis was performed to introduce the appropriate restriction enzyme sites and remove other unwanted sites. mCherry and Katushka reporter inserts were ordered and ligated into RhoPGEMT-Easy and Gnat1PGEMT-Teasy vector backbones respectively (Figure 4.11B). Successful generation of these reporter constructs were validated by restriction digest and Sanger sequencing (Figure 4.11C). In addition, both pairs of U6 and H1 guides for Rhodopsin and Gnat1 have been successfully cloned into separate pUC backbones.

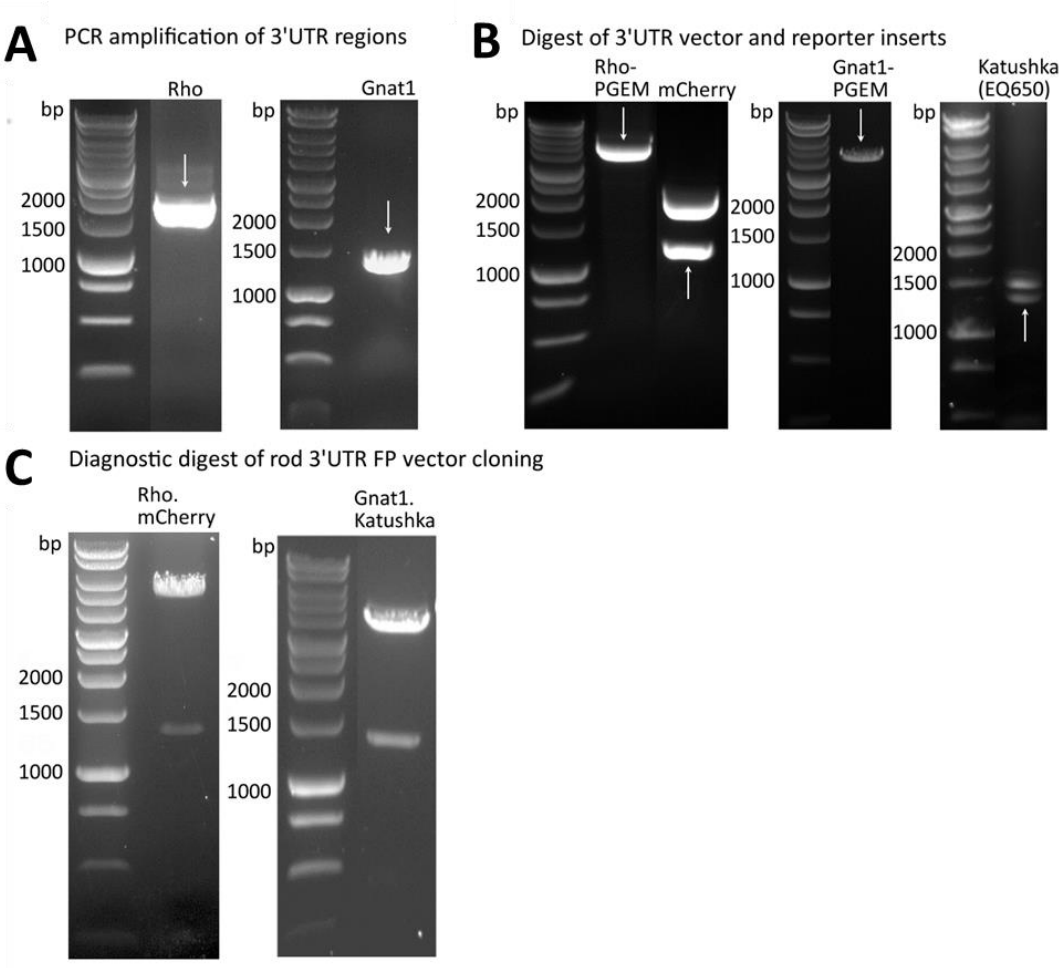

Figure 4.11: UV images of DNA bands obtained at various stages of the cloning strategy for Rho and Gnat1. A. Correct amplicons were obtained for each sample from PCR amplification (Rho (1925bp) and Gnat1 (1444bp)). B. Bands from restriction digestions showing correct DNA band sizes of 3'UTR regions in PGEMT-Easy vector and fluorescent protein inserts, which were subsequently extracted for ligation. C. Bands obtained from restriction digest of vectors showing expected band sizes for Rho.mCherry and Gnat1.Katushka constructs.

4.3 Discussion

Previous work by our group has shown that following the transplantation of mESC-derived virus-labelled Rhodopsin.GFP$^+$ rod precursors from day 29 of culture into *Gnat1*$^{-/-}$ recipient mice, GFP$^+$ rod-like cells expressing *Gnat1* were present in the host ONL (Gonzalez-Cordero et al., 2013), albeit in lower numbers than that achieved with the transplantation of donor-derived P4-8 Nrl.GFP$^+$ rod precursors. Having optimised the transplantation protocol, I next explored the use of an endogenous reporter line – the Crx.GFP mESC line – to facilitate the detection of emerging photoreceptors in *in vitro* cultures and in recipient retinas post-transplantation without the need for viral-labelling.

Retinal development in *in vitro* mESC differentiation cultures can differ between mESC lines and are dependent on culture conditions, too (REFS). As such, I first sought to characterise the time course of photoreceptor birth in the Crx.GFP line. EdU was chosen over BrdU as a nucleoside analogue for *in vitro* birth dating in view of its ease of immunohistochemical detection and compatibility with flow cytometry, which will allow for more quantitative measurements compared with BrdU. Indeed, successful use of EdU for *in vitro* birth dating has been demonstrated in other studies (Decembrini et al., 2014; Ning et al., 2013). Unfortunately, in our system, EdU was found to severely compromise embryoid body viability and neuroepithelial morphology, especially when added at the early stages of differentiation. These findings are in line with recent observations made by other groups, who similarly found that EdU severely reduced cell viability, particularly that of stem cells (Andersen et al., 2013; Neef and Luedtke, 2011; Ligasová et al., 2015). While the mechanisms for EdU-induced cytotoxicity remain unclear, it appears to be positively correlated to the efficiency of its incorporation, which varies across different cell types (Diermeier-Daucher et al., 2009). By reducing the length of the pulse as well as the EdU concentration used, I was able to estimate the peak of photoreceptor birth based on immunohistochemical staining, but not by flow cytometry due to poor viability following dissociation. The proportion of Crx.GFP$^+$/EdU$^+$ cells present in the neuroepithelia of day 26 Crx.GFP EBs was highest in EBs that had been given an EdU pulse on day 19 of culture. Furthermore, Ki67 staining in neuroepithelial regions appeared to peak between day 16-19 of culture. The largest increase in the number of Crx.GFP$^+$ cells was also seen between day 16 and 19, suggesting that majority of

photoreceptors were born by day 19 in culture. This surge in the number of Crx.GFP-expressing cells is likely to be due to rod birth rather than cone birth, as cones are born much earlier than rods. Taken together, the peak of rod photoreceptor birth in the Crx.GFP ESC line appears to occur on day 19 in culture, therefore placing EBs at day 19 in culture at a similar developmental stage to P0 *in vivo*.

Immunohistochemical characterisation of photoreceptor maturation in the Crx.GFP line confirmed that Crx.GFP differentiation cultures followed a pattern of photoreceptor development very similar to that observed *in vivo.* Compared to the E16 line and to *in vivo* development, however, the onset of rod development appeared to occur slightly earlier, and at a slightly accelerated pace; although ideally qPCR should be done to confirm this. With the Crx.GFP line, Crx was first detected at day 12 in culture, and expression, as assessed by IHC, was maintained at a high level till day 29; whereas in the E16 line, Crx was only weakly detected at day 18 and peaked between day 20-24 before decreasing after day 26. In agreement with Lakowski et al. (2010), Crx expression was confined to post-mitotic photoreceptor cells, as demonstrated by the lack of Ki67 expression in the Crx.GFP$^+$ population. The onset of Rhodopsin was also earlier in the Crx.GFP line, coming on faintly at day 19 compared to day 24 in the E16 lines. Expression of rhodopsin in mice begins at approximately P2, which falls within the range of our estimated peak of rod birth, at day 19. Rod α-transducin was expressed around the same time in both cell lines, at around day 30. These differences between mESC lines demonstrate the need for thorough characterisation of individual ESC lines.

Finally, we observed a significant increase in the number of GFP$^+$ cells present in the host ONL following the transplantation of day 26 Crx.GFP$^+$ cells compared to Crx.GFP$^+$ cells from earlier or later days in culture. This is in keeping with the time course of photoreceptor birth and development that was estimated from our immunohistochemical staining, and indicates that Crx.GFP$^+$ cells obtained from day 26 in culture are most similar to P8 rod precursors. In addition, the average number of GFP$^+$ cells present in the host ONL following the transplantation of day 26 Crx.GFP$^+$ cells (1,815 ± 423.3) is comparable to the average seen following the transplantation of day 29 virus-labelled Rhop.GFP$^+$ cells (1,750 ± 285.1), with a slight increase in the highest number observed (5,358 vs. 3,606 respectively). Given the consistently higher yields of transplantation-competent cells from each batch of differentiation culture,

as well as the lack of viral labelling required, which reduces the risk of viral particle carry-over into eyes receiving transplants, subsequent experiments to assess visual function following the transplantation of mESC-derived photoreceptor precursors were therefore carried out using D26 Crx.GFP^{+} donor cells.

Endogenous reporter lines like the Crx.GFP mESC line facilitate the detection of emerging photoreceptors without relying on viral transfection of promoter-driven reporter genes, which run the risk of integrating at undetermined genomic sites that may be subject to silencing. With the tools offered by CRISPR-Cas9 technology, additional reporters can be inserted into the Crx.GFP mESC line to expand the use of the line. Therefore, I sought to apply CRISPR-Cas9 technology combined with the inherent repair of DNA DSBs by homologous recombination to generate a mature reporter line which harbours reporter genes as 3' terminal fusion of endogenous rhodopsin and rod α-transducin. Generating a 3'UTR reporter fusion presents several advantages, such as maintenance of the full-length gene sequence with less likelihood of disruption of the coding sequence while maximising the similarity of reporter expression to that of the endogenous gene, since they are both under the same transcriptional control, and can therefore give a more accurate representation of a gene's activity. However, despite having successfully made the Rho.mCherry and Gnat1.Katushka reporter repair templates as well as the corresponding guides, I was unable to detect successful integration of the repair templates following electroporation of the plasmids into Crx.GFP ESCs. Indeed, precise genome editing tools like CRISPR-Cas9 are limited by the notoriously low efficiency of HDR compared with the NHEJ pathway. The use of adjunct methods, such as the suppression of players in the NHEJ pathway (Chu et al., 2015; Lin et al., 2016), may enhance HDR. Additional work is also necessary to optimise conditions for detecting successful integration and screening colonies for successfully-edited clones.

To date, studies using reporter-based selection of murine photoreceptor precursor cells have been very successful in demonstrating that the ontogenetic stage of the donor cell has a critical influence on the number of reporter-labelled cells present in the host retina after transplantation (MacLaren et al., 2006; Bartsch et al., 2008; Pearson et al., 2012; Eberle et al., 2011). The generation of endogenous reporter ESC lines to assess the activity of developmental markers is therefore important for facilitating the move from donor-derived cells to ESC-derived cells as a source of

donor cells for cell replacement therapy. Moreover, it will improve our understanding of *in vitro* derived retinal structures for studying development and for providing testing platforms for drug screening (Rowntree and McNeish, 2010; Inoue and Yamanaka, 2011). Reporter genes inserted in the ESCs will persist in the differentiating cells arising from the ESCs, and the expression of the reporter gene at a distinct stage in differentiation will facilitate the use of FACS to purify stage-specific cells during development. Apart from being able to compare the transplantation competence of cell populations at various developmental stages, stage-specific cells can be profiled for unique surface markers that can be used for selecting transplantation-competent cells. Given the advancements in hESC and hiPSC differentiation, the development of a similar hESC or hiPSC line with endogenous reporters for photoreceptor markers (Crx, rhodopsin, Gnat1) will be an excellent tool to determine the optimal ontogenetic window of hESCs and hiPSCs in differentiation cultures for functional integration into the host retina following transplantation, and also to identify cell surface markers that can be used to purify desired cell populations at the optimal ontogenetic stage for transplantation.

Chapter 5 : Assessment of retinal function following the transplantation of mESC-derived photoreceptors into mouse models of retinal degeneration

5.1 Introduction

The ultimate aim of photoreceptor replacement therapy is the rescue of visual function. To this end, transplanted photoreceptor precursors need to mature *in vivo,* developing photoreceptor outer segments and forming functional synapses with the host inner retinal circuitry. In the previous two chapters, I demonstrated a significant increase in the number of GFP^+ cells present in the host ONL following the transplantation of GFP-labelled mESC-derived photoreceptor precursors by improving the transplantation protocol, as well as establishing the optimal developmental stage of mESC-derived photoreceptor precursors for transplantation. I next sought to assess whether mESC-derived photoreceptor precursors transplanted into the subretinal spaces of recipient mice would be able to generate electrical signals in response to light stimulation and propagate these signals to the inner retina.

To do this, I recorded the spiking activity of retinal ganglion cells (RGCs) from retinal explants using a multi-electrode array (MEA). This technique was chosen over other methods of assessing retinal function for several reasons: firstly, because of the number of GFP-labelled cells in the ONL following transplantation. The sensitivity of the commonly-utilised electroretinography (ERG) is insufficient for detecting and evaluating small improvements in focal areas of the retina. ERGs measure the summated neural activity of the retina, and previous work from our lab has demonstrated with gene replacement therapy that generation of a reproducible scotopic ERG response requires at least approximately 150,000 donor reporter-labelled cells (Pearson et al., 2012). On the other hand, single-cell intracellular electrode recordings by patch-clamp can provide detailed information about single neurons, but do not allow for the study of population interactions (Shlens et al., 2009; Gauthier et al., 2009; Stafford et al., 2009). Calcium imaging allows for the study of populations of neurons, but it is technically difficult to achieve selectivity and specificity of cell labelling, particularly for light-sensitive cells, which require laser spot activation of the outer segment (Nakatani et al., 2002). The use of a MEA overcomes these aforementioned limitations, as extracellular electrical action

potentials can be simultaneously recorded from numerous neurons in a single retinal explant over an extended period of time, allowing for the study of population features without loss of temporal resolution (Meister et al., 1994). Furthermore, downstream spike sorting of the recorded spikes offers the possibility of isolating single neurons, thereby overcoming a limitation fundamental to most extracellular recording techniques. Finally, the retina is particularly amenable to MEA recordings as RGCs, the output cells of the retina, are very accessible and can be brought into close proximity with the MEA. Numerous studies in recent years have indeed demonstrated the use of MEAs for high-throughput, simultaneous recordings of retinal responses to presented visual stimuli (Fiscella et al., 2012; Tikidji-Hamburyan et al., 2014; Santos-Ferreira et al., 2014; Meister et al., 1994; Reinhard et al., 2014; Field et al., 2010).

In brief (see Sections 2.14 and 2.15 for further detail), for *in vitro* MEA recordings from isolated retinal slices, the retina is dissected out of the eye and mounted with the ganglion cell layer in close apposition to the MEA electrodes. The light stimulus is applied from the top and is first detected by photoreceptors in the ONL. Light-evoked signals are transmitted from each rod or cone photoreceptor to bipolar cells, which in turn each connect directly or indirectly to RGCs. The signals are modified along the way by lateral interactions mediated by horizontal and amacrine cells at the photoreceptor and bipolar cell level respectively (Masland, 2001; Wassle, 2004). The final retinal output is generated as extracellular action potentials in RGC axons, which can be detected by the electrodes of the MEA (Figure 5.1).

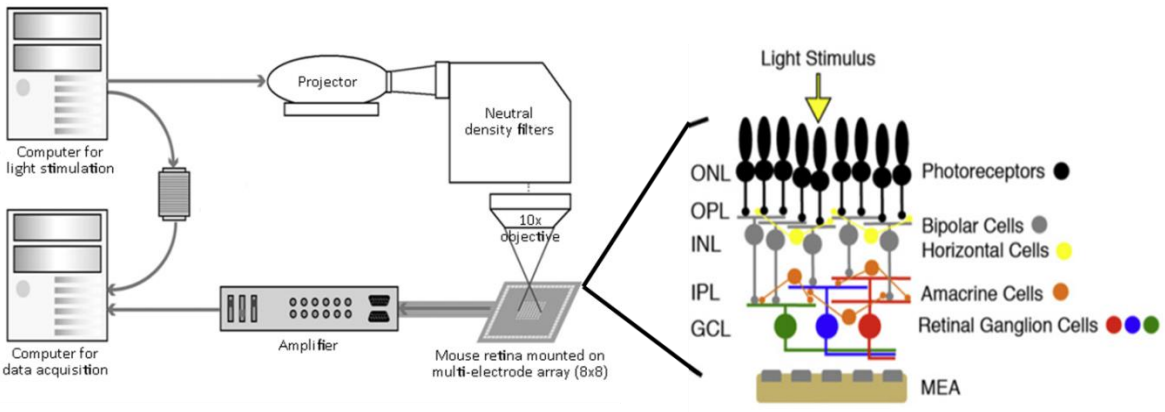

Figure 5.1: Schematic of MEA experimental set up. The visual stimulus is projected onto the photoreceptors of the mounted retina explant, and extracellular voltage traces are recorded from the multiple electrodes of the MEA in contact with the retinal ganglion cell layer.

The number of GFP+ cells in the recipient ONL following transplantation has been shown to vary significantly depending on characteristics of each model of retinal disease, such as glial scarring and outer limiting membrane integrity (Barber et al., 2013). In addition, the extent to which inner circuitry is maintained in the absence of functioning photoreceptors has been shown to vary across models with different rates of degeneration (Strettoi, 2015; Marc et al., 2003). As such, the extent of visual function restored after photoreceptor replacement therapy can be expected to vary across models. Therefore, I performed the assessment of retinal function through MEA recordings in the WT retina as well as three transgenic mice models of inherited photoreceptor degeneration. These models exhibit different rates of disease progression and retinal degeneration – namely, the *Gnat1*$^{-/-}$, the *Opn4*$^{-/-}$ *Gnat1*$^{-/-}$ *Cnga3*$^{-/-}$ (*OGC*) triple-knockout mouse, and the *Aipl1*$^{-/-}$ mouse.

The *Gnat1*$^{-/-}$ mouse has been the model of choice for our previous transplantation studies, and is a model of congenital stationary night blindness that lacks high-sensitivity rod function while retaining normal cone function. In contrast, targeted deletion of the genes encoding for Gnat1, cone cyclic nucleotide gated channel α3 subunit (Cnga3), and melanopsin (Opn4) is expected to completely abolish photoreception in the *OGC* triple-knockout mouse model, since rods, cones, and melanopsin-containing intrinsically photosensitive RGCs (ipRGCs) are understood to account for all photosensitivity in the mammalian retina. Indeed, functional studies employing this model have shown a lack of scotopic and photopic ERG responses as well as accessory visual functions (Hattar et al., 2003; Allen et al., 2010), as would be expected in the absence of these critical elements of phototransduction. The absence of these proteins does not appear to affect the genesis, development, survival, and connectivity of photoreceptors and RGCs; correspondingly, retinal morphology of the *OGC* retina appears similar to the healthy wild-type retina (Hattar et al., 2003). Of particular clinical interest is the extent to which visual function can be restored following transplantation into a model of advanced retinal degeneration, where little or none of the host ONL is left, as photoreceptor replacement therapy is likely to be most necessary in such cases. In contrast to the *Gnat1*$^{-/-}$ and *OGC* triple-knockout mouse models, the *Aipl1*$^{-/-}$ mouse displays a rapid rate of retinal degeneration, with the death of all photoreceptors by 4 weeks of age, followed by complete loss of the ONL beyond this age (Ramamurthy et al., 2004; Dyer et al., 2004). Targeted disruption in the *Aipl1* gene prevents the production of the aryl hydrocarbon receptor-

interacting protein-like 1 (Aipl1) protein, which is expressed exclusively in both rod and cone photoreceptors (van der Spuy et al., 2002). Aipl1 is not essential for the genesis and development of photoreceptors; as such, normal retinal histology and photoreceptor morphology is observed at birth (Dyer et al., 2004; Ramamurthy et al., 2004). It is, however, essential for rod and cone photoreceptor survival and function, and in its absence there is a drastic destabilisation and rapid degradation of both rod and cone phosphodiesterase (PDE) subunits (Kirschman et al., 2010). The loss of PDE activity leads to the accumulation of cGMP, resulting in a continuous Ca^{2+} influx through cGMP- and voltage-gated Ca^{2+} channels. The calcium overload is thought to trigger apoptotic cell death in the photoreceptors (Fain and Lisman, 1999). This mechanism of photoreceptor death is similar to that in the commonly-used *rd1/rd1* mouse model of retinitis pigmentosa, where there is a null mutation in the *Pde6b* gene encoding the β6-subunit of rod PDE. A key difference, however, is that in the *rd1/rd1* model, cone loss occurs secondary to rapid rod loss and cones are still functional during the initial phase of rod degeneration (Strettoi et al., 2002); whereas in *Aipl1*$^{-/-}$ mice, both rods and cones degenerate simultaneously and are functionally quiescent at all ages tested (Ramamurthy et al., 2004).

The main aims of this study were firstly, to design an MEA set up and stimulus protocol that will enable the detection and characterisation of RGC responses in the retinas of wild-type (WT), *Gnat1*$^{-/-}$, *OGC*, and *Aipl1*$^{-/-}$ mouse models of retinal degeneration; and secondly, to assess the extent to which retinal function may be restored in selected mice models following the transplantation of mESC-derived photoreceptor precursors, through the use of the MEA.

5.2 Results

5.2.1 Designing a MEA setup and light stimulus protocol for the detection of rod-driven RGC responses in the dark-adapted WT retina

5.2.1.1 Designing the MEA setup

The fundamental MEA set up is as described above in , whereby the retinal explant is mounted ganglion cell side down on the MEA, so that any retinal output generated as extracellular action potentials can be detected by the electrodes.

When preparing the retinal explant, it was important to remove the vitreous thoroughly for good electrode contact, which is not always easy to achieve if the eye is heavily diseased, as the vitreous tends to be strongly attached to retina, or if the retina is very thin. Care had to be taken to avoid introducing tears in the retina especially when removing the optic nerve, as any holes in the explant might cause turbulence in the flow through the perforations in the array, and also to avoid causing focal damage to the outer segments.

A perforated 60-electrode MEA was chosen to improve signal-to-noise ratio by ensuring better contact between electrodes and the strongly-curved mouse retinal explant, to increase oxygen and nutrient supply to the explant, as well as to minimise tissue displacement during recordings (Reinhard et al., 2014). An upper perfusion loop was set up to supply the explant with fresh oxygenated solution, while a lower perfusion loop controlled the amount of negative pressure on the explant. It was particularly important to ensure that the negative pressure applied to the underside of the retinal explant was sufficiently high to allow the retinal slice to flatten and achieve good explant-electrode contact, without tearing the explant tissue and causing it to be suctioned through the perforations in the array.

In order to probe for rod-driven RGC responses, it was important to ensure that rods were not photobleached prior to recording. All MEA recordings were therefore performed on retinal explants obtained from dark-adapted mice in the dark under dim red light (λ_{MAX} = 650nm), which is reported to be below the spectral sensitivity of murine detection and has minimal impact on rod photopigment activation (Govardovskii et al., 2000). In addition, prior to recording, all retinal slices were perfused for 30 minutes with 9-*cis*-retinal, which is an artificial analogue of the chromophore11-*cis*-retinal. This is performed to enable regeneration of Rhodopsin in

the absence of RPE, as the exposure to GFP-excitation light, used to search for areas with transplanted cells, may have resulted in the depletion of usable 11-cis retinal for Rhodopsin regeneration and subsequent rod photobleaching (Schadel et al., 2003; Lamb and Pugh, 2004). Moreover, this adaptation period was also to allow the retina to settle and adapt to the new environment, as well as for spontaneous activity of RGCs to appear, as this can be sparse at the beginning of the experiment.

A square pulse of white light was generated by the projector and projected onto each retinal explant as brief flashes. The light intensity of the flash stimulus was set by placing neutral density (ND) filters in the light path to keep all other factors constant apart from the light intensity of the stimulus. Recordings were made in discrete 1 log unit increments, from the lowest light intensity (ND5) to the highest (ND0), in order to avoid bleaching by the stimulus. A 10-minute adaptation period following each neutral density filter change was included to allow for the retina to adapt to the new ambient light level before each recording. Although the inclusion of this adaption period further lengthened the duration of the protocol, it is necessary to minimize the effects of light adaptation, especially at higher intensities of the flash stimulus.

As alluded to earlier, the reliability of the MEA data collected is inevitably user-dependent, and the success of each preparation is dependent on numerous factors, such as the thickness of the retina handled, the time taken to isolate the retina and mount the explant, and the ability to gauge a suitable degree of negative pressure to apply to the explant. The rejection rate of preparations indeed decreased over time as my skill in manipulating the retina and adjusting pressure improved with practice. To minimise any skill-related bias, only preparations that showed good retinal health throughout the entire recording were subject to downstream analysis, i.e. (1) majority (at least 40 out of 60) of electrodes should show spontaneous spiking activity; and when inspecting the high-pass filtered data, (2) the noise level should not exceed 20 μV and (3) spiking activity should have an amplitude of 100–250 μV (Figure 5.2). Recordings were rejected from further downstream analysis if there was reason to suspect that the health of the retina might have been compromised in the course of recording. Finally, as far as possible, treated and control retinal explants had to be taken from age-matched animals rather than from the same animal, because it was

observed that the viability of retinal explants taken from the second eye tended to be compromised due to the length of each set of recordings.

This recording setup using a perforated MEA has been optimised to allow long-term, stable spike recordings from RGCs in retinal explants. The use of a perforated MEA has proven to be particularly crucial for enhancing signal-to-noise ratios, which is crucial for downstream spike-sorting into single neuron units. Spike-sorted units can be analysed by a multiplicity of methods to elucidate information about individual neuronal characteristics, relationships with other neurons, and RGC response properties, etc. The range of neutral density filters and corresponding light intensities employed in our setup further allows for the detection of RGC responses driven by both rod and cone photoreceptors, as shown in Section 5.2.1.2. The use of this setup can be extended through the use of different stimuli, such as a binary checkerboard (Reinhard et al., 2014) or a Gaussian white noise (Koehler et al., 2011) stimulus, to answer various questions.

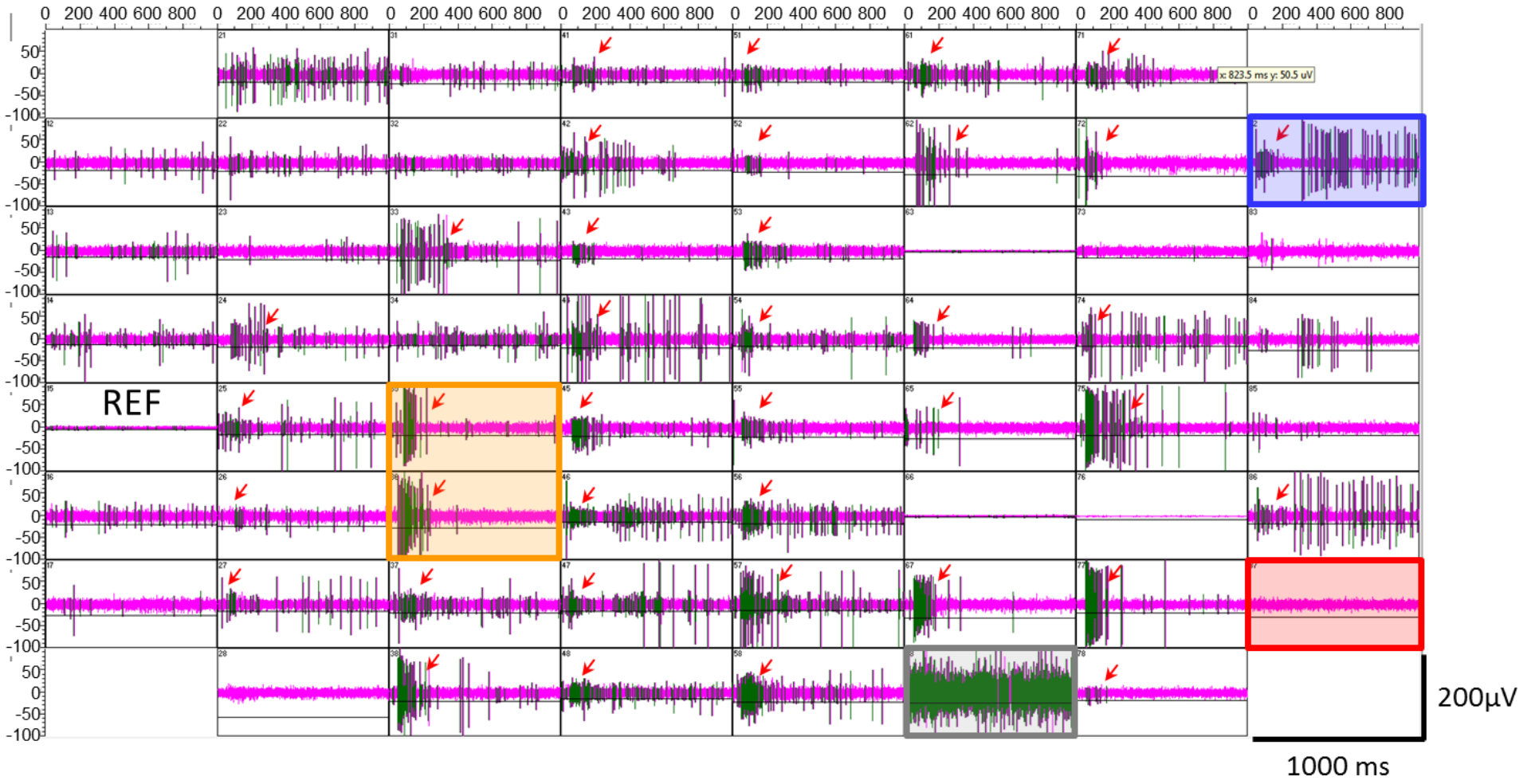

Figure 5.2: Representative image of a 500Hz high-pass filtered MC_Rack display. Spontaneous spiking activity with good signal-to-noise ratio is visible on majority of the electrodes. In optimal recordings, all electrodes would have activity with amplitudes such as the electrode marked in "blue", although a signal-to-noise ratio and activity level like on the "orange" electrodes are also sufficient. On the "red" electrode, the signal-to-noise ratio is too small. The "grey" electrode shows a noisy channel. Red arrows indicate a sudden increase in spiking in response to light stimulus that has just been triggered. In this example, most of the channels show light-responsive spike bursts.

5.2.1.2 Designing a light stimulus protocol for the detection photoreceptor-driven RGC responses in the WT retina

Having designed the MEA setup, I next sought to determine suitable stimulus parameters for detecting photoreceptor-driven RGC responses. For each light level, the length of the flash stimulus presented as well as the inter-stimulus recovery interval was varied in order to determine the optimal conditions for eliciting a functional response from both endogenous and transplanted photoreceptors. I hypothesized that the photosensitivity, response time, and/or recovery kinetics of transplanted photoreceptors would be less efficient than that of endogenous wild-type rods, even after maturation in the recipient retina by 3 weeks post-transplantation. This is because any small reduction in outer segment disc formation, and thus Rhodopsin expression, in transplanted rods is likely to lower the probability of a photon activating a Rhodopsin molecule, such that higher light intensities and/or a longer length of flash stimulus may be required to elicit a response. Additionally, transplanted photoreceptors may attempt to signal without normal ribbon synapses, which would likely to need a longer integration time at downstream bipolar cells in order for the signal to be above the level of what would otherwise be considered noise.

Taking this into consideration, I compared 3 different stimulus protocols on dark-adapted 8-12 week old C57BL6/J WT retinal explants (n=3 retinae): a 50ms stimulus with a short 2s inter-stimulus recovery interval (Figure 5.3A and A'), a 100ms stimulus with a long 20s inter-stimulus recovery interval (Figure 5.3B and B'), and a 500ms stimulus with a long 20s inter-stimulus recovery interval (Figure 5.3C and C'). 50ms was chosen as a baseline because previous MEA experiments conducted by colleagues in our lab had observed good responses to 50ms-long stimuli in wild-type, rod and cone α-transducin double mutant *rd17*, and *cpfl1* retinas. Furthermore, the flicker fusion threshold, which is how fast a flicker needs to be before it is perceived as a steady light, is approximately 15Hz (a 66ms flash) for rods, and 60Hz (a 16.67ms flash) for cones (Sharpe and Stockman, 1999). Our tested stimulus lengths of 50ms, 100ms, and 500ms on a black background are therefore expected to be visible to functioning photoreceptors.

As expected, RGC responses could be evoked by a flash stimulus as short as 50ms in duration, even at the lowest light intensities (ND5 and 4). However, we observed that the shorter stimulus lengths (50ms and 100ms) were consistently less

able to elicit OFF responses, compared to the 500ms-long stimuli. In addition, at high light intensities (ND1 and ND0), the shorter 2s inter-stimulus recovery interval between flashes appeared to be insufficient for photoreceptors to remain dark-adapted, and stimulation with the brightest flash stimulus often resulted in relatively rapid bleaching and reduction of subsequent responses. Therefore, for subsequent experiments, I decided to use the 500ms-long flash stimulus with a long 20s inter-stimulus recovery interval in order to maximise the possibility of detecting light-driven RGC responses.

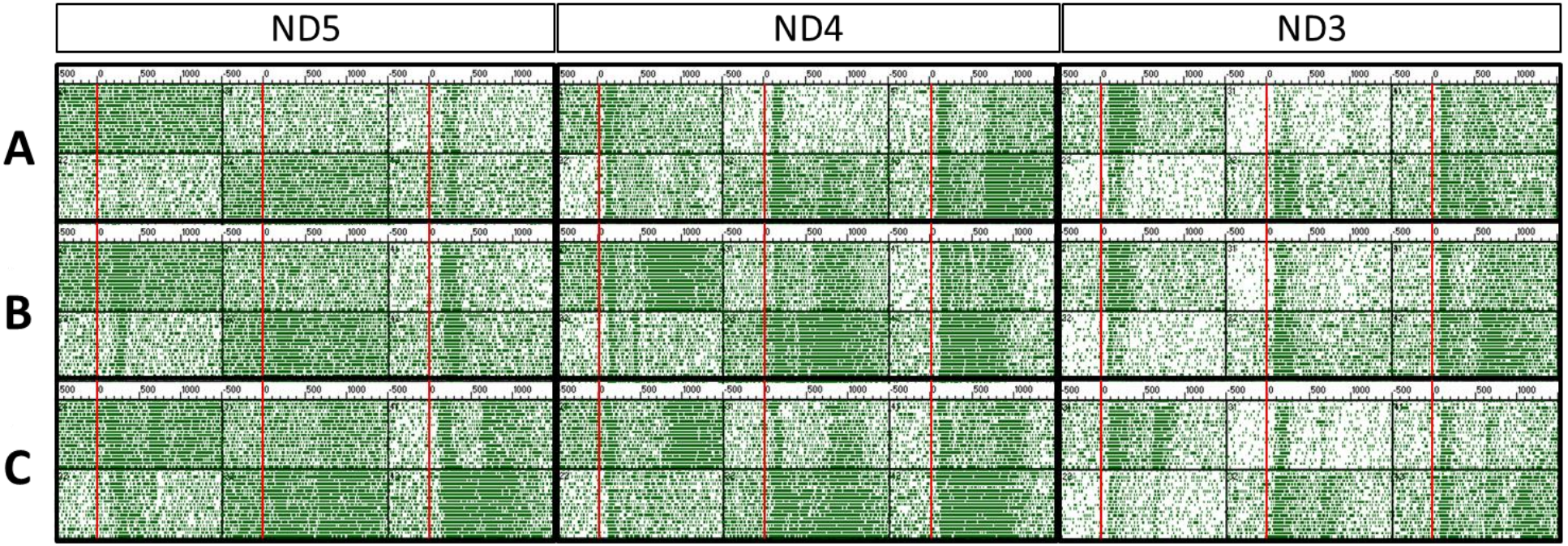
ND5
ND4
ND3
A
B
C

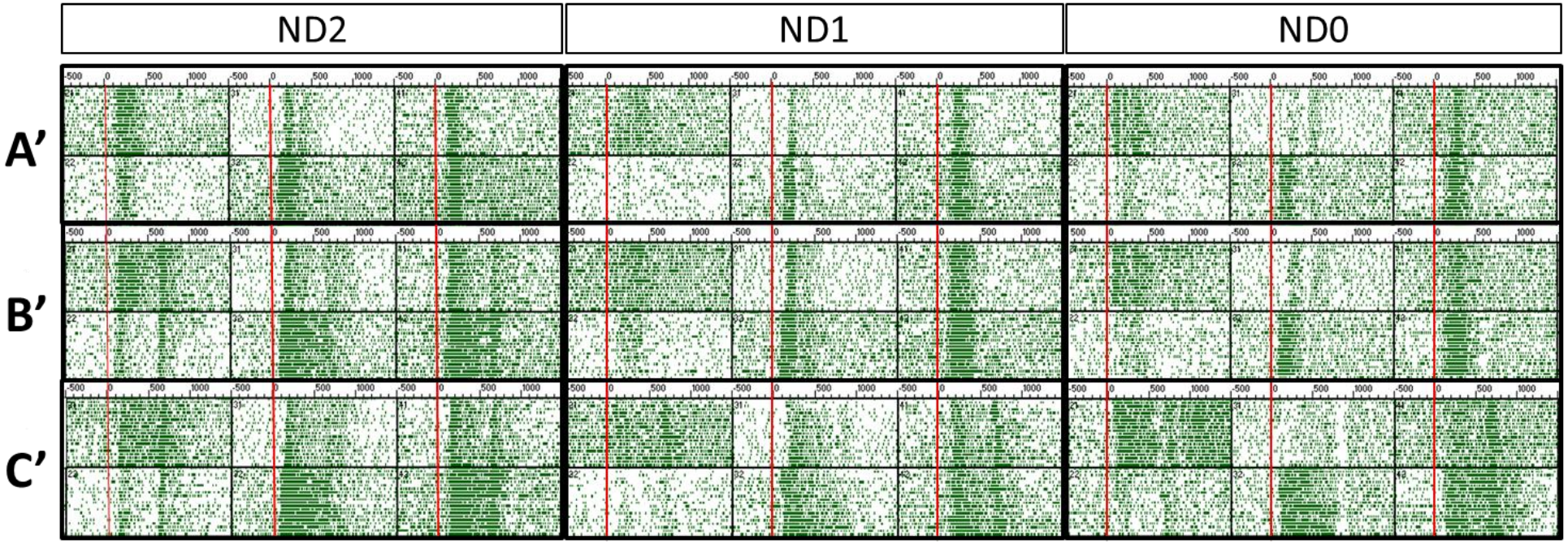

Figure 5.3: Comparison of stimulus protocols using varying lengths of flash stimulus and inter-stimulus recovery intervals. A-C'. Representative raster plots of unsorted responses seen on the same 6 channels using the 3 different stimulus protocols, moving from low (ND5) to high (ND0) light stimulus intensities. A. Channels with 50ms stimulus, 2s recovery. B. Channels with 100ms stimulus, 20s recovery. C. Channels with 500ms stimulus, 20s recovery. In each plot, a baseline pre-stimulus window of 500ms is shown prior to the presentation of the flash stimulus at time 0, indicated by the red line, followed by a post-stimulus window of 1500ms.

5.2.2 Characterising light stimulus-driven RGC responses in the WT retina

In order to validate the setup and stimulus protocol, I next sought to characterise the RGC responses recorded from the WT retina.

5.2.2.1 Defining light stimulus-evoked RGC responses

Spikes were first extracted from the raw voltage traces recorded from each electrode using a threshold of 3 standard deviations. It is important to note that the responses recorded in one channel may originate from more than one RGC, and multiple channels may reflect the response from the same RGC if its axon and/or cell body were in contact with multiple electrodes.

A custom-written Matlab script (written by M.R. Robinson, a PhD student in the lab) was used to generate plots to visualise the extracted spikes recorded in every channel, and also to classify the recorded response in each channel as 'significant' or not. An example of the generated plots is shown in Figure 5.4; in each plot, a baseline pre-stimulus window of 1000ms is shown prior to the presentation of the 500ms flash stimulus at time 0, followed by a post-stimulus window of 2000ms.

A raster plot is represented in Figure 5.4A, showing the spike traces of all 20 repeated trials ("sweep") by denoting the occurrence of a spike at a specific time in a sweep with a vertical tick mark, with each sweep shown on a different line. In this particular example of a transient ON response, the frequency of spiking increases sharply relative to the pre-stimulus baseline, at approximately 200ms after presentation of the light stimulus at time = 0 (indicated by the vertical red line). Here, the increase in spiking frequency is transient and there is a quick return to baseline levels of spiking even as the stimulus is maintained; however, other types of responses to the light stimulus were observed as well, and will be classified in Section 5.2.2.2.

As variability from trial to trial can be large, a peri-stimulus time histogram (PSTH, Figure 5.4B) is constructed by plotting the trial-averaged spike rate (in mean impulses per ms) as a histogram in 10ms time 'bins'. In this example, a clear peak in average spike rate is seen at approximately 200ms after stimulus presentation, followed by a quick return to baseline spike rate.

Figure 5.4C is a cumulative sum (CUSUM) plot derived from the PSTH, showing the cumulative deviation of each bin in the PSTH from the expected average baseline spike rate, which is calculated based on the 1000ms pre-stimulus window. In doing so, it offers a clear visual depiction of the change in PSTH in response to a stimulus, and the slope of the CUSUM provides a quantitative estimate of change. Limits (denoted by the diverging red lines) are set at 3 standard deviations of the CUSUM (Davey et al., 1986). If either the upper or lower limit is crossed for more than 8 time bins, the software automatically classifies the response as significant.

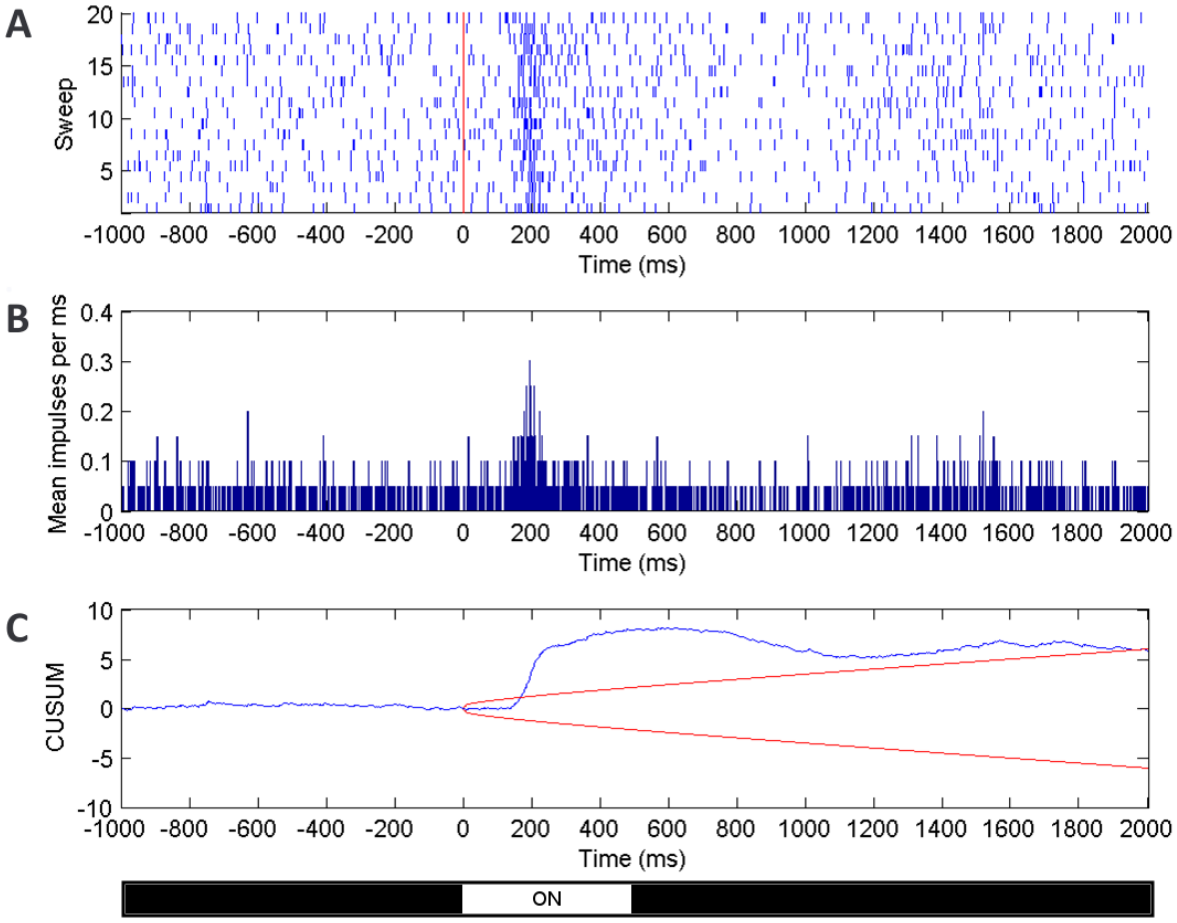

Figure 5.4: Example of the plots generated for each recorded channel. A. In each plot, a baseline pre-stimulus window of 1000ms is shown prior to the presentation of the 500ms flash stimulus at time 0, followed by a post-stimulus window of 2000ms. A raster plot showing the spike trains of all 20 sweeps. Each tick mark denotes the occurrence of a spike at a specific time in a sweep. B. A peri-stimulus time histogram (PSTH) showing the trial-averaged spike rate (in mean impulses per ms) for each 10ms time interval. C. A cumulative sum (CUSUM) plot showing the cumulative deviation of the PSTH from the baseline average spike rate, as set by the 1000ms pre-window.

Additional checks of all channels identified as light-responsive by the algorithm were carried out by hand to discriminate true from false positive responses (Figure 5.5). Short (<10ms) violations of the threshold limits (Figure 5.5A), as well as instances in which the spike rate narrowly crossed the expected limits for a reasonable duration but did not appear to be in response to light stimulus onset or offset (Figure 5.5B), were excluded from downstream analysis. Channels with a very low baseline spike rate (5 or less spikes per sweep, or an average firing rate of <0.1 impulses per ms) and a lack of consistency were excluded as well due to the inability of the algorithm to accurately calculate threshold limits for such cases (Figure 5.5C).

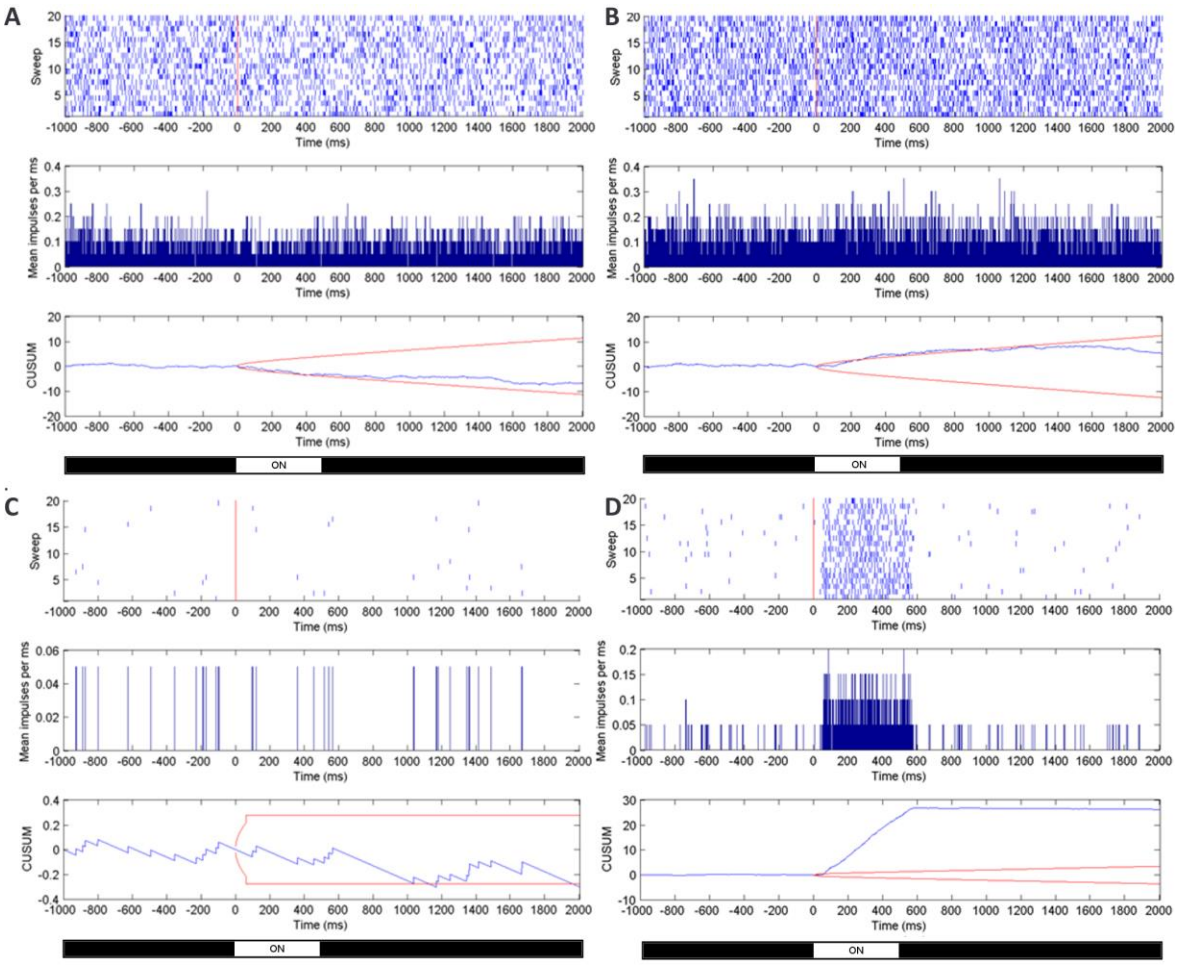

Figure 5.5: Examples of false positive 'responses' excluded from downstream analysis, as seen on the raster plots, PSTHs and CUSUM plots. A. A short (<10ms) violation of the threshold limits B. Slight crossing of threshold limits for a reasonable duration, but not in response to light stimulus onset or offset. C. Low baseline spike rate (5 or less spikes per sweep, or an average firing rate of <0.1 impulses per ms) and a lack of consistency between sweeps, resulting in inaccurate calculation of threshold limits. D. Suspected electrical artefact created by high intensity light hitting a bare electrode.

Figure 5.5D shows the example of a 'response' that was initially included in downstream analysis. However, retrospective examination of all occurrences of this 'response' led us to conclude that this is unlikely to be a physiological response. It was occasionally observed in MEA recordings taken from retinal explants across all tested different models, occurring only at the highest light level, ND0, with the exception of one preparation where it was observed at ND1 as well. This response is unlike a typical sustained 'ON' response (described in Section 5.2.2.2) in a number of ways – the latency of onset is evidently shorter, approximately 50ms after the stimulus is triggered; the duration consistently exactly 500ms long, corresponding to the length of the stimulus, and the strength of the response is constant throughout without the usual tailing off, giving it a classic stereotypic profile. It is, therefore, perhaps more plausibly an electrical artefact created by the light stimulus hitting a bare electrode at a high light intensity. Furthermore, it is not unreasonable to suspect the likelihood of this occurring is higher towards the end of the recording, as the explant may have been sucked through the perforations, thereby exposing an electrode; alternatively, the explant may have shifted in the course of the recording.

Finally, there were also instances of stimulus-evoked responses that were not identified by the algorithm as light-responsive (Figure 5.6). Figure 5.6A and B show examples of weak but distinct ON and OFF responses respectively that fail to cross the threshold limits. However, these were very rare, indicating that the employed algorithm was sufficiently sensitive in identifying majority of true light stimulus-evoked responses. These false negatives were taken note of when they occurred, but were not included in downstream analysis. Based on the frequency and sporadic manner of occurrence, there was no indication that the threshold detection method was systematically failing to pick up on a certain class of response.

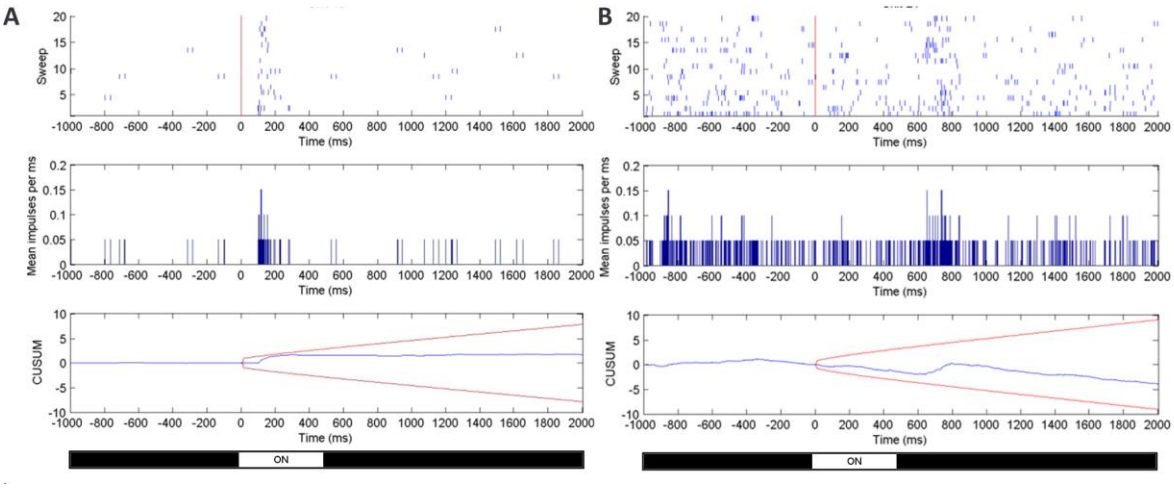

Figure 5.6: Examples of false negative responses. A. ON and B. OFF responses that failed to cross the threshold limits and were therefore not identified by the algorithm as light-responsive.

5.2.2.2 Classification of light-evoked RGC responses in the WT retina

Numerous studies of the mouse retina using various electrophysiological techniques have classified RGC responses as ON, OFF, and ON-OFF, based on changes in RGC spiking rate relative to stimulus onset and offset (Nirenberg and Meister, 1997; Tian and Copenhagen, 2003; Stone and Pinto, 1992; Tikidji-Hamburyan et al., 2014; Santos-Ferreira et al., 2014). These response classes appear to correspond to morphologically and functionally distinct classes of RGCs. In keeping with these reports, a range of light-evoked RGC responses were detected from the WT retina across the 5 log units of light intensities surveyed, which could likewise be classified into different response types by visual inspection of changes in spike rate (Figure 5.7 and Figure 5.8, n = 3 retinas). An ON response was defined as an increase in spike rate during the period of light stimulus (Figure 5.7A, B); an OFF response as an increase in spike rate following termination of the light stimulus (Figure 5.7C, D); and an ON-OFF response as increases in spiking to both light onset and offset (Figure 5.7E). The distribution of ON responses in the degree of transiency appeared to fall into two distinct groups – some were sustained throughout the length of the 500ms stimulus (Figure 5.7A), whereas others were brisk and transient, lasting for approximately 100ms (Figure 5.7B). Similarly, OFF responses were either sustained (Figure 5.7C) or transient (Figure 5.7D).

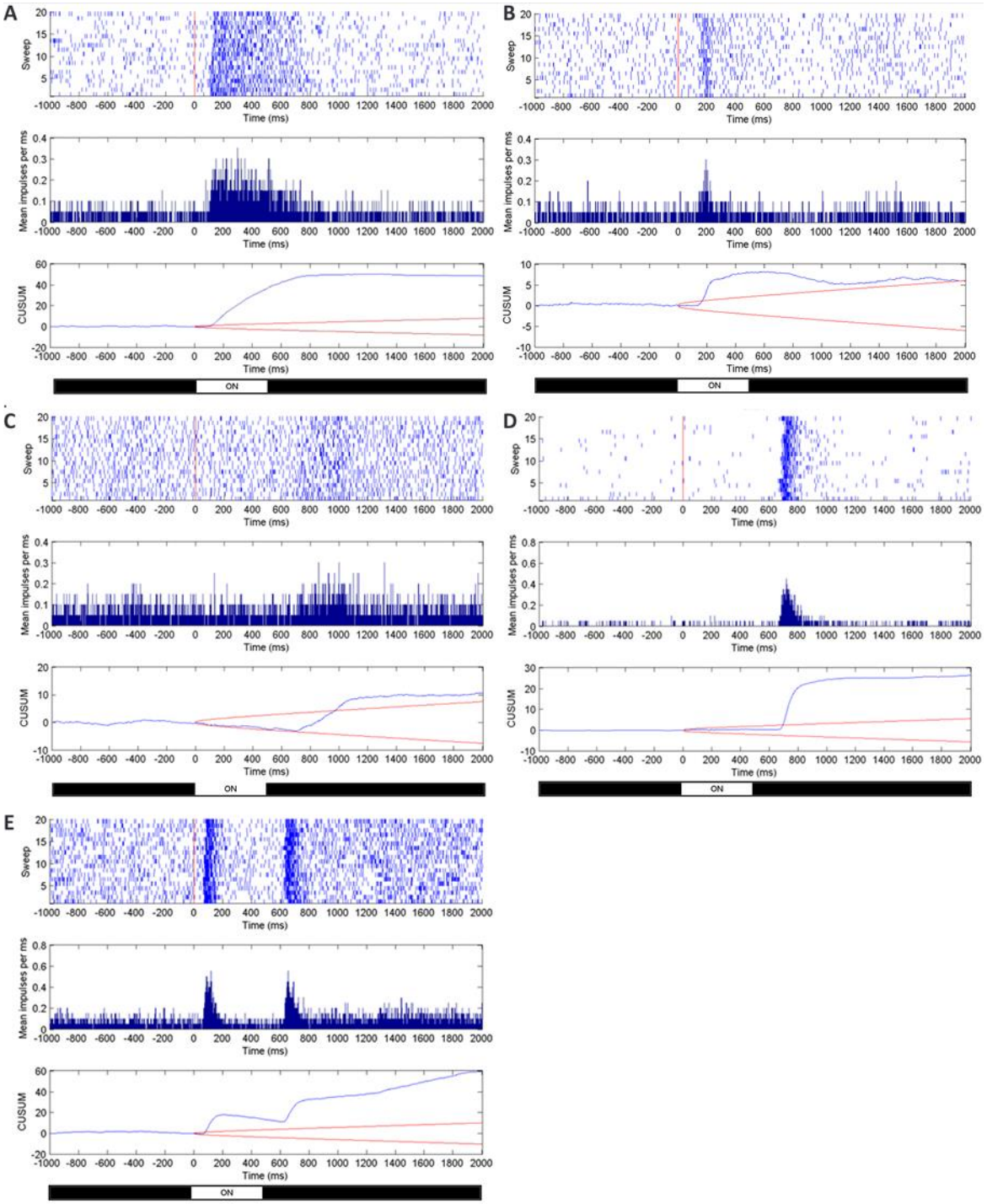

Figure 5.7: Representative examples of ON (A, B), OFF (C,D), and ON-OFF (E) RGC responses to a 500ms light pulse triggered at time 0. Each tick mark on the raster plot represents the occurrence of one action potential ('spike'). RGC spiking was recorded from the MEAs 2000ms before and 3000ms after stimulation with a 500ms-long flash; these examples only display the 1000ms before and 2000ms after. The flash stimulus was presented 20 times ('sweeps') at each tested light intensity. Responses were classified based on the change in spiking pattern relative to light onset and offset, and were either transient (B, D, E) or sustained (A, C).

Interestingly, the type and duration of RGC response detected by each electrode was frequently observed to change as the light intensity of the stimulus was increased (Figure 5.8). It was rare to find channels in which the type and duration of the response was consistent throughout all 6 light intensities.

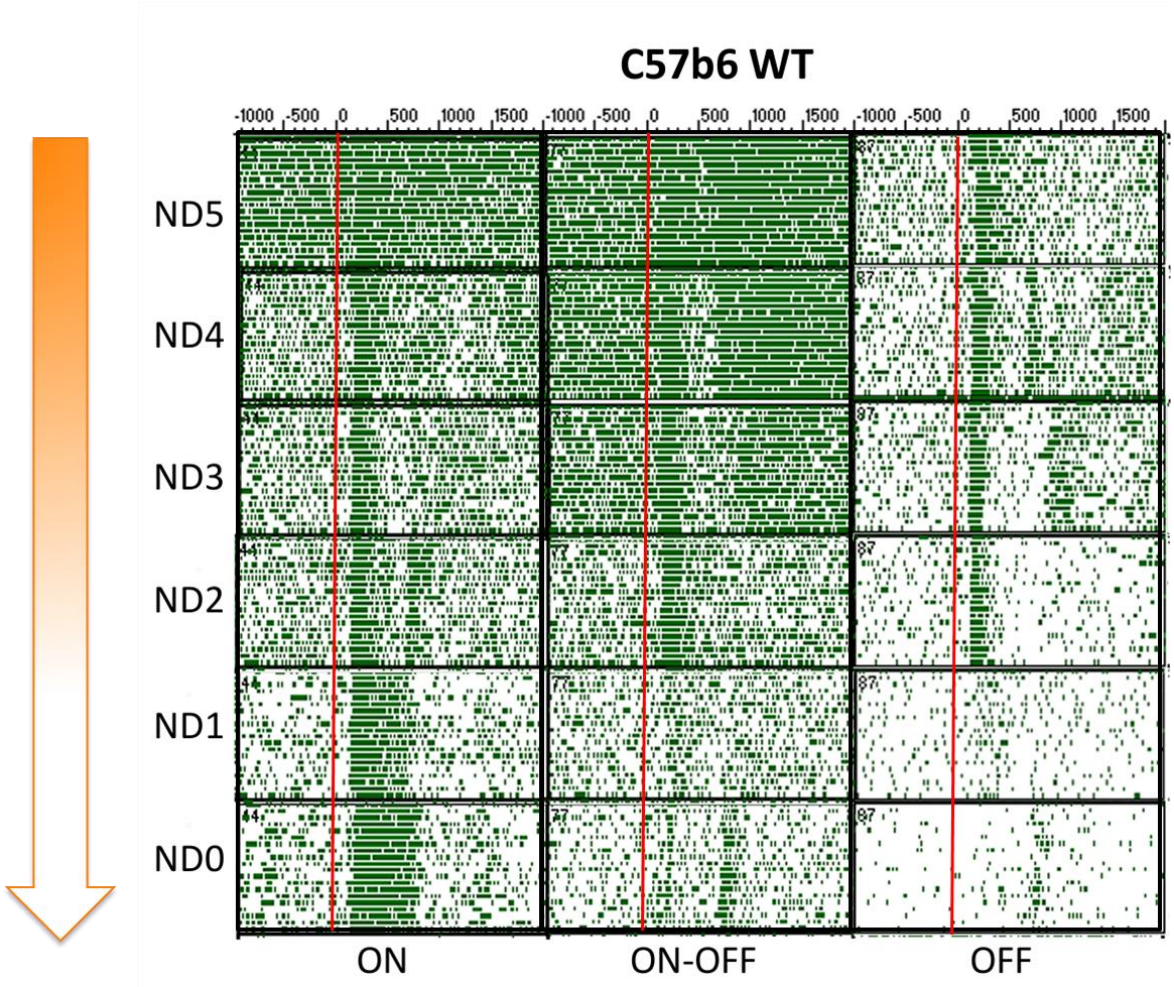

Figure 5.8: RGC responses to a 500ms light pulse from a C57BL6/J WT mouse retina. Representative responses beginning from the lowest (ND5) to highest (ND0) light intensities, as recorded on a sample of 3 channels. ON, ON-OFF, and OFF response types could be observed across all light levels. Additionally, the type of RGC response detected in each channel can be seen to change as the light intensity of the stimulus is increased. Red line represents the onset of light stimulus.

To establish the number and proportion of light-responsive channels that showed ON, OFF, or ON-OFF response types on a WT retina MEA recordings were analysed and quantified (Figure 5.9 A, B; n=3 different retinae, represented in the graphs as individual columns). The total number of light-responsive channels varied across retinal preparations, but for a preparation with good tissue-electrode contact, it was possible to achieve a maximum of approximately 45-55 responding channels (Figure 5.9A). There was a significant variation in the proportion of each response type between preparations (Figure 5.9B), especially at the lowest light intensity, ND5. However, it is apparent that all 3 response types are present at all light intensities, with the exception of ND3, where no OFF responses were recorded. OFF responses were consistently less frequently observed compared to ON and ON-OFF responses at all light intensities.

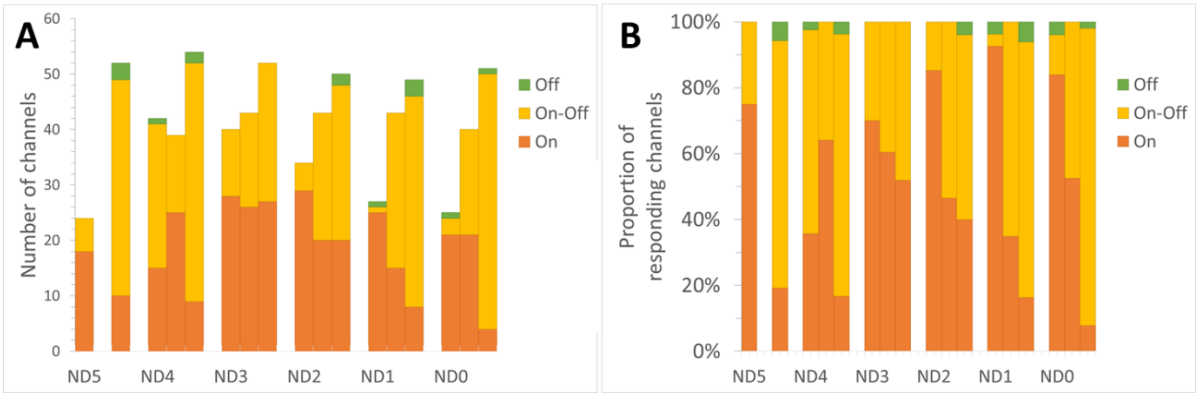

Figure 5.9: Quantification of response types in the WT retina. The A. number and B. proportion of light-responsive channels showing ON, OFF, or ON-OFF response types at each light intensity, quantified from MEA recordings from WT retinal explants (n = 3 retinas).

5.2.3 Investigating light stimulus-driven RGC responses in the Gnat1$^{-/-}$ retina

5.2.3.1 Characterisation of RGC responses in the Gnat1$^{-/-}$ retina

Having shown that the MEA set up and stimulus protocol is able to detect all major types of RGC responses across a large range of light intensities in the WT retina, I next sought to investigate light-evoked responses in the *Gnat1*$^{-/-}$ retina, which has been the model of choice for our previous transplantation studies. *Gnat1*$^{-/-}$ mice have been reported (Calvert et al., 2000; Umino et al., 2008) and verified by others in our lab to lack high-sensitivity rod function, while retaining normal cone function; as such, light levels at which *Gnat1*$^{-/-}$ mice are lacking a light stimulus-driven response can be inferred to correspond to a scotopic dim light range.

Although rods respond in dim scotopic conditions and cones respond in bright photopic ones, there is a degree of overlap in the light intensity range in which both rods and cones respond to, which is known as the mesopic range. The full response thresholds of light detection by cones must therefore be determined in the context of our experimental parameters, as cone-driven signals may overlap with and mask signals from transplanted rods. To this end, the cone response threshold was determined by comparing RGC responses of the *Gnat1*$^{-/-}$ mice lacking rod function to the previously-characterised C57BL6/J WT mice at different light intensities.

MEA recordings were made from *Gnat1*$^{-/-}$ retinas stimulated with same 500ms flash stimulus as above, in order of increasing light intensity from ND5 to ND0. Robust ON, OFF, and ON-OFF RGC responses to the light stimulus, similar to that observed in the WT retina, were observed at light intensities only from ND3 upwards in *Gnat1*$^{-/-}$ retinas (Figure 5.10, n = 3 retinas). Similar to the WT retina, the type of response recorded by an electrode was often observed to change from one light intensity to the other. However, there was a complete absence of RGC response in the *Gnat1*$^{-/-}$ retinas at ND5 and ND4. shows representative raster plots of the spiking recorded from 3 channels in response to the stimulus in order of increasing light intensity, with blue boxes indicating an absence of response to the light stimulus.

The absence of light-evoked response in the *Gnat1*$^{-/-}$ retina at ND5 and ND4 was unlike the WT retina, where robust RGC responses to light stimuli were still observed at ND5 and 4. This difference reflects the absence of rod function and loss of cone-driven responses in the *Gnat1*$^{-/-}$ retina. On this basis, I estimated that ND5 and 4 corresponded to baseline 'scotopic' light levels below the cone response threshold in the *Gnat1*$^{-/-}$ retina. ND3 is likely to be at the very bottom of the 'mesopic' range in the *Gnat1*$^{-/-}$ retina and the highest light intensities, ND1 and ND0, were estimated to correspond to 'photopic' levels and acted as positive controls of cone function.

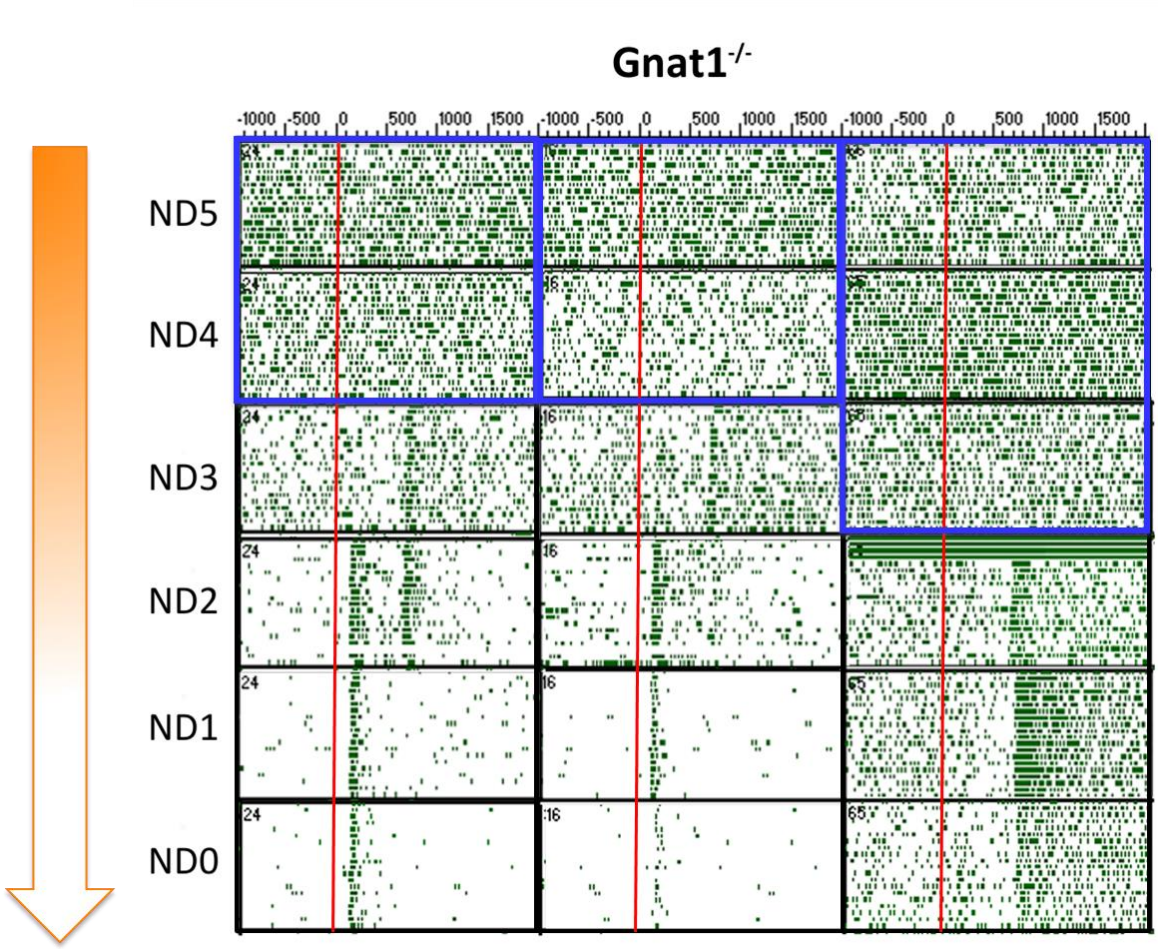

Figure 5.10: RGC responses to a 500ms light pulse from an untreated *Gnat1*$^{-/-}$ mouse retina. Representative examples of responses beginning from the lowest (ND5) to highest (ND0) light intensities, as recorded on a sample of 3 channels. At ND4 and ND5, RGC responses could not be detected in *Gnat1*$^{-/-}$ retinas, unlike in WT retinas. Red line represents the onset of light stimulus.

Next, to characterise the type of responses observed in the *Gnat1*$^{-/-}$ model, the number and proportions of ON, ON-OFF, and OFF responses were quantified (Figure 5.11A and B respectively, n=3 retinae, represented on separate columns). As mentioned above, no responses were observed for ND5 and ND4. The number of responsive channels was similar to the WT retinas from ND2 to ND0. However, there was a noticeably lower number of light-responsive channels in the *Gnat1*$^{-/-}$ retina at ND3, as compared to the WT retina. OFF responses were also observed at ND3 in *Gnat1*$^{-/-}$ retinas in a consistently larger proportion compared to ON and ON-OFF response types at the other tested light levels; whereas OFF responses appeared to be absent in WT retinas at ND3 (Figure 5.11A). Finally, the proportion of response types from ND2 to ND0 appear to be similar in the *Gnat1*$^{-/-}$ and WT retinas (Figure 5.11B).

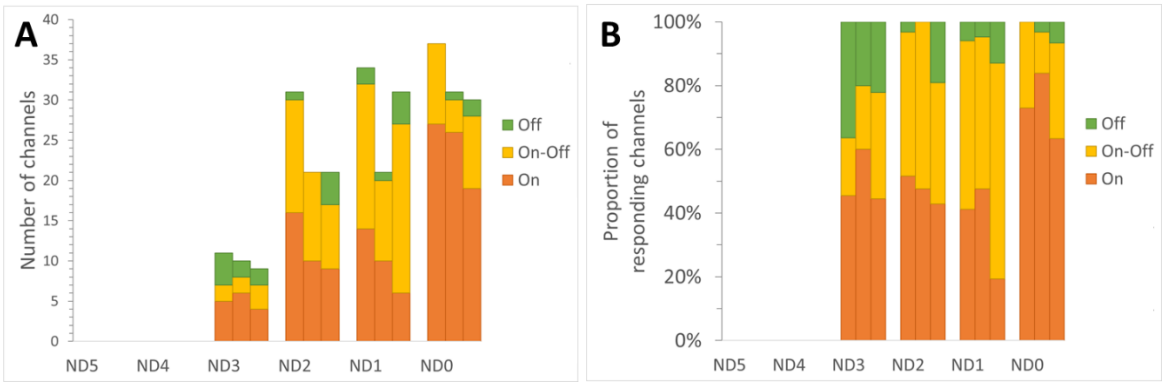

Figure 5.11: Quantification of response types in the *Gnat1*$^{-/-}$ retinas. The A. number and B. proportion of light-responsive channels showing ON, OFF, or ON-OFF response types at each light intensity, quantified from MEA recordings from untreated *Gnat1*$^{-/-}$ retinal explants (n = 3 retinas).

The results presented here establish the ranges of light intensities within which rod- and cone-driven RGC responses can be detected in the *Gnat1*$^{-/-}$ mouse model. This characterisation is essential for instructing the analysis of MEA recordings following mESC-derived rod photoreceptor transplantation.

5.2.3.2 Assessing the restoration of retinal function in mESC-derived photoreceptor precursor treated Gnat1$^{-/-}$ mice

Based on our comparison of the *Gnat1*$^{-/-}$ and WT responses, ND5 and ND4 were established to correspond to scotopic levels of solely rod function. Any light-driven RGC responses seen at ND5 and ND4 light intensities in a treated *Gnat1*$^{-/-}$ retina would therefore be likely to be attributed solely to rod function from transplanted rod photoreceptors. Therefore, I next attempted to establish if mESC-derived photoreceptors could respond to light stimulus following transplantation.

MEA recordings were performed on a *Gnat1*$^{-/-}$ retina transplanted with D26 Crx.GFP^{+} photoreceptor precursors 3 weeks post transplantation. Unfortunately, only one treated retinal explant displayed good MEA recordings. This single eye showed an absence of light-evoked RGC responses at the scotopic levels, ND5 and 4 (Figure 5.12A). Interestingly, a slightly larger proportion of OFF responses at the higher light intensities was observed in the treated eye (Figure 5.12B, striped columns). However, it is not possible to distinguish these from endogenous OFF responses.

It is important to emphasise that the 2 log units of light intensity, ND4 and ND5, may represent a very narrow window to detect RGC responses driven by transplanted mESC-derived rods. Moreover, cone-driven RGC responses in the *Gnat1*$^{-/-}$ retina were apparent as early as ND3 onwards, whereas transplanted rods may be less photosensitive and respond at light levels on this stimulus range. It is possible that small improvements by transplanted rods may be detected at light levels above conventional rod-response levels.

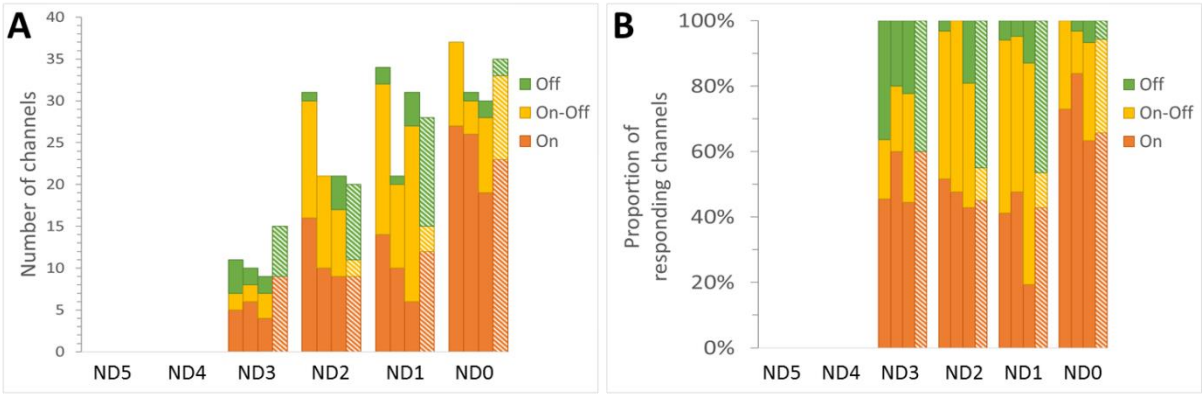

Figure 5.12: Quantification of response types in the untreated and treated *Gnat1*$^{-/-}$ retinas. The A. number and B. proportion of light-responsive channels showing ON, OFF, or ON-OFF response types at each light intensity, quantified from MEA recordings from untreated *Gnat1*$^{-/-}$ retinal explants (n = 3 retinas, represented on separate columns in solid fill) and a treated *Gnat1*$^{-/-}$ retinal explant (n = 1 retina, represented by the striped column.

Therefore, to confidently detect any change in function brought about by transplanted mESC-derived photoreceptors, we characterised a triple-knockout *Opn4*$^{-/-}$ *Gnat1*$^{-/-}$ *Cnga3*$^{-/-}$ (*OGC*) mouse model, which was presumed to lack all phototransduction capabilities due to targeted deletion of specific components of all three photoreception cascades – melanopsin (or opsin 4, Opn4), rod α-transducin (Gnat1) and cone cyclic nucleotide gated channel α3 subunit (Cnga3).

5.2.4 Investigating light stimulus-driven RGC responses in the Opn4$^{-/-}$ Gnat1-/- Cnga3$^{-/-}$ retina

5.2.4.1 Characterisation of RGC responses in the OGC retina

Despite the absence of Opn4, Gnat1, and Cnga3, the retinas of these mice look morphologically normal at 8 weeks, with no apparent loss of photoreceptors or thinning of the ONL (Hattar et al., 2003). To verify that *OGC* mice do not show any response to light, MEA recordings were performed as above on *OGC* mice retinas. Consistent with previous reports (Calvert et al., 2000; Umino et al., 2008) and my results presented here that mice lacking Gnat1 expression do not show high sensitivity vision at scotopic levels (Figure 5.11), we did not observe any light-evoked response in dark-adapted *OGC* mice at scotopic light intensities ND5 and ND4 (Figure 5.20, n=3 retinae). In addition, although spontaneous RGC spiking activity could be observed at all light levels, these retinae showed a complete lack of light-evoked RGC spiking at mesopic (ND3) and photopic intensities (ND2 to ND0) (Figure 5.13 , n=3 retinae).

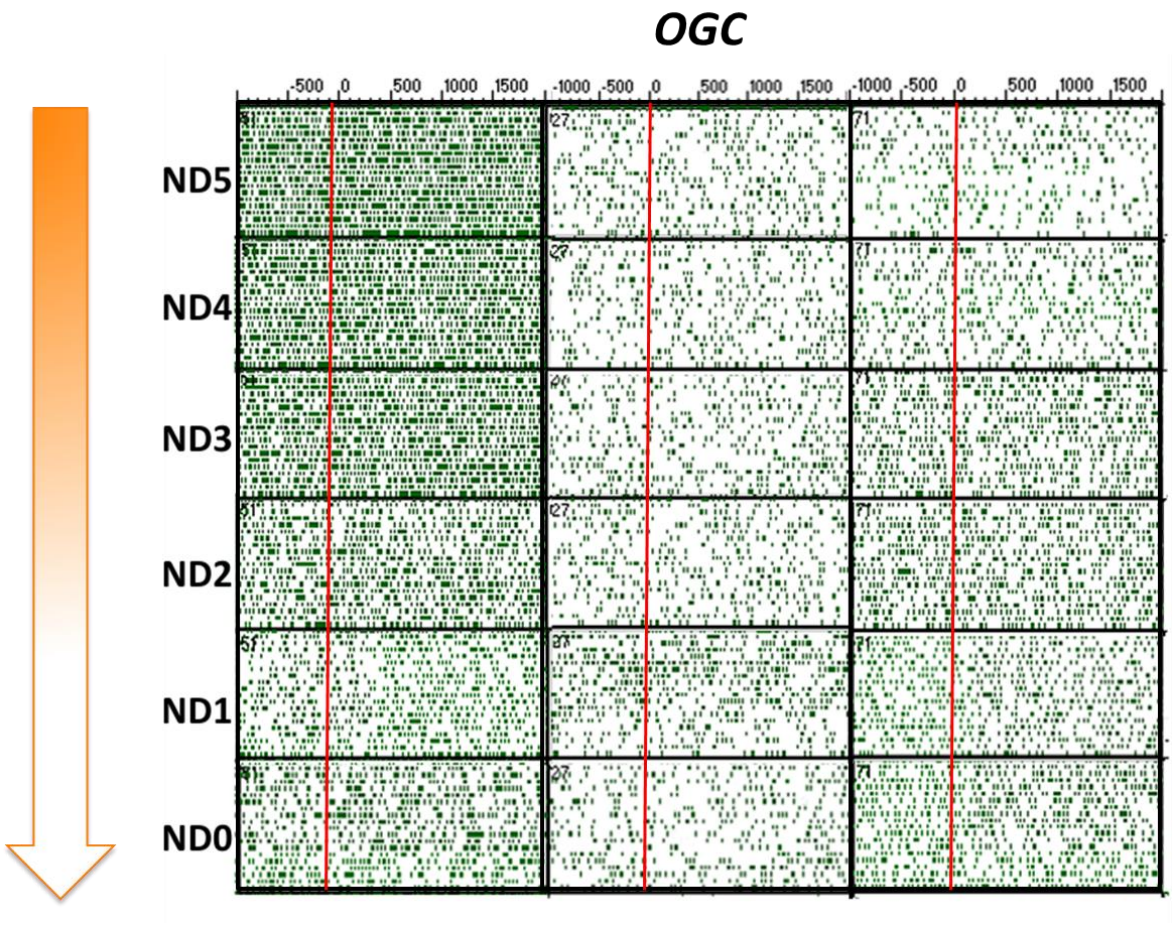

Figure 5.13: RGC responses to a 500ms light pulse from *OGC* mouse retina. Representative examples of responses beginning from the lowest (ND5) to highest (ND0) light intensities, as recorded on a sample of 3 channels. There was a complete absence of RGC responses at all tested light levels in all the *OGC* mouse retinas tested. Red line represents the onset of light stimulus.

In conclusion, the *OGC* model of retinal degeneration did not appear to show any light evoked response at any of the light intensities tested. In comparison to the *Gnat1*$^{-/-}$ model, the *OGC* model offers a much wider 5 log-unit window within which we could assess the functional capabilities of transplanted ESC-derived photoreceptors, with minimal interference from endogenous responses.

5.2.4.2 Gnat1 virus-mediated rescue of light sensitivity in OGC retinas

The complete lack of visual response in the *OGC* mouse model of retinal degeneration is of relevance for experiments designed to assess visual function of transplanted photoreceptors. However, the ability of the endogenous retina to transmit light evoked responses is still unknown. Thus, to verify the possibility of demonstrating visual rescue in the *OGC* retina we delivered the Gnat1 gene to photoreceptors by gene therapy. *OGC* mice were given superior subretinal injections of AAV9.CMV.Gnat1.GFP virus and culled 10-12 weeks later to assess the RGC responses in virus-treated retinas. The superior half of the treated retina was dissected out for MEA recordings to be performed on. Encouragingly, vector-mediated expression of *Gnat1* in the *OGC* retina rescued photosensitivity in 3 out of 3 *Gnat1* virus-transduced *OGC* retinas. Interestingly, robust light-evoked RGC responses could be detected at all light levels (Figure 5.14A), with a maximum of approximately 38-54 responding channels across all 3 preparations (Figure 5.14B). ON, ON-OFF, and OFF responses could be observed, and like the WT retina, OFF responses were significantly less frequent than ON and ON-OFF responses. OFF responses were only observed at scotopic levels (ND5 and ND4), whereas interestingly, at photopic levels (ND1 and ND0) only ON responses were observed. The large number of ON responses from ND3 to ND0 as well as the presence of ON-OFF responses from ND3 to ND2 suggest that these recorded responses were due to vector-mediated expression of *Gnat1* in photoreceptors.

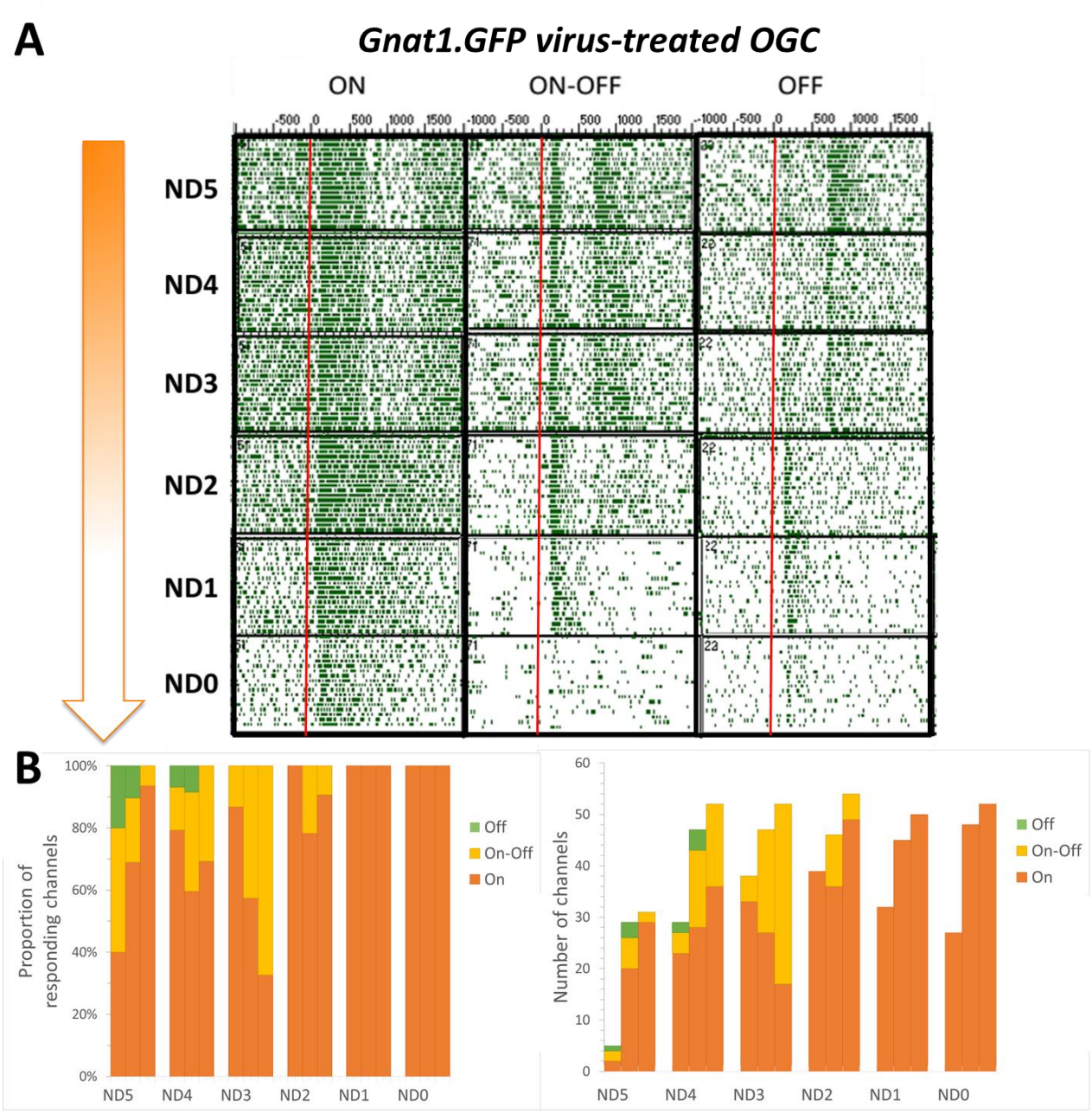

Figure 5.14: A. Examples of RGC responses to a 500ms light pulse from one of the Gnat1.GFP virus-treated *OGC* mouse retinas, beginning from the lowest (ND5) to highest (ND0) light intensities, as recorded on a sample of 3 channels. B. The number and proportion of light-responsive channels showing ON, OFF, or ON-OFF response types at each light intensity, quantified from MEA recordings from Gnat1.GFP virus-treated *OGC* retinal explants (n = 3 retinas). Red line represents the onset of light stimulus.

5.2.4.3 Assessing the restoration of retinal function in mESC-derived photoreceptor precursor-treated OGC mice

Having verified that it was indeed possible to demonstrate visual rescue in the *OGC* retina using the established MEA set up and stimulus protocol, I next sought to assess the extent to which retinal function may be restored in retinas transplanted with optimally-staged mESC-derived photoreceptor precursors. To this end, single superior subretinal injections of D26 Crx.GFP^{+} photoreceptor precursors were performed in 6-8 week old *OGC* recipients, and their retinas were harvested for MEA recording 3 weeks post-transplantation.

Following transplantation, similar to untreated OGC retinas, 8 out of 10 *OGC* retinas did not show any light-driven RGC responses at all tested light levels. However, in 2 of the treated *OGC* retinas, 1-2 channels identified by the Matlab algorithm as light-responsive (i.e. response passed the threshold on CUSUM plot) showed an ON response (Figure 5.15). In one of the channels, the ON response could be observed at a light intensity as low as ND3 (Figure 5.15A, blue box), whereas in other channels, an response was observed only with the use of the high intensity light stimuli (ND1 and ND0) (Figure 5.15B and B'). No ON-OFF or OFF responses were otherwise observed in any of treated *OGC* retinas.

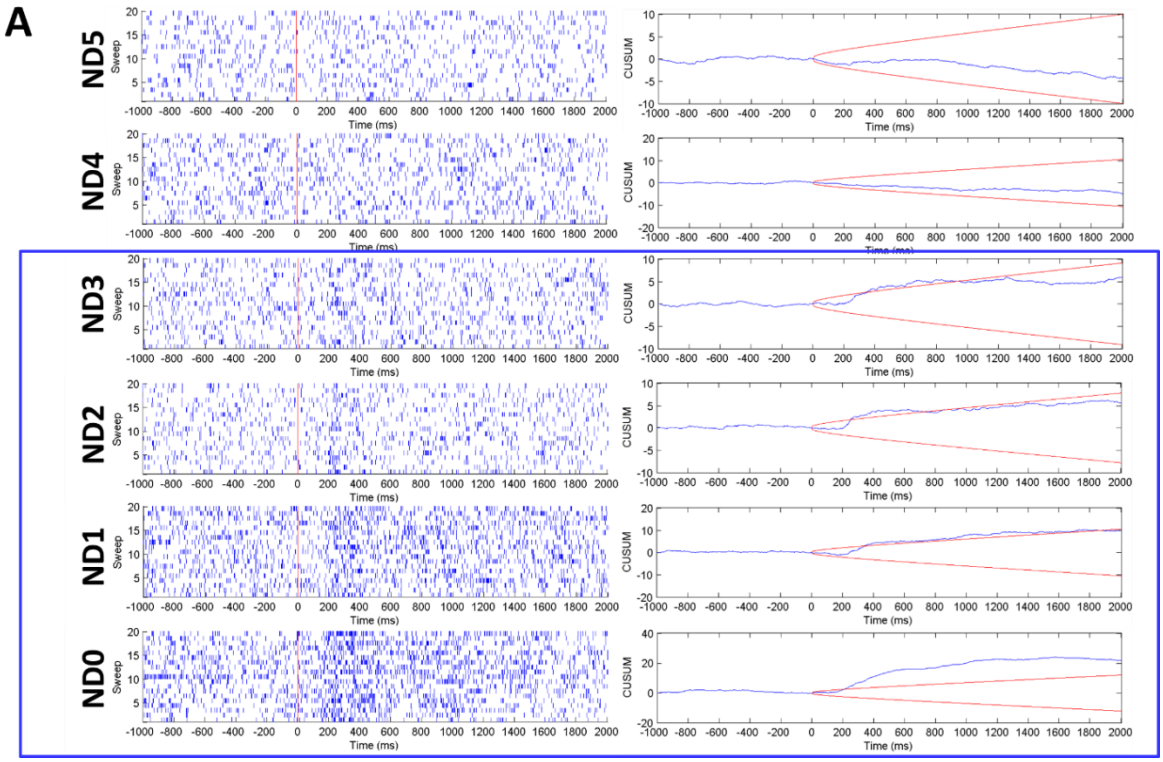

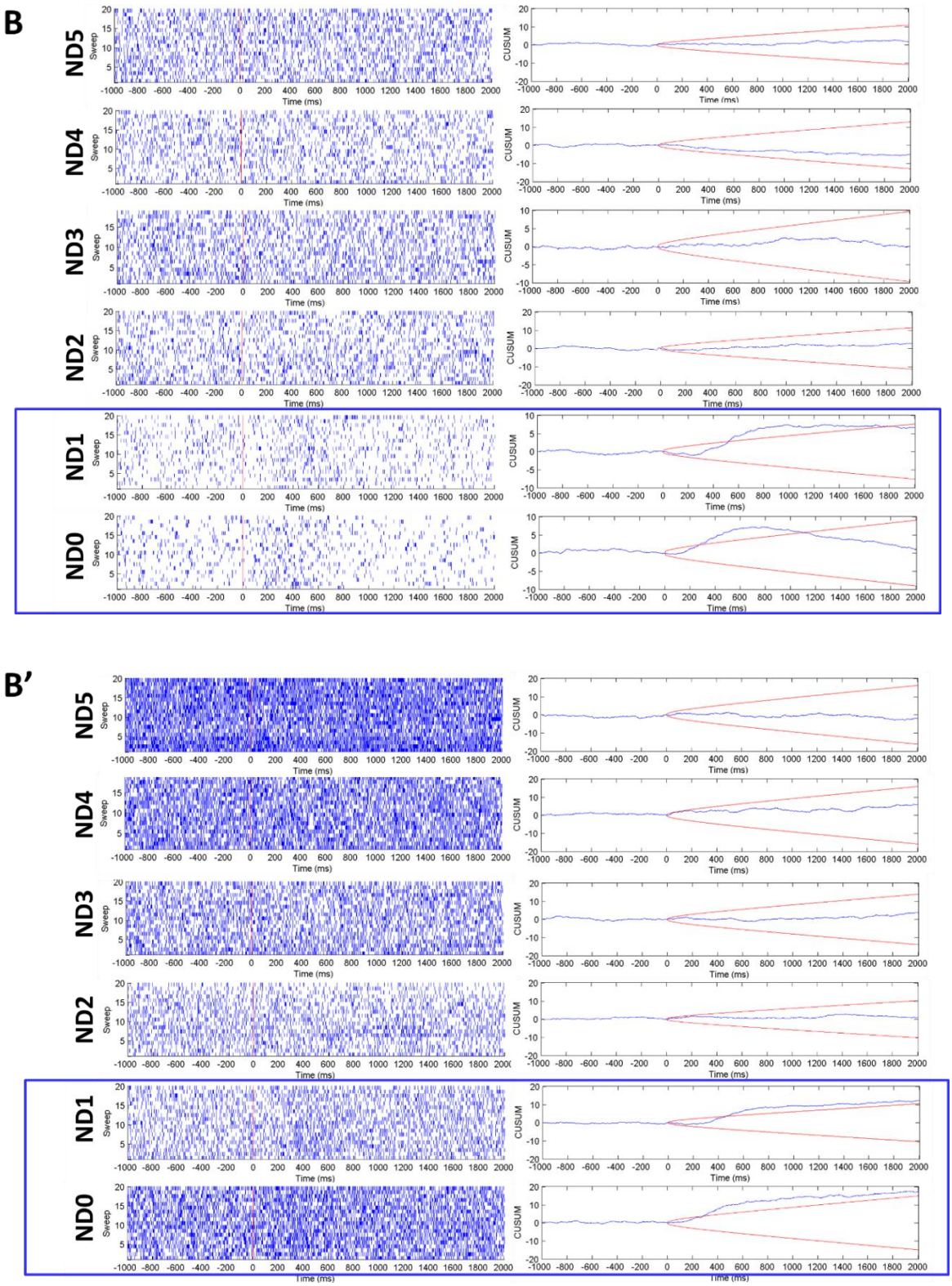

Figure 5.15: Representative raster and CUSUM plots. (A, B) Raster and CUSUM plots of ON responses observed across 2 independent *OGC mice* retinal explants transplanted with D26 Crx.GFP^{+} photoreceptor precursor cells. B and B' are examples of ON responses derived from the same retinal preparation. ON responses are indicated by the blue boxes.

Despite the small number of ON responses observed in the treated eyes, these results were very encouraging. Thus, to further investigate the nature of these responses, specific response parameters were measured and compared to those of ON responses from WT retinas.

5.2.4.3.1 Measuring parameters of the RGC response time course on the WT retina

Several important parameters of the RGC response time course – response latency, response duration, peak frequency, and peak latency – can be measured from the CUSUM plots and PSTHs (examples are shown in Figure 5.16).

To better understand the ON response observed on treated retinas I first investigated these parameters on the WT retina. Response latency was measured from the onset or offset of the light stimulus to the onset of the response (e.g. On_1 and On_2), which was determined at the point of gradient change (Figure 5.16, bottom CUSUM plot). Response duration was measured as the time interval between response onset and offset (e.g. On_1 to Off_1 and On_2 to Off_2), where offset was determined as the point of gradient resolution, or where there was no apparent plateau in gradient, the point where the frequency dropped by 15% of its highest frequency (Wang et al., 2007) (Figure 5.16, bottom CUSUM plot). Peak latency was measured from the onset or offset of the light stimulus to the point at which the gradient of the CUSUM slope was the steepest, which reflects when the rate of increase in spike rate was the greatest. Finally, peak frequency, which is a measure of the magnitude of the response to the light stimulus, was determined from the PSTH by measuring the maximum spike rate achieved in the duration of the response (Figure 5.16, middle PSTH plot).

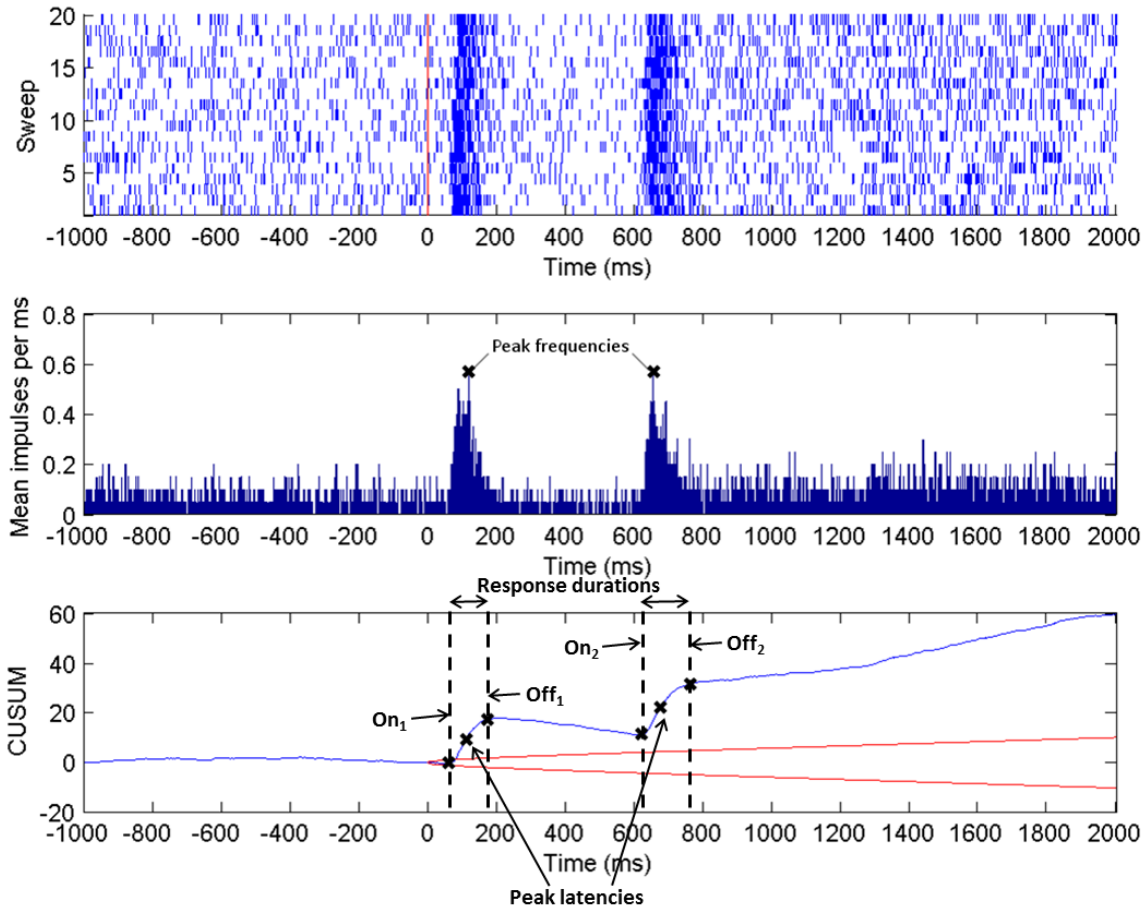

Figure 5.16: Measuring parameters of the RGC response time course. Representative example of an ON-OFF response in a WT retina; Top: response latencies (On_1 and On_2), Middle: response durations (e.g. On_1 to Off_1 and On_2 to Off_2), Bottom. CUSUM, peak frequencies, and peak latencies.

To visualise the distribution of these measured response properties in the light-responsive channels of the WT retinas these parameters were plotted as histograms at each light level (Figure 5.17). The properties of ON (Figure 5.17A) and OFF (Figure 5.17B) responses were examined separately, and ON-OFF responses were broken down into their component ON and OFF parts (Wang et al., 2007).

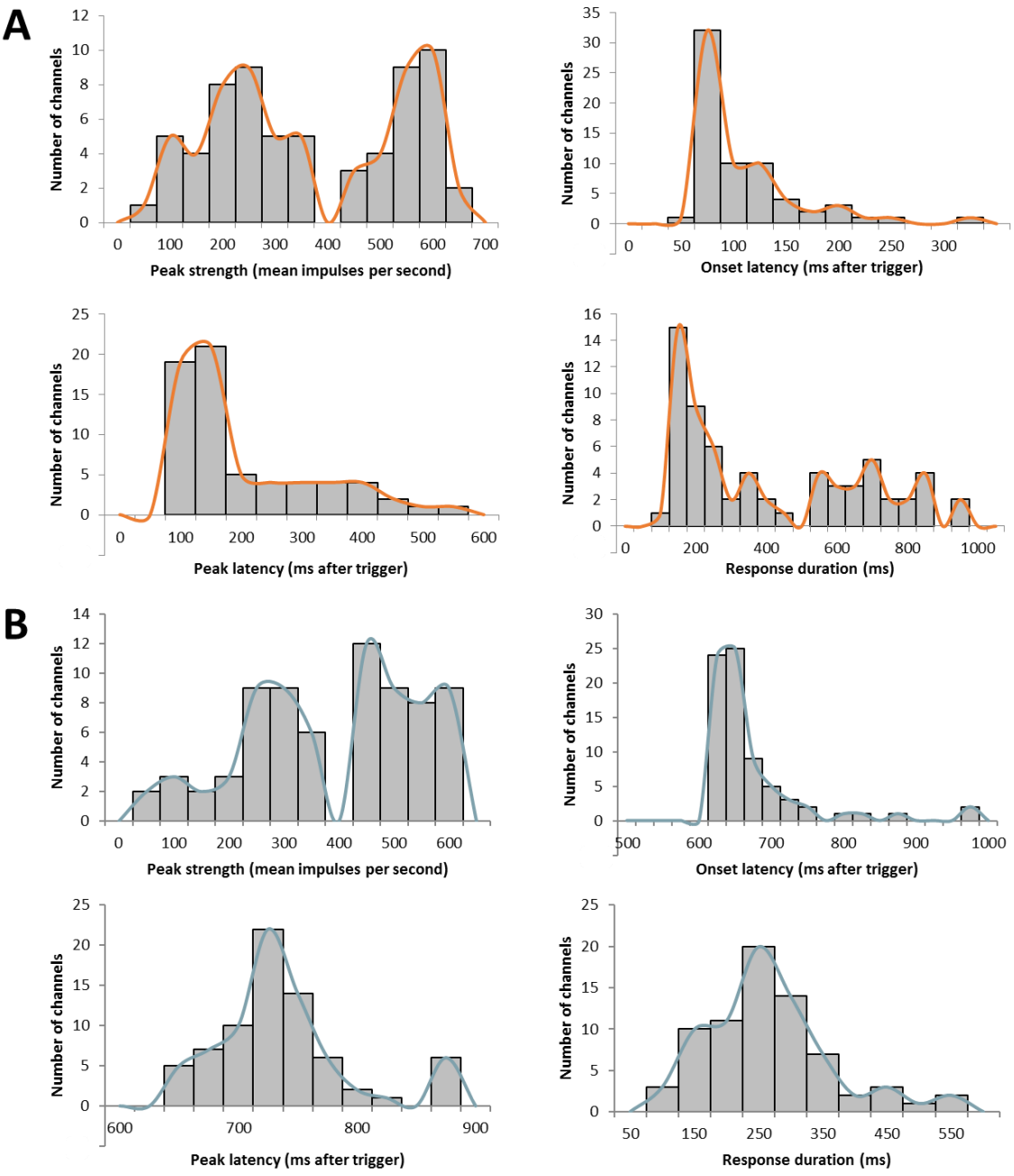

Figure 5.17: Example of histograms showing the distribution of measured response properties (peak strength, onset latency, peak latency, and response duration) across all A. ON and B. OFF responses in a WT retina at ND0.

Having established the RGC response parameters, I carefully characterised ON (Figure 5.18) and OFF (Figure 5.19) responses in the C57BL6/J WT retina (n=3 retinas).

The peak strength of ON responses in the WT retina appeared to cluster into two different groups, with the peak of the first cluster occurring around 200-250 impulses per second, and the second occurring around 550-600 impulses per second at ND0. This division was most pronounced at photopic light levels (ND1 and ND0), whereas at mesopic and scotopic levels, most responses had a relatively higher average number of impulses per second. The onset latencies of ON responses were clustered in one group, and the duration between the trigger of the stimulus and the onset of the ON response was observed to decrease in length slightly as the light intensity of the stimulus was increased. At ND0, the time to onset of the WT ON response was around 75ms after the stimulus was triggered. Similarly, the greatest increase in spiking rate, as indicated by the peak latency, occurred relatively instantaneously in WT retinas around 100-150ms after the stimulus was triggered, and was observed to decrease in duration as the light intensity of the stimulus was increased from ND5 to ND0. Finally, in the WT retina, ON responses were mostly brisk and transient, lasting for around 150ms.

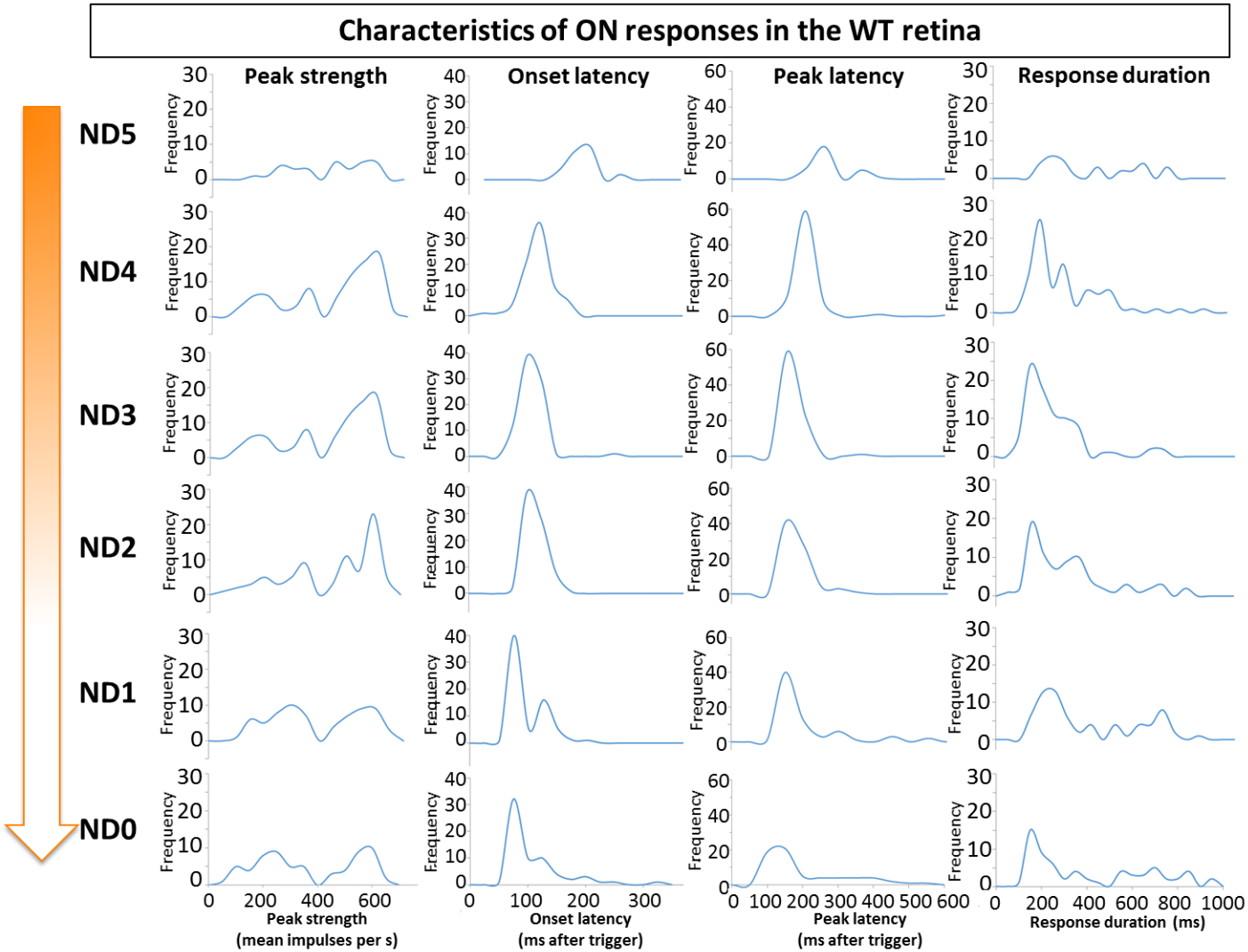

Figure 5.18: Characterisation of ON responses in the WT retina.

OFF responses in the WT retina appeared to cluster evenly into two different groups based on peak strength of the response, with the peak of the first distribution occurring between an average of 250-350 impulses per second, and the second occurring at 450-500 impulses per second. The frequency of OFF responses was also observed to increase as the intensity of the delivered light stimulus was increased. At the highest light intensity (ND0), the maximum peak strength of WT OFF responses was 600 impulses per second. The onset latencies of OFF responses in the WT were clustered in one group, and appeared to decrease slightly as the intensity of the light stimulus was increased – at ND5, the peak of the distribution occurred around 650-700ms after the stimulus was triggered, whereas at ND0, the peak of the distribution occurred between 625-650ms. The peak latencies of the OFF responses in the WT retina could be seen to fall into two clusters, which was most evident at ND0. The peak of the first cluster occurred between 700-750ms after the stimulus was triggered, which may suggest a brisk response where the peak strength of the response was attained relatively instantaneously at stimulus offset. Conversely, the peak of the second cluster occurred past 900ms after the stimulus was triggered, which may suggest a gradual, sustained response. Finally, the OFF responses in the WT retina were mostly transient, lasting for approximately 250-300ms.

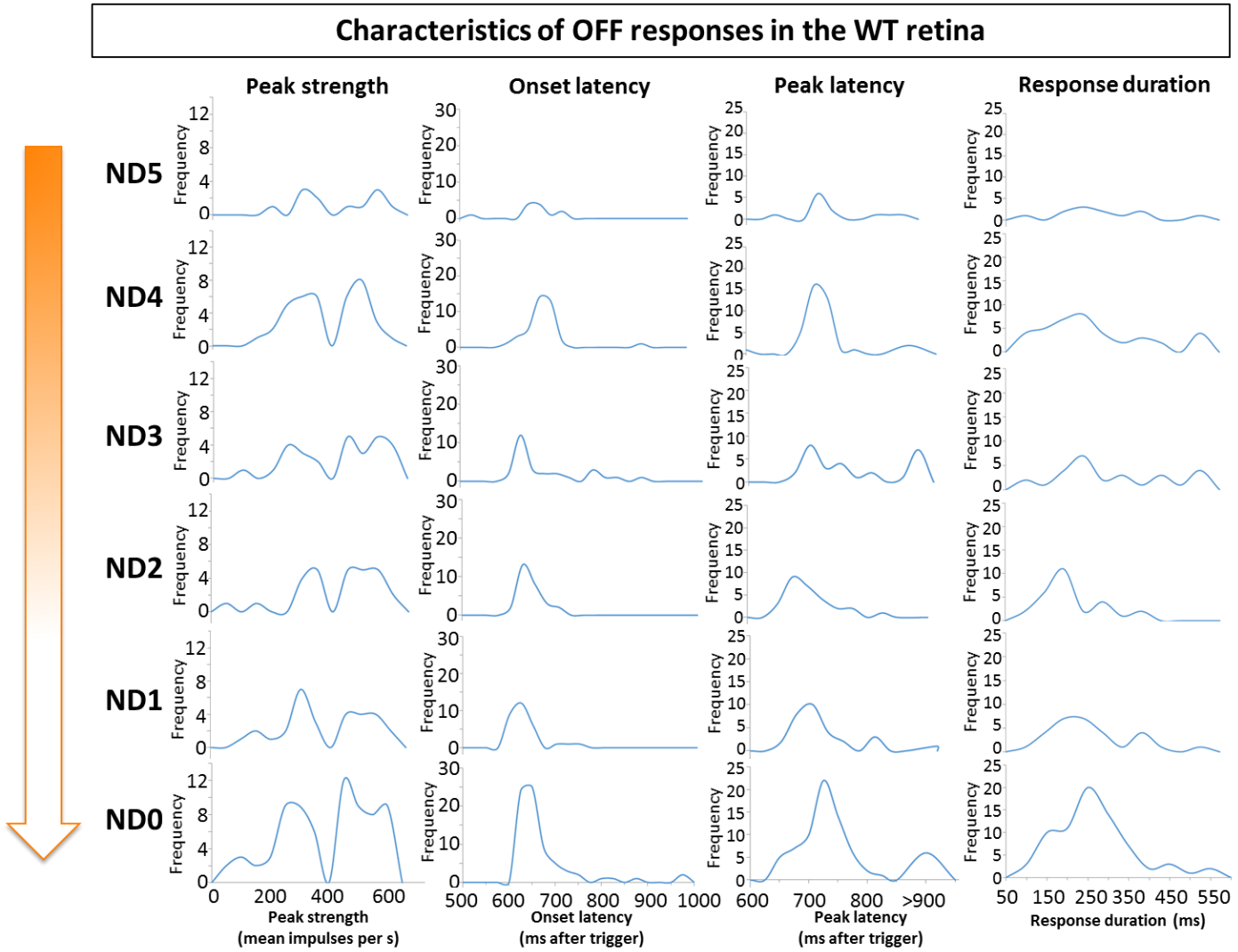

Figure 5.19: Characterisation of OFF responses in the WT retina.

5.2.4.3.2 Comparing light-evoked responses in the treated *OGC* retina to the WT retina

Having established the characteristics of ON and OFF responses in the WT retina, I then compared the ON responses observed in the treated *OGC* retinas to the ON responses of the WT retina (Figure 5.20).

Similar to ON responses in the WT retina, the peak strength of the ON responses detected in the treated *OGC* retina ranged from between 210-410 impulses per second and the strength of the response appeared to increase as the intensity of the light stimulus was increased. Interestingly, in comparison, the onset latencies of all the detected ON responses were longer, occurring more than 200ms after the stimulus was triggered. In treated *OGC* retinas, the latency to peak was around 400ms after the stimulus was triggered, even at the highest light intensity. This may suggest that in the treated *OGC* retina, RGC spiking rate increased very gradually in response to light onset. Finally, the ON responses in the treated *OGC* retina showed little sign of recovery, with spike rate remaining elevated relative to baseline for over 200ms following light offset.

Summary of ON responses detected in the *OGC* retina after transplantation

Retinal explant	ND	Peak strength (mean impulses per s)	Onset latency (ms after trigger)	Peak latency (ms after trigger)	Response duration (ms)
A	3	210	218	252	303
	2	210	234	220	215
	1	250	271	310	200
	0	330	284	408	402
B	1	330	316	556	457
	0	410	218	380	305
B(i)	1	210	345	572	550
	0	210	220	405	505

Figure 5.20: Characterisation of the ON responses detected in 3 channels (A, B and B(i) across 2 independent retinal explants (A and B) derived from *OGC* mice injected with D26 Crx.GFP^{+} photoreceptor precursor cells, as shown in).

Despite the low number of responses and their differences when compared to the normal WT retina, the experiments presented here demonstrate for the first time light responses in the OGC mouse model of retinal degeneration following the transplantation of mESC-derived photoreceptors.

5.2.4.4 Morphological characterisation of OGC mice treated with mESC-derived photoreceptor precursors

Next, we sought to assess if the observations from our functional assessment could be correlated to the immunohistochemical appearance of transplanted D26 Crx.GFP$^+$ photoreceptor precursors in the host ONL. Unfortunately, due to the stress placed on the retinas during the long MEA recordings, IHC could not be done on the same retinas from which MEA recordings were performed. Instead, age-matched *OGC* mice treated with D26 Crx.GFP$^+$ photoreceptor precursors were culled 3 weeks post-transplantation for immunohistochemical assessment.

GFP$^+$ cells were observed in the recipient *OGC* ONL and appeared to be morphologically similar to wild-type rods, displaying correct polarity within the host ONL with well-organised long outer segments extending towards the RPE and synaptic buttons evident near the INL (Figure 5.21A and A'). The majority of these GFP$^+$ cells contained Gnat1 protein, which may indicate maturation of the transplanted photoreceptor precursors within the host retina (Figure 5.21B and B'). The number of GFP$^+$ cells present in the host ONL following transplantation of D26 Crx.GFP$^+$ photoreceptors was significantly lower in the recipient *OGC* retina (745.8 ± 237.6, n=5) compared to the *Gnat1*$^{-/-}$ retina (2698.7 ± 631.9, n=7) (Figure 5.21C; $p < 0.05$, Mann-Whitney). The difference in the number of GFP+ cells in the ONL is interesting, as morphologically these retinas appear to be very similar. Future studies will further investigate structural differences between these two diseased models, such as glial scarring and outer limiting membrane integrity.

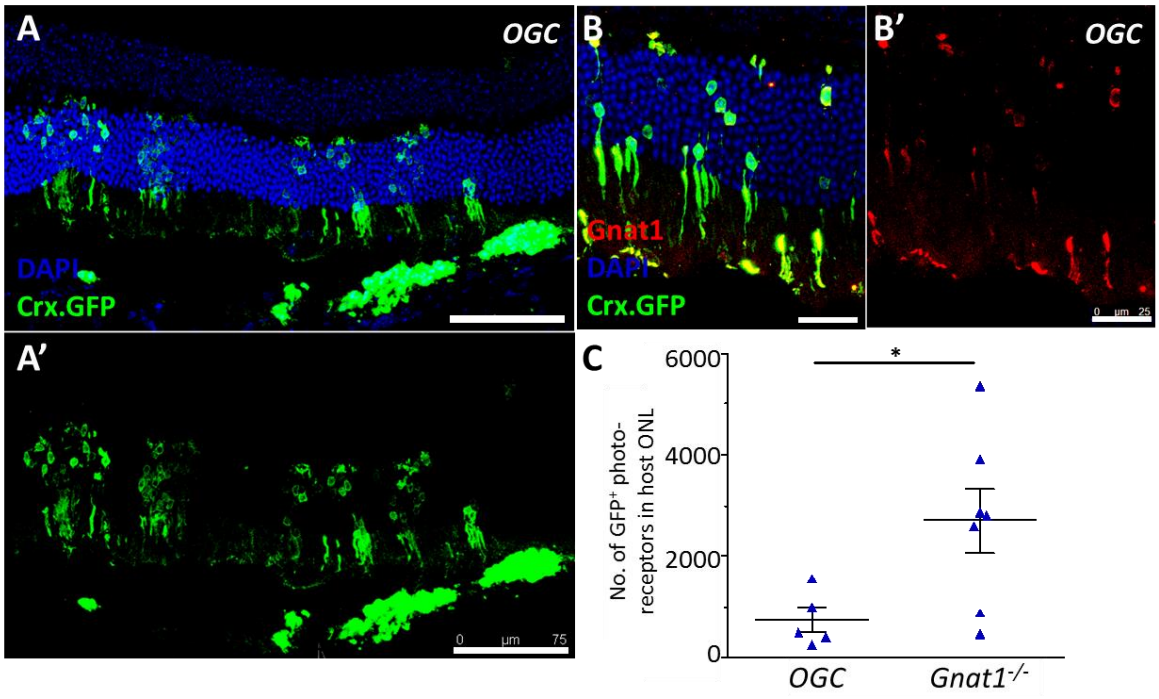

Figure 5.21: Transplantation of ESC-derived D26 Crx.GFP⁺ cells into the triple knockout *OGC* mouse . A and A'. Tile-scan confocal images (10X) of GFP-labelled photoreceptors in the host ONL of an *OGC* recipient at 3 weeks post-transplantation. B and B'. Projection confocal images (40X) of GFP-labelled photoreceptors expressing *Gnat1*, in an *OGC* recipient. C. Number of GFP-labelled cells present in the host ONL in *OGC* recipients compared to the *Gnat1*$^{-/-}$ mouse model. Scale bars: A and A' – 75µm; B and B' – 25µm.

Together, these data suggest that mESC-derived photoreceptor precursors are capable of surviving and maturing *in vivo* following transplantation into a recipient with an intact ONL, and may be able to transmit light-evoked visual signals.

5.2.5 Investigating light stimulus-driven RGC responses in the Aipl1$^{-/-}$ retina

Next, we aimed to characterise and transplant mESC-derived photoreceptors into the *Aipl1*$^{-/-}$ mouse, a model of end-stage retinal disease, which would more closely reflect the clinical scenario of patients in future clinical trials. *Aipl1*$^{-/-}$ mice have been used in numerous studies as a model of Leber congenital amaurosis (LCA4), an early onset and extremely severe form of congenital retinal dystrophy (Dyer et al., 2004; Sun et al., 2010; Kirschman et al., 2010; Singh et al., 2014). In this severe retinal degeneration model, the death of all rod and cone photoreceptors occurs by 1 month, beyond which all of the ONL is lost (Ramamurthy et al., 2004). In our experiments, we used mice aged between 1.5-2 months old, and our characterisation of the photoreceptor presence in these animals is described in the following section.

5.2.5.1 Characterisation of photoreceptor presence in the Aipl1$^{-/-}$ retina

To characterise the pattern of photoreceptor degeneration in *Aipl1*$^{-/-}$ mice, we performed immunohistochemical staining for cone and rod photoreceptor markers, Arrestin and Rhodopsin respectively, on eyes from 1- to 6 months-old *Aipl1*$^{-/-}$ mice (Figure 5.22, n = 2 eyes per time point). At 1 month of age, a thin ONL comprising a single layer of Arrestin-positive cones could still be seen; whereas by 2 months, there was complete absence of an ONL in all eyes assessed. Occasional isolated Arrestin-positive cones could be spotted in eyes up to 6 months (<10 cells per eye), which was the latest time-point assessed. However, none of the Arrestin-positive cones displayed normal cone morphology; most of them did not extend processes towards the INL or RPE in a polarised manner, and only a few were observed to elaborate stunted processes. Rhodopsin-positive cells were rarely seen by 2 months (<6 cells per eye), and these did not display normal rod morphology.

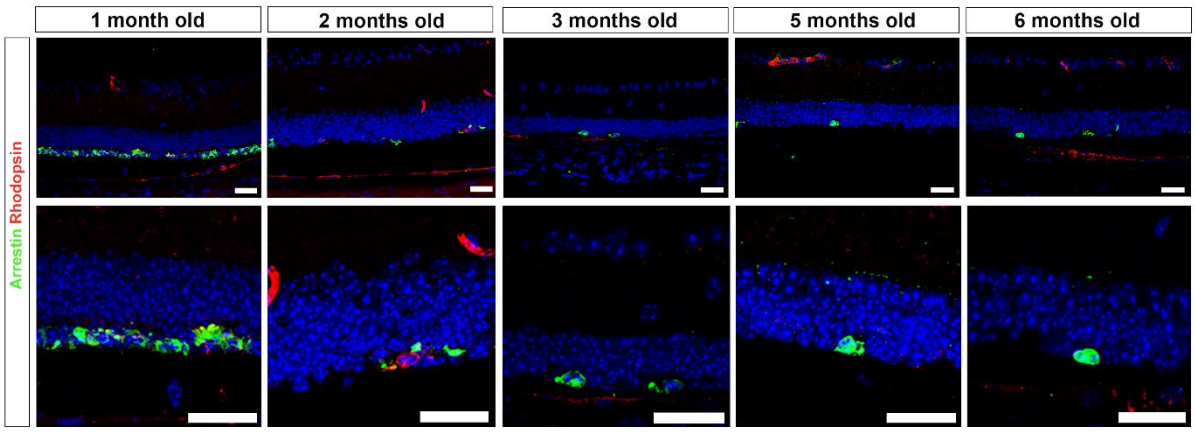

Figure 5.22: Photoreceptor loss in the *Aipl1*$^{-/-}$ mouse. Rods are labelled with the Rhodopsin antibody, while cones are labelled with the arrestin antibody. Scale bars, 25µm.

Next, to survey the impact of this abrupt photoreceptor degeneration on the morphology of the interneurons that would normally contact photoreceptors we performed immunohistochemical analysis for the α-isoenzyme of protein kinase C (PKCα) rod bipolar cells. In *Aipl1*$^{-/-}$ eyes at the time of transplantation (1.5-2 months), rod bipolar cell bodies appeared to be well-aligned, with most axons projecting to the IPL with large lobular terminals (Figure 5.23, arrows), although there appeared to be a lack of dendrites (Figure 5.23, arrowheads). However, by 3 months of age, which would correspond approximately to 3 weeks post-transplantation, there was an impression of increased disorganisation in the IPL, with some rod bipolar cell axonal terminals appearing as rudimentary dots (Figure 5.23, arrows), which may suggest stunted axonal arborisation, and the presence of cell bodies that were not well-aligned (Figure 5.23, asterisk).

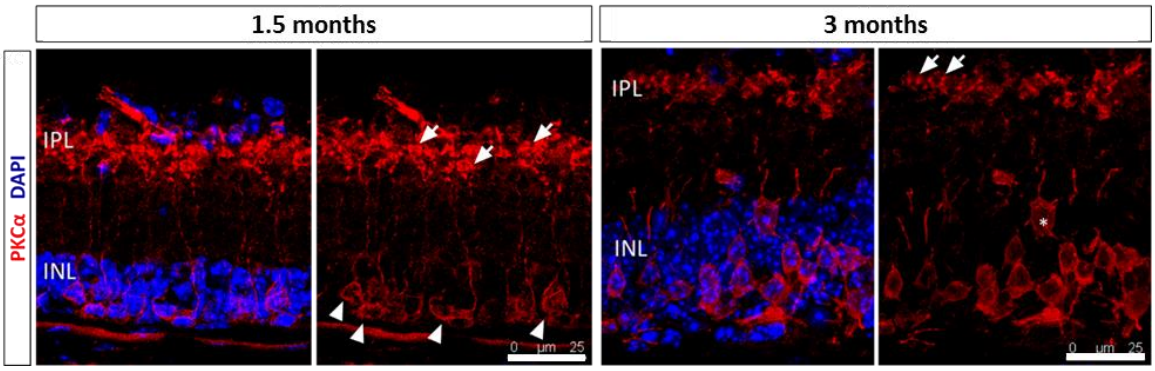

Figure 5.23: Changes in rod bipolar cell morphology with photoreceptor loss.

5.2.5.2 Characterisation of RGC responses in the Aipl1$^{-/-}$ retina

To characterise light responses on *Aipl1*$^{-/-}$ mouse retinas MEA recordings were performed as described above. Unsurprisingly, although spontaneous RGC spiking activity could be observed, we did not observe any light-evoked RGC responses in retinas (n = 7) of dark-adapted 6-9 week old *Aipl1*$^{-/-}$ mice at all light intensities tested (ND5 to ND0; Figure 5.24). This offered us a wide 5 log unit window of light intensities to probe for light-evoked RGC responses driven by transplanted mESC-derived photoreceptor precursors.

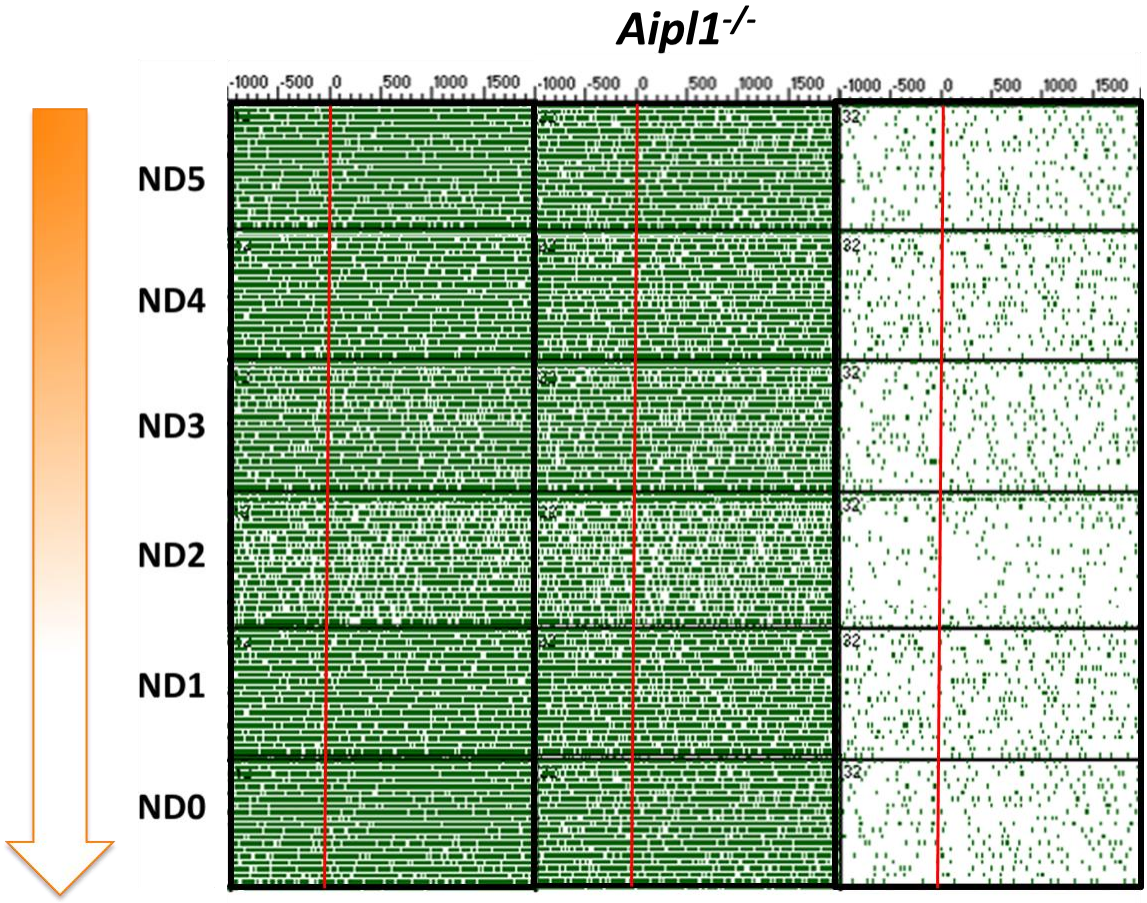

Figure 5.24: RGC responses to a 500ms light pulse from an untreated *Aipl1*$^{-/-}$ mouse retina. Representative examples of responses beginning from the lowest (ND5) to highest (ND0) light intensities, as recorded on a sample of 3 channels. There was a complete absence of RGC responses at all tested light levels in all the *Aipl1*$^{-/-}$ mouse retinas tested. Red line represents the onset of light stimulus.

5.2.5.3 Assessing the restoration of retinal function in mESC-derived photoreceptor precursor-treated Aipl1$^{-/-}$ mice

To assess the extent to which retinal function may be restored in *Aipl1*$^{-/-}$ retinas transplanted with optimally-staged mESC-derived photoreceptor precursors, single superior subretinal injections of D26 Crx.GFP+ photoreceptor precursors were performed in 6-9 week old *Aipl1*$^{-/-}$ recipients, and their retinas were harvested for MEA recording 3 weeks post-transplantation.

Following transplantation, 7 out of 10 retinas showed a complete absence of light-evoked RGC responses at all tested light intensities. However, 3 retinas had 1-2 channels identified by the Matlab algorithm as light-responsive, that showed a clear response at high light intensities (ND1 or 0).

In the first responding retina (herein referred to as retinal explant A), examination of the raster and CUSUM plots at all tested light intensities from the channel with the algorithm-identified response at ND0, revealed the presence of a weak response beginning at light intensities as low as ND3 (Figure 5.25, blue box). This retina was from the eye of an *Aipl1*$^{-/-}$ recipient that was 12 weeks old at the time of recording, and it is therefore very unlikely that this response is mediated by endogenous photoreceptors.

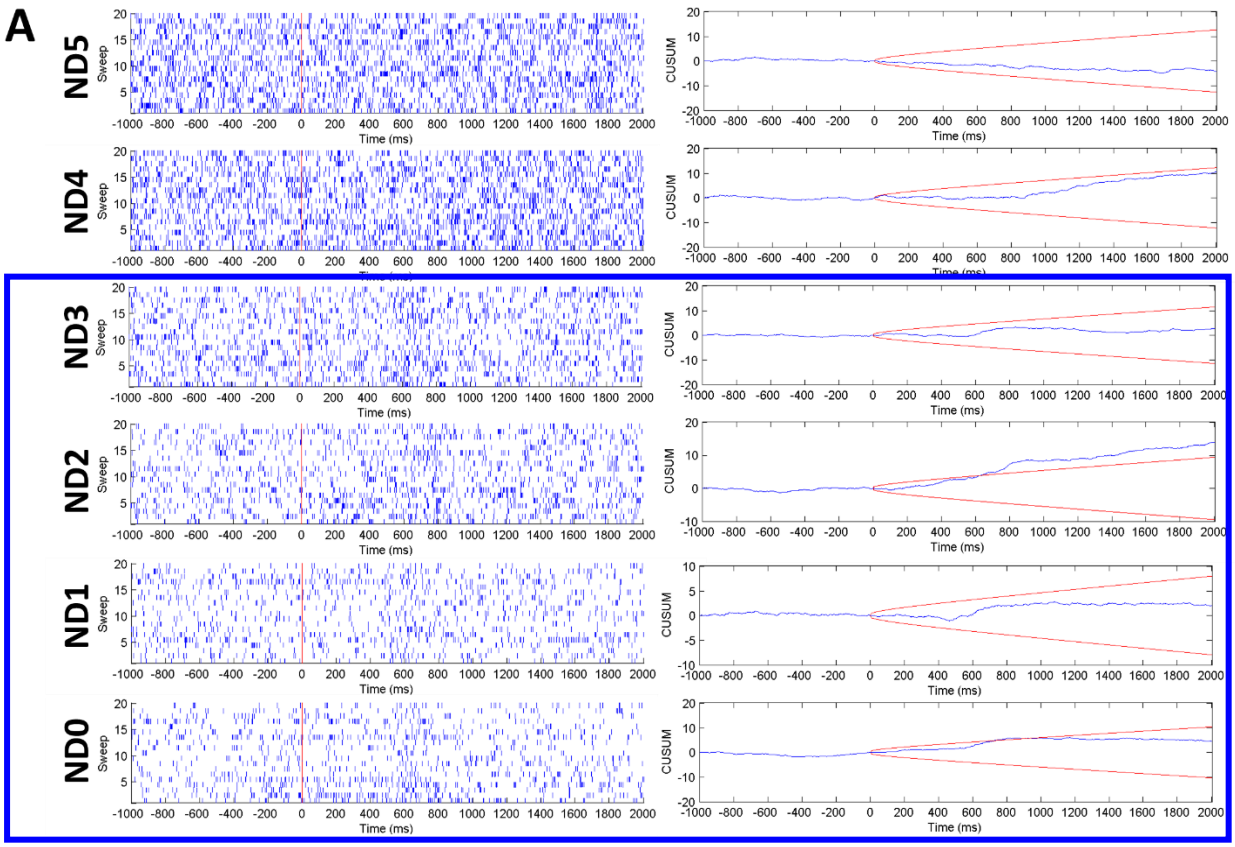

Figure 5.25: Raster and CUSUM plots of responses recorded across all tested light intensities from a channel that demonstrated a response to the light stimulus at ND0 (herein referred to as retinal explant A). A weak response could be seen as early at ND3, although this was not automatically detected by the algorithm. Responses are indicated by the blue boxes.

In the other responding channel of a 13-week old retina (herein referred to as retinal explant B), a clear response was only observed in response to a high light intensity stimulus at ND0 (Figure 5.26, blue box).

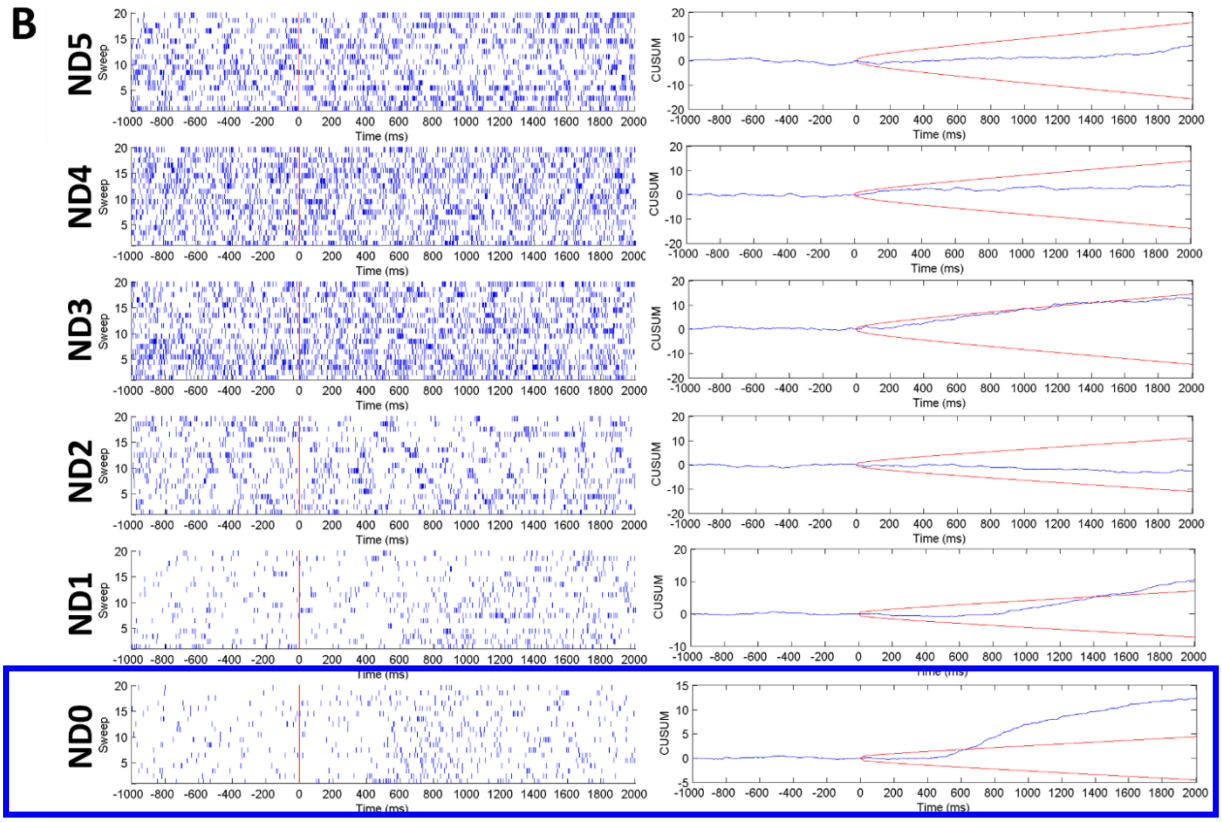

Figure 5.26: Raster and CUSUM plots of responses recorded across all tested light intensities from a channel that demonstrated a response to the light stimulus at ND0 (herein referred to as retinal explant B). A weak response could be seen from ND1 onwards. Responses are indicated by the blue boxes.

Finally, the third retinal preparation that demonstrated responses (herein referred to as sample C) was 10 weeks of age, and showed two separate channels responding at ND1 and ND0 (Figure 5.27).

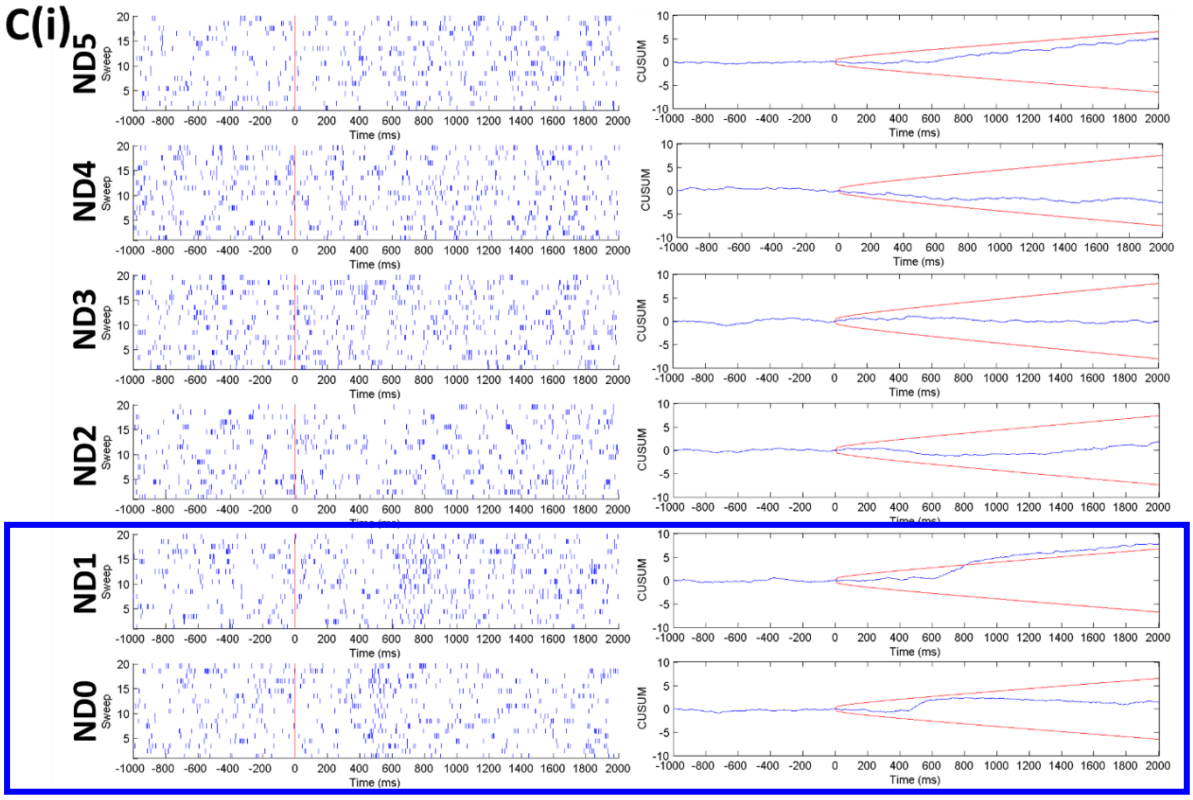

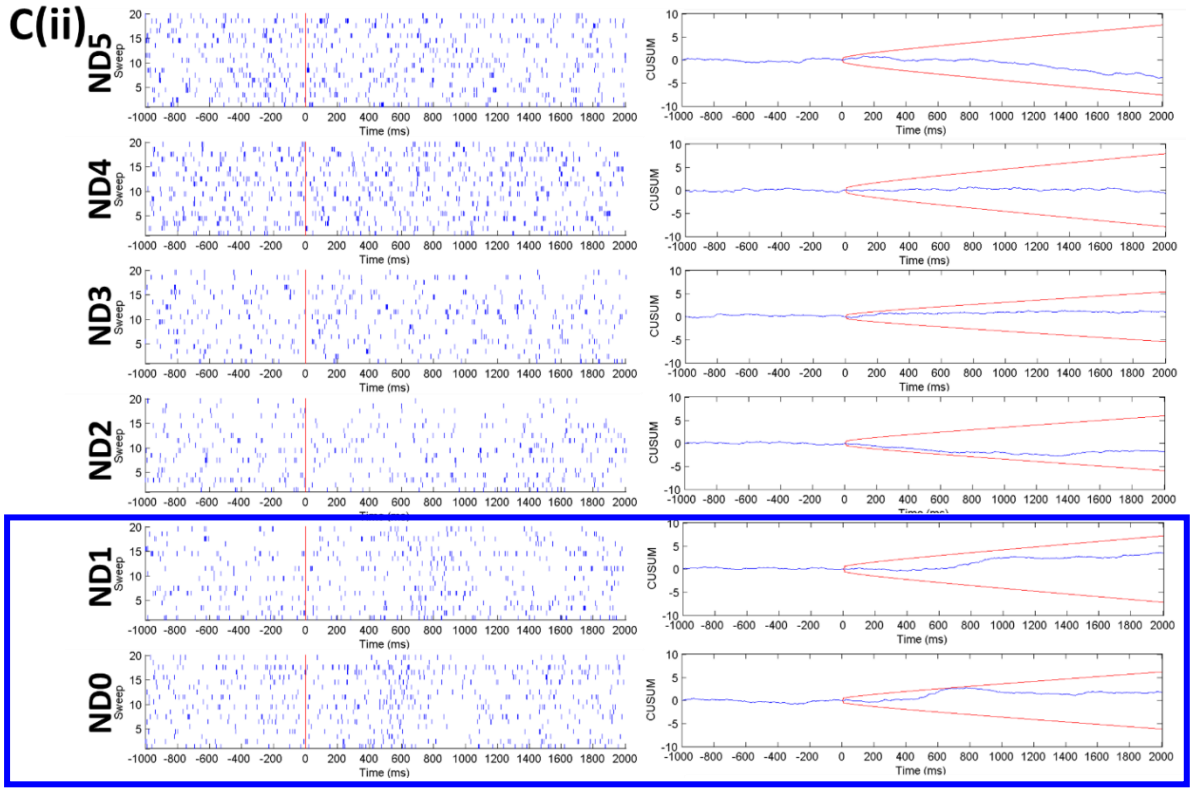

Figure 5.27: Raster and CUSUM plots of responses recorded across all tested light intensities from two channels ((i) and (ii)) that demonstrated responses to the light stimulus at ND0 (herein referred to as sample C). In both channels, a weak response could be seen from ND1 onwards. Responses are indicated by the blue boxes.

To further investigate the nature of these responses, specific parameters of these responses were measured, as done previously in Section 5.2.4.3.1 (Figure 5.28).

The responses observed in treated *Aipl1*$^{-/-}$ retinas appeared to be markedly weaker, ranging between 150 to 250 impulses per second at ND0. Notably, the onset latency of the detected responses in the treated *Aipl1*$^{-/-}$ retinas ranged from 559 to 454ms at ND0. Given that some of the responses occurred before the light stimulus was turned off (i.e. onset latency < 500ms), it is more likely that these are slow ON responses with long onset latencies, as opposed to 'early' OFF responses with unusually short onset latencies. Majority of the OFF responses in the WT retina had onset latencies between 625-650ms, and it is unlikely that transplanted cells could respond to the stimulus more quickly than cells in the WT retina. Correspondingly, in the majority of the responses detected in treated *Aipl1*$^{-/-}$ retinas, the greatest increase in spike rate occurred after a noticeable delay relative to the stimulus onset. Finally, the responses detected in the treated *Aipl1*$^{-/-}$ retinas were mostly transient, lasting for approximately 250ms.

Summary of responses detected in the *Aipl1*$^{-/-}$ retina after transplantation

Retinal explant	ND	Peak strength (mean impulses per s)	Onset latency (ms after trigger)	Peak latency (ms after trigger)	Response duration (ms)
A	3	210	551	657	253
	2	270	582	764	255
	1	210	469	500	275
	0	250	559	662	266
B	0	150	556	718	459
C(i)	1	210	628	766	234
	0	160	471	576	203
C(ii)	1	160	738	829	245
	0	160	454	529	166

Figure 5.28: Characterisation of the responses detected in 4 channels across 3 independent retinal explants (A, B, and C) derived from *Aipi1*$^{-/-}$ mice injected with D26 Crx.GFP^{+} photoreceptor precursor cells, as shown in Figure 5.25, Figure 5.26, and Figure 5.27).

5.2.5.4 Morphological characterisation of Aipl1$^{-/-}$ mice treated with mESC-derived photoreceptor precursors

To examine whether the observations from functional assessment could be correlated to the expression patterns of photoreceptor markers or morphological disturbances in the recipient retina, age-matched *Aipl1*$^{-/-}$ mice transplanted with D26 Crx.GFP+ photoreceptor precursors were culled 3 weeks post-transplantation for immunohistochemical assessment. Due to the stress placed on retinal explants during the long MEA recordings, immunostaining could not be done on the same retinas from which MEA recordings were performed on.

As before, mouse ESC-derived Crx.GFP+ photoreceptor precursors demonstrated robust survival in the subretinal space, with sizable cell masses observed in 6 out of 8 treated eyes. These were mostly well-spread across a wide surface area of the host retina to form a thin, 2-3 cell-thick layer (~ 15µM) between the host INL and the RPE, although it was difficult to discern any form of clear organisation (Figure 5.29).

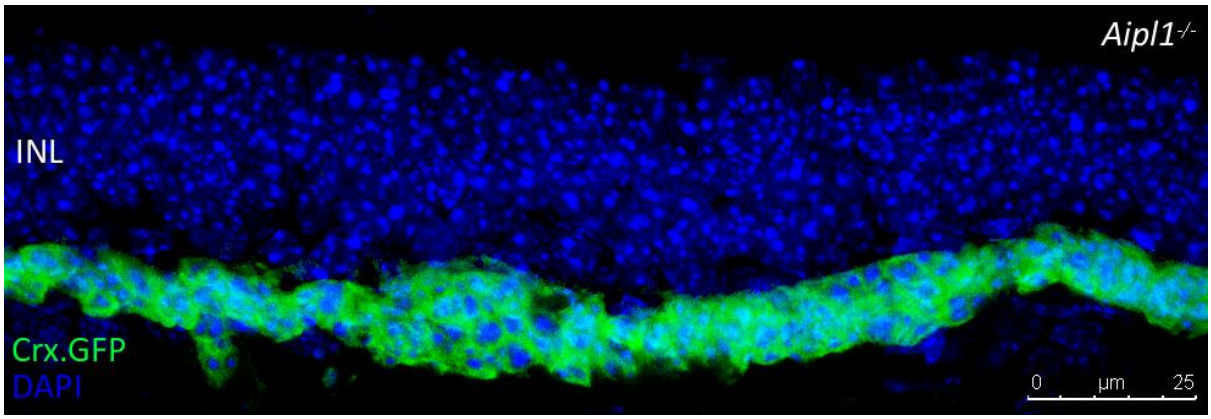

Figure 5.29: Spread of mESC-derived Crx.GFP+ photoreceptor precursors in subretinal space of the *Aipl1*$^{-/-}$ host retina.

Furthermore, a number of the transplanted Crx.GFP+ photoreceptor precursors contained proteins involved in phototransduction, such as Rhodopsin, Gnat1 and Recoverin indicating maturation of transplanted photoreceptor precursors within the host retina (Figure 5.30 A-C''). The antibody against Recoverin labels not only photoreceptors, but also cone bipolar cells (Günhan et al., 2003), which are the Recoverin+ cells in the INL (Figure 5.30C-C'').

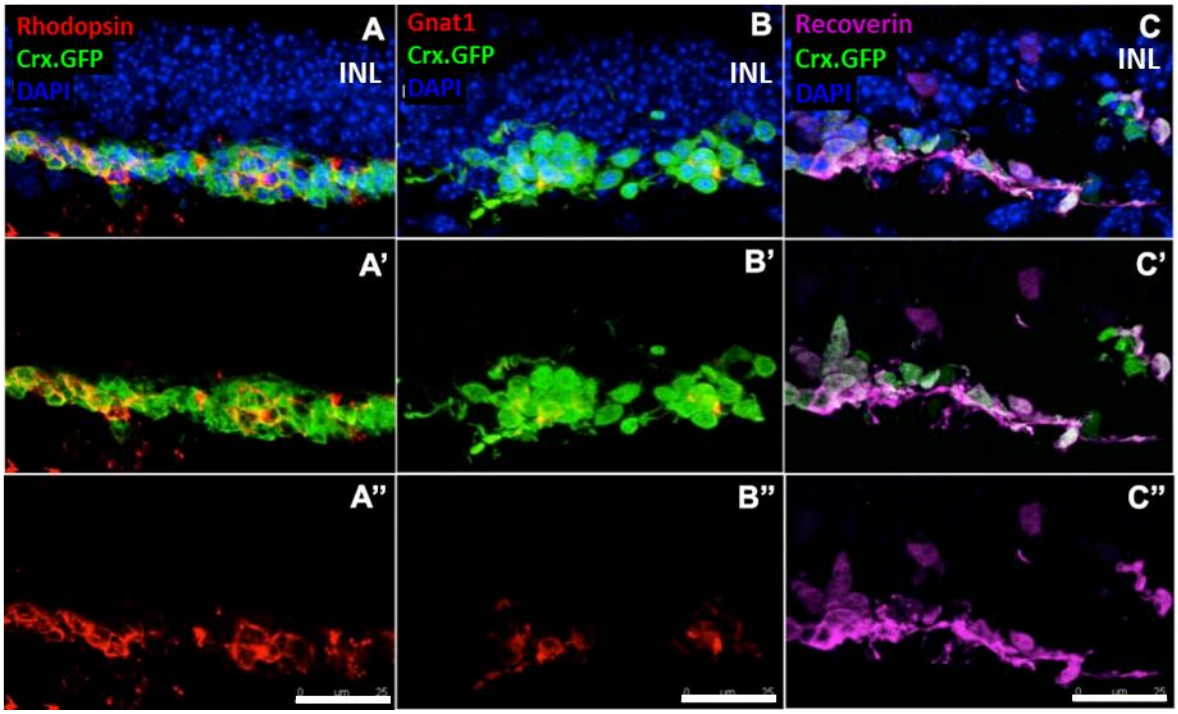

Figure 5.30: Expression of mature photoreceptor markers in transplanted mESC-derived Crx.GFP+ cells within the host *Aipl1*$^{-/-}$ retina. A-C''. Immunohistochemistry analysis showing the presence of Rhodopsin (A-A''), Gnat1 (B-B'') and Recoverin (C-C''). Scale bar: 25 µm.

In contrast to the *OGC* and *Gnat1*$^{-/-}$ recipients where the ONL does not degenerate and thus was present before transplantation, in the fully degenerate *Aipl1*$^{-/-}$ retina, transplanted Crx.GFP+ cells did not display obvious polarity. They were observed to extend processes, suggesting attempts to connect with second-order interneurons in the host inner retina, which is necessary for the transmission of visual signals.

To further investigate the relationship between transplanted Crx.GFP+ cells and the host INL, we used immunostaining for the photoreceptor ribbon synapse protein Ribeye, the synaptic vesicle protein Synaptophysin, as well asthe rod bipolar cell marker PKCα. Some of the transplanted Crx.GFP+ cells presented with processes, which terminated as round, synaptic bouton-like structures that expressed both Ribeye (Figure 5.31A) and Synaptophysin (Figure 5.31B).

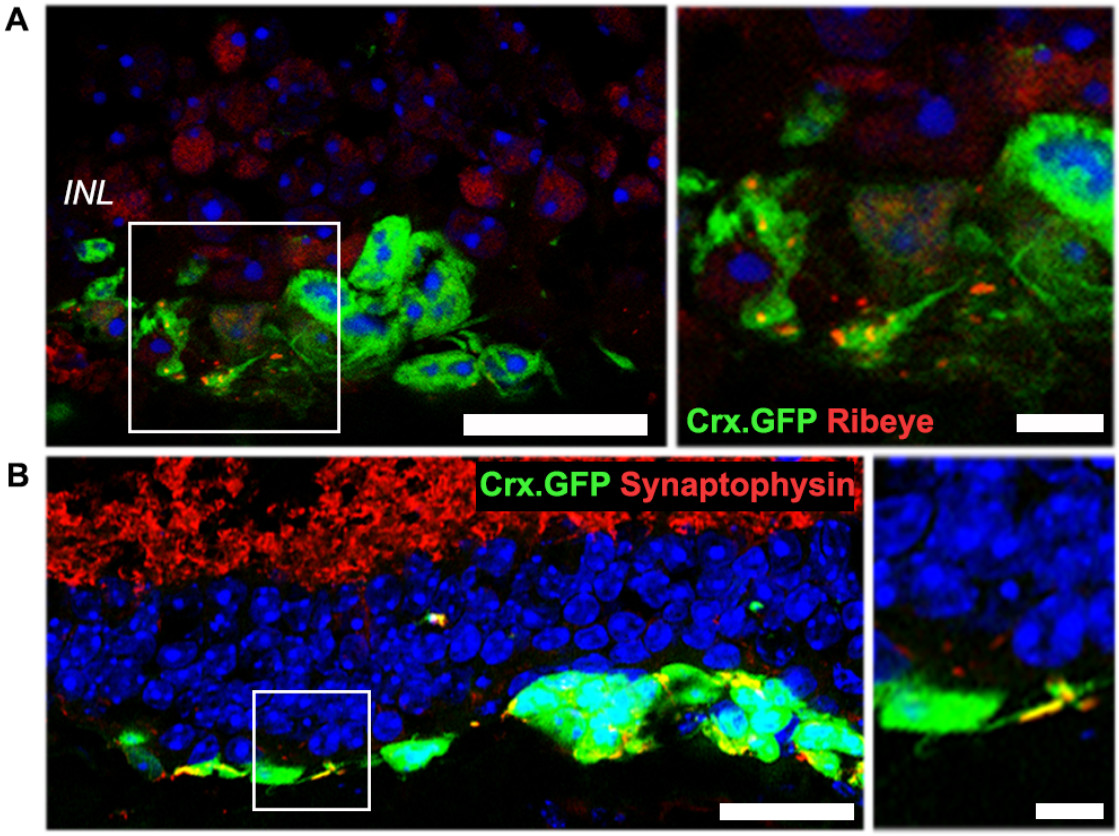

Figure 5.31: Expression of synaptic proteins A. Ribeye and B. Synaptophysin in transplanted mESC-derived Crx.GFP+ cells within the host *Aipl1*$^{-/-}$ retina. Scale bars, A. 25µm (5 µm in high magnification panel), B. 30µm (5 µm in high magnification panel).

Furthermore, several PKCα+ host *Aipl1*$^{-/-}$ rod bipolar cells appeared to extend dendrites to contact the processes of transplanted Crx.GFP+ cells (Figure 5.32, arrowheads). Given the close apposition between the processes of the host rod bipolar cells and transplanted cells, it is possible that this may be a potential mechanism of donor-host interaction in severe retinal degeneration where the ONL is absent.

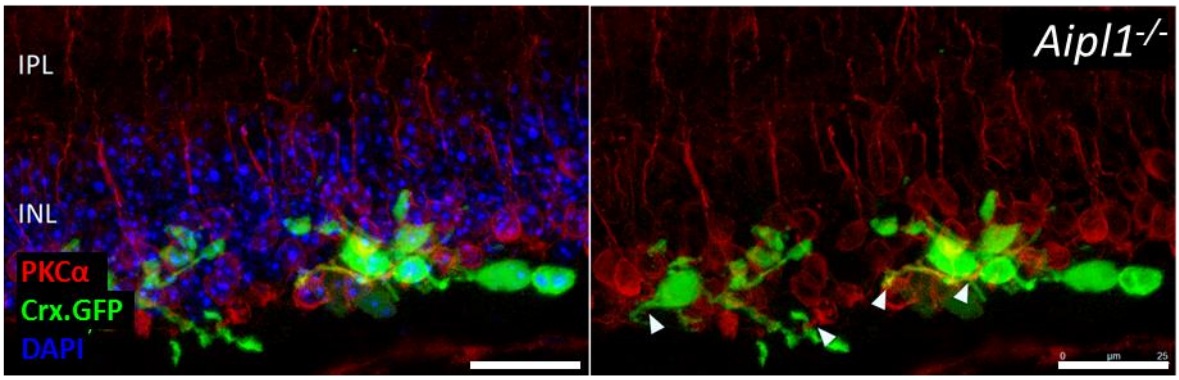

Figure 5.32: Interaction of transplanted Crx.GFP+ cells with host rod bipolar cells in the INL. Image showing the presence of Crx.GFP+ cells in the subretinal space of the *Aipl1*-/- eye in close apposition to bipolar cells (PKCa, red) with some dentrites contacting the transplanted photoreceptors (arrowheads). Scale bar: 25µm.

Finally, studies by our group and others have suggested that during retinal degeneration, reactive gliosis by Müller glial cells may form an outer retinal glial barrier impeding the interaction of transplanted cells with host cells (Jones et al., 2003; Kinouchi et al., 2003; Hippert et al., 2015). Using immunostaining for anti-glial fibrillary acid protein (GFAP), we observed reactive GFAP+ Müller glial cells throughout the *Aipl1*$^{-/-}$ retina, indicating Müller glial activation to photoreceptor degeneration in the *Aipl1*$^{-/-}$ eye, as with other models of end-stage photoreceptor degeneration. Importantly, at the region of the transplanted cell mass, Müller glial cell processes were observed to extend from the host GCL into and past the Crx.GFP+ mass without a significant glial barrier forming between them (Figure 5.33).

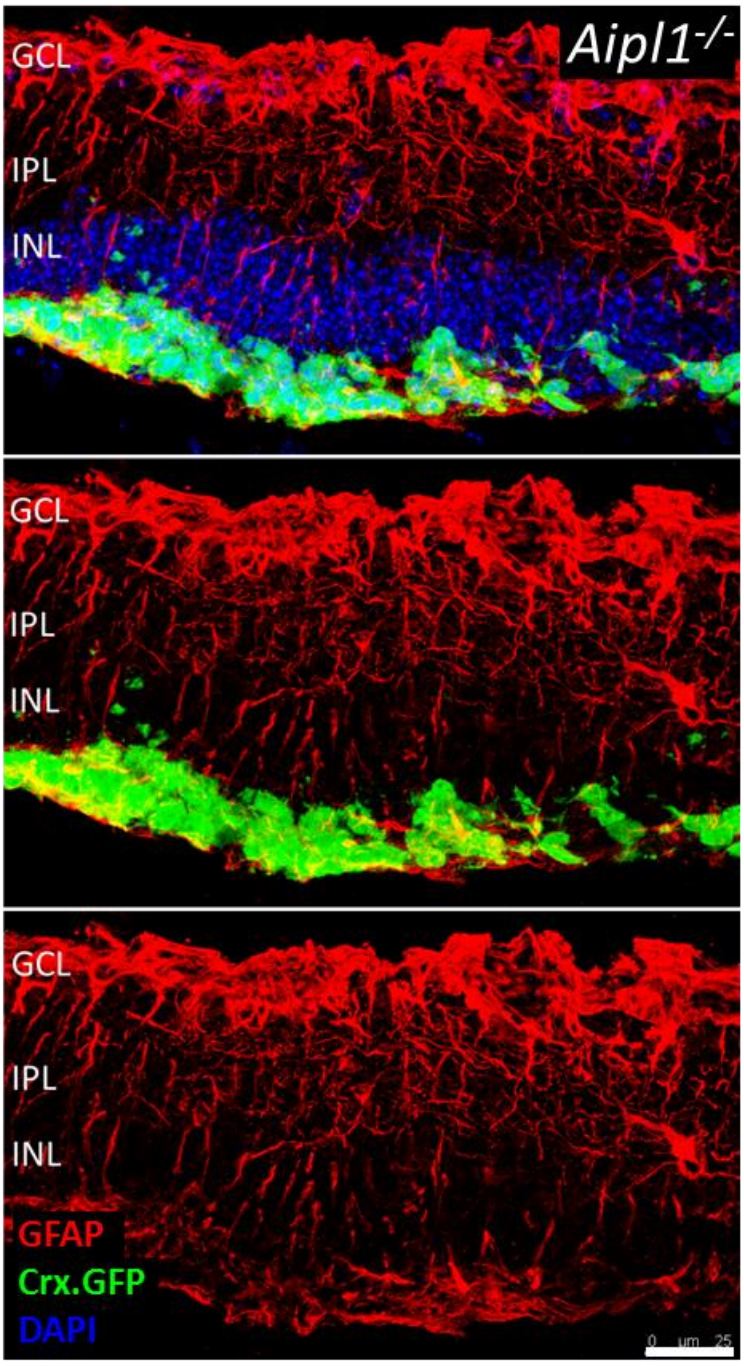

Figure 5.33: Reactive Müller glial cells in the host *Aipl1*$^{-/-}$ retina do not appear to form a glial barrier between transplanted Crx.GFP+ cells and the host inner retina. Scale bar: 25µm.

Together, these data demonstrate that mESC-derived photoreceptor precursors are capable of surviving and maturing following transplantation in a model of end-stage retinal degeneration. They go to express markers of phototransduction and interact with the host inner retina to transmit light-evoked visual signals.

5.3 Discussion

The objectives of this study were, firstly, to design an MEA set up and stimulus protocol that would enable the detection and characterisation of RGC responses in the retinas of various mouse models; and secondly, to assess the extent to which function may be restored following the transplantation of mESC-derived photoreceptor precursors, through the use of the MEA.

5.3.1 Characterising light stimulus-driven RGC responses in the WT retina

Using our MEA set up and stimulus protocol, we were able to detect a range of light-evoked RGC responses from WT retinas, across the 5 log units of light intensities surveyed. These responses could be classified based on changes in spike rate relative to light onset and offset, as ON, OFF, or ON-OFF response types, which is in keeping with numerous other electrophysiological studies of the mouse retina (Nirenberg and Meister, 1997; Tian and Copenhagen, 2003; Stone and Pinto, 1992; Tikidji-Hamburyan et al., 2014; Santos-Ferreira et al., 2014). These response types plausibly correspond to biologically distinct classes of RGCs, which enable functional segregation of ON and OFF signals in the visual pathway (Famiglietti and Kolb, 1976; Nelson et al., 1978).

In addition, in this study we demonstrated that ON and OFF RGC responses varied in duration – some were transient while others were sustained, and this variation is presumed to be reflective of differing synaptic inputs and intrinsic properties, as characterised in other studies (Margolis and Detwiler, 2007; Arman and Sampath, 2012; van Wyk et al., 2010; Hensley et al., 1993). In contrast, the majority of ON-OFF responses observed here were transient, which is in line with observations by other studies (Awatramani and Slaughter, 2000; Tian and Copenhagen, 2003). Occasionally, ON-OFF responses with a sustained component were observed, which may be accounted for by the detection of separate ON-sustained and OFF-transient RGCs (or vice versa) by the same electrode. As spike sorting (the assignment of spikes to individual RGCs) was not performed on the raw datasets, the responses recorded by one electrode may originate from more than one RGC, and multiple electrodes may detect the response from the same RGC if both its axon and cell body were in contact with multiple electrodes.

RGC responses recorded from the same electrodes were also frequently observed to change response type as the light intensity of the stimulus increased. While this may be attributed to the firing of different RGCs at varying light intensities, it may also reflect a luminance-dependent RGC response change, which was recently investigated by Tikidji-Hamburyan et al. (2014). This study showed that RGC response properties are dependent on the ambient luminance; as such, a RGC identified as an ON cell at one light intensity may behave as an ON-OFF cell at another light intensity, even within the same broad brightness range (scotopic, mesopic, or photopic). While the mechanism underlying luminance-dependent changes in response type has yet to be elucidated, the study showed that this mechanism may differ between RGC classes, and even a single RGC might employ various mechanisms at different luminance changes (Tikidji-Hamburyan et al., 2014). As such, in the present study, recorded RGC responses were classified in terms of response types rather than RGC class, as classification into RGC classes based on response type at a particular light intensity may be misleading.

We observed consistently larger proportions of ON and ON-OFF responses compared to OFF responses at all tested light intensities, which is in agreement with several studies that characterised MEA recordings from adult WT retinas. Tian and Copenhagen (2003) reported approximately 2% OFF, 21.5% ON-OFF, and majority ON responses; Cowan et al. (2016) reported 6% OFF, 67% ON-OFF, and 19% ON; while Nirenberg et al. (1997) reported 17% OFF, 12% ON-OFF, and 52% ON. Without further spike sorting, it is difficult to compare our results with other studies and assess the accuracy of our sampling. Nonetheless, the variation in stimulus protocol, luminance conditions, age of animals, and stringency of defining ON/OFF/ON-OFF responses, compound the difficulty of making comparisons across studies and may account for the discrepancy in estimates between studies.

Furthermore, different electrophysiological sampling methods may lead to under-sampling of certain RGC classes. Tian and Copenhagen (2003) proposed that the MEA tends to under-sample OFF RGCs, because their somata are further from the electrodes compared to the ON and ON-OFF RGC somata; this may account for the higher proportion of OFF RGCs detected by Stone and Pinto (1992), who utilised single extracellular electrodes instead of the MEA, and reported 44% OFF cells (Stone and Pinto, 1992). On the contrary, the smaller soma sizes of ON-OFF RGCs (Sun et al., 2002) may have resulted in under-sampling with the single electrode approach, which detected only 9% ON-OFF cells (Stone and Pinto, 1992).

5.3.2 Characterising light stimulus-driven RGC responses in the Gnat1$^{-/-}$ retina

Comparison of WT RGC responses with RGC responses recorded from the functionless-rods of *Gnat1*$^{-/-}$ retinas allowed for empirical determination of scotopic levels, as an absence of light-evoked RGC responses in the *Gnat1*$^{-/-}$ retina would presumably be indicative of a lack of rod input. The absence of RGC responses in the *Gnat1*$^{-/-}$ retina at the lowest light levels tested, ND5 and ND4, confirmed the abolishment of high sensitivity rod-driven visual responses, in agreement with previous reports (Calvert et al., 2000; Umino et al., 2008; Cowan et al., 2016). Correspondingly, RGC responses seen in the WT retina at these light levels were necessarily solely rod-driven. In addition, the *Gnat1*$^{-/-}$ retina appeared to display a partial loss of light responsiveness at ND3, with consistently fewer recorded RGCs displaying light-evoked responses. This may reflect the lack of rod input at what is likely to correspond to a mesopic light level, at which both rods and cones would normally be responsive. There also appeared to be a lower number of ON and ON-OFF responses at this light level compared to the WT retina, which may similarly reflect the lack of rod input, as high-sensitivity responses to light onset at low light levels tend to be rod-dominant (Cowan et al., 2016). From ND2 to ND0, the *Gnat1*$^{-/-}$ retinas appeared to have similar proportions of ON, ON-OFF, and OFF responses to WT retinas, which is in agreement with the observations of Cowan et al. (2016), and presumably reflects normal cone function.

Next, to assess if mouse ESC-derived rod precursors are responsive to light stimulation we performed MEA recordings on *Gnat1*$^{-/-}$ mice transplanted with D26 Crx.GFP^{+} photoreceptors. There were no discernible differences in the pattern of RGC responses between treated and untreated *Gnat1*$^{-/-}$ retinas, apart from what seemed to be a slightly greater number of OFF responses in the treated retina. As the *Gnat1*$^{-/-}$ mouse model could offer only a narrow window of light intensities for us to probe for RGC responses driven by transplanted ESC-derived photoreceptor precursors, we decided to seek an alternative model that would allow us to confidently detect changes in retinal function following transplantation into animals that lack sensitivity in a wider window of light intensities. Since transplanted rod precursors may be less photosensitive and improvements in retinal function may therefore occur at levels above conventional rod-response levels, we explored the use of the triple-knockout *Opn4*$^{-/-}$ *Gnat1*$^{-/-}$ *Cnga3*$^{-/-}$ (*OGC*) mouse model. *OGC* mice lack essential components of the phototransduction pathway in each of the known photosensitive cell types in the retina (rod α-transducin Gnat1 in rods, cyclic GMP-gated channel A3-subunit Cnga3 in cones, and melanopsin Opn4 in intrinsically-photosensitive RGCs), and were therefore expected to exhibit a complete loss of light sensitivity.

5.3.3 Investigating light stimulus-driven RGC responses in the Opn4$^{-/-}$ Gnat1$^{-/-}$ Cnga3$^{-/-}$ retina

As expected, the MEA recordings performed on untreated triple-knockout *OGC* retinas showed an absence of light-evoked RGC responses at all tested light levels, giving us a wide 5 log unit-wide window to probe for visual rescue. To this end, we were able to successfully demonstrate restoration of retinal function in *OGC* retinas following subretinal injection of AAV9.CMV.Gnat1.GFP virus, which can lead to expression of the G protein rod transducin α-subunit that is necessary for rod phototransduction in transduced recipient retinal cells. Surprisingly, robust light-evoked responses were observed not only at scotopic and mesopic levels but also at photopic levels, and the number of responding channels at all light levels was comparable to that seen in the WT retina. The vector-expressed Gnat1 was able to restore robust ON, ON-OFF, and OFF responses at scotopic levels; however, at mesopic levels, only ON and ON-OFF responses were observed, and at photopic levels, only ON responses were present.

In the *Gnat1* virus-transduced *OGC* retina, the ON, ON-OFF and OFF responses seen at scotopic levels are presumably due to the transmission of rod input by three different pathways (Volgyi, 2004; Wassle, 2004). Conversely, the absence of OFF responses at mesopic and photopic levels may reflect a relative lack of cone input. Unlike Gnat1, Cnga3 (the A3 subunit of the cone CNG channel) cannot be substituted by other subunits, and as it is involved in the final stage of cone phototransduction, RGCs in the *OGC* retina are unlikely to receive any cone input. ON responses at mesopic levels may be attributed to rod input via the highly-sensitive primary pathway through rod ON bipolar cells and bistratified AII amacrine cells to cone ON bipolar cells, which then provide synaptic input to the light onset response of ON and ON-OFF RGCs. Rods can also signal to cone OFF bipolar cells indirectly via the primary pathway or directly via the tertiary pathway (Soucy et al., 1998), giving rise to the light offset response of ON-OFF RGCs (Cowan et al., 2016). It is interesting to note that at photopic levels, there is a complete lack of response to light offset, and instead all RGC responses are in response to light onset. It is possible that these may be attributable to rods which possess less rhodopsin and are therefore less sensitive, requiring a greater light intensity stimulus to elicit a response.

While the precise mechanisms driving the observed responses in the *Gnat1* virus-transduced *OGC* retina remain to be investigated, the evident rescue of retinal function in the *OGC* retina following *Gnat1* virus transduction provided important validation for the use of the established MEA set up and protocol, as well as the *OGC* mouse as a suitable model to detect rescue of retinal function by transplanted mESC-derived photoreceptor precursors.

Following the transplantation of optimally-aged Crx.GFP$^+$ ESC-derived photoreceptor precursors, we detected weak ON responses in 1-2 channels in MEA recordings from 2 out of 10 treated *OGC* retinas at mesopic and photopic levels. We were unable to detect any response at scotopic levels, nor any responses to light offset. Immunohistochemical staining of Crx.GFP$^+$ photoreceptor precursor-treated *OGC* retinas revealed the presence of numerous GFP$^+$ rod-like cells extending long, Gnat1-positive outer segments in the host *OGC* ONL. While the median number of GFP$^+$ cells present in the host ONL appeared to be significantly lower in the *OGC* model compared to the *Gnat1*$^{-/-}$ model, this may be due to the small sample size; given that approximately 30-45% of mESC-derived photoreceptor transplants were rejected in the *Gnat1*$^{-/-}$ model, it may be necessary to have a larger sample size of treated *OGC*

retinas to verify if there is a true difference between the two models in the number of GFP^+ cells present in the host ONL following transplantation of mESC-derived photoreceptor precursors.

While the small number of ON responses observed in 2 out of 10 treated *OGC* retinas may be attributed to successful integration of transplanted mESC-derived photoreceptors with the host inner circuitry, it is important to note that residual, albeit attenuated, responses have been observed in the untreated *OGC* mouse at cone-response light levels. Hattar et al. (2003) reported the infrequent occurrence of a transient but significant pupillary reflex in response to bright 480 nm light (Hattar et al., 2003), while Vugler and colleagues described the retention of a small dark-adapted flash ERG response at fairly low to moderate light levels and evidence of visual responses from the lateral geniculate nucleus (LGN) and visual cortex of these mice (Allen et al., 2010), as well as a slight degree of behavioural light aversion (Semo et al., 2010). More recently, efforts by Hughes et al. (2016) to investigate the mechanism underlying these residual responses using MEA recordings confirmed the presence of robust micro-ERG type responses to 500nm light at moderate to bright light levels, and weaker responses to 360nm UV light at only high light levels. However, they were unable to detect any corresponding changes in RGC spike rate from *OGC* retinae stimulated under similar conditions, apart from a single electrode that detected a sluggish ON response to bright 360nm UV light (Hughes et al., 2016).

We did not observe any such residual responses in the 3 untreated *OGC* control retinal explants that we recorded from. However, it is not possible to conclude that responses were not seen in the untreated *OGC* control retinas compared to the treated *OGC* retinas, given the small number of untreated control *OGC* retinas compared to the number of treated *OGC* retinas (Fisher's Exact Test, $p = 1$). Given that we were only able to detect 3 positive channels out of 10 treated retinas at the highest light level (ND0), which equates to 1 positive channel in every 200 recorded channels, it would only be possible to conclude a statistically significant absence of response in the untreated *OGC* retinas with about 18 untreated *OGC* retinas that do not respond to the light stimulus.

Nonetheless, to verify if the nature of the ON responses observed in the treated *OGC* retinas was similar to that described in the aforementioned studies, we measured specific properties of the response time course in these responses and compared

them to ON responses in the WT retina. In agreement with Allen et al. (2010) and Hughes et al. (2016), in the treated *OGC* retina, we observed an increase in the peak strength of the responses as the intensity of the delivered light stimulus was increased. Moreover, the peak latency of the observed ON responses in the treated *OGC* retinas were greater than that of ON responses in the WT retina, suggesting that the RGC spiking rate increased very gradually in response to light onset. This delayed latency of response points to a photoreceptor-driven response rather than an early receptor potential, which occurs almost instantaneously on light presentation only at high light intensities, and has been previously proposed as a possible source of the residual responses observed in *OGC* retinas (Hattar et al., 2003). In addition, our observed responses similarly showed little sign of recovery, with spike rate remaining elevated relative to baseline for at least 200ms following light offset. Finally, in agreement with Hughes et al. (2016), only ON responses were observed in the treated *OGC* retina, whereas no OFF responses could be detected. Given these similarities, although we did not see any responses in our untreated *OGC* retinas, we cannot exclude the possibility that the low-amplitude long-latency responses that we observed in a small number of channels at cone-response levels in these particular *OGC* retinas, were a result of residual endogenous responses in the *OGC* recipient retina, as opposed to mESC-derived photoreceptor-driven responses.

Several studies have attempted to investigate the specific cellular mechanism(s) underlying these residual light-evoked RGC responses in the *OGC* retina, as well as the retinal pathway(s) by which they are propagated. While the targeted loss of melanopsin (*Opn4*) gene expression completely abolishes photoresponses from ipRGCs, both rods and cones in the *OGC* retina retain expression of their photopigments, and photosensitivity in these photoreceptors is lost instead through the removal of components further downstream in their phototransduction cascades (Gnat1 in rods, and Cnga3 in cones). This, therefore, allows for the possibility that phototransduction may still occur via alternative signalling pathways or by functional substitution of missing components in rods and cones. The first evidence that Gnat1-independent signalling pathways may exist within rod photoreceptors came from Calvert et al. (2000)'s study on the *Gnat1*$^{-/-}$ mouse model, where he noted a small subset of rods (less than 1%) that displayed a light-evoked rod response with a spectral efficiency equivalent to that of rhodopsin, but only at light intensities within the sensitivity range of cones. Allen et al. (2010)'s study similarly found that the

threshold irradiance of residual responses in the *OGC* retina was approximately 1 cd/m^2, which is similar to that for a cone-dependent ERG response; however, it could not be evoked under light-adapted conditions, indicating that it was atypical of cones. Subsequent spectral sensitivity analysis showed that this dark-adapted ERG response was rhodopsin-dependent, which is consistent with Calvert et al. (2000)'s observation. The authors proposed that the coupling of rhodopsin to cone α-transducin (Gnat2) present in rods was the most likely mechanism for this Gnat1-independent rod response, providing immunocytochemical evidence for low-level *Gnat2* expression in rods and showing that the Gnat1-independent rod response is lost in *Gnat1*$^{-/-}$ *Gnat2*$^{cpfl3/cpfl3}$ mice lacking both *Gnat1* and *Gnat2* expression (Allen et al., 2010). In additional support of this, separate studies have reported that rod and cone α-transducins (Gnat1 and Gnat2) are functionally interchangeable in the rod phototransduction cascade (Deng et al., 2009; Mao et al., 2013; Chen et al., 2010). Following on from these findings, more recently, Hughes et al. (2016) showed that residual rod-driven responses in the *OGC* retina were propagated to rod ON bipolar cells, and activated downstream a small but distinct population of atypical AII amacrine cells that are neither glycinergic nor GABAergic (Hughes et al., 2016).

Taken together, it is possible that the observed ON responses in treated *OGC* retinas may be attributed to the same rhodopsin-dependent, Gnat1-independent rod-driven mechanism described in the above studies. The lack of mESC-derived photoreceptor-driven responses could potentially be attributed to inner retinal remodelling, which to date has not been characterised in the *OGC* model. While Hattar et al. (2003) showed that there was no apparent loss of ONL thickness nor loss of Opn4-associated RGC connectivity in the *OGC* retina (Hattar et al., 2003), remodelling of the bipolar cells in the IPL may occur to a greater degree in the *OGC* retina due to the complete lack of photoreceptor input. Indeed, Haverkamp et al. (2006) have demonstrated that Cnga3 deficiency leads to inner retinal remodelling, beginning with loss of rod bipolars. However, this study also showed that cone bipolar cells in *Cnga3*$^{-/-}$ mice were able to react to the loss of light-driven output by forming functional ectopic synapses with rod spherules (Haverkamp et al., 2006). It would be interesting to investigate if similar rewiring events can occur in the *OGC* model, and if transplanting mESC-derived photoreceptor precursors during this window of rewiring may increase the possibility of rescuing visual function in this model.

At the time of experimentation, ongoing work by colleagues in the lab (see Chapter 6 and Appendix (Pearson et al., 2016)) yielded observations which suggested that a large proportion of the GFP+ cells observed in the ONL of recipient mice following transplantation arises as a result of what appears to be the transfer of RNA and/or protein between donor and host photoreceptors, rather than true integration of the donor photoreceptor cells. As the mechanisms underlying both processes remain unknown, it would have been difficult to determine the contribution of either process to any observed improvement in retinal function. As such, we decided to turn our efforts to investigating the extent to which retinal function could be improved in the rod-less and cone-less *Aipl1*$^{-/-}$ mouse model, in which any transfer of RNA and/or protein between transplanted cells and host photoreceptors presumably cannot occur.

5.3.4 Investigating light stimulus-driven RGC responses in the Aipl1$^{-/-}$ retina

In the *Aipl1*$^{-/-}$ model of end-stage retinal degeneration, we observed a pattern of retinal degeneration that was consistent with Ramamurthy et al. (2004), who observed rapid degeneration of both rods and cones after day 12, progressing from central to peripheral retina, resulting in complete ONL degeneration by 4 weeks (Ramamurthy et al., 2004). Although we could still observe the presence of a thin ONL comprising rods and cones at the 1-month time-point, this was completely absent by 2 months. Finally, the evident loss of both rods and cones from *Aipl1*$^{-/-}$ retinas between 1 and 2 months of age is in support of their findings that rods and cones appear to undergo degeneration at similar rates in this model (Ramamurthy et al., 2004).

Crx.GFP+ photoreceptor precursors transplanted into the subretinal space of *Aipl1*$^{-/-}$ eyes were able to survive, produce mature photoreceptor phototransduction proteins, and transmit light-evoked responses to host RGCs. In the majority of *Aipl1*$^{-/-}$ eyes receiving transplants, the transplanted cell mass was more well-spread as compared to in the treated *OGC* or *Gnat1*$^{-/-}$ models, probably due to the lack of a pre-existing host ONL. Some of the transplanted photoreceptor precursors expressed late phototransduction markers, although most did not display clear organised morphology or elaborate long outer segments similar to those in the WT retina, which is in fact in keeping with observations by other studies investigating the transplantation of photoreceptor precursors in severe retinal degeneration (Singh et al., 2013; Barnea-Cramer et al., 2016). These observations may be attributable to a

combination of factors such as the absence of a pre-existing photoreceptor layer to guide directional extension of processes, errant cues from the inner retina undergoing remodelling, or a lack of structural support that a pre-existing photoreceptor layer would otherwise provide. Nonetheless, we were able to observe processes extending from the transplanted Crx.GFP+ photoreceptor precursors towards the host INL, which terminated in synaptic bouton-like structures expressing synaptic proteins. These were in close apposition to host PKCα+ bipolar cells, which may indicate attempts by transplanted Crx.GFP+ photoreceptor precursors to connect with the host inner circuitry.

The absence of long outer segments in transplanted photoreceptor precursors may not necessarily preclude photoreceptor function and the transmission of visual signals to the inner retina. A small degree of light sensitivity was restored in severely degenerate retinas even without the elaboration of typical photoreceptors layering and the formation of long outer segments by transplanted human PSC-derived photoreceptor precursor cells (Lamba et al., 2009; Barnea-Cramer et al., 2016), while structurally-impaired murine photoreceptors have been shown to be capable of supporting a basic level of visual function (Thompson et al., 2014; Barber et al., 2013; Reuter and Sanyal, 1984; Singh et al., 2013). For example, even in the complete absence of outer segments, *rds* mice still demonstrate a small, albeit attenuated ERG response in the early stages of life (Reuter and Sanyal, 1984) . However, it is likely that this lack of normal outer segment morphology in transplanted photoreceptor precursors will reduce their sensitivity to light, and a higher number of cells may be required to compensate for the compromised light sensitivities of individual cells.

As in other models of end-stage retinal degeneration, changes in the inner retinal circuitry as well as glial scarring may present further challenges to the restoration of functional vision with photoreceptor transplantation.

Singh et al. (2014) observed that synapse development in *Aipl1*$^{-/-}$ retinas is arrested prior to photoreceptor degeneration, and synapses between photoreceptor terminals and second-order bipolar cells are not properly formed early on in development. In the early stages of photoreceptor degeneration, there is a reduction in bipolar cell dendritic arborisation and retraction from the OPL, without a decrease in the number of bipolar axons. In late stages of degeneration, bipolar cell bodies appear to lose their tight orientation and alignment, along with loss of large lobular

rod bipolar axon terminals (Singh et al., 2014), and we saw indications of both in our 3 month-old *Aipl1*$^{-/-}$ eyes. This pattern of inner retinal degeneration in *Aipl1*$^{-/-}$ is unlike that in *rd1* mice, where synaptic connections between photoreceptors and bipolar cells develop normally, and are lost only after photoreceptor degeneration (Puthussery and Taylor, 2010). Nonetheless, transplanted photoreceptors may be still able to transmit electrical signals in a manner similar to that of a subretinal electronic implant, and influence second-order bipolar cells even in the absence of conventional synapses, provided the grafted photoreceptors and host bipolar cells are closely apposed. As there is a lack of literature characterising inner retinal degeneration in the *Aipl1*$^{-/-}$ mouse model, further studies investigated pre- and post-synaptic formation in this model are warranted.

Using the MEA, we were only able to detect a small improvement in retinal function in *Aipl1*$^{-/-}$ retinas transplanted with Crx.GFP+ photoreceptor precursors, which may be reflective of the difficulties encountered in establishing graft:host connectivity in this particular end-stage model of retinal degeneration. However, as with the *OGC* retinas, we cannot conclude that there was a statistically significant absence of response in the untreated *Aipl1*$^{-/-}$ retinas compared to the treated *Aipl1*$^{-/-}$ retinas (Fisher's Exact Test, p = 0.15), due to an insufficient number of untreated control *Aipl1*$^{-/-}$ retinas. Given that we were only able to detect 4 responsive channels out of 10 treated retinas (600 recorded channels) at the highest light level (ND0), whereas we did not detect any responsive channels out of 7 control retinas (420 recorded channels), it would only be possible to conclude a statistically significant absence of response in the untreated *Aipl1*$^{-/-}$ retinas with about 12 untreated *Aipl1*$^{-/-}$ retinas that do not respond to the light stimulus. These calculations are based on the assumption that all recorded channels were usable; however, as indicated in Section 5.2.2.1, in every recording there was a variable number of false positive channels that were excluded, as well as noisy channels and channels with small signal-to-noise ratios, which would affect our estimates. Regardless, a larger number of untreated control retinas would increase our confidence in determining the effect of transplanted photoreceptor precursors on retinal function in the *Aipl1*$^{-/-}$ retina.

Nonetheless, our findings indicate that it may be possible for transplanted photoreceptors to reconnect, provided they are transplanted at the right stage of degeneration. Studies characterising inner retinal remodelling during retinal degeneration have shown that bipolar cells can seek out alternative functioning

photoreceptors in response to the loss of their original afferent photoreceptors, and establish new synaptic connections (Haverkamp et al., 2006). It may therefore be necessary to characterise the changes in the inner retinal circuitry in different forms of retinal degenerative diseases, which has already been done in various models of RP (Gayet-Primo and Puthussery, 2015; Cuenca et al., 2014; Jones et al., 2012), in order to determine the optimal stage for transplantation, which would conceivably be when inner retinal neurons are seeking out photoreceptors to reconnect with.

In addition, interestingly, the few responses observed appeared to be ON responses with a prolonged onset latency. While our findings must be interpreted with caution, given the small number of channels from which these responses were recorded as well as the small number of untreated control retinas, these delayed ON responses would be in keeping with our observations of the Crx.GFP+ cells following transplantation into the subretinal space of *Aipl1*$^{-/-}$ mice. The transplanted cells in the *Aipl1*$^{-/-}$ retina did not display obvious polarity nor extend long outer segments, despite exhibiting markers of mature photoreceptors and synaptic proteins. In comparison, the transplanted cells in the *OGC* retina were well-orientated and extended long outer segments as well as synaptic terminals, yet the ON responses observed in treated *OGC* mice displayed similar prolonged onset latencies, albeit to a smaller degree. While the source of the ON responses observed in treated *OGC* mice remains unclear, the markedly prolonged onset latency of the ON responses observed in treated *Aipl1*$^{-/-}$ mice may not be entirely unexpected if the ON responses observed in treated *OGC* mice originated from transplanted cells.

The methods and data presented in this chapter thus represent the first steps towards demonstrating that mouse ESC-derived photoreceptor precursors may be able to rescue a basic level of visual function in a mouse model of severe retinal degeneration.

Chapter 6 : Conclusion

6.1 Restoration of visual responses following transplantation of mouse ESC-derived photoreceptor precursors

The main aims of this study were to optimise the transplantation of mouse ESC-derived rod photoreceptor precursors into mouse models of retinal disease, and to thereafter assess the extent to which visual responses could be restored in these models. Much progress has been made in recent years in the field of photoreceptor replacement therapy, particularly in the use of 3D ESC culture systems to recapitulate retinal development *in vivo* and thereby provide a renewable source of photoreceptor cells for transplantation. Indeed, the presence of donor-reporter labelled cells in the host ONL have been observed following the transplantation of rod photoreceptor precursors isolated from 3D mouse ESC-derived retinal cultures, albeit at lower numbers than those isolated directly from the neonatal retina. The research detailed in this thesis builds on previous studies in the lab by refining the transplantation protocol in order to generate high numbers of a healthy and developmentally-homogenous mouse ESC-derived rod photoreceptor population for transplantation. This resulted in a significantly increased number of GFP+ cells correctly located within the host ONL following transplantation. Following that, we established the use of the multi-electrode array as a sensitive method of detecting visual responses and assessing the restoration of visual function in models of retinal disease. Most importantly, we were able to demonstrate for the first time that mouse ESC-derived photoreceptor precursors were capable of transmitting light-evoked responses following transplantation into a mouse model of severe retinal degeneration.

As mentioned in Chapter 5, at the time of writing, ongoing work by colleagues in the lab ((Pearson et al., 2016), see Appendix), as well as by Ader and colleagues (Santos-Ferreira et al., 2016), yielded observations which suggested that, while a small number of donor photoreceptor precursors do migrate and integrate into the host ONL following transplantation, a large proportion of the GFP+ cells observed in the host ONL following transplantation arises instead as a result of what appears to be the transfer of RNA and/or protein between donor and host photoreceptors. While the precise cellular mechanism(s) underlying this process has yet to be determined, our data thus far has ruled out the possibility of 1) classic donor cell-host cell nuclear fusion, 2) the uptake of free-floating protein from the extracellular environment and

3) the uptake of free nucleic acid released by donor cells that were damaged during the cell preparation process. Having excluded these possibilities, we postulate that RNA and/or protein may be transferred between donor and host photoreceptors *in vivo* following transplantation, resulting in the robust expression by host photoreceptors of a variety of proteins that are specific only to donor photoreceptors and otherwise absent from diseased host photoreceptors (for example, rod □-transducin in *Gnat1*$^{-/-}$ mice). This had previously been regarded as evidence for the integration of donor cells into the host ONL; however, our findings now indicate that integration is not the only mechanism that can lead to such expression.

Observations from additional experiments conducted by Pearson and colleagues suggest that this process, which we have termed cytoplasmic material transfer, is a specific property of post-mitotic photoreceptor precursors, but not of more immature cells or other cell types. It occurs in a fairly widespread and frequent, yet transient, manner; as such, the duration of protein expression resulting from material transfer is likely to be dependent on the half-life of the protein as well as viability of the donor cell population. Moreover, while material transfer from donor photoreceptor precursors to photoreceptors in the host ONL could occur via a direct physical cell-cell connection, a sustained connection between donor and host cells does not appear to be essential. We can speculate that an indirect mechanism such as intercellular trafficking of RNA and/or protein between cells within microvesicles or tunnelling nanotubules may be involved. Whatever the underlying mechanism is, it will need to be set in the context of a vast literature that, until recently, supported the notion of donor cell integration as the predominant process occurring after transplantation – for instance, the ability to increase the number of GFP-labelled cells in the host ONL following transplantation by manipulating OLM integrity (Barber et al., 2013; West et al., 2008; Pearson et al., 2010) or glial scar formation (Barber et al., 2013; Singhal et al., 2008; Jing Yao et al., 2011) in the host retina. That said, it must be borne in mind that integration does occur alongside cytoplasmic material transfer and may do so at differing rates in the degenerated, compared to the intact, retina. Indeed, recent unpublished data in the lab has indicated just this: transplantation of cones into the *Nrl*$^{-/-}$ host retina, which is cone-rich, with a disrupted OLM, yields markedly higher levels of integration (as opposed to material transfer) compared to transplants into the rod-dominant, intact wildtype retina.

Additionally, we find it hard to explain why ESC-derived photoreceptor precursors appear to be less efficient at material transfer than donor-derived photoreceptor precursors of a similar developmental stage, as suggested by the lower number of GFP-labelled cells in the host ONL following transplantation of ESC-derived photoreceptor precursors.

Nonetheless, aside from elucidating the underlying mechanisms, cytoplasmic material transfer may represent a novel therapeutic avenue for introducing functional proteins into otherwise diseased photoreceptors. Reporter-labelled donor cells in the host ONL have been shown by a number of studies to be light-responsive in a manner that is comparable to that of normal wild-type photoreceptors, based on single cell (Pearson et al., 2012) and whole retinal (MacLaren et al., 2006; Santos-Ferreira et al., 2014; Lamba et al., 2009; Neves et al., 2016) recordings in various mouse models of retinal degeneration, all of which had intact ONLs at the point of analysis. In addition, there appears to be a strong positive correlation between the number of reporter-labelled donor cells in the host ONL and the likelihood that a positive response is detected in a functional assay (Pearson et al., 2012; Barber et al., 2013; MacLaren et al., 2006; Lamba et al., 2009; Neves et al., 2016). Moreover, the presence of sufficiently large numbers of reporter-labelled donor cells in the host ONL allows for the transmission of visual signals from the retina to higher visual centres, as seen from the detection of light-evoked activity in the visual cortex and improvements in visually-guided behaviour (Pearson et al., 2012), optokinetic head-tracking behaviour in response to scotopic stimuli (Barber et al., 2013), and the restoration of pupillary light responses (MacLaren et al., 2006), all of which were absent in uninjected and sham-injected animals.

In routine quantitative analysis of recipients with an intact ONL, it is difficult to distinguish between material transfer of protein and/or RNA from donor cells to host cells, and true integration of transplanted cells with formation of synaptic connections to the host circuitry. Without knowing the mechanisms underlying both processes, it will be challenging to experimentally discern which is responsible for mediating visual rescue, or even which specific aspect of visual rescue each process may be mediating. As such, it will be essential to investigate the extent to which retinal function can be restored by the transplantation of photoreceptor precursor cells in severely degenerated retinas lacking an ONL, where material transfer from

transplanted donor cells to pre-existing host photoreceptors presumably cannot take place.

Our investigations in the rod-less and cone-less *Aipl1*$^{-/-}$ model exclude the possibility of material transfer between transplanted immature mouse ESC-derived photoreceptor precursors and host cells. In the experiments described in Chapter 5, we demonstrated that transplanted mouse ESC-derived photoreceptor precursors may be capable of forming functional connections with host inner circuitry and transmitting light-evoked responses to retinal ganglion cells in the *Aipl1*$^{-/-}$ model. The morphologies and orientation of the transplanted cells do not appear normal. This is in keeping with observations by other groups (Singh et al., 2013; Barnea-Cramer et al., 2016) and is to be expected for photoreceptor transplantation in the absence of other pre-existing host ONL photoreceptors. This may compromise the light sensitivity of transplanted photoreceptor precursors and compound the difficulty of restoring retinal function to levels of detection in degenerate retinas, although it does not necessarily preclude photoreceptor function. Transplanted mouse ESC-derived photoreceptor precursors were observed to extend processes towards the host INL, and may generate electrical currents that are transmitted to closely apposed bipolar and horizontal cells in the inner retina without the need for conventional synapses; this would be more akin to having an electronic retina implant in the subretinal space. Work done in parallel by colleagues in the lab on the transplantation of human PSC-derived L/Mopsin.GFP^{+} cone precursors (Gonzalez-Cordero et al., manuscript under review) or mouse ESC-derived cone precursors (Kruczek et al., manuscript in revision) into the *Aipl1*$^{-/-}$ model similarly demonstrated evidence of transplanted cones extending neurites, which show punctate Ribeye-positive ribbon synapses, towards the host INL.

Moreover, previous studies have demonstrated that light sensitivity is possible in photoreceptors with short (Thompson et al., 2014; Barber et al., 2013) or no outer segments (Lamba et al., 2009; Barnea-Cramer et al., 2016; Reuter and Sanyal, 1984). Plasticity and signal gain at the level of the visual cortical circuits (Davis, 2006; Nelson and Turrigiano, 2008) as well as photoreceptors and/or second-order neurons (Thompson et al., 2014) may allow photoreceptors with a reduced capacity for photon capture to generate useful, albeit limited, vision.

Few studies have investigated the restoration of visual function following photoreceptor transplantation in end-stage retinal degeneration mouse models lacking an ONL. Singh et al. (2013) reported that when Nrl.GFP-labelled rod precursors derived from postnatal mice pups were transplanted into 10-12 week old *rd1* mice lacking an ONL, at 2 weeks post-transplantation, the transplanted cells appeared to reconstitute an ONL between the host INL and RPE, with more than half of the transplanted rods extending short outer segments toward the RPE, and some making connections with the host rod bipolar cells. This appeared to be sufficient for functional improvements in pupillary light responses and light avoidance behaviour, as well as changes in cerebral visual cortical blood flow (Singh et al., 2013). However, it must be noted that the pupillary light reflex is an autonomous reflex that may also be mediated by intrinsically-photosensitive melanopsin-expressing RGCs (Semo et al., 2003; Vugler et al., 2008), bypassing the need for photoreceptors (Fu et al., 2005). The observed improvements in pupillary light responses therefore may not be related to the number of photoreceptors transplanted (Kovalevsky et al., 1995), and should be interpreted with caution if the contributions from ipRGCs are not definitively eliminated. Furthermore, the *rd1* strain used in most, if not all studies since 1948, are likely to possess a naturally-occurring mutation in the *Gpr179* gene, which specifically abolishes function in the ON bipolar cells (Nishiguchi et al., 2015). This makes it highly unlikely that the observed connections between transplanted rods and host rod bipolar cells can account for the reported improvements in visual function, and necessitates an alternative signalling pathway, possibly involving a novel rewiring involving cone OFF bipolar cells, to explain these findings. In addition, while the evidence of the CNS visual centre's activation is comparatively more robust, neuroprotection and functional rescue of residual host cones in the *rd1* retina by transplanted cells (Sun et al., 2015; Punzo and Cepko, 2007) were not excluded as an alternative explanation for the observed functional improvements. The recent study by Barnea-Cramer et al. (2016) reporting a small improvement in light sensitivity following the transplantation of human PSC-derived photoreceptor precursor cells into *rd1* mice will therefore also need to be interpreted with caution, in light of the abovementioned considerations pertaining to use of the *rd1* mouse model of end-stage retinal degeneration.

The electrophysiological data presented in this thesis thus provide proof of concept that mouse ESC-derived photoreceptor precursors are capable of restoring light sensitivity in an end-stage degenerate retina in which there is a complete absence of rods and cones. The next main aim of our work will be to increase the frequency of RGC responses detected by the MEA, assess the quality of these responses, and subsequently investigate the activation of the visual cortex and behavioural response to physiologically-relevant visual stimuli following the transplantation of mouse ESC-derived photoreceptors. In addition, in parallel with our investigations with mouse ESC-derived photoreceptors, we have also been able to generate and transplant photoreceptors from human ESCs and iPSCs, and will be looking to assess the function of human ESC- and iPSC-derived photoreceptors following transplantation in a similar manner (see Section 6.3.1).

6.2 Considerations for stem cell replacement therapy

The work presented in this thesis on the differentiation of photoreceptor precursors from mouse ESCs for transplantation into mouse models of retinal degeneration has important implications for ongoing work with human PSCs, and can inform the translation of pre-clinical studies to clinically-useful therapy. Although human PSCs do not necessarily behave the same as mouse ESCs, the use of mouse ESCs in these studies can nonetheless establish important principles and methods to be taken forward to studies employing human PSCs, such as the importance of the ontogenetic stage of ESC-derived donor cells, and the development of techniques for surveying immune responses to transplanted cells or assessing the functional capabilities of transplanted cells. In addition, the use of animal models that accurately reflect human disease is critical not only for justifying continued development of a therapeutic strategy for clinical use, but also for predicting clinical outcomes. In this study, we used the *Aipl1*$^{-/-}$ mouse, which has been found to be a useful model for AIPL1-associated Leber's Congenital Amaurosis (Dyer et al., 2004; Tan et al., 2009), as well as the *Gnat1*$^{-/-}$ mouse, which has been used as a model for congenital stationary night blindness (Calvert et al., 2000). Given the heterogeneity in clinical presentations and aetiologies of retinal degenerative diseases, it may be necessary to find suitable animal models that mirror different points on the disease spectrum, although some studies have suggested that the regressive events occurring in retinal degeneration are largely mutation- and species-independent (Hippert et al., 2015), and findings in

rodents and rabbits can be only broadly predictive of disease progression and treatment outcomes in humans (Cuenca et al., 2014).

In addition to establishing important principles and methods, some of the experiments conducted in this thesis have raised several considerations for the field of stem cell replacement therapy, which will be elaborated on in the following sections. Addressing these considerations may facilitate the detection of visual responses following transplantation.

6.2.1 Understanding inner retinal remodelling in retinal degenerative diseases

Regenerative strategies for treating degenerative diseases of the outer retina typically assume that the inner retinal circuitry remain intact. However, in recent years, there has been a growing body of evidence pointing to the gradual deconstruction of inner retina circuitry accompanying and following the death of rods and cones, regardless of the mechanism or sequence of photoreceptor loss (see reviews by (Jones et al., 2005; Cuenca et al., 2014; Strettoi, 2015)). For stem cell therapy to be clinically viable, it is essential to understand the molecular triggers and early processes of inner retinal remodelling, since cells of the inner retina play a critical role in accurately transmitting visual information to the brain, and are likely to influence clinical outcomes following transplantation. In addition, understanding the processes driving inner retinal remodelling may enable the development of strategies to attenuate or delay remodelling, which will thereby extend the therapeutic window for stem cell therapy, and possibly make the host retina more receptive for transplanted cells.

In the early stages of retinal degeneration, the loss of afferent input from photoreceptors appears to trigger a range of rewiring events in the inner retina, beginning with the second-order bipolar cells (Jones et al., 2003; Marc and Jones, 2003; Marc et al., 2003). Bipolar cells have been observed to initially retract their dendrites, but then subsequently extend their dendrites into the ONL, seeking out other functional pre-synaptic photoreceptors to establish new, ectopic contacts with (Haverkamp et al., 2006). Notably, the ON pathway, which is characterised by the expression of the metabotropic glutamate receptor-6 (mGluR6), appears to be more susceptible to photoreceptor loss (Cuenca et al., 2004; Strettoi and Pignatelli, 2000). Across studies on various animal models of RP, a common observation has been that rod ON bipolar cells are the first inner retinal cells to undergo both anatomical and

functional remodelling changes, followed by cone ON bipolars, and lastly cone OFF bipolar cells (Gayet-Primo and Puthussery, 2015; Cuenca et al., 2014; Jones et al., 2012). These changes include a switch from ON to OFF functional phenotypes due to altered glutamate receptor expression at the bipolar cell dendrites (Marc et al., 2007; Jones et al., 2012).

In addition to such extensive remodelling of inner retinal circuitry, Müller glial cells typically become reactive. They produce inhibitory extracellular matrix molecules such as chondroitin proteoglycans (CSPGs), which have been negatively correlated with transplantation outcome (Singhal et al., 2008; Suzuki et al., 2007; Barber et al., 2013). Other reports have indicated that the hypertrophic terminal processes of reactive Muller glial cells may present a physical barrier to graft:host interactions (Kinouchi et al., 2003; Zhang et al., 2003). Conversely, the gliotic 'scar' can regress in very advanced degeneration, becoming restricted to the inner retina (Barber et al., 2013; Hippert et al., 2015). This may actually leave the severely degenerated retina more amenable to rescue than some mid-stage aetiologies. Regardless, understanding inner retinal remodelling and glial activation in late stages of retinal degeneration will be essential to predicting the likelihood of restoration of visual function by stem cell therapy.

As such, it is important to identify a therapeutic window of opportunity in animal models and in humans, and determine the optimal stage of retinal degeneration for cell replacement therapy to be maximally efficacious. Intervening at the right stage of retinal degeneration may allow us to use inner retinal remodelling to our advantage; for example, introducing donor cells at earlier stages of retinal degeneration, when bipolar cells are searching for new synaptic targets to reconnect with, may improve the chances of donor cells forming new connections with the inner retinal circuitry.

6.2.2 Method of cell delivery

In theory, for maximally efficient restoration of visual function in end-stage retinal degeneration, transplanted photoreceptor precursors should ideally form a polarised ONL after transplantation, to enable both the establishment of specialized synaptic connections with residual bipolar and horizontal cells, as well as proper interactions with RPE cells. While the results by our group, and others, in severely degenerate mouse models hint at the possibility of this, the low occurrence of restored

RGC responses, as well as the inability of most transplanted cells in the donor cell mass to assume a normal orientation and form a laminated ONL-like structure, highlight the challenge of reconstructing an organised, functional ONL de novo in a model with a complete loss of the ONL by transplanting photoreceptor precursors in a cell suspension.

In the absence of any anatomical or functional baseline ONL structure, transplanted photoreceptor precursors may require more structural support in order to assume the right orientation and morphology. Early work by Seiler et al. (2010) has demonstrated that transplanted fetal rat retinal sheets are able to extend neuronal processes into the host IPL of severely degenerate rat retina, restoring robust – albeit delayed – visual responses in the superior colliculus, where over 95% of RGC axons project to, at mesopic light levels. Interestingly, connectivity with host retinal circuitry was found to occur via inner retinal neurons of the transplanted retinal sheet rather than those of the host INL; furthermore, few classic ribbon synapses were observed between donor and host cells, suggesting alternative communication pathways (Seiler et al., 2010). More recently, Assawachananont et al. (2014) showed considerable success with generating laminated retinal tissue *in vitro* from mouse ESCs and iPSCs, and transplanting these as whole retinal sheets into the subretinal space of *rd1* mice. Mouse ESC- and mouse iPSC-derived retinal sheets were able to differentiate and mature into well-organised, laminated retina-like structures when transplanted into severely degenerate retinas at the right age. Photoreceptors in the putative ONL of the retinal sheet were able to develop inner and outer segments, although functional assessment of whether light responses were restored following transplantation was not performed. However, in contrast to Seiler et al. (2010), the authors observed that connection to the host inner circuitry occurred via direct synapses between donor photoreceptors and host bipolar cells rather than donor bipolar cells (Assawachananont et al., 2014), raising the possibility of synaptic switching of donor photoreceptors from donor bipolar cells to host bipolar cells (Sher et al., 2013).

While it is not possible to directly compare these two studies' observations, it does raise questions about the use of full-thickness retinal sheets, as the donor graft inner retinal layer may hinder interactions between transplanted photoreceptors and host inner retinal neurons. Developing methods of generating partial-thickness retinal sheets, where only an organised photoreceptor layer is present but not an inner retinal layer, may therefore be an approach warranting further investigation (Pearson, 2014). To this end, advances in tissue engineering may offer a variety of scaffolds on which to culture photoreceptor precursor cells for delivery to the subretinal space (see reviews by (Hynes and Lavik, 2010; Kundu et al., 2014). This approach could also allow for the possibility of co-transplanting RPE and photoreceptors simultaneously for the treatment of retinal diseases that result in the loss of multiple cell types, such as AMD.

6.2.3 Adjunctive neuroprotective strategies

All retinal degenerative diseases, regardless of their aetiology, inevitably involve the activation of oxidative stress, inflammation and apoptosis pathways, all of which can compromise the survival and maturation of transplanted cells. Few studies on photoreceptor replacement therapy have evaluated the long-term survival of transplanted photoreceptor precursors. As such, it may be necessary to refine methods to increase the long-term survival and function of ESC-derived photoreceptors post transplantation. The administration of neuroprotective compounds, such as neurotrophic factors (West et al., 2012; Seiler et al., 2008; Jung et al., 2013; Ma et al., 2011) , anti-apoptotic (Jingyu Yao et al., 2011), or anti-inflammatory (Neves et al., 2016) molecules, as an adjunct to cell transplantation may prolong the preservation of host retinal integrity, thereby broadening the therapeutic window particularly in early stages of retinal degeneration, and also improve the health and long-term survival of transplanted cells. For example, the use of brain-derived neurotrophic factor (BDNF) has been shown to promote the formation of synaptic connections and improve functional outcomes following photoreceptor transplantation (Seiler et al., 2008). The use of adjunctive neuroprotective strategies may therefore increase the receptiveness of the host retina to transplanted donor photoreceptors.

6.3 Prospects for clinical application

6.3.1 Differentiation and transplantation of photoreceptor precursors from human ES and iPS cells

Findings based on investigations conducted with mouse ESC cultures have facilitated rapid progress in the differentiation of retinal cells from human PSCs (Meyer et al., 2009; Nakano et al., 2012; Reichman et al., 2014; Zhong et al., 2014). Ongoing work by colleagues in our lab has demonstrated the efficient generation of rod and cone photoreceptor precursors from human ES and iPS cell lines, using a combined 2D/3D differentiation protocol (Gonzalez-Cordero et al., manuscript submitted). This combined protocol allows for the efficient and reproducible generation of transplantation-competent donor cells in a manner reflecting normal retinal development in humans, and supports the *in vitro* maturation of rod and cone photoreceptors to late developmental stages, as evidenced by positive immunohistochemical staining for inner and outer segments, connecting cilia, and pre-synaptic ribbon synapses. Crx expression was first observed at week 6 followed by Nrl at week 7, then Recoverin at week 10 and Rhodopsin around week 12. A similar expression pattern was seen in hiPSC differentiation cultures.

The next step forward will therefore be to determine the capacity of transplanted human photoreceptors to mediate light-evoked responses in the degenerate mouse retina, using similar methods to that described in this thesis. Lamba et al. (2009) showed that GFP-labelled hESC-derived retinal cells were able to restore visual function in a $Crx^{-/-}$ mouse model with an intact ONL; however, the GFP-labelled cells in the host ONL appear strikingly similar in morphology to host photoreceptors (Lamba et al., 2009). In light of the above-mentioned studies by Pearson et al. (2016) and Santos-Ferreira et al. (2016), the possibility of material transfer accounting for these observations cannot be excluded. A more recent study by Barnea-Cramer et al. (2016) showed that human ESC- and iPSC-derived photoreceptor progenitors transplanted into end-stage 10-12 week old *rd1* mice were able to express phototransduction proteins and generate primitive outer segments, even though the morphology and orientation was not normal. Nonetheless, they were able to demonstrate the restoration of basic light avoidance behaviour and optomotor responses in *rd1* eyes receiving transplants (Barnea-Cramer et al., 2016). Although promising, it is also important to note that as mentioned above, for these studies conducted in *rd1* mice, neuroprotection and functional rescue of residual host cones

by transplanted cells (Sun et al., 2015; Punzo and Cepko, 2007) cannot be excluded as an alternative explanation for the observed restoration of visual function.

The latest work by our group (Gonzalez-Cordero et al., manuscript submitted) has unequivocally established that human ESC-derived cone photoreceptors can undergo integration, not only into the cone-rich *Nrl*$^{-/-}$ mouse model, but also into the *Aipl1*$^{-/-}$ model of end-stage retinal degeneration, where there is a complete absence of host rods and cones. These human NUCLEI+, M-opsin.GFP+ integrated hESC-derived cones exhibited features of nascent inner and outer segments, and also extended processes that displayed the presence of ribbon synapses, towards host bipolar cells. Further studies into whether these hESC-derived cones can survive for an extended period of time, mature, and restore functional vision in end-stage degenerate retinas is required. To this end, the use of larger animal models with retinas that have cone-rich regions and are more structurally-similar to the human retina may be necessary.

The ability of PSC-derived human photoreceptors to successfully contribute to light-mediated responses and restore functional vision in models of severe retinal degeneration remains to be conclusively determined. Nonetheless, these recent results support further development of stem cell-derived photoreceptor replacement therapy as a treatment strategy for retinal degenerative diseases.

6.3.2 Stem cells in clinical trials for retinal disease

Remarkable progress has been made in the past decade, not only in the differentiation of mouse and human ES and iPS cells towards retinal cells, but also in the approaches for transplantation into animal models, as well as the development of methods to assess visual function. Some of these advances have been addressed in this thesis and discussed above. These represent the first steps towards translating stem cell technology to clinical therapy.

In terms of clinical trials, the derivation and transplantation of human ES cell-derived RPE has advanced comparatively more quickly than photoreceptors, as Good Manufacturing Practice-compliant RPE differentiation has been comparatively easier to achieve. To date, a total of nine clinical trials are ongoing for PSC-derived RPEs in the treatment of macular degenerative diseases, eight of which involve hESC-derived RPE (see (Kimbrel and Lanza, 2015) for details). The ninth trial, initiated in 2014 by the Riken Institute (Japan) for the treatment of wet AMD, is the first human iPSC-

based therapy to be approved for trial in humans (Reardon and Cyranoski, 2014). The primary goal of these clinical trials is to assess the safety and tolerability of the intervention, and, if safe, the long-term prevention of photoreceptor loss. Encouragingly, recent reports from the first clinical trial using hESC-derived RPE cells for transplantation into patients with Stargardt's macular dystrophy and dry AMD (Schwartz et al., 2012) has provided evidence of the medium- to long-term safety, survival, and possible biological activity of the transplanted hESC-derived RPE, although an improvement in baseline visual acuity has yet to be observed (Schwartz et al., 2015). Nonetheless, if results from these clinical trials continue to demonstrate the safety of PSC-derived retinal cells, this will certainly pave the way for the translation of human PSC-derived photoreceptor transplantation to the clinic.

6.4 Concluding thoughts

The studies presented in this thesis have demonstrated the efficient generation of large numbers of healthy, developmentally-homogenous rod photoreceptor precursors from 3D mouse ESC cultures for transplantation into mouse models of retinal disease, as well as a sensitive, preliminary method for detecting visual responses and assessing the restoration of visual function following transplantation. These findings and methods have been and will continue to be important for informing ongoing work in deriving and transplanting photoreceptor precursors from human PSCs. Notably, we were also able to demonstrate for the first time that mouse ESC-derived photoreceptor precursors are capable of transmitting light-evoked responses following transplantation into a mouse model of severe retinal degeneration, and our findings in this aspect have surfaced several important issues that warrant further investigation in order for PSC-derived photoreceptor transplantation to be suitable for use in humans. Taken together with the recent progress by our lab (Gonzalez-Cordero et al., manuscript submitted) and others (Barnea-Cramer et al., 2016; Lamba et al., 2010, 2009) in generating and transplanting homogeneous populations of photoreceptor precursor cells from human PSCs, the possibility of stem cell-derived photoreceptor replacement therapy for the treatment of retinal degenerative diseases is certainly not far from sight.

References

Akimoto, M. et al. (2006) Targeting of GFP to newborn rods by Nrl promoter and temporal expression profiling of flow-sorted photoreceptors. *Proceedings of the National Academy of Sciences of the United States of America*. 103 (10), 3890–3895.

Allen, A. E. et al. (2010) Visual Responses in Mice Lacking Critical Components of All Known Retinal Phototransduction Cascades Paul A. Bartell (ed.). *PLoS ONE*. 5 (11), e15063.

Alves, C. H. et al. (2014) The CRB1 and adherens junction complex proteins in retinal development and maintenance. *Progress in Retinal and Eye Research*. 40 (November 2016), 35–52.

Anchan, R. M. et al. (1991) EGF and TGF-alpha stimulate retinal neuroepithelial cell proliferation in vitro. *Neuron*. 6 (6), 923–936.

Andersen, D. C. et al. (2013) Stem cell survival is severely compromised by the thymidineanalog EdU (5-ethynyl-2′-deoxyuridine), an alternative to BrdU for proliferation assays and stem cell tracing. *Analytical and Bioanalytical Chemistry*. 405 (29), 9585–9591.

Anderson, D. H. et al. (2002) A role for local inflammation in the formation of drusen in the aging eye. *American journal of ophthalmology*. 134 (3), 411–431.

Andreazzoli, M. (2009) Molecular regulation of vertebrate retina cell fate. *Birth defects research. Part C, Embryo today : reviews*. 87 (3), 284–295.

Anosova, N. G. et al. (2001) Antigenicity and immunogenicity of allogeneic retinal transplants. *Journal of Clinical Investigation*. 108 (8), 1175–1183.

Arman, A. C. & Sampath, A. P. (2012) Dark-adapted response threshold of OFF ganglion cells is not set by OFF bipolar cells in the mouse retina. *J Neurophysiol*. 107 (10), 2649–2659.

Assawachananont, J. et al. (2014) Transplantation of Embryonic and Induced Pluripotent Stem Cell-Derived 3D Retinal Sheets into Retinal Degenerative Mice. *Stem Cell Reports*. 2 (5), 662–674.

Asteriti, S. et al. (2014) Mouse rods signal through gap junctions with cones. *eLife*. 3.

Awatramani, G. B. & Slaughter, M. M. (2000) Origin of Transient and Sustained Responses in Ganglion Cells of the Retina. *Journal of Neurosc*. 20 (18), 7087–7095.

B. Jensen, M. (2012) Injected Versus Oral Cyclosporine for Human Neural Progenitor Grafting in Rats. *Journal of Stem Cell Research & Therapy*. 1 (S10), 3.

Bainbridge, J. W. B. et al. (2015) Long-Term Effect of Gene Therapy on Leber's Congenital Amaurosis. *New England Journal of Medicine*. 372 (20), 1887–1897.

Barber, A. C. et al. (2013) Repair of the degenerate retina by photoreceptor transplantation. *PNAS*. 110 (1), 354–359.

Barnea-Cramer, A. O. et al. (2016) Function of human pluripotent stem cell-derived photoreceptor progenitors in blind mice. *Scientific Reports*. 6 (July), 29784.

Bartsch, U. et al. (2008) Retinal cells integrate into the outer nuclear layer and differentiate into mature photoreceptors after subretinal transplantation into adult mice. *Experimental eye research*. 86 (4), 691–700.

Bäumer, N. et al. (2003) Retinal pigmented epithelium determination requires the redundant activities of Pax2 and Pax6. *Development (Cambridge, England)*. 130 (13), 2903–2915.

Berson, E. L. (2007) Long-term visual prognoses in patients with retinitis pigmentosa: The Ludwig von Sallmann lecture. *Experimental Eye Research*. 85 (1), 7–14.

Bharti, K. et al. (2008) Alternative promoter use in eye development: the complex role and regulation of the transcription factor MITF. *Development (Cambridge, England)*. 135 (6), 1169–1178.

Bharti, K. et al. (2006) The other pigment cell: specification and development of the pigmented epithelium of the vertebrate eye. *Pigment cell research / sponsored by the European Society for Pigment Cell Research and the International Pigment Cell Society*. 19 (5), 380–394.

Bibb, L. C. et al. (2001) Temporal and spatial expression patterns of the CRX transcription factor and its downstream targets. Critical differences during human and mouse eye development. *Human molecular genetics*. 10 (15), 1571–1579.

Boisgérault, F. et al. (2001) Role of CD4+ and CD8+ T cells in allorecognition: lessons from corneal transplantation. *Journal of immunology (Baltimore, Md. : 1950)*. 167 (4), 1891–1899.

Bunce, C. et al. (2010) Causes of blind and partial sight certifications in England and Wales: April 2007-March 2008. *Eye (London, England)*. 24 (11), 1692–1699.

Burke, B. (2001) Lamins and apoptosis: A two-way street? *Journal of Cell Biology*. 152 (3), 5–8.

Burmeister, M. et al. (1996) Ocular retardation mouse caused by Chx10 homeobox null allele: impaired retinal progenitor proliferation and bipolar cell differentiation. *Nature genetics*. 12 (4), 376–384.

Cai, Z. et al. (2010) Temporal requirement of the protein tyrosine phosphatase Shp2 in establishing the neuronal fate in early retinal development. *The Journal of neuroscience : the official journal of the Society for Neuroscience*. 30 (11), 4110–4119.

Calvert, P. D. et al. (2000) Phototransduction in transgenic mice after targeted deletion of the rod transducin alpha -subunit. *Proceedings of the National Academy of Sciences of the United States of America*. 97 (25), 13913–13918.

Carter-Dawson, L. D. & LaVail, M. M. (1979) Rods and cones in the mouse retina. II. Autoradiographic analysis of cell generation using tritiated thymidine. *The Journal of comparative neurology*. 188 (2), 263–272.

Cepko, C. (2014) Intrinsically different retinal progenitor cells produce specific types of progeny. *Nature Reviews Neuroscience*. 15 (9), 615–627.

Cepko, C. L. (1999) The roles of intrinsic and extrinsic cues and bHLH genes in the determination of retinal cell fates. *Current opinion in neurobiology*. 9 (1), 37–46.

Chacko, D. M. et al. (2000) Survival and differentiation of cultured retinal progenitors transplanted in the subretinal space of the rat. *Biochemical and biophysical research communications*. 268 (3), 842–846.

Chen, C.-K. et al. (2010) Replacing the rod with the cone transducin subunit decreases sensitivity and accelerates response decay. *The Journal of physiology*. 588 (2010), 3231–3241.

Chen, S. et al. (2012) Defective FGF signaling causes coloboma formation and disrupts retinal neurogenesis. *Cell Research*. 23 (2), 254–273.

Chu, V. T. et al. (2015) Increasing the efficiency of homology-directed repair for CRISPR-Cas9-induced precise gene editing in mammalian cells. *Nature Biotechnology*. 33 (5), 543–548.

Cowan, C. S. et al. (2016) Connexin 36 and rod bipolar cell independent rod pathways drive retinal ganglion cells and optokinetic reflexes. *Vision Research*. 11999–109.

Cuenca, N. et al. (2014) Cellular responses following retinal injuries and therapeutic approaches for neurodegenerative diseases. *Progress in Retinal and Eye research*. 4317–75.

Curcio, C. A. et al. (1996) Photoreceptor loss in age-related macular degeneration. *Investigative ophthalmology & visual science*. 37 (7), 1236–1249.

Damiani, D. et al. (2012) Undersized dendritic arborizations in retinal ganglion cells of the rd1 mutant mouse: A paradigm of early onset photoreceptor degeneration. *The Journal of Comparative Neurology*. 520 (7), 1406–1423.

Davey, N. J. et al. (1986) Statistical limits for detecting change in the cumulative sum derivative of the peristimulus time histogram. *Journal of neuroscience methods*. 17 (2–3), 153–166.

Davidoff, A. M. et al. (2004) Purification of recombinant adeno-associated virus type 8 vectors by ion exchange chromatography generates clinical grade vector stock. *Journal of virological methods*. 121 (2), 209–215.

Davis, G. W. (2006) Homeostatic control of neural activity: from phenomenology to molecular design. *Annual review of neuroscience*. 29307–323.

Decembrini, S. et al. (2014) Derivation of Traceable and Transplantable Photoreceptors from Mouse Embryonic Stem Cells. *Stem Cell Reports*. 2 (6), 853–865.

Deng, W.-T. et al. (2009) Functional interchangeability of rod and cone transducin alpha-subunits. *Proceedings of the National Academy of Sciences of the United States of America*. 106 (42), 17681–17686.

DeVries, S. H. (2000) Bipolar cells use kainate and AMPA receptors to filter visual information into separate channels. *Neuron*. 28 (3), 847–856.

Diermeier-Daucher, S. et al. (2009) Cell type specific applicability of 5-ethynyl-2'-deoxyuridine (EdU) for dynamic proliferation assessment in flow cytometry. *Cytometry. Part A : the journal of the International Society for Analytical Cytology*. 75 (6), 535–546.

Donoso, L. A. et al. (2006) The role of inflammation in the pathogenesis of age-related macular degeneration. *Survey of ophthalmology*. 51 (2), 137–152.

Dyer, M. A. et al. (2004) 'Retinal degeneration in Aipl1-deficient mice: A new genetic model of Leber congenital amaurosis', in *Molecular Brain Research*. . 2004 pp. 208–220.

Eberle, D. et al. (2011) Increased integration of transplanted CD73-positive photoreceptor precursors into adult mouse retina. *Investigative ophthalmology & visual science*. 52 (9), 6462–6471.

Eberle, D. et al. (2012) Outer segment formation of transplanted photoreceptor precursor cells. *PloS one*. 7 (9), e46305.

Eberle, D. et al. (2014) Subretinal transplantation of MACS purified photoreceptor precursor cells into the adult mouse retina. *Journal of visualized experiments : JoVE*. (84), e50932.

Eiraku, M. et al. (2011) Self-organizing optic-cup morphogenesis in three-dimensional culture. *Nature*. 472 (7341), 51–56.

Evans, J. R. (2001) Risk factors for age-related macular degeneration. *Progress in retinal and eye research*. 20 (2), 227–253.

Fain, G. L. & Lisman, J. E. (1999) Light, Ca2+, and photoreceptor death: new evidence for the equivalent-light hypothesis from arrestin knockout mice. *Investigative ophthalmology & visual science*. 40 (12), 2770–2772.

Famiglietti, E. V & Kolb, H. (1976) Structural basis for ON-and OFF-center responses in retinal ganglion cells. *Science (New York, N.Y.)*. 194 (4261), 193–195.

Fan, Y. & Bergmann, A. (2008) Apoptosis-induced compensatory proliferation. The Cell is dead. Long live the Cell! *Trends in cell biology*. 18 (10), 467–473.

Field, G. D. et al. (2010) Functional connectivity in the retina at the resolution of photoreceptors. *Nature*. 467 (7316), 673–677.

Fiscella, M. et al. (2012) Recording from defined populations of retinal ganglion cells using a high-density CMOS-integrated microelectrode array with real-time switchable electrode selection. *Journal of Neuroscience Methods*. 211 (1), 103–113.

Fitzgerald, S. C. et al. (1992) In search of the central respiratory neurons: I. Dissociated cell cultures of respiratory areas from the upper medulla. *Journal of neuroscience research*. 33 (4), 579–589.

Fu, Y. et al. (2005) Intrinsically photosensitive retinal ganglion cells detect light with a vitamin A-based photopigment, melanopsin. *Proceedings of the National Academy of Sciences of the United States of America*. 102 (29), 10339–10344.

Fuhrmann, S. et al. (2000) Extraocular mesenchyme patterns the optic vesicle during early eye development in the embryonic chick. *Development (Cambridge, England)*. 127 (21), 4599–4609.

Fuhrmann, S. (2010) Eye Morphogenesis and Patterning of the Optic Vesicle. *October*. 9361–84.

Fuhrmann, S. (2008) Wnt signaling in eye organogenesis. *Organogenesis*. 4 (April 2015), 60–67.

Furukawa, T. et al. (1999) Retinopathy and attenuated circadian entrainment in Crx-deficient mice. *Nature genetics*. 23 (4), 466–470.

Gao, G. et al. (2002) Rep/Cap gene amplification and high-yield production of AAV in an A549 cell line expressing Rep/Cap. *Molecular therapy : the journal of the American Society of Gene Therapy*. 5 (5 Pt 1), 644–649.

Gauthier, J. L. et al. (2009) Receptive fields in primate retina are coordinated to sample visual space more uniformly. *PLoS biology*. 7 (4), e1000063.

Gayet-Primo, J. & Puthussery, T. (2015) Alterations in Kainate Receptor and TRPM1 Localization in Bipolar Cells after Retinal Photoreceptor Degeneration. *Front Cell Neurosci*. 9 (December), 486.

Gonzalez-Cordero, A. et al. (2013) Photoreceptor precursors derived from three-dimensional embryonic stem cell cultures integrate and mature within adult degenerate retina. *Nature Biotechnology*. (July), 1–9.

Govardovskii, V. I. et al. (2000) In search of the visual pigment template. *Visual Neuroscience*. 17 (4), 509–528.

Green, E. S. et al. (2003) Genetic rescue of cell number in a mouse model of microphthalmia: interactions between Chx10 and G1-phase cell cycle regulators. *Development (Cambridge, England)*. 130 (3), 539–552.

Gregory, C. D. & Pound, J. D. (2011) Cell death in the neighbourhood: direct microenvironmental effects of apoptosis in normal and neoplastic tissues. *The Journal of pathology*. 223 (2), 177–194.

Gregory, C. D. & Pound, J. D. (2010) Microenvironmental influences of apoptosis in vivo and in vitro. *Apoptosis : an international journal on programmed cell death*. 15 (9), 1029–1049.

Günhan, E. et al. (2003) Ectopic photoreceptors and cone bipolar cells in the developing and mature retina. *The Journal of neuroscience : the official journal of the Society for Neuroscience*. 23 (4), 1383–1389.

Gust, J. & Reh, T. A. (2011) Adult donor rod photoreceptors integrate into the mature mouse retina. *Investigative ophthalmology & visual science*. 52 (8), 5266–5272.

Hack, I. et al. (1999) An alternative pathway for rod signals in the rodent retina: rod photoreceptors, cone bipolar cells, and the localization of glutamate receptors. *Proceedings of the National Academy of Sciences of the United States of America*. 96 (24), 14130–14135.

Haines, J. L. et al. (2005) Complement factor H variant increases the risk of age-related macular degeneration. *Science (New York, N.Y.)*. 308 (5720), 419–421.

Hartong, D. T. et al. (2006) Retinitis pigmentosa. *Lancet*. 368 (9549), 1795–1809.

Hatakeyama, J. & Kageyama, R. (2004) Retinal cell fate determination and bHLH factors. *Seminars in cell & developmental biology*. 15 (1), 83–89.

Hattar, S. et al. (2003) Melanopsin and rod-cone photoreceptive systems account for all major accessory visual functions in mice. *Nature*. 424 (6944), 76–81.

Haverkamp, S. et al. (2006) Synaptic plasticity in CNGA3(-/-) mice: cone bipolar cells react on the missing cone input and form ectopic synapses with rods. *The Journal of neuroscience : the official journal of the Society for Neuroscience*. 26 (19), 5248–5255.

Hennig, A. K. et al. (2008) Regulation of photoreceptor gene expression by Crx-associated transcription factor network. *Brain research*. 1192114–133.

Hensley, S. H. et al. (1993) Relative contribution of rod and cone inputs to bipolar cells and ganglion cells in the tiger salamander retina. *J Neurophysiol*. 69 (6), 2086–2098.

Hilgenberg, L. G. W. & Smith, M. A. (2007) Preparation of dissociated mouse cortical neuron cultures. *Journal of visualized experiments : JoVE*. (10), 562.

Hippert, C. et al. (2015) Müller Glia Activation in Response to Inherited Retinal Degeneration Is Highly Varied and Disease-Specific. *Plos One*. 10 (3), e0120415.

Van Hoffelen, S. J. et al. (2003) Incorporation of murine brain progenitor cells into the developing mammalian retina. *Investigative ophthalmology & visual science*. 44 (1), 426–434.

Holt, C. E. et al. (1988) Cellular determination in the Xenopus retina is independent of lineage and birth date. *Neuron*. 1 (1), 15–26.

Horsford, D. J. et al. (2005) Chx10 repression of Mitf is required for the maintenance of mammalian neuroretinal identity. *Development*. 132 (1), 177–187.

Hsu, P. D. et al. (2014) Development and Applications of CRISPR-Cas9 for Genome Engineering. *Cell*. 157 (6), 1262–1278.

Huettner, J. E. & Baughman, R. W. (1986) Primary culture of identified neurons from the visual cortex of postnatal rats. *The Journal of neuroscience : the official journal of the Society for Neuroscience*. 6 (October), 3044–3060.

Hughes, S. et al. (2016) Characterisation of light responses in the retina of mice lacking principle components of rod, cone and melanopsin phototransduction signalling pathways. *Scientific Reports*. 628086.

Humayun, M. S. et al. (2000) Human neural retinal transplantation. *Investigative ophthalmology & visual science*. 41 (10), 3100–3106.

Hynes, S. R. & Lavik, E. B. (2010) A tissue-engineered approach towards retinal repair: Scaffolds for cell transplantation to the subretinal space. Graefe's Archive for Clinical and Experimental Ophthalmology 248 (6) p.763–778.

Ikeda, H. et al. (2005) Generation of Rx+/Pax6+ neural retinal precursors from embryonic stem cells. *Proceedings of the National Academy of Sciences of the United States of America*. 102 (32), 11331–11336.

Inoue, H. & Yamanaka, S. (2011) The Use of Induced Pluripotent Stem Cells in Drug Development. *Clinical Pharmacology & Therapeutics*. 89 (5), 655–661.

Jager, R. D. et al. (2008) Age-related macular degeneration. *The New England journal of medicine*. 358 (24), 2606–2617.

Janssen, E. M. et al. (2003) CD4+ T cells are required for secondary expansion and memory in CD8+ T lymphocytes. *Nature*. 421 (6925), 852–856.

Jayakody, S. a et al. (2015) Cellular strategies for retinal repair by photoreceptor replacement. *Progress in Retinal and Eye Research*. 46 (May 2015), 31–66.

Jensen, A. M. & Wallace, V. A. (1997) Expression of Sonic hedgehog and its putative role as a precursor cell mitogen in the developing mouse retina. *Development (Cambridge, England)*. 124 (2), 363–371.

Jia, L. et al. (2009) Retinoid-related orphan nuclear receptor RORbeta is an early-acting factor in rod photoreceptor development. *Proceedings of the National Academy of Sciences of the United States of America*. 106 (41), 17534–17539.

Jiang, L. Q. et al. (1993) Subretinal space and vitreous cavity as immunologically privileged sites for retinal allografts. *Investigative Ophthalmology and Visual Science*. 34 (12), 3347–3354.

Jiang, L. Q. et al. (1995) Unconventional rejection of neural retinal allografts implanted into the immunologically privileged site of the eye. *Transplantation*. 59 (8), 1201–1207.

Johansen, P. et al. (2004) CD4 T cells guarantee optimal competitive fitness of CD8 memory T cells. *European journal of immunology*. 34 (1), 91–97.

Jones, B. W. et al. (2012) Retinal remodeling. Japanese Journal of Ophthalmology 56 (4) p.289–306.

Jones, B. W. et al. (2003) Retinal remodeling triggered by photoreceptor degenerations. *The Journal of comparative neurology*. 464 (1), 1–16.

Jones, B. W. et al. (2005) Retinal remodelling. *Clinical and Experimental Optometry*. 88 (5), 282–291.

Jones, N. D. et al. (2000) CD40-CD40 ligand-independent activation of CD8+ T cells can trigger allograft rejection. *Journal of immunology (Baltimore, Md. : 1950)*. 165 (2), 1111–1118.

Jones, N. D. et al. (2006) Effector and memory CD8+ T cells can be generated in response to alloantigen independently of CD4+ T cell help. *J Immunol*. 176 (4), 2316–2323.

Jung, G. et al. (2013) Genetically modified neural stem cells for a local and sustained delivery of neuroprotective factors to the dystrophic mouse retina. *Stem cells translational medicine*. 2 (12), 1001–1010.

Kaestel, C. G. et al. (2005) The immune privilege of the eye: human retinal pigment epithelial cells selectively modulate T-cell activation in vitro. *Current eye research*. 30 (5), 375–383.

Kaiser, O. et al. (2013) Dissociated neurons and glial cells derived from rat inferior colliculi after digestion with papain. *PLoS ONE*. 8 (12), 1–14.

Katamay, R. & Nussenblatt, R. B. (2013) 'Blood–Retinal Barrier, Immune Privilege, and Autoimmunity', in *Retina*. Fifth Edit . Elsevier. pp. 579–589.

Kimbrel, E. a. & Lanza, R. (2015) Current status of pluripotent stem cells: moving the first therapies to the clinic. *Nature Reviews Drug Discovery*. 14 (September), 681–692.

Kinouchi, R. et al. (2003) Robust neural integration from retinal transplants in mice deficient in GFAP and vimentin. *Nature neuroscience*. 6 (8), 863–868.

Kirschman, L. T. et al. (2010) The leber congenital amaurosis protein, AIPL1, is needed for the viability and functioning of cone photoreceptor cells. *Human Molecular Genetics*. 19 (6), 1076–1087.

Klassen, H. et al. (2007) Neural precursors isolated from the developing cat brain show retinal integration following transplantation to the retina of the dystrophic cat. *Veterinary ophthalmology*. 10 (4), 245–253.

Klein, R. J. et al. (2005) Complement factor H polymorphism in age-related macular degeneration. *Science (New York, N.Y.)*. 308 (5720), 385–389.

Koehler, C. L. et al. (2011) Receptive field center size decreases and firing properties mature in ON and OFF retinal ganglion cells after eye opening in the mouse. *Journal of neurophysiology*. 106 (2), 895–904.

Kolb, H. et al. (1995) *Cone Pathways through the Retina* [online]. Available from: http://webvision.med.utah.edu/book/part-iii-retinal-circuits/cone-pathways-through-the-retina/ (Accessed 15 March 2016).

Koso, H. et al. (2009) CD73, a novel cell surface antigen that characterizes retinal photoreceptor precursor cells. *Investigative ophthalmology & visual science*. 50 (11), 5411–5418.

Kovalevsky, G. et al. (1995) The intensity of the pupillary light reflex does not correlate with the number of retinal photoreceptor cells. *Experimental neurology*. 133 (1), 43–49.

Kundu, J. et al. (2014) Approaches to cell delivery: substrates and scaffolds for cell therapy. *Developments in ophthalmology*. 53143–154.

Lakowski, J. et al. (2010) Cone and rod photoreceptor transplantation in models of the childhood retinopathy Leber congenital amaurosis using flow-sorted Crx-positive donor cells. *Human molecular genetics*. 19 (23), 4545–4559.

Lakowski, J. et al. (2011) Effective Transplantation of Photoreceptor Precursor Cells Selected via Cell Surface Antigen Expression. *Stem Cells*. 29 (9), 1391–1404.

Lakowski, J. et al. (2015) Transplantation of Photoreceptor Precursors Isolated via a Cell Surface Biomarker Panel from Embryonic Stem Cell-Derived Self-Forming Retina. *Stem cells*. 33 (8), 2469–2482.

Lamb, T. D. et al. (2007) Evolution of the vertebrate eye: opsins, photoreceptors, retina and eye cup. *Nature reviews. Neuroscience*. 8 (12), 960–976.

Lamb, T. D. & Pugh, E. N. (2004) Dark adaptation and the retinoid cycle of vision. Progress in Retinal and Eye Research 23 (3) p.307–380.

Lamba, D. a et al. (2006) Efficient generation of retinal progenitor cells from human embryonic stem cells. *Proceedings of the National Academy of Sciences of the United States of America*. 103 (34), 12769–12774.

Lamba, D. a et al. (2009) Transplantation of human embryonic stem cell-derived photoreceptors restores some visual function in Crx-deficient mice. *Cell stem cell*. 4 (1), 73–79.

Lamba, D. A. et al. (2010) Generation, Purification and Transplantation of Photoreceptors Derived from Human Induced Pluripotent Stem Cells Rafael Linden (ed.). *PLoS ONE*. 5 (1), e8763.

Le, T. T. et al. (2006) Math5 is required for both early retinal neuron differentiation and cell cycle progression. *Developmental Biology*. 295 (2), 764–778.

Leskov, I. B. et al. (2000) The gain of rod phototransduction: reconciliation of biochemical and electrophysiological measurements. *Neuron*. 27 (3), 525–537.

Levine, E. M. et al. (1997) Sonic hedgehog promotes rod photoreceptor differentiation in mammalian retinal cells in vitro. *The Journal of neuroscience : the official journal of the Society for Neuroscience*. 17 (16), 6277–6288.

Ligasová, A. et al. (2015) A fatal combination: A thymidylate synthase inhibitor with DNA damaging activity. *PLoS ONE*. 10 (2), 1–21.

Lillien, L. (1995) Changes in retinal cell fate induced by overexpression of EGF receptor. *Nature*. 377 (6545), 158–162.

Lillien, L. & Cepko, C. (1992) Control of proliferation in the retina: temporal changes in responsiveness to FGF and TGF alpha. *Development*. 115 (1), 253–266.

Lin, C. et al. (2016) Increasing the Efficiency of CRISPR/Cas9-mediated Precise Genome Editing of HSV-1 Virus in Human Cells. *Scientific Reports*. 634531.

Lu, X. et al. (1996) Effect of cyclosporine and some derivatives on chronic rejection. *Transplantation proceedings*. 28 (6), 3152–3153.

Ma, J. et al. (2011) Combining chondroitinase ABC and growth factors promotes the integration of murine retinal progenitor cells transplanted into Rho(-/-) mice. *Molecular vision*. 17 (June), 1759–1770.

MacLaren, R. E. et al. (2006) Retinal repair by transplantation of photoreceptor precursors. *Nature*. 444 (7116), 203–207.

Mali, P. et al. (2013) Cas9 as a versatile tool for engineering biology. *Nature methods*. 10 (10), 957–963.

Mao, W. et al. (2013) Functional comparison of rod and cone Gα(t) on the regulation of light sensitivity. *The Journal of biological chemistry*. 288 (8), 5257–5267.

Marc, R. E. et al. (2003) Neural remodeling in retinal degeneration. Progress in Retinal and Eye Research 22 (5) p.607–655.

Marc, R. E. et al. (2007) Neural Reprogramming in Retinal Degeneration. *Investigative Opthalmology & Visual Science*. 48 (7), 3364.

Marc, R. E. & Jones, B. W. (2003) Retinal remodeling in inherited photoreceptor degenerations. *Molecular neurobiology*. 28 (2), 139–147.

Margolis, D. J. & Detwiler, P. B. (2007) Different Mechanisms Generate Maintained Activity in ON and OFF Retinal Ganglion Cells. *Journal of Neuroscience*. 27 (22), 5994–6005.

Marquardt, T. (2003) Transcriptional control of neuronal diversification in the retina. *Progress in retinal and eye research*. 22 (5), 567–577.

Marquardt, T. & Gruss, P. (2002) Generating neuronal diversity in the retina: one for nearly all. *Trends in neurosciences*. 25 (1), 32–38.

Martinez-Morales, J. R. et al. (2003) OTX2 Activates the Molecular Network Underlying Retina Pigment Epithelium Differentiation. *Journal of Biological Chemistry*. 278 (24), 21721–21731.

Martinez-Morales, J. R. et al. (2001) Otx genes are required for tissue specification in the developing eye. *Development (Cambridge, England)*. 128 (11), 2019–2030.

Martínez-Morales, J. R. et al. (2004) Eye development: a view from the retina pigmented epithelium. *BioEssays : news and reviews in molecular, cellular and developmental biology*. 26 (7), 766–777.

Masland, R. H. (2001) The fundamental plan of the retina. *Nature neuroscience*. 4 (9), 877–886.

Mazzoni, F. et al. (2008) Retinal Ganglion Cells Survive and Maintain Normal Dendritic Morphology in a Mouse Model of Inherited Photoreceptor Degeneration. *Journal of Neuroscience*. 28 (52), 14282–14292.

Medawar, P. B. (1948) Immunity to homologous grafted skin; the fate of skin homografts transplanted to the brain, to subcutaneous tissue, and to the anterior chamber of the eye. *British journal of experimental pathology*. 29 (1), 58–69.

Meister, M. et al. (1994) Multi-neuronal signals from the retina: acquisition and analysis. *Journal of Neuroscience Methods*. 51 (1), 95–106.

Mellough, C. B. et al. (2007) Treatment of adult neural progenitor cells prior to transplantation affects graft survival and integration in a neonatal and adult rat model of selective retinal ganglion cell depletion. *Restorative neurology and neuroscience*. 25 (2), 177–190.

Meyer, J. S. et al. (2009) Modeling early retinal development with human embryonic and induced pluripotent stem cells. *Proceedings of the National Academy of Sciences of the United States of America*. 106 (39), 16698–16703.

Minassian, D. C. et al. (2011) Modelling the prevalence of age-related macular degeneration (2010-2020) in the UK: expected impact of anti-vascular endothelial growth factor (VEGF) therapy. *British Journal of Ophthalmology*. 95 (10), 1433–1436.

Morcillo, J. et al. (2006) Proper patterning of the optic fissure requires the sequential activity of BMP7 and SHH. *Development (Cambridge, England)*. 133 (16), 3179–3190.

Morrow, E. M. et al. (1998) Vertebrate photoreceptor cell development and disease. *Trends in cell biology*. 8 (9), 353–358.

Murali, D. et al. (2005) Distinct developmental programs require different levels of Bmp signaling during mouse retinal development. *Development*. 132 (5), 913–923.

Nakano, T. et al. (2012) Self-formation of optic cups and storable stratified neural retina from human ESCs. *Cell stem cell*. 10 (6), 771–785.

Nakatani, K. et al. (2002) Calcium Diffusion Coefficient in Rod Photoreceptor Outer Segments. *Biophysical Journal*. 82 (2), 728–739.

Nasonkin, I. O. & Koliatsos, V. E. (2006) Nonhuman sialic acid Neu5Gc is very low in human embryonic stem cell-derived neural precursors differentiated with B27/N2 and noggin: implications for transplantation. *Experimental neurology*. 201 (2), 525–529.

Nawy, S. & Jahr, C. E. (1991) cGMP-gated conductance in retinal bipolar cells is suppressed by the photoreceptor transmitter. *Neuron*. 7 (4), 677–683.

Neef, a. B. & Luedtke, N. W. (2011) Dynamic metabolic labeling of DNA in vivo with arabinosyl nucleosides. *Proceedings of the National Academy of Sciences*. 108 (51), 20404–20409.

Nelson, R. et al. (1978) Intracellular staining reveals different levels of stratification for on- and off-center ganglion cells in cat retina. *Journal of neurophysiology*. 41 (2), 472–483.

Nelson, R. & Kolb, H. (1983) Synaptic patterns and response properties of bipolar and ganglion cells in the cat retina. *Vision research*. 23 (10), 1183–1195.

Nelson, S. B. & Turrigiano, G. G. (2008) Strength through diversity. *Neuron*. 60 (3), 477–482.

Neves, J. et al. (2016) Immune modulation by MANF promotes tissue repair and regenerative success in the retina. *Science*. 353 (6294), aaf3646.

Ng, L. et al. (2001) A thyroid hormone receptor that is required for the development of green cone photoreceptors. *Nature genetics*. 27 (1), 94–98.

Ng, L. et al. (2009) Developmental expression of thyroid hormone receptor beta2 protein in cone photoreceptors in the mouse. *Neuroreport*. 20 (6), 627–631.

Nguyen, M. & Arnheiter, H. (2000) Signaling and transcriptional regulation in early mammalian eye development: a link between FGF and MITF. *Development*. 127 (16), 3581–3591.

Nicholson, D. W. et al. (1995) Identification and inhibition of the ICE/CED-3 protease necessary for mammalian apoptosis. *Nature*. 376 (6535), 37–43.

Niederkorn, J. Y., Streilein, J. W., et al. (1981) Deviant immune responses to allogeneic tumors injected intracamerally and subcutaneously in mice. *Investigative Ophthalmology & Visual Science*. 20 (3), 355–363.

Niederkorn, J. Y., Shadduck, J. A., et al. (1981) Immunogenetic basis for immunologic privilege in the anterior chamber of the eye. *Immunogenetics*. 13 (3), 227–236.

Ning, H. et al. (2013) Effects of EdU labeling on mesenchymal stem cells. *Cytotherapy*. 15 (1), 57–63.

Nirenberg, S. & Meister, M. (1997) The light response of retinal ganglion cells is truncated by a displaced amacrine circuit. *Neuron*. 18 (4), 637–650.

Nishida, A. et al. (2003) Otx2 homeobox gene controls retinal photoreceptor cell fate and pineal gland development. *Nature neuroscience*. 6 (12), 1255–1263.

Nishiguchi, K. M. et al. (2015) Gene therapy restores vision in rd1 mice after removal of a confounding mutation in Gpr179. *Nature Communications*. 66006.

Oh, E. C. T. et al. (2008) Rod differentiation factor NRL activates the expression of nuclear receptor NR2E3 to suppress the development of cone photoreceptors. *Brain research*. 123616–29.

Osakada, F. et al. (2009) Stem cell biology and cell transplantation therapy in the retina. *Biotechnology and Genetic Engineering Reviews*. 26 (1), 297–334.

Osakada, F. et al. (2008) Toward the generation of rod and cone photoreceptors from mouse, monkey and human embryonic stem cells. *Nature biotechnology*. 26 (2), 215–224.

Owen, C. G. et al. (2012) The estimated prevalence and incidence of late stage age related macular degeneration in the UK. *The British journal of ophthalmology*. 96 (5), 752–756.

Panchision, D. M. et al. (2007) Optimized flow cytometric analysis of central nervous system tissue reveals novel functional relationships among cells expressing CD133, CD15, and CD24. *Stem cells*. 25 (6), 1560–1570.

Pang, J.-J. et al. (2012) Rod, M-cone and M/S-cone inputs to hyperpolarizing bipolar cells in the mouse retina. *The Journal of Physiology*. 590 (4), 845–854.

Pearson, R. A. (2014) Advances in repairing the degenerate retina by rod photoreceptor transplantation. *Biotechnology advances*. 32 (2), 485–491.

Pearson, R. A. et al. (2016) Donor and host photoreceptors engage in material transfer following transplantation of post-mitotic photoreceptor precursors. *Nature Communications*. 713029.

Pearson, R. A. et al. (2012) Restoration of vision after transplantation of photoreceptors. *Nature*. 485 (7396), 99–103.

Pearson, R. A. et al. (2010) Targeted Disruption of Outer Limiting Membrane Junctional Proteins (Crb1 and ZO-1) Increases Integration of Transplanted Photoreceptor Precursors Into the Adult Wild-Type and Degenerating Retina. *Cell Transplant*. 19 (4), 487–503.

Pennartz, S. et al. (2009) Generation of single-cell suspensions from mouse neural tissue. *Journal of visualized experiments : JoVE*. (29), .

Popp, S. et al. (2004) Developmental changes of aggrecan, versican and neurocan in the retina and optic nerve. *Experimental Eye Research*. 79 (3), 351–356.

Postel, K. et al. (2013) Analysis of cell surface markers specific for transplantable rod photoreceptors. *Molecular vision*. 192058–2067.

Pugh, E. N. & Lamb, T. D. (2000) Chapter 5 Phototransduction in vertebrate rods and cones: Molecular mechanisms of amplification, recovery and light adaptation. *Handbook of Biological Physics*. 3 (C), 183–255.

Punzo, C. & Cepko, C. (2007) Cellular Responses to Photoreceptor Death in the *rd1* Mouse Model of Retinal Degeneration. *Investigative Opthalmology & Visual Science*. 48 (2), 849.

Puthussery, T. & Taylor, W. R. (2010) Functional changes in inner retinal neurons in animal models of photoreceptor degeneration. *Advances in experimental medicine and biology*. 664525–532.

Radtke, N. D. et al. (1999) Preliminary report: indications of improved visual function after retinal sheet transplantation in retinitis pigmentosa patients. *American journal of ophthalmology*. 128 (3), 384–387.

Ramamurthy, V. et al. (2004) Leber congenital amaurosis linked to AIPL1: a mouse model reveals destabilization of cGMP phosphodiesterase. *Proceedings of the National Academy of Sciences of the United States of America*. 101 (38), 13897–13902.

Ran, F. A. et al. (2013) Genome engineering using the CRISPR-Cas9 system. *Nature protocols*. 8 (11), 2281–2308.

Rapaport, D. H. et al. (2004) Timing and topography of cell genesis in the rat retina. *The Journal of Comparative Neurology*. 474 (2), 304–324.

Reardon, S. & Cyranoski, D. (2014) Japan stem-cell trial stirs envy. *Nature*. 513 (7518), 287–288.

Reh, T. A. (2013) *The Development of the Retina*. Fifth Edit. [Online]. Elsevier Inc.

Reichman, S. et al. (2014) From confluent human iPS cells to self-forming neural retina and retinal pigmented epithelium. *Proceedings of the National Academy of Sciences of the United States of America*. 111 (23), 8518–8523.

Reinhard, K. et al. (2014) Step-by-step instructions for retina recordings with perforated multi electrode arrays. *PloS one*. 9 (8), e106148.

Reuter, J. H. & Sanyal, S. (1984) Development and degeneration of retina in rds mutant mice: the electroretinogram. *Neuroscience letters*. 48 (2), 231–237.

Roberts, M. R. et al. (2006) Making the gradient: thyroid hormone regulates cone opsin expression in the developing mouse retina. *Proceedings of the National Academy of Sciences of the United States of America*. 103 (16), 6218–6223.

Roberts, M. R. et al. (2005) Retinoid X receptor (gamma) is necessary to establish the S-opsin gradient in cone photoreceptors of the developing mouse retina. *Investigative ophthalmology & visual science*. 46 (8), 2897–2904.

Rojas-Muñoz, A. et al. (2005) chokh/rx3 specifies the retinal pigment epithelium fate independently of eye morphogenesis. *Developmental biology*. 288 (2), 348–362.

Rowan, S. et al. (2004) Transdifferentiation of the retina into pigmented cells in ocular retardation mice defines a new function of the homeodomain gene Chx10. *Development (Cambridge, England)*. 131 (20), 5139–5152.

Rowntree, R. K. & McNeish, J. D. (2010) Induced pluripotent stem cells: opportunities as research and development tools in 21st century drug discovery. *Regenerative medicine*. 5 (4), 557–568.

Sakaguchi, D. S. et al. (2005) Neural Progenitor Cell Transplants into the Developing and Mature Central Nervous System. *Annals of the New York Academy of Sciences*. 1049 (1), 118–134.

Sakaguchi, D. S. et al. (2004) Transplantation of neural progenitor cells into the developing retina of the Brazilian opossum: an in vivo system for studying stem/progenitor cell plasticity. *Developmental neuroscience*. 26 (5–6), 336–345.

Sam, T. N. et al. (2006) Engrafted neural progenitor cells express a tissue-restricted reporter gene associated with differentiated retinal photoreceptor cells. *Cell transplantation*. 15 (2), 147–160.

Samson, M. et al. (2009) Robust marking of photoreceptor cells and pinealocytes with several reporters under control of the Crx gene. *Dev Dynamics*. 238 (12), 3218–3225.

Sander, J. D. & Joung, J. K. (2014) CRISPR-Cas systems for editing, regulating and targeting genomes. *Nature biotechnology*. 32 (4), 347–355.

Santos, A. et al. (1997) Preservation of the inner retina in retinitis pigmentosa. A morphometric analysis. *Archives of ophthalmology (Chicago, Ill. : 1960)*. 115 (4), 511–515.

Santos-Ferreira, T. et al. (2014) Daylight vision repair by cell transplantation. *Stem cells*. (1), 1–15.

Santos-Ferreira, T. et al. (2016) Retinal transplantation of photoreceptors results in donor–host cytoplasmic exchange. *Nature Communications*. 713028.

Schadel, S. A. et al. (2003) Ligand channeling within a G-protein-coupled receptor: The entry and exit of retinals in native opsin. *Journal of Biological Chemistry*. 278 (27), 24896–24903.

Schmitz, F. et al. (2012) EF hand-mediated Ca- and cGMP-signaling in photoreceptor synaptic terminals. *Frontiers in molecular neuroscience*. 526.

Schwartz, S. D. et al. (2012) Embryonic stem cell trials for macular degeneration: a preliminary report. *The Lancet*. 379 (9817), 713–720.

Schwartz, S. D. et al. (2015) Human embryonic stem cell-derived retinal pigment epithelium in patients with age-related macular degeneration and Stargardt's macular dystrophy: Follow-up of two open-label phase 1/2 studies. *The Lancet*. 385 (9967), 509–516.

Seeliger, M. W. et al. (2011) Modulation of rod photoreceptor output by HCN1 channels is essential for regular mesopic cone vision. *Nature communications*. 2532.

Seiler, M. J. et al. (2008) BDNF-treated retinal progenitor sheets transplanted to degenerate rats: improved restoration of visual function. *Experimental eye research*. 86 (1), 92–104.

Seiler, M. J. et al. (2010) Visual restoration and transplant connectivity in degenerate rats implanted with retinal progenitor sheets. *European Journal of Neuroscience*. 31 (3), 508–520.

Semo, M. et al. (2010) Dissecting a role for melanopsin in behavioural light aversion reveals a response independent of conventional photoreception Steven Barnes (ed.). *PLoS ONE*. 5 (11), e15009.

Semo, M. et al. (2003) Melanopsin retinal ganglion cells and the maintenance of circadian and pupillary responses to light in aged rodless/coneless (rd/rd cl) mice. *The European journal of neuroscience*. 17 (9), 1793–1801.

Sharpe, L. & Stockman, A. (1999) Rod pathways: The importance of seeing nothing. *Trends in Neurosciences.* 22 (11), 497-504.

Shedlock, D. J. & Shen, H. (2003) Requirement for CD4 T cell help in generating functional CD8 T cell memory. *Science (New York, N.Y.)*. 300 (5617), 337–339.

Shen, J. K. et al. (2007) Oxidative damage in age-related macular degeneration. *Histology and histopathology*. 22 (12), 1301–1308.

Sher, A. et al. (2013) Restoration of retinal structure and function after selective photocoagulation. *The Journal of neuroscience : the official journal of the Society for Neuroscience*. 33 (16), 6800–6808.

Shintani, K. et al. (2009) Review and update: current treatment trends for patients with retinitis pigmentosa. *Optometry*. 80 (7), 384–401.

Shlens, J. et al. (2009) The Structure of Large-Scale Synchronized Firing in Primate Retina. *Journal of Neuroscience*. 29 (15), 5022–5031.

Singh, M. S. et al. (2013) Reversal of end-stage retinal degeneration and restoration of visual function by photoreceptor transplantation. *Proceedings of the National Academy of Sciences of the United States of America*. 110 (3), 1101–1106.

Singh, R. K. et al. (2014) Early Alteration of Retinal Neurons in Aipl1 -/- Animals. *Investigative Ophthalmology and Visual Science*. 55 (5), 3081–3092.

Singhal, S. et al. (2008) Chondroitin Sulfate Proteoglycans and Microglia Prevent Migration and Integration of Grafted Müller Stem Cells into Degenerating Retina. *Stem Cells*. 261074–1082.

Snyder, S. H., Lai, M. M., et al. (1998) Immunophilins in the nervous system. *Neuron*. 21 (2), 283–294.

Snyder, S. H., Sabatini, D. M., et al. (1998) Neural actions of immunophilin ligands. *Trends in pharmacological sciences*. 19 (1), 21–26.

Soucy, E. et al. (1998) *A Novel Signaling Pathway from Rod Photoreceptors to Ganglion Cells in Mammalian Retina*. 21481–493.

van der Spuy, J. et al. (2002) The Leber congenital amaurosis gene product AIPL1 is localized exclusively in rod photoreceptors of the adult human retina. *Human molecular genetics*. 11 (7), 823–831.

Srinivas, M. et al. (2006) Activation of the blue opsin gene in cone photoreceptor development by retinoid-related orphan receptor beta. *Molecular endocrinology*. 20 (8), 1728–1741.

Stafford, B. K. et al. (2009) Spatial-temporal patterns of retinal waves underlying activity-dependent refinement of retinofugal projections. *Neuron*. 64 (2), 200–212.

Stein-Streilein, J. & Streilein, J. W. (2002) Anterior chamber associated immune deviation (ACAID): regulation, biological relevance, and implications for therapy. *International reviews of immunology*. 21 (2–3), 123–152.

Stone, C. & Pinto, L. H. (1992) Receptive field organization of retinal ganglion cells in the spastic mutant mouse. *The Journal of physiology*. 456125–142.

Streilein, J. W. et al. (2002) Immunobiology and privilege of neuronal retina and pigment epithelium transplants. *Vision Research*. 42 (4), 487–495.

Streilein, J. W. (1999) Immunologic privilege of the eye. *Springer Seminars in Immunopathology*. 21 (2), 95–111.

Streilein, J. W. (1999) Regional immunity and ocular immune privilege. *Chemical immunology*. 7311–38.

Streilein, J. W. et al. (1980) Systemic immune unresponsiveness induced in adult mice by anterior chamber presentation of minor histocompatibility antigens. *The Journal of experimental medicine*. 152 (4), 1121–1125.

Streilein, J. W. & Niederkorn, J. Y. (1985) Characterization of the suppressor cell(s) responsible for anterior chamber-associated immune deviation (ACAID) induced in BALB/c mice by P815 cells. *Journal of immunology (Baltimore, Md. : 1950)*. 134 (3), 1381–1387.

Strettoi, E. (2015) A Survey of Retinal Remodeling. *Frontiers in cellular neuroscience*. 9494.

Strettoi, E. et al. (2002) Morphological and functional abnormalities in the inner retina of the rd/rd mouse. *J Neurosci*. 22 (13), 5492–5504.

Sun, J. et al. (2015) Protective Effects of Human iPS-Derived Retinal Pigmented Epithelial Cells in Comparison with Human Mesenchymal Stromal Cells and Human Neural Stem Cells on the Degenerating Retina in *rd1* mice. *STEM CELLS*. 33 (5), 1543–1553.

Sun, W. et al. (2002) Large-scale morphological survey of mouse retinal ganglion cells. *The Journal of Comparative Neurology*. 451 (2), 115–126.

Sun, X. et al. (2010) Gene therapy with a promoter targeting both rods and cones rescues retinal degeneration caused by AIPL1 mutations. *Gene therapy*. 17 (1), 117–131.

Suzuki, T. et al. (2007) Chondroitinase ABC treatment enhances synaptogenesis between transplant and host neurons in model of retinal degeneration. *Cell transplantation*. 16 (5), 493–503.

Swaroop, A. et al. (2010) Transcriptional regulation of photoreceptor development and homeostasis in the mammalian retina. *Nature reviews. Neuroscience*. 11 (8), 563–576.

Tabata, T. et al. (2000) A reliable method for culture of dissociated mouse cerebellar cells enriched for Purkinje neurons. *Journal of Neuroscience Methods*. 104 (1), 45–53.

Tan, M. H. et al. (2009) Gene therapy for retinitis pigmentosa and Leber congenital amaurosis caused by defects in AIPL1: Effective rescue of mouse models of partial and complete Aipl1 deficiency using AAV2/2 and AAV2/8 vectors. *Human Molecular Genetics*. 18 (12), 2099–2114.

Tang, C. et al. (2013) Immunogenicity of in vitro maintained and matured populations: potential barriers to engraftment of human pluripotent stem cell derivatives. *Methods in molecular biology*. 102917–31.

Tepass, U. (2002) Adherens junctions: new insight into assembly, modulation and function. *BioEssays : news and reviews in molecular, cellular and developmental biology*. 24 (8), 690–695.

Tezel, T. H. et al. (2004) Pathogenesis of age-related macular degeneration. *Trends in molecular medicine*. 10 (9), 417–420.

Thompson, S. et al. (2014) Photoreceptor cells with profound structural deficits can support useful vision in mice. *Investigative ophthalmology & visual science*. 55 (3), 1859–1866.

Tian, N. & Copenhagen, D. R. (2003) Visual Stimulation Is Required for Refinement of ON and OFF Pathways in Postnatal Retina. *Neuron*. 39 (1), 85–96.

Tikidji-Hamburyan, A. et al. (2014) Retinal output changes qualitatively with every change in ambient illuminance. *Nature Neuroscience*. 18 (1), 66–74.

Trambley, J. et al. (1999) Asialo GM1(+) CD8(+) T cells play a critical role in costimulation blockade-resistant allograft rejection. *The Journal of clinical investigation*. 104 (12), 1715–1722.

Tsukamoto, Y. et al. (2001) Microcircuits for night vision in mouse retina. *The Journal of neuroscience : the official journal of the Society for Neuroscience*. 21 (21), 8616–

8623.

Tsukamoto, Y. & Omi, N. (2013) Functional allocation of synaptic contacts in microcircuits from rods via rod bipolar to AII amacrine cells in the mouse retina. *Journal of Comparative Neurology*. 521 (15), 3541–3555.

Turner, D. L. et al. (1990) Lineage-independent determination of cell type in the embryonic mouse retina. *Neuron*. 4 (6), 833–845.

Turner, D. L. & Cepko, C. L. (1987) A common progenitor for neurons and glia persists in rat retina late in development. *Nature*. 328 (6126), 131–136.

Umino, Y. et al. (2008) Speed, spatial, and temporal tuning of rod and cone vision in mouse. *The Journal of neuroscience : the official journal of the Society for Neuroscience*. 28 (1), 189–198.

Vergara, M. N. & Canto-Soler, M. V. (2012) Rediscovering the chick embryo as a model to study retinal development. *Neural development*. 7 (1), 22.

Volgyi, B. (2004) Convergence and Segregation of the Multiple Rod Pathways in Mammalian Retina. *Journal of Neuroscience*. 24 (49), 11182–11192.

Vosshenrich, C. A. J. et al. (2005) Distinguishing features of developing natural killer cells. *Current Opinion in Immunology*. 17 (2), 151–158.

Vugler, A. A. et al. (2008) Survival and remodeling of melanopsin cells during retinal dystrophy. *Visual neuroscience*. 25 (2), 125–138.

Wang, G.-Y. et al. (2007) The sensitivity of light-evoked responses of retinal ganglion cells is decreased in nitric oxide synthase gene knockout mice. *Journal of Vision*. 7 (14), 7.

Wassle, H. (2004) Parallel processing in the mammalian retina. *Nat Rev Neurosci*. 5 (10), 747–757.

Watanabe, K. et al. (2005) Directed differentiation of telencephalic precursors from embryonic stem cells. *Nature neuroscience*. 8 (3), 288–296.

Wenkel, H. et al. (1999) Immune privilege is extended, then withdrawn, from allogeneic tumor cell grafts placed in the subretinal space. *Investigative ophthalmology & visual science*. 40 (13), 3202–3208.

Wenkel, H. & Streilein, J. W. (1998) Analysis of immune deviation elicited by antigens injected into the subretinal space. *Investigative Ophthalmology and Visual Science*. 39 (10), 1823–1834.

Wert, K. J. et al. (2014) General pathophysiology in retinal degeneration. *Dev Opthalmology*. 5333–43.

West, E. et al. (2012) Manipulation of the recipient retinal environment by ectopic expression of neurotrophic growth factors can improve transplanted photoreceptor integration and survival. *Cell Transplant*. 21 (5), 871–887.

West, E. L. et al. (2010) Long-term survival of photoreceptors transplanted into the adult murine neural retina requires immune modulation. *Stem cells*. 28 (11), 1997–2007.

West, E. L. et al. (2008) Pharmacological disruption of the outer limiting membrane leads to increased retinal integration of transplanted photoreceptor precursors. *Experimental eye research*. 86 (4), 601–611.

Westenskow, P. et al. (2009) Beta-catenin controls differentiation of the retinal pigment epithelium in the mouse optic cup by regulating Mitf and Otx2 expression. *Development (Cambridge, England)*. 136 (15), 2505–2510.

Wilbanks, G. A. & Streilein, J. W. (1990) Characterization of suppressor cells in anterior chamber-associated immune deviation (ACAID) induced by soluble antigen. Evidence of two functionally and phenotypically distinct T-suppressor cell populations. *Immunology*. 71 (3), 383–389.

Wong, K. A. et al. (2015) Efficient retina formation requires suppression of both Activin and BMP signaling pathways in pluripotent cells. *Biology open*. 4 (4), 573–583.

Wood, K. J. et al. (2016) Understanding Stem Cell Immunogenicity in Therapeutic Applications. *Trends in immunology*. 37 (1), 5–16.

Wu, D. C. et al. (2008) Embryonic stem cells and their differentiated derivatives have a fragile immune privilege but still represent novel targets of immune attack. *Stem cells*. 26 (0), 1939–1950.

van Wyk, M. et al. (2010) Receptive field properties of ON- and OFF-ganglion cells in the mouse retina. *Visual neuroscience*. 26 (3), 297–308.

Yang, C.-Y. et al. (2003) Differential synaptic organization of GABAergic bipolar cells and non-GABAergic (glutamatergic) bipolar cells in the tiger salamander retina. *The Journal of comparative neurology*. 455 (2), 187–197.

Yang, H.-J. et al. (2015) Vision from next generation sequencing: Multi-dimensional genome-wide analysis for producing gene regulatory networks underlying retinal development, aging and disease. *Progress in Retinal and Eye Research*. 461–30.

Yang, P. et al. (2002) Differential lineage restriction of rat retinal progenitor cells in vitro and in vivo. *Journal of neuroscience research*. 69 (4), 466–476.

Yao, J. et al. (2011) Robust cell integration from co-transplantation of biodegradable MMP2-PLGA microspheres with retinal progenitor cells. *Biomaterials*. 32 (4), 1041–1050.

Yao, J. et al. (2011) XIAP therapy increases survival of transplanted rod precursors in a degenerating host retina. *Investigative ophthalmology & visual science*. 52 (3), 1567–1572.

Yau, K. W. (1994) Phototransduction mechanism in retinal rods and cones. The Friedenwald lecture. *Investigative Ophthalmology and Visual Science*. 35 (1), 9–32.

Young, M. J. et al. (2000) Neuronal differentiation and morphological integration of hippocampal progenitor cells transplanted to the retina of immature and mature dystrophic rats. *Molecular and cellular neurosciences*. 16 (3), 197–205.

Young, R. W. (1985) Cell differentiation in the retina of the mouse. *The Anatomical record*. 212 (2), 199–205.

Zamiri, P. et al. (2005) Thrombospondin plays a vital role in the immune privilege of the eye. *Investigative ophthalmology & visual science*. 46 (3), 908–919.

Zhang, L. (2011) Voluntary oral administration of drugs in mice. *Protocol Exchange*. 1–11.

Zhang, Y. et al. (2003) Neuronal Integration in an Abutting-Retinas Culture System. *Investigative Opthalmology & Visual Science*. 44 (11), 4936.

Zhong, X. et al. (2014) Generation of three-dimensional retinal tissue with functional photoreceptors from human iPSCs. *Nature communications*. 54047.

Zuber, M. E. et al. (2003) Specification of the vertebrate eye by a network of eye field transcription factors. *Development*. 130 (21), 5155–5167.

Appendix